Dual roles of p97 in DNA damage repair

Shudong Li

University College



Supervisor: Prof Kristijan Ramadan

A thesis submitted to the University of Oxford for the degree of Doctor of Philosophy

Michaelmas Term 2021

Medical Research Council
Oxford Institute for Radiation Oncology

1. Contents

Acknowledgements ***1***

Declaration ***2***

Abstract ***3***

List of Figures ***4***

List of abbreviations ***5***

1. Introduction ***10***

1.1. Base excision repair (BER) **11**

1.2. Single strand break (SSB) repair **12**

1.3. Double strand break (DSB) repair **15**

1.3.1. Homologous recombination (HR) 16

1.3.2. NHEJ 17

1.3.3. Alternative DSB repair pathways 18

1.4. Regulation of DSB repair **21**

1.4.1. Ubiquitin/SUMO regulation of DSB repair 21

1.5. DNA protein crosslinks (DPCs) **26**

1.5.1. Replication/SPRTN dependent DPC repair 29

1.5.2. Proteasome-mediated DPC repair 32

1.6. p97 ..... **34**

1.6.1. p97 in cancer 38

1.7. DNA damage in cancer **40**

1.7.1. DNA damaging agents in cancer chemotherapy 42

1.7.2. PARP1 inhibitors 43

1.8. Aim of this study **48**

2. Materials and methods ***49***

2.1. Buffers **49**

2.1.1. 10x Phosphate buffer saline (PBS) 49

2.1.2. 10x Tris Buffered Saline (TBS) 49

2.1.3. 10x Tris/Glycine buffer 49

2.1.4. 5x Laemmli Buffer 50

2.1.5. Crystal violet staining (colony forming assays) 50

2.2. Cell culture **50**

2.2.1. Cell line buffers and maintenance 50

2.2.2. Generation of cell lines 51

2.2.3. Plasmids 51

2.2.4. Antibodies 52

2.2.5. Cell treatment reagents 53

2.2.6. Western blotting 53

2.2.7. Whole cell lysates 54

2.2.8. Cellular fractionation immunoprecipitation 54

2.2.9. Whole cell Immunoprecipitation 55
2.2.10. Denaturing IP 55
2.2.11. Colony forming assay 56
2.2.12. Apex2-mediated Proximity-Labelling 56
2.2.13. Rapid immunoprecipitation mass spectrometry of tagged protein (RIME-based approach) 57
2.2.14. Mass spectrometry and data analysis 58
2.2.15. Proximity ligation assay (PLA) 60
2.2.16. Immunofluorescence 60
2.2.17. Rapid Approach to DNA Adduct Recovery (RADAR) 61
2.2.18. Statistics and reproducibility 61

3. Results 62

3.1. p97 functions in DNA damage repair and signalling 62
3.1.1. p97 is a DNA damage repair protein 62
3.1.2. p97 is a DNA damage signalling protein 67

3.2. Identifying the trapped PARP1 repair pathway 71
3.2.1. Mass spectrometric analysis of trapped PARP1 protein interactions 71
3.2.2. Ubiquitination and SUMOylation of trapped PARP1 78
3.2.3. RNF4 ubiquitinates trapped PARP1 86
3.2.4. Trapped PARP1 triggers ubiquitin-dependent p97 activity 90
3.2.5. The RNF4-UFD1-p97 axis repairs trapped PARP1 100
3.2.6. Targeting RNF4-UFD1-p97 sensitises to PARPi 109

3.3. The p97 cofactor SPRTN and trapped PARP1 114
3.3.1. Deficiency in the p97 cofactor SPRTN causes PARPi sensitivity 114
3.3.2. SPRTN deficiency causes ineffective trapped PARP1 repair 118

4. Discussion 121

4.1. p97 and DNA damage 123
4.1.1. p97 and DSBs 123
4.1.2. p97 and TOP1ccs – nuclear periphery-based repair 125

4.2. Trapped PARP1 - mechanistic insights into DPC repair 127
4.2.1. Insights from mass spectrometric analysis 127
4.2.2. Novel mechanism of PARP1 dissociation 129
4.2.3. SUMOylation and STUbLs 131
4.2.4. Physiological trapped PARP1 135

4.3. PARPis and cancer 137
4.3.1. PARPi synthetic lethality revised 138
4.3.2. Clinical implications 142
4.3.3. Further Work 144

5. References 145

Acknowledgements

Thank you to Kristijan for supervising me throughout my studies, for motivating me when I was down. Your enthusiasm was addictive and you became the person I knew I could rely on when I was lost. Thank you Ignacio and Abhay for helping to troubleshoot my endless problems and for never losing patience. Thank you Ignacio for always keeping the lab organised and the tiring work you do in the background and Abhay for never saying no to helping me finish off an experiment so I can finish early. Annamaria, I always looked forward to seeing you in the lab, whether that's because I knew I had someone to dump my scientific worries on or to gossip with. I could always come to you for advice when I was not confident enough to make a decision and you were my guide to taking the next step. To John, I am so glad you were there during the beginning of my DPhil, you were the supportive senior student which every new DPhil candidate dreams of. If it is true when they say imitation is the greatest form of flattery, then you should feel smug by my attempts to model myself on you. I hope we see each other again to talk rubbish. Thank you to Sam for always being around to talk science, you were always supportive of every result, good or bad and I wish you the best for your future in the clinic. Thank you to Drago for being the best collaborator a scientist could hope for.

Thank you to all the students we have had join the lab in the last few years, you were all a breath of fresh air. Thank you to Martina for teaching me how to have an attitude. Thank you to Pauline for being always being a good laugh and also being one of the toughest people I know. Thank you to Cristiano for providing us unforgettable memories during our lab days off. Thank you for Ftoon for putting up with me as a desk buddy, I know you were sat in between me and John and you were always too kind to tell us to shut up. Thank you to Gwennie for being the easiest DPhil student one could be asked to supervise.

Thank you to Emily for being my biggest supporter, you got me through the tough times and made the bright times brighter.

Declaration

I declare that the work presented in this thesis is my own except where explicitly stated otherwise in the text, and that this work has not been submitted for any other degree at this or any other university.

Abstract

An organism's genome is perpetually challenged by multiple types of DNA lesions. The variety of insults is reflected by an equally diverse range of overlapping DNA repair mechanisms essential for an organism to survive. One protein which has roles in multiple DNA damage repair (DDR) pathways is the segregase/unfoldase p97. p97 acts in a ubiquitin dependent manner to unfold and remove modified substrates, facilitating the enzyme cascades required for efficient DNA damage repair. We show here how p97 has dual actions in DNA damage repair. It can act as a facilitator of DNA damage signalling, through mediating ubiquitin signalling at double strand breaks (DSBs), while also acting as a direct DNA damage repair protein. p97 is able to directly repair DNA-protein crosslinks (DPCs) and DPC-like lesions, such as Top1-ccs and trapped PARP1 respectively. These are deleterious protein adducts on chromatin which otherwise cause cell death by blocking replication fork progression and global transcription.

Importantly, we find that p97 directly removes and repairs PARP inhibitor (PARPi) - induced damage, namely trapped PARP1. PARPi are of special significance as they are the first approved targeted DNA damage chemotherapy to be used in the clinic. We reveal here, novel mechanistic details of how cancer cells respond to the trapped PARP1 lesion. Trapped PARP1 is first SUMOylated by PIAS4 and sequentially ubiquitinated by the SUMO-targeted ubiquitin ligase (STUbL), RNF4. Trapped PARP1 ubiquitination recruits p97 via its cofactor UFD1. By inhibiting the PIAS4-RNF4-UFD1-p97 axis, we were able to cause substantial accumulation of cytotoxic trapped PARP1. Using inhibitors of p97, including CuET, the metabolite of approved anti-alcohol abuse drug disulfiram, we potentiated PARPi cytotoxicity in cancer cell lines. Of additional interest, we show that a cofactor of p97, the essential protease SPRTN, also acts to prevent accumulation of trapped PARP1.

List of Figures

Figure 1. Model of overlapping BER and SSB repair
Figure 2. DSB repair by HR and NHEJ
Figure 3. Alternative DSB repair mechanisms
Figure 4. RNF8-RNF168 DSB ubiquitin signalling cascade
Figure 5. p97 and SUMO in DSB repair
Figure 6. DPC summary
Figure 7. Replication coupled SPRTN DPC repair
Figure 8. p97 unfolds proteins through its central pore
Figure 9. PARPi mechanism of action
Figure 10. TEX264 acts to recruit p97 for TOP1cc repair
Figure 11. TEX264 functions at the nuclear periphery to recruit p97 to TOP1ccs
Figure 12. p97 regulates RNF8 E3 ubiquitin ligase at DSB sites
Figure 13. p97 regulates RNF8 E3 ubiquitin ligase at DSB sites
Figure 14. Generating and validating model cell lines for trapped PARP1 mass spectrometry
Figure 15. RIME mass spectrometry identifies trapped PARP1 interaction partners
Figure 16. Apex2-mediated proximity-labelling mass spectrometry identifies trapped PARP1 interaction partners
Figure 17. PARP1 forms high MW isoforms upon trapping on chromatin by PARPi.
Figure 18. Trapped PARP1 is modified by ubiquitin on chromatin.
Figure 19. Trapped PARP1 is modified by SUMOylation
Figure 20. SUMOylation triggers ubiquitination of trapped PARP1 and recruits RNF4
Figure 21. RNF4 siRNA depletion prevents trapped PARP1 ubiquitination
Figure 22. RNF4$^{-/-}$ cells and RNF4 dominant negative mutant confirms E3 ubiquitin ligase activity on trapped PARP1
Figure 23. p97 intearcts with PARP1 in a trapped PARP1 dependent manner
Figure 24. p97 interacts with trapped PARP1 in a ubiquitin/UFD1 dependent manner.
Figure 25. p97 ATPase inhibition by CB-5083 treatment causes increased trapped PARP1 ubiquitination (K48 linked) and p97 interaction
Figure 26. ATPase deficient p97^{E578Q} mutant interacts with trapped PARP1 upon PARPi treatment
Figure 27. Inhibiting the RNF4-UFD1-p97 axis causes increased trapped PARP1 on chromatin
Figure 28. Pre-extraction based immunofluorescence microscopy enables visualisation of trapped PARP1
Figure 29. Immunofluorescence microscopy shows p97^{E578Q} expression causes trapped PARP1 accumulation
Figure 30. Inhibiting RNF4 and p97 slows the kinetics of trapped PARP1 repair (i)
Figure 31. Inhibiting RNF4 and p97 slows the kinetics of trapped PARP1 repair (ii)
Figure 32. CB5083 and CuET sensitises to PARPi in a trapped PARP1 dependent manner
Figure 33. Proposed model for trapped PARP1 repair by p97
Figure 34. SPRTN deficiency causes increased cytotoxicity to PARPis in HeLa and RPE WT hTERT
Figure 35. PARPi induced cytotoxicity in SPRTN deficient cells is PARP1 trapping dependent
Figure 36. PARPi induces more trapped PARP1 in SPRTN deficient cells
Figure 37. SPRTN deficiency causes trapped PARP1 accumulation and inhibits repair

List of abbreviations

53BP1	p53 Binding Protein 1
5-aza-dC	5-aza-2′-deoxycytidine
6-4 PP	6-4 Photoproduct
8-oxoG	8-oxoguanine
A	Alanine
ALDH	Aldehyde Dehydrogenase
ANOVA	Analysis Of Variance
AP	Apurinic/apyrimidinic
ATM	Ataxia-Telangiectasia Mutated
ATP	Adenosine Triphosphate
ATR	Ataxia Telangiectasia and Rad3-Related Protein
BER	Base Excision Repair
BP	Base Pair
BRCA	Breast Cancer Susceptibility Gene
C	Carboxy/cytosine
CB-5083	Cleave Biosciences 5083
Cdc	Cell Division Cycle
CDT1	Chromatin Licensing and DNA Replication Factor 1
CHK	Checkpoint Kinase
CMG	CDC45, GINS, MCM
CPT	Camptothecin
CRL	Cullin RING-Based E3 Ligase
CtIP	C-Terminal Binding Protein 1 Interacting Protein
CUL	Cullin
D	Aspartic Acid
Da	Dalton
DAPI	4',6-Diamidino-2-Phenylindole
DDB	DNA Damage-Binding Protein
ddH2O	Double Distilled Water
DMSO	Dimethyl Sulfoxide
DNA	Deoxyribonucleic Acid
DNA2	DNA Replication Helicase/Nuclease 2
DNA-PKcs	DNA-Dependent Protein Kinase Catalytic Subunit
DNMT	DNA Methyltransferase

DOX	Doxycycline
DPC	DNA-Protein Crosslink
DSB	Double Strand Break
dsDNA	Double Stranded DNA
E	Glutamic Acid
EDTA	Ethylene Diamine Tetraacetic Acid
EdU	5-ethynyl-2'-deoxyuridine
ER	Endoplasmic Reticulum
ERCC1	Excision Repair Cross-Complementation Group 1 (XPF)
EXO1	Exonuclease 1
F	Phenylalanine
FA	Fanconi Anaemia
FAF1	Fas Associated Factor 1
FANC	FA Complementation Group
FBS	Fetal Bovine Serum
FDA	Food and Drug Administration
GFP	Green Fluorescent Protein
GINS	Go, Ichi, Nii and San
Gy	Gray
HEK293	Human Embryonic Kidney 293
His	Histidine
HR	Homologous Recombination
hr	Hour(s)
ICL	Inter-Strand Crosslink
INM	Inner Nuclear Membrane
iPOND	Isolation of Proteins On Nascent DNA
IR	Ionising Radiation
K	Lysine
kDa	Kilodalton
L	Leucine/Litre
LRR	Leucine-Rich Repeat
M	Molar
MCM	Minichromosome Maintenance
MDC1	Mediator of DNA Damage Checkpoint Protein 1
Met	Methionine
min	Minute(s)
mM	Millimolar

MMS	Methyl Methansulfonate
MRC	Medical Research Council
MRE11	Meiotic Recombination 11
MRN	MRE11-RAD50-NBS1
mRNA	Messenger Ribonucleic Acid
MS	Mass Spectrometry
N	Amino
NBS1	Nijmegen Breakage Syndrome Protein 1
NCI	National Cancer Institute
NHEJ	Non-Homologous End Joining
nM	Nanomole
nm	Nanometre(s)
NPL4	Nuclear Protein Localisation Protein 4
ns	Not Significant
OGG1	8-Oxoguanine DNA Glycosylase
PAGE	Polyacrylamide Gel Electrophoresis
PALB2	Partner and Localizer of BRCA2
PARP1/2	Poly (ADP-Ribose) Polymerase 1/2
PARPi	Poly (ADP-Ribose) Polymerase Inhibitor
PAXX	Paralog of XRCC4 and XLF
PBS	Phosphate-Buffered Saline
PCNA	Proliferating Cell Nuclear Antigen
PCR	Polymerase Chain Reaction
PIP	PCNA-Interacting Protein
Pol	Polymerase
PSMD	26S Proteasome Non-ATPase Regulatory Subunit
PTM	Posttranslational Modification
Q	Glutamine
RADAR	Rapid Approach to DNA Adducts Recovery
REV	Reversionless
RIF1	Rap1-Interacting Factor 1
RING	Really Interesting New Gene
RIPA	Radioimmunoprecipitation Assay
RJALS	Ruijs-Aalfs Syndrome
RNA	Ribonucleic Acid
RNF	RING Finger Protein
ROS	Reactive Oxygen Species

RPA	Replication Protein A
RPE-1	Retinal Pigmented Epithelial 1
S Phase	Synthesis Phase
S/Ser	Serine
SDS	Sodium Dodecyl Sulphate
SEM/SD	Standard Error of the Mean/Standard Deviation
SHP	Src Homology 2-containing Phosphatase
SIM	SUMO Interacting Motif
siRNA	Short Interfering RNA
SPRTN	SprT-like N-terminal domain
SSBs	Single Strand Breaks
ssDNA	Single Stranded DNA
SSH	Strep-Strep- haemagglutinin
STUbl	SUMO-Targeted Ubiquitin Ligase
SUMO	Small Ubiquitin-Like Modifier
TBS	Tris-Buffered Saline
TDP	Tyrosyl-DNA Phosphodiesterase
TEX264	Testes Expressed 264
TOP	Topoisomerase
TOP-cc	Topoisomerase Cleavage Complex
TRAIP	TRAF Interacting Protein
U2OS	U2-Osteosarcoma
Ub	Ubiquitin
UBC	Ubiquitin-Conjugating
UBL	Ubiquitin-like proteins
UBXD	UBX Domain-containing protein
UBZ	Ubiquitin-Binding Zinc Finger
UFD1	Ubiquitin Fusion Degradation Protein 1
UV	Ultraviolet
VCP	Valosin Containing Protein
W	Tryptophan
WCE	Whole Cell Extract
WT	Wild-Type
XLF	XRCC4-Like Factor Ubiquitin Like with PHD and Ring Finger Domains
XP	Xeroderma Pigmentosum Complementation Group
XRCC	X-Ray Repair Cross Complementing
Y	Tyrosine

YFP	Yellow Fluorescent Protein
ZNF	Zinc Finger
γH2AX	Phosphorylated histone H2AX
Δ	Deletion

1. Introduction

Genetic material is the constant through which living organisms survive. Through its genome, an organism is able to function and respond in its environment, during which it looks to pass on the same successful blueprint to its next generation (Bruce Alberts, 2015). Through an organisms' lifetime, its genome is bombarded by a variety of endogenous and exogenous agents which cause DNA damage (Basu, 2018; Ciccia & Elledge, 2010; Jackson & Bartek, 2009). When left unchecked, this can lead to deleterious mutations and chromosomal aberrations leading to the loss of cell fitness. Thus, to survive, a complex system of pathways exist to preserve genome stability.

Genomic DNA damage occurs in several forms and this is mirrored by the equally wide range of DNA repair proteins required to maintain genome stability. These repair proteins are categorised into separate pathways, each repairing different forms of DNA damage (Jackson & Bartek, 2009). The necessity of DNA damage repair (DDR) for survival is made evident by the essentiality of many proteins in these pathways. Furthermore, cell death and senescence pathways are triggered by p53 when a cell is judged to be overburdened with DNA damage (Surova & Zhivotovsky, 2012).

The ability to cause cell death through the induction of DNA damage has been utilised even before the discovery of DNA itself. This includes radiation therapy and subsequent chemotherapies (camptothecin derivatives), which cause cell death through the induction of DSBs (Gianfaldoni et al., 2017; Martino et al., 2017). Through genetic analysis, malignancies themselves have been shown to have severe innate genomic instability (Hanahan & Weinberg, 2011), establishing it as one of the enabling characteristics of cancer. This has lead to a need to further our understanding of DDR to successfully apply our knowledge for clinical applications (Chatterjee & Walker, 2017; Lord & Ashworth, 2012).

Broadly, DNA damage repair (DDR) can be split into pathways which are distinct for the lesions they repair. However, the same DDR protein can function in several different pathways for the repair of different lesions.

1.1. Base excision repair (BER)

DNA bases are the most reactive part of the nucleotide (Masuda et al., 1980) and can be modified by oxidation, alkylation and deamination to become a DNA lesion. 1000s of these lesions occur per cell per day, on which the base excision repair pathway acts (Ciccia & Elledge, 2010). BER is initiated by the detection of these modified bases by one of the 11 known glycosylases, of which each are specialised for a particular base lesion. For example, the glycosylase 8-Oxoguanine DNA Glycosylase (OGG1) repairs reactive oxygen species-(ROS) induced base damage to the guanosine base, termed 8-oxoG. (Bauer et al., 2015; Chatterjee & Walker, 2017; Krokan & Bjørås, 2013).

All BER starts with the cleavage of the damaged DNA base by glycosylases leaving an abasic (AP) site. These sites are then cleaved to form a single strand break (SSB) intermediate by either AP-endonuclease 1 (APE1), lyase activity from DNA polymerase (pol) β or AP lyase (Figure 1) (Barnes & Lindahl, 2004; Fortini & Dogliotti, 2007). Depending on the type of lesion and glycosylase, the break site is repaired by either short-patch or long-patch BER. At the centre of mediating this pathway is the molecular scaffold XRCC1. XRCC1 is non-catalytic but has multiple interactions with proteins involved in both short and long-patch BER including APE1, pol β, polynucleotide kinase 3'-phosphatase (PNKP) and proliferating cell nuclear antigen (PCNA), among others (Figure 1).

Short-patch BER involves the insertion of a single nucleotide by pol β followed by strand ligation by DNA Ligase III (LIG3) (Barnes & Lindahl, 2004). Long-patch BER utilises pol β and also processive DNA polymerases δ and ε to synthesise 2 or more nucleotides (Figure 1). The resulting single strand flap is cleaved by flap endonuclease 1 (FEN1), and the nick is ligated by DNA ligase I (LIG1) in coordination with PCNA. Before ligation can occur, DNA end

processing is needed to create viable substrates for the DNA ligases. This is achieved by many of the BER factors already mentioned, which depending on the nature of the broken ends, requires pol β, aprataxin (APTX), PNKP, (Tyrosyl-DNA phosphodiesterase 1) TDP1 and APE1 (Figure 1) (Caldecott, 2008).

One thing to note is that in addition to AP sites generated by glycosylase, 10,000s of AP sites occur spontaneously due to the hydrolytic removal of DNA bases from the sugar-phosphate backbone. After DNA end-processing, these lesions are then repaired by BER pathways (Ciccia & Elledge, 2010; Fortini & Dogliotti, 2007).

1.2. Single strand break (SSB) repair

Single strand breaks occur when the sugar-phosphate backbone on one strand of DNA is broken. ROS, of which hydrogen peroxide (H2O2) is the most relevant physiological source can cause SSBs by oxidising and disintegrating sugars on DNA (Caldecott, 2008) (Figure 1).

SSBs are sensed by the DNA damage sensor poly(ADP-ribose) polymerase 1 (PARP1) (Figure 1). PARP1 has catalytic activity which generates chains of ADP-ribose sugar on itself, nearby proteins and DNA (Ray Chaudhuri & Nussenzweig, 2017). These poly(ADP-ribose) (PAR) chains act as the first signal for SSB lesion detection (Aleksandrov et al., 2018), promoting subsequent repair by recruiting the major SSB repair protein XRCC1 (Caldecott, 2019). XRCC1 acts as a molecular scaffold, coordinating and mediating several complexes with PNKP1, Pol β, LIG3 and others depending on the nature of the SSB (Figure 1). Antagonising PARP1 activity is the glycohydrolase, PARG, which restores PARP1 to its pre-activated state. This regulates recruitment of PAR-binding proteins and allows PARP1 to detect other SSBs (Figure 1) (Caldecott, 2008).

There is significant overlap between SSB repair and BER, as an universal intermediate in BER is the SSB formed after a nick is created in the single stranded DNA (ssDNA) of the abasic site (Caldecott, 2008; Krokan & Bjørås, 2013). Direct SSBs are repaired similarly but not identically to indirect SSBs formed during BER. For example XRCC1 is involved in both

and this is followed by the principles of DNA gap-filling and ligase activity (Figure 1). However different factors, not limited to, cell cycle, DNA replication fork proximity and repair protein expression levels affect which specific proteins are employed in SSB and BER repair (Bauer et al., 2015; Caldecott, 2008; Fortini & Dogliotti, 2007; Krokan & Bjørås, 2013).

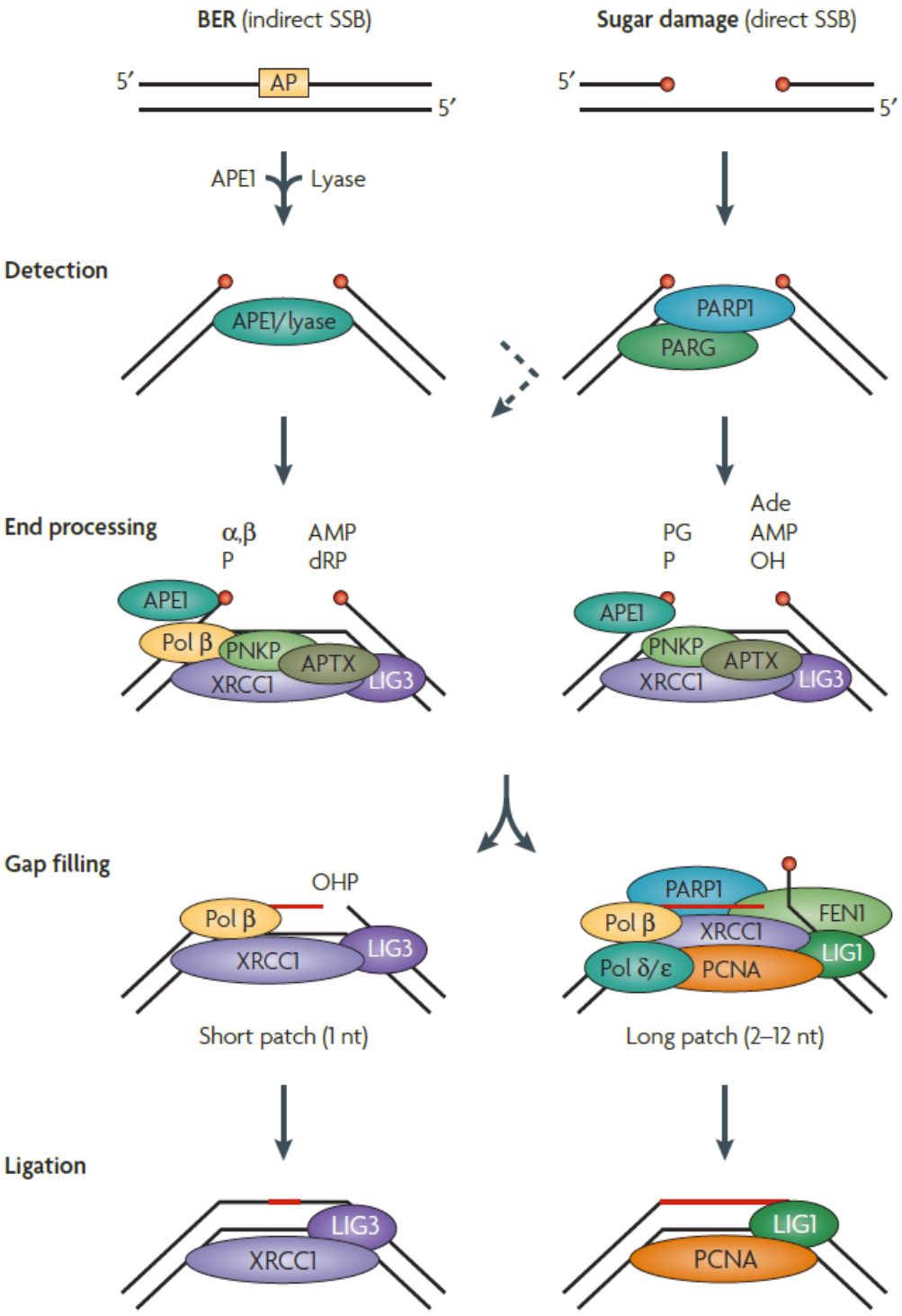


Figure 1. Model of overlapping BER and SSB repair

SSBs arise either directly or as an intermediate during BER repair. AP sites are processed during BER repair by APE1 to create an indirect SSB, whereas direct SSBs can be formed spontaneously. Both types of lesions require end-processing, coordinated by the central scaffold protein XRCC1. Depending on the nature of the DNA ends, PNKP, APTX, TDP1, pol β or APE1 can generate viable ends for ligation. The lesion can then undergo either short patch or long patch repair. With short patch relying on XRCC1-LIG3 whereas long patch utilises PCNA-LIG1 after FEN1 endonucleolytic cleavage of the displaced DNA strand. Image taken from (Caldecott, 2008).

1.3. Double strand break (DSB) repair

DSBs are the most cytotoxic lesion that can occur on the genome. A single DSB can cause cell death if it occurs on an essential gene (Rich et al., 2000). Repair mechanisms for DSBs require the tethering of the broken strands which are then processed before they are ligated back together. These mechanisms can, but not always, result in the loss of genetic information (Chatterjee & Walker, 2017).

The cytotoxicity of DSBs has been exploited to treat malignancies through the use of exogenous agents such as ionising radiation (IR) (Khanna & Jackson, 2001) and chemotherapies such as irinotecan (Kciuk et al., 2020). Endogenously, ROS can cause SSBs which when occurring on opposite strands and close in proximity, can spontaneously cause DSBs. Furthermore, when replication forks encounter SSBs, the helicase-mediated unwinding of duplex DNA can lead to a DSB on either the leading or lagging strand, this is named "replication fork runoff" (Berti & Vindigni, 2016; Kuzminov, 1999).

There are two main mechanisms of DSB repair, homologous recombination (HR) and non-homologous end joining (NHEJ), along with distinct secondary pathways such as alternative-NHEJ (a-NHEJ) and single strand annealing (SSA) (Figure 2, 3). The pathway which a DSB is repaired by is heavily reliant on the cell cycle stage as HR requires the presence of an identical copy of the chromosome. It is only active on post-replicative parts of the genome (Khanna & Jackson, 2001). In interphase, cells are reliant on NHEJ, which is more error-prone than HR.

Once a DSB forms, the broken ends can be bound by either PARP1 or the Ku70/80 complex. This recruitment occurs with equally fast kinetics (Aleksandrov et al., 2018; G. Yang et al., 2018). Interestingly in G1, Ku70/80 occupies all of the DSB sites, whereas in S/G2 phase, the amount of PARP1 recruited to DSB increased (G. Yang et al., 2018). The binding of Ku70/80 guides the repair pathway towards NHEJ (Fell & Schild-Poulter, 2012) whereas PARP1 has been shown to recruit the MRN (MRE11, RAD50, NBS1) complex which favours

HR (Haince et al., 2008), additional components which influence DSB repair pathway choice are discussed below.

1.3.1. Homologous recombination (HR)

HR is reliant on DNA end resection to create 3'-hydroxyl overhangs which can anneal to homologous regions on sister chromatids (Figure 2). This begins by the action of the MRN complex, this complex binds near the broken ends of DNA (Figure 2) (Jackson & Bartek, 2009). The nuclease MRE11, activated by CtIP (Anand et al., 2016), first creates a nick on the 5' strand using its endonuclease activity, then it uses its 3' to 5' exonuclease activity and creates a 3' single-stranded DNA (ssDNA) overhang (Figure 2). This activity allows more long-range resection to occur, carried out by nucleases, EXO1 or BLM-DNA2 (Gravel et al., 2008; Mimitou & Symington, 2008; Z. Zhu et al., 2008). The generation of the ssDNA 3' overhangs initially leads to the recruitment of RPA, which acts to protect ssDNA from further nuclease activity and unwanted secondary structures (Wold, 1997). RPA is then replaced by the recombinase RAD51, whose binding to DNA is dependent on it binding to ATP (Baumann et al., 1996). This binding of ssDNA and RAD51 produces the nucleoprotein filament. As RPA binds ssDNA with a higher affinity, the RAD51 binding process requires activity from Rad52 in yeast (Benson et al., 1998) and BRCA2 in humans (Jensen et al., 2010).

During this process, ubiquitin signalling (discussed later) recruits RAP80, which in turn recruits BRCA1-BARD1 to the DSB site (H. Kim et al., 2007). BRCA1 has many roles promoting HR including increasing RAD51 recombinase activity (W. Zhao et al., 2017). It has multiple mechanistic functions as it forms several complexes with PALB2, RAD51, BRCA2 and other HR factors, which are functionally distinct (Figure 2) (Savage & Harkin, 2015).

The nucleoprotein filament then undergoes a process termed homology-search on the sister chromatid. This is promoted by the dsDNA translocase RAD54 (Petukhova et al., 1998). This creates a D-loop structure where RAD54 then uses its ATPase activity to remove RAD51 from the nucleoprotein filament (Solinger et al., 2002). From this, synthesis of DNA using the

sister chromatid as a template then leads to synthesis-dependent strand annealing, creating a final product with no crossover event (Figure 2).

The D-loop can also become a platform for which the opposite end of the DSB anneals to, its 3' overhang is able to bind to the displaced ssDNA of the D-loop (Figure 2). This is catalysed by Rad52 in yeast (Nimonkar et al., 2009), creating a stabilised D-loop structure where DNA synthesis by either polymerases δ (Li et al., 2009) or ε (Hicks et al., 2010) can occur followed by eventual ligation and possible crossover. These events can then result in loss of heterozygosity by gene conversion as one template is used for both maternal and paternal chromosomes (Bishop & Schiestl, 2000).

1.3.2. NHEJ

The binding of Ku70/80 channels DSB repair towards NHEJ by protecting ends against resection (Mimitou & Symington, 2010). Its major role is in the recruitment of core NHEJ factors, DNA-PKcs (Uematsu et al., 2007), XRCC4 (Mari et al., 2006) and XLF (Yano et al., 2008) (Figure 2). The general steps of NHEJ includes firstly the processing of DNA ends of the DSB, this is achieved in concert by the main nuclease Artemis and DNA-PKcs kinase activity. Artemis has 5' exonuclease, 5 and 3' endonuclease activity. In addition to Artemis, polymerases λ, μ and terminal deoxynucleotidyl transferase (TdT) synthesises DNA to prepare it for ligation (Davis & Chen, 2013; Scully et al., 2019). The ends are then ligated by XRCC4-LIG4, a process promoted by XLF and paralog of XRCC4 (PAXX), which both have similar structure to XRCC4 (Chang et al., 2017). This process is thought to be iterative whereby the single DNA strand ligation by XRCC4-LIG4 is reversible until a final satisfactory configuration can be found (B. Zhao et al., 2020) and both strands are covalently bonded. As a result of NHEJ, often, but not always, the processing of DNA ends by nuclease activity leads to the loss of genetic information.

1.3.3. Alternative DSB repair pathways

When canonical NHEJ or HR is not an option due to deficiency in NHEJ or HR factors such as Ku70/80 and BRCA1, a-NHEJ can use micro-homology of up to 20bp between resected DNA strands to anneal DSBs (Figure 3) (B. Zhao et al., 2020). a-NHEJ occurs independently of LIG4 and is more error-prone than canonical NHEJ. In the absence of Ku70/80, PARP1 binds to DSBs recruiting MRE11. MRE11-mediated resection of DNA promotes a-NHEJ by revealing microhomologies (Audebert et al., 2004; Xie et al., 2009). PARP1's ADP-ribosylation (PARylation) activity also recruits polymerase θ (Ceccaldi et al., 2015; Mateos-Gomez et al., 2015), the central component in a-NHEJ, which searches for microhomology and performs gap-filling before ligation by LIG3 (Simsek et al., 2011).

Similarly to a-NHEJ, SSA uses homologous repeat sequences near the ends of the DSB to cause erroneous annealing and deleterious repair (Figure 3). SSA is an alternative DSB repair pathway that requires more extensive strand annealing than a-NHEJ (Bhargava et al., 2016). When a DSB occurs in between homologous repeats and resection generates 3' ssDNA exposing the homologous repeats, complementary annealing occurs. The strands are then processed leading to a loss of the genetic material in between the repeats (Figure 2). It is distinct from a-NHEJ in its need for longer homologous sequences rather than microhomologies and does not require pol θ or PARP1 activity.

SSA is dependent on CtIP, a factor which promotes the resection necessary for exposing the homologous repeats for annealing (Muñoz et al., 2012). Factors which inhibit end-resection such as 53BP1 and RNF168 are also inhibitory to the occurrence of SSA (Bothmer et al., 2010; B. R. Chen et al., 2021). After the homologous repeats have annealed, RAD52 and ERCC1 work together to remove the overhang tails which represent the sequences in between the two homologous repeats (Figure 3) (Gottifredi & Wiesmüller, 2020; Rothenberg et al., 2008). After this, DNA polymerases fill in the remaining gap and DNA ligation occurs. One key distinction between HR and SSA, is the requirement for RAD51, SSA is RAD51 independent and no homology search occurs however SSA requires RAD52.

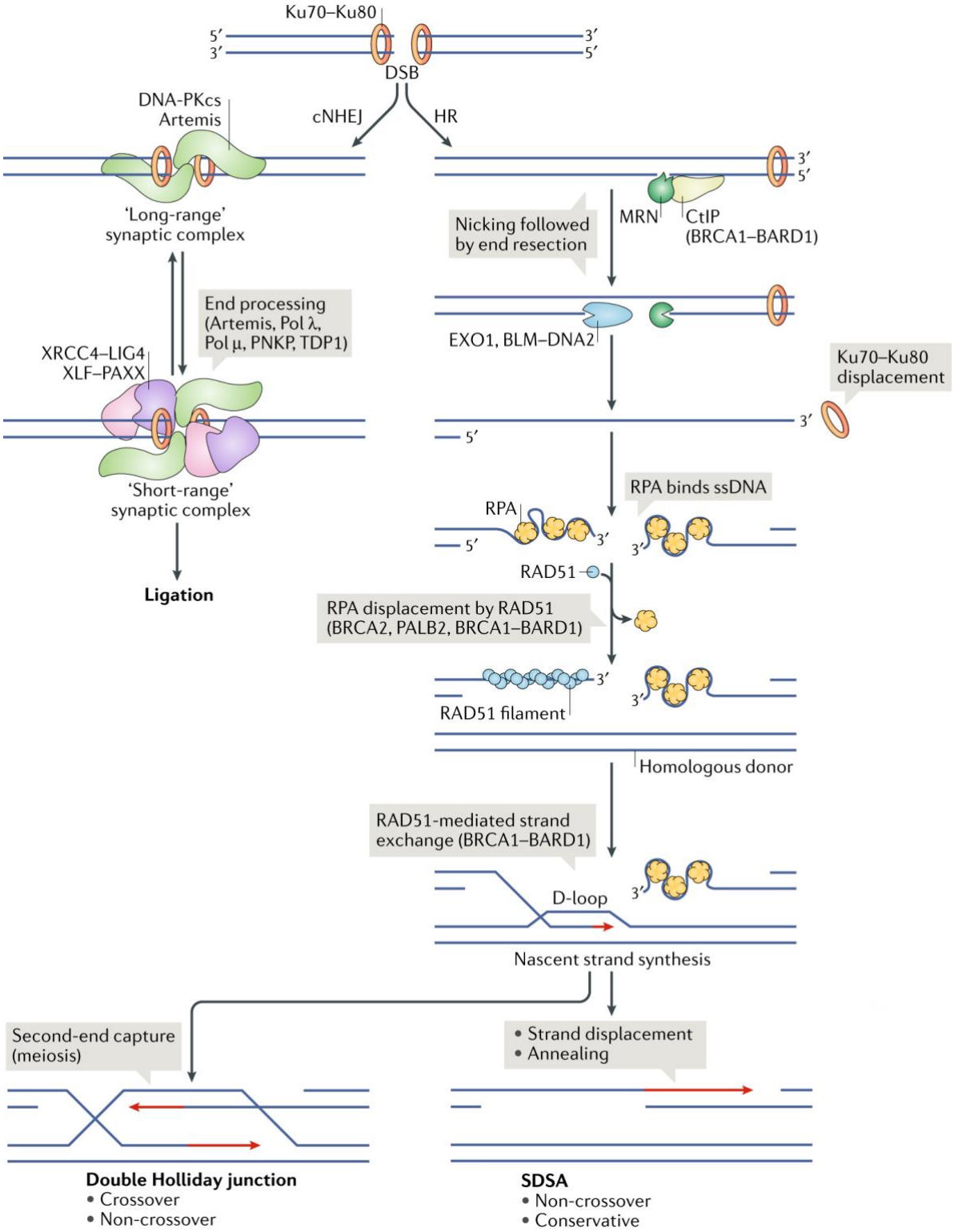


Figure 2. DSB repair by HR and NHEJ

DSB ends are bound by Ku70/80 which promotes NHEJ by recruiting NHEJ factors such as DNA-PKcs. As the main NHEJ regulator, DNA-PKCs coordinates end processing by Artemis and other factors such as TDP1, PNKP, pol λ and pol μ. DSB end ligation during NHEJ is carried out by XRCC4-LIG4 which can be promoted by XLF and PAXX. During S-phase, Ku70/80 is displaced by MRN complex-mediated 3' to 5' resection to begin HR. This allows more extensive end resection by EXO1 and BLM-DNA2 exonucleases. Exposed ssDNA is bound by RPA then by RAD51, which along with BRCA1/2 and PALB2 promotes homology directed repair of DSBs. Image taken from (Scully et al., 2019).

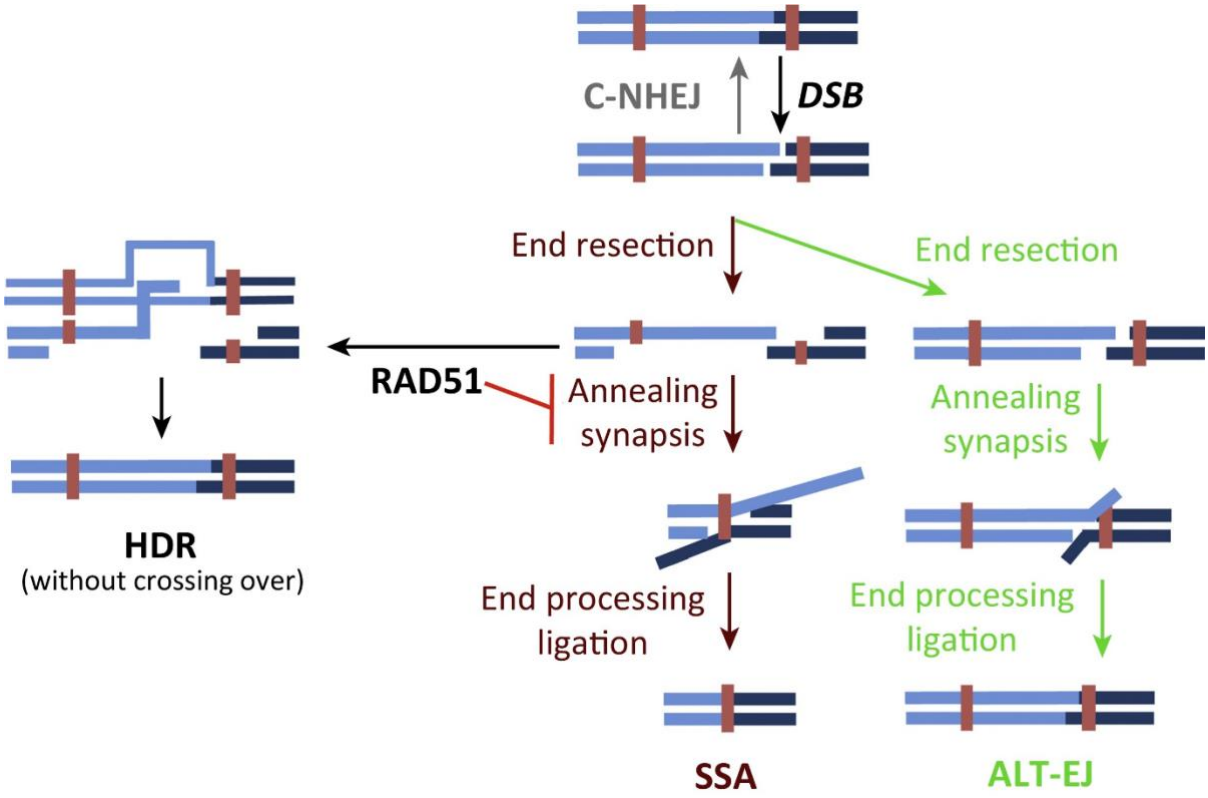


Figure 3. Alternative DSB repair mechanisms

End resection during DSB repair can lead to SSA (red) when extensive resection occurs revealing repeat sequences of homology (red blocks). These homologous repeat sequences anneal erroneously from different parts of the genome. SSA leads to the loss of all genetic material in between the two repeat sequences. Prior to this, RAD51 can antagonise SSA by binding resected DNA, channelling the repair towards HR. In contrast a-NHEJ (green) does not require extensive resection but instead occurs at sequences of microhomology. Pol θ plays a central role in a-NHEJ where it searches for microhomology, trims non-homologous tails and synthesises DNA to allow DSB end joining. Image taken from (Bhargava et al., 2016).

1.4. Regulation of DSB repair

Throughout DSB repair, post-translational modifications (PTMs) regulate the DDR response in both HR and NHEJ. Protein phosphorylation by the apical phosphoinositide 3-kinase related kinases (PIKKs), ATM, ATR and DNA-PKcs play a critical role in this. They are recruited to DSBs by NBS1 (of the MRN complex), ATRIP and Ku80 respectively (Blackford & Jackson, 2017). In NHEJ, DNA-PKc-mediated auto-phosphorylation is thought to allow DNA-end alignment (Graham et al., 2016) and also recruit core NHEJ factors such as the nuclease Artemis (Malu et al., 2012). Whereas ATR is thought to be the apical kinase in response to replication stress, ATM is the apical kinase for DSB repair. ATM possesses autophosphorylation activity (Kozlov et al., 2011) and activates other DSB repair pathway kinases such as CHK2 (Matsuoka et al., 1998). In response to DSBs, ATM and other kinases target several proteins including MDC1 and the histone variant H2AX (Goldberg et al., 2003; Rogakou et al., 1998). Phosphorylation on H2AX is commonly named γ-H2AX and is used as a universal marker for DNA damage.

These described phosphorylation sites then form a platform on which other PTMs such as ubiquitin, SUMO, NEDD8 regulate DSB repair and repair pathway choice (Schwertman et al., 2016).

1.4.1. Ubiquitin/SUMO regulation of DSB repair

Ubiquitin and ubiquitin-like modifiers (UBLs) are involved in nearly all cellular processes, the dynamic nature by which they can be attached and removed make them ideal for regulatory purposes (Damgaard, 2021; Oh et al., 2018). The 76 amino-acid protein ubiquitin and its associated proteins are expressed in all eukaryotes. This PTM consists of an isopeptide bond between the carboxy terminus of ubiquitin to lysine residues found on its target substrates. Further regulatory capacity is afforded by the formation of different chains of ubiquitin which can occur on a range of lysines found on ubiquitin itself, including but not limited to K6, K33, K48 and K63 (Oh et al., 2018). These can then be bound by different

ubiquitin binding domains with different functions, for example K48 chains are associated with protein degradation.

Ubiquitin and UBLs such as SUMO and NEDD8 are all attached onto substrates in a cascade involving three enzymatic steps, first an E1 ubiquitin-activating enzyme, second an E2 ubiquitin-conjugating enzyme and then a final E3 ubiquitin ligase. In the human genome, there are two E1 enzymes, around 30 E2 enzymes and 600-1000 E3 enzymes (Kliza & Husnjak, 2020). Furthermore, ubiquitin can be rapidly removed from its substrate through the action of deubiquitinases (DUBs), of which there are around 100 (Reyes-Turcu et al., 2009). One of the primary effects of ubiquitin modification is the shuttling of substrate proteins for controlled protein degradation by the proteasome (Damgaard, 2021; Deshaies, 2014).

In DSB repair, the E3 ubiquitin ligase RNF8 is recruited to DSB sites by binding to ATM phosphorylation sites on MDC1 (Figure 4) (Huen et al., 2007; Kolas et al., 2007; Mailand et al., 2007). RNF8 decorates H1 linker histones with the K63 ubiquitin chain linkage with the E2 enzyme UBC13 as part of its enzymatic cascade (Thorslund et al., 2015). The K63 signal recruits RNF168 which itself ubiquitylates H2A (Panier et al., 2012). This recruits key repair factors BRCA1 and 53BP1 to break sites (Figure 4), from which pathway choice of either HR through BRCA1 or NHEJ through 53BP1 is decided.

53BP1 and BRCA1 play antagonistic roles in pathway choice, made most evident by the finding that 53BP1 deletion rescues viability in HR-deficient BRCA1- mutated mice (Cao et al., 2009). The molecular details of this antagonism involves the protein RIF1 and the Shieldin complex which are recruited to 53BP1 (Dev et al., 2018a; Gupta et al., 2018; Noordermeer et al., 2018; Schwertman et al., 2016). The recruitment of Shieldin channels DSB repair towards NHEJ by either physically preventing DSB end-resection or promoting CTC1-STN1-TEN1 (CST) complex recruitment leading to gap-filling of resected DNA (Mirman et al., 2018; Setiaputra & Durocher, 2019).

In addition to E3 ubiquitin ligases, the SUMO E3 ligases PIAS1 and PIAS4 are found to be active at DSB sites and target proteins such as MDC1, 53BP1, BRCA1 and RNF168 (Schwertman et al., 2016). Although much of its downstream effects are unknown, it is thought to promote protein-protein interaction and regulate enzyme activity. For example, PIAS1/4 are needed for efficient ligase activity of BRCA1-BARD1 (Figure 5A) (Morris et al., 2009). SUMOylation pathways in DSB repair are interesting as they possess functional crosstalk with ubiquitin. SUMO-targeted ubiquitin ligases (STUbLs), of which two are known, RNF4 and RNF111, contain SIMs (SUMO interaction motifs) which allow binding to SUMO moieties and trigger their E3 ubiquitin ligase activity on these SUMOylated substrates (Prudden et al., 2007). This activity is best characterised by RNF4 and its role in conjugating K48 linked chains to remove MDC1 and RPA from DNA lesion sites (Figure 5B) (Luo et al., 2012; Yin et al., 2012). Once modified by ubiquitin, these substrates are then targeted for degradation by the ubiquitin-proteasome system.

In addition to proteasome-mediated degradation being a downstream result of ubiquitination, the AAA+ ATPAse p97 (aka valosin-containing protein or VCP) has also been heavily implicated in DSB repair (Torrecilla et al., 2017). At DSBs, it uses its ATPase activity to unfold substrates (Stach & Freemont, 2017), inhibition of this activity causes an accumulation of RNF8-mediated K48 linked ubiquitinated substrates at DSB sites (Meerang et al., 2011). Through its role in removing ubiquitinated substrates, p97 can influence the pathway choice of DSB repair by contributing to the recruitment of 53BP1. 53BP1 is recruited to DSBs by binding to mono/di-methylated H4-Lys-20 residues and ubiquitinated H2A-Lys-15 (Botuyan et al., 2006; Fradet-Turcotte et al., 2013). One of p97's substrates is L3MBTL1, which when removed, exposes H4-Lys-20me2 and allows the recruitment of 53BP1 to DSB sites, thus promoting NHEJ (Acs et al., 2011) (Figure 5C).

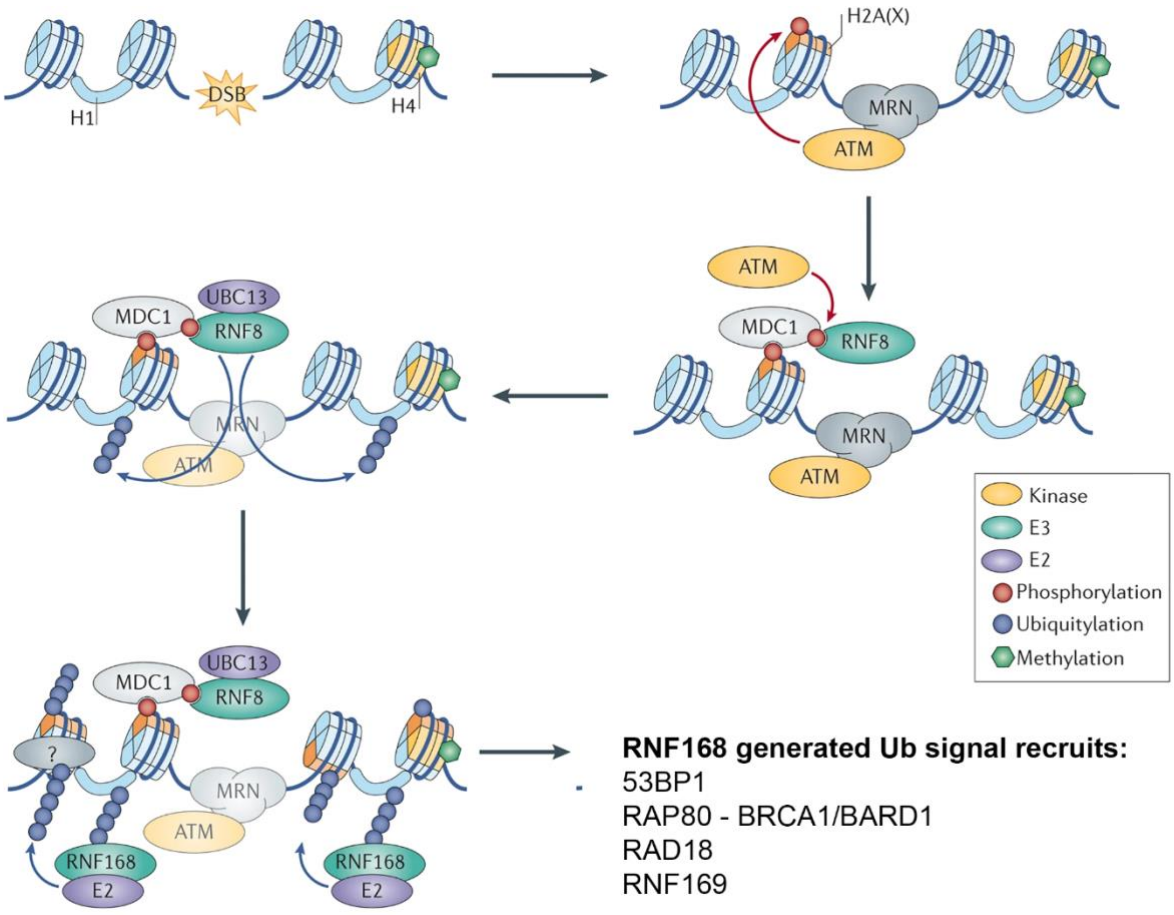


Figure 4. RNF8-RNF168 DSB ubiquitin signalling cascade

DSB triggers rapid recruitment of the MRN complex and ATM. ATM phosphorylates histone variant H2AX which recruits the DDR repair scaffold protein MDC1, which itself is phosphorylated by ATM. RNF8 is then recruited by phosphorylated MDC1. RNF8 then produces both K48 chains for targeted degradation of DDR proteins and K63 chains on histone H1. These chains recruit RNF168 which along with its E2 ubiquitin-conjugating enzyme UBC13, generates local Ub signals on histone H2A. This signal recruits proteins from both HR and NHEJ pathways including 53BP1, RAP80, RAD18, RNF169. Image taken from (Schwertman et al., 2016).

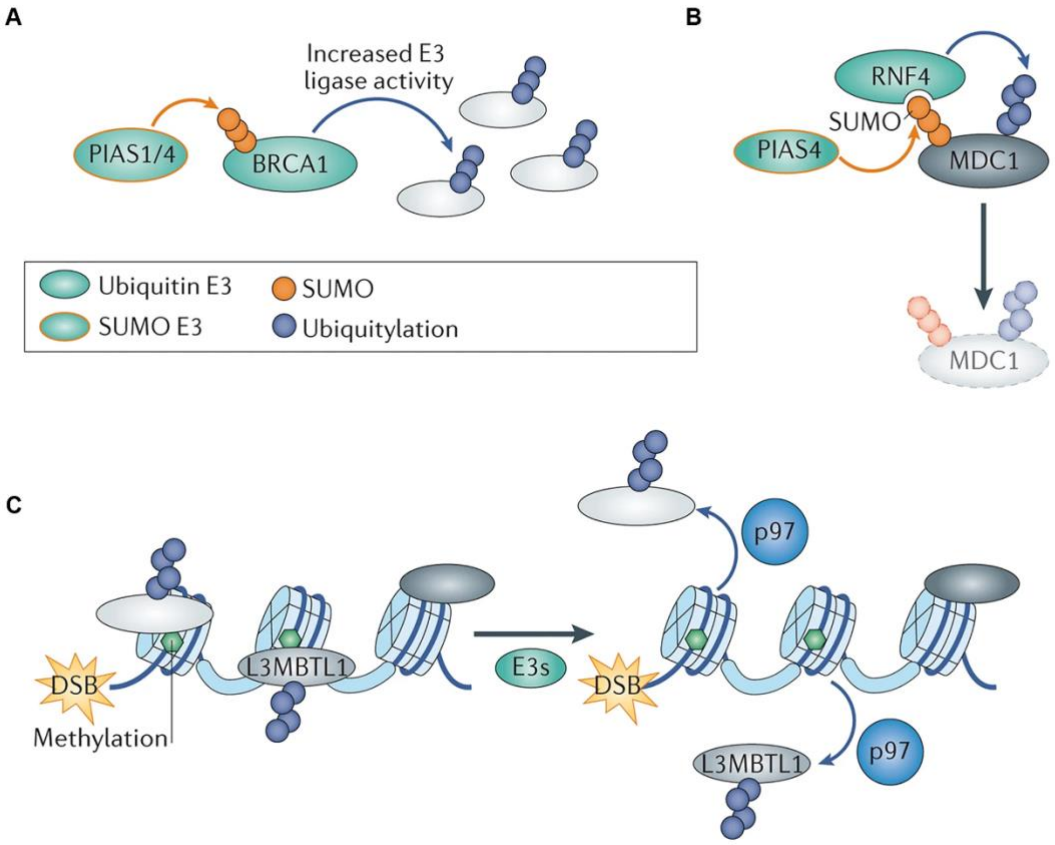


Figure 5. SUMO and p97 in DSB repair

(**A**) PIAS4 E3 SUMO ligase signalling can initiate targeted protein degradation at DSB sites. PIAS4 modifies MDC1 which in turn recruits the STUbL E3 ligase RNF4. RNF4 modifies MDC1 with K48 linked ubiquitin causing its proteasomal degradation. (**B**) PIAS1/4 SUMOylation can also promote enzymatic activity at DSB sites. It can increase the ubiquitin ligase activity of BRCA1 by modifying it directly with SUMO. (**C**) The ATPase p97 uses its unfoldase activity to remove targeted proteins from DSB sites for degradation. It is recruited by K48 ubiquitin chains and acts on multiple substrates at the lesion including Ku80, L3MBTL1 and KAP1. Removal of L3MBTL1 reveals the H4K20me2 histone modification which allows 53BP1 recruitment. Image taken from (Schwertman et al., 2016).

1.5. DNA protein crosslinks (DPCs)

DPCs are a type of DNA damage which is formed when proteins become covalently linked to DNA (Fielden et al., 2018; Stingele et al., 2017; Vaz et al., 2017). Whereas in BER, SSB repair and DSB repair, the deleterious lesion is based on DNA modifications, DPCs' main disruptive component is the peptide which is covalently linked onto DNA (Figure 6). This bulky adduct prevents the normal function of almost all genomic processes including transcription, DNA replication and chromatin remodelling. Induction of DPCs, like DSBs, have been widely used in traditional chemotherapeutics due to their cytotoxicity. Similar to DSBs, they are particularly more toxic to proliferative cells, thus enabling broad-targeting of malignancies.

The agency-approved chemotherapeutics which cause DPCs such as platinum salts, 5-aza-2'-deoxycytidine (5-aza-dC), camptothecin analogues and eotoposide analogues, do so by either creating specific or promiscuous DPCs (Figure 6) (Stingele et al., 2017). For example, 5-aza-dC becomes incorporated into the genome from where it then becomes a substrate for DNA methyl-transferase 1 (DNMT1). Processing this incorporated nucleotide analogue by DNMT1 causes its enzymatic cross-linking to the genome (Maslov et al., 2012). Camptothecin and etoposide act in a similar fashion by causing abortive topoisomerase-1 (TOP1) and topoisomerase-2 (TOP2) DPCs, TOP1ccs and TOP2ccs respectively (Sun, Saha, et al., 2020). PARP inhibitors, a targeted chemotherapy against HR deficient malignancies have also been shown to cause DPC-like lesions. These trapped PARP1 lesions lack a covalent linkage but are effectively DPCs as PARP1 is prevented from leaving chromatin once PARP1 binds to DNA lesions (Murai et al., 2012; Pommier & Murai, 2015; Stingele et al., 2017). Platinum salts such as cisplatin on the other hand, crosslink chromatin interacting proteins by forming non-specific covalent linkages between DNA and nearby proteins, with itself being the intermediate (Ming et al., 2017). For example, proteins such as histones, high mobility group (HMG) proteins and transcription elongation factors have all been identified as DPCs caused by cisplatin.

Alternatively, endogenous DPCs can form as a result of abortive complexes that occur during normal physiological function, such as when TOP1 carries out its enzymatic activity near DNA distortions (Pommier et al., 2014). Alternatively, *in* vitro experiments suggest a whole host of DPCs can form by the innate cross-linking properties of abasic sites on DNA, which can react with nearby chromatin associated proteins such as histones to form DPCs (Sczepanski et al., 2010). Furthermore, endogenous agents such as reactive aldehydes, especially formaldehyde which form during histone demethylation, can also effectively crosslink protein to DNA (Shi et al., 2004).

Recently and contrary to the acquired knowledge of DPCs so far, DPCs have been shown to have a protective role in cell survival. 5-hydroxymethylcytosine (5hmC) binding ESC-specific (HMCES) protein has been shown to form suicidal crosslinks with DNA by seeking out abasic sites during DNA replication (Halabelian et al., 2019; Mehta et al., 2020; Mohni et al., 2019). HMCES is evolutionarily-conserved in all domains of life and its bacterial orthologs also possess the same ability to sense and seek out abasic sites. By shielding these abasic sites at replication forks, HMCES is thought to prevent cytotoxic outcomes of chronic abasic sites. These include endonuclease-mediated formation of DSB breaks during replication, error-prone DNA replication and DPC formation (Halabelian et al., 2019; Mohni et al., 2019).

Like other types of DNA damage, there exist specialised pathways for DPC repair. A picture has begun to emerge of DPC repair pathways that are similar to DSB repair. Pathways that are differentially employed depending on the cellular context.

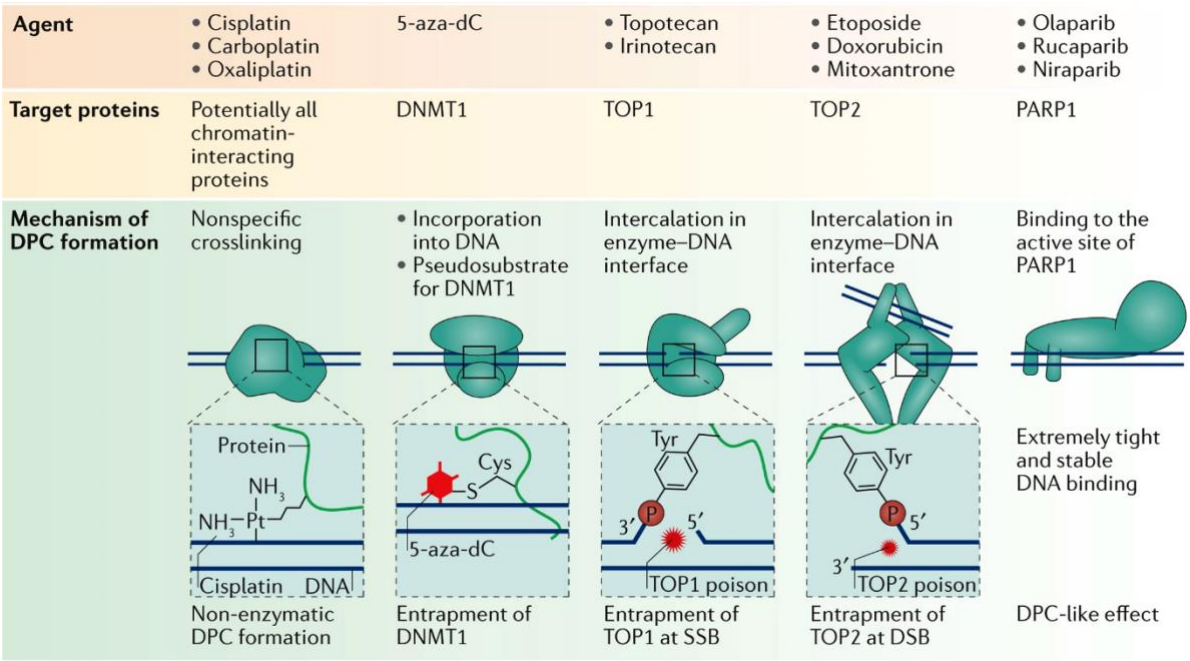


Figure 6. DPC summary

Table of approved DPC causing agents for chemotherapy. Cisplatin, carboplatins and oxaliplatins cause DPCs from potentially all chromatin interacting proteins. They do so by bridging the DNA and protein with a covalent bond. 5-aza-dC, topotecan, irinotecan, etoposide, doxorubicin and mitoxantrone cause enzymatic DPCs. These are dependent on enzymes which act on the chromatin, these agents cause covalent bonds to occur during the normal catalytic cycle of their target enzymes. Olaparib, rucaparib and niraparib trap PARP1 on chromatin in a non-covalent manner. PARP1 retention at sites of DNA damage by PARPis causes DPC-like effects. Image taken from (Stingele et al., 2017).

1.5.1. Replication/SPRTN dependent DPC repair

To repair DPCs and allow the resumption of chromatin processes, the protein component of the DPCs has to be removed. Often the covalent linkage between protein and DNA is hidden/shielded by the peptide component, thus this needs to be processed first (Figure 7) (Fielden et al., 2018; Ruggiano & Ramadan, 2021; Stingele et al., 2017; Vaz et al., 2017).

Work has identified a novel essential metalloprotease SprT-Like N-terminal domain (SPRTN) which carries out this function on a range of substrates in human cells (Stingele et al., 2016; Vaz et al., 2016). This protease is present in all metazoans and knockout of SPRTN causes embryonic lethality in mice (Maskey et al., 2014). Mutations in SPRTN causes the autosomal recessive progeroid disease Ruijs-Aalfs syndrome, which is characterised by early onset hepatocellular carcinoma and genomic instability (Lessel et al., 2014). SPRTN contains both SUMO (SIMs) and ubiquitin-interacting domains (UBZ), along with a PIP box (PCNA interacting domain) and a SHP box (p97 interacting domain). Its function allows the progression of DNA replication forks after they encounter a DPC (Figure 7) (Vaz et al., 2016). To achieve this, it is recruited to stalled replication forks where it then proteolytically cleaves the bulky adduct to allow continuation of the fork (Stingele et al., 2016; Vaz et al., 2017).

The best characterised substrate of SPRTN based DPC repair is of TOP1ccs. In addition to SPRTN, TOP1ccs have a dedicated enzyme for its removal, tyrosyl-DNA phosphodiesterase-1 (TDP1) (Das et al., 2014; S. W. Yang et al., 1996). TDP1 hydrolyses the phosphodiester bond between TOP1 peptide and DNA formed during abortive TOP1 activity. However, it was found that SPRTN and its yeast ortholog Wss1 both also play roles in TOP1cc repair, upstream of TDP1 (Balakirev et al., 2015; Fielden et al., 2020). In humans, SPRTN forms a complex with p97 and the p97 adaptor TEX264. It then functions after p97-mediated unfolding of TOP1ccs where it proteolytically cleaves the peptide in a replication-dependent manner (Fielden et al., 2020). This reduced peptide fragment is then excised by the dedicated activity of TDP1. This process was shown to be regulated by TOP1 SUMOylation.

SPRTN is a promiscuous protease with a large active site, proposed to allow indiscriminate cleavage of proteins presented to it (Ruggiano & Ramadan, 2021; Stingele et al., 2016). Thus its recruitment and activation have been shown to be tightly regulated to prevent deleterious proteolytic activity at the replication fork. Activation of SPRTN is contingent on the presence of DNA and the removal of an internal mono-ubiquitin switch (Stingele et al., 2016; S. Zhao et al., 2021). It was shown that SPRTN is particularly activated by ss/dsDNA hybrid binding (Reinking et al., 2020). This suggests that at the replication fork, when active DNA polymerases come into close proximity to DPCs on ssDNA, SPRTN is activated by the half-replicated DNA structure.

SPRTN resides in a repressed state when SPRTN is mono-ubiquitinated, it is degraded either via polyubiquitination and proteasome-mediated degradation, or by promoting *trans* DNA-dependent autocleavage of SPRTN (Figure 7B) (S. Zhao et al., 2021). In the presence of DPCs, the DUB USP7 deubiquitinates SPRTN, activating its proteolytic cleavage activity. Whether SPRTN substrates require SUMO/ubiquitination modification for it to act or whether it does so purely through DNA structures is still uncertain (Larsen et al., 2019; Ruggiano et al., 2021).

Furthermore, its initial recruitment to its substrates is also tightly controlled, for example in the context of TOP1ccs, it is recruited by forming a complex with p97 and TEX264, the latter which, binds specifically to TOP1 (Fielden et al., 2020).

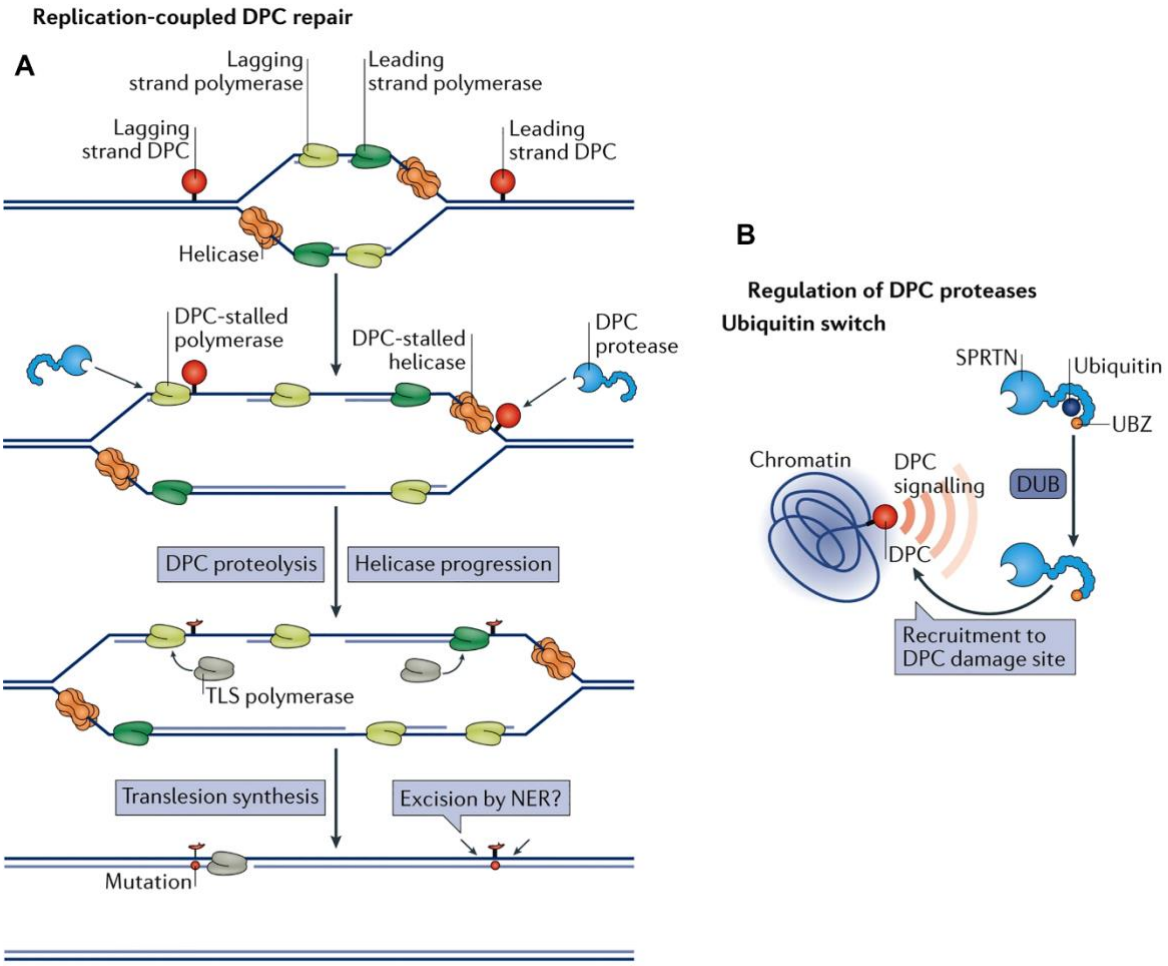


Figure 7. Replication coupled SPRTN DPC repair

(**A**) Schematic of SPRTN-mediated DPC repair at the replication fork. SPRTN acts at replication forks to remove DPCs using its proteolytic activity. By removing the peptide component of DPCs, SPRTN allows replication forks to bypass the remnants of the DPCs and restart fork progression. (**B**) SPRTN is regulated by an internal ubiquitin switch. Mono-ubiquitination of SPRTN causes binding by its own UBZ domain and inactivation of its catalytic activity. Image taken from (Stingele et al., 2017).

1.5.2. Proteasome-mediated DPC repair

Before the discovery of SPRTN and its replication-dependent repair of DPCs, it was assumed that the 26S proteasome, which acts on ubiquitinated substrates, was the main pathway for DPC repair together with nucleotide excision repair for DPCs smaller that 14 kDa. Using *Xenopus laevi* cell-free extract systems and mammalian cells, we now know for certain that DPCs are modified by SUMO and ubiquitin independently of DNA replication (Liu et al., 2021; Sun, Jenkins, et al., 2020). Furthermore, this signalling pathway is suggested to function independently to SPRTN-mediated degradation, instead directing DPCs towards proteasomal-mediated degradation.

The proteasome acts specifically on ubiquitylated substrates, and it requires ubiquitin E3 ligases to mark its substrates. Although there is some evidence to show that the E3 ubiquitin ligase TRAIP is partially responsible for DPC ubiquitination (Larsen et al., 2019), there is now a growing body of evidence that suggests the SUMO/STUbL-PIAS4/RNF4 -mediated ubiquitination pathway is crucial for signalling leading to proteasome dependent repair (Borgermann et al., 2019; Liu et al., 2021; Sun et al., 2019). This has now been shown for DNMT1 DPCs, TOP1ccs and the synthetic DPC HpaII. These recent works also showed that DPC SUMOylation and ubiquitination by the SUMO/STUbL-PIAS4/RNF4 pathway occurs in the absence of DNA replication and also neither inhibits nor stimulates SPRTN-dependent DPC repair (which is replication-dependent) (Liu et al., 2021).

It is worthy of note however that there is interplay between the SPRTN-dependent DPC repair pathway and SUMOylation/ubiquitination but it is independent of PIAS4/RNF4. It is known that SUMOylated DPCs accumulate in SPRTN-deficient cells after DPC induction and that SPRTN's ubiquitin-binding UBZ domain is essential for localisation to lesion sites (Ruggiano et al., 2021). The components of this separate SUMOylation/ubiquitination-mediated regulation of SPRTN are yet to be identified, but it is clear that SUMOylation and ubiquitination have central signalling roles in DPC repair.

How exactly DPCs are detected for SUMOylation is unknown. However we do know that SUMOylation of DPCs leads to recruitment of the STUbL, RNF4, which carries out the ubiquitin ligation reaction onto the SUMOylated substrate. In the case of TOP1ccs, RNF4 KO was epistatic to proteasomal inhibition suggesting they function in the same pathway (Sun, Jenkins, et al., 2020). However, all these studies show that proteasome was only partially responsible for the removal of ubiquitylated DPCs, suggesting alternative pathways may remove these adducts in the absence of proteasome activity.

Interestingly, it was found that DPCs do not elicit a classical DNA damage checkpoint response. However during mitosis, these unresolved DPCs cause abnormal chromosomal segregation and abnormal nuclei (Liu et al., 2021).

These findings suggest that the SUMO-STUbL DPC repair pathway can function independently outside of DNA replication/S-phase to ensure cell survival, whereas SPRTN-mediated degradation is solely active during DNA replication. This is similar to DSB repair where NHEJ is active outside of S-phase whereas HR occurs in S and G2-phases of the cell cycle.

1.6. p97

One protein which has been found to function in both SPRTN- and proteasome-dependent DPC repair pathways is the AAA+ ATPase p97 (or VCP – valosin containing protein) (Fielden et al., 2020; van den Boom & Meyer, 2018). p97 is an unfoldase/segregase, it consists of: an N-terminal domain, where the majority of its cofactors and binding partners interact; and a D1 and D2 domain, where its catalytic activity is generated (Figure 8A) (Ye et al., 2017). p97 forms a hexameric barrel-like structure where a central pore is formed. p97 is targeted to ubiquitinated and SUMOylated substrates by its cofactors. It then uses energy from ATP hydrolysis to pull the substrate through its central pore, unfolding it and extracting it from various macromolecules and cellular locations, including the chromatin environment (Figure 8B, C) (Blythe et al., 2017; Bodnar & Rapoport, 2017a; Køhler et al., 2015; Weith et al., 2018).

In addition to DDR, p97 helps to maintain protein homeostasis (proteostasis) through a number of different pathways. It was originally found to be part of protein quality control at the endoplasmic reticulum (ER), where it provides the driving force behind the process of removing misfolded proteins of the secretory pathway (van den Boom & Meyer, 2018; Ye et al., 2001). In mammalian ER-associated degradation (ERAD), ubiquitin ligases such as Hrd1, ubiquitinate substrates at the ER-membrane, these proteins are then unfolded through the central pore of p97. This enables substrate delivery to the proteasome where it is degraded.

p97 works with a range of cofactors which possess the SUMO- and ubiquitin-binding motifs needed to target it to its substrates, as p97 itself lacks innate SUMO/ubiquitin binding ability. Two “core” cofactors are thought to be necessary for normal function, UFD1-NPL4, which form a heterodimeric complex (Stach & Freemont, 2017). This heterodimer is required for binding to ERAD substrates (Ye et al., 2003). Through its cofactors, p97 is able to interact with specifically linked ubiquitin chains, allowing an additional level of regulation. The main chain linkage for p97-mediated degradation is the K48 linked ubiquitin chain (Stach & Freemont, 2017).

As has been described above, there have been newfound roles of p97 in the nucleus. The first identification of this was the removal of Aurora B kinase from the chromatin by p97 (Ramadan et al., 2007). A well-studied p97 substrate is the helicase MCM2-7, which form part of the CMG complex responsible for unwinding duplex DNA for DNA replication (Maric et al., 2014). p97 acts at the termination of replication and removes MCM2-7. It does so by segregating ubiquitinated MCM7 from the chromatin, a target of either the E3 ubiquitin ligase $CRL2^{LRR1}$ during S-Phase or TRAIP during mitosis (Dewar et al., 2017; Villa et al., 2021). This then allows recruitment of the p97-NPL4-UFD1 complex which carries out the removal of MCM7 (Figure 8B).

p97 has further been implicated in regulating ubiquitin signalling and ubiquitinated substrates during DNA damage (Torrecilla et al., 2017). As mentioned above, it can act to remove L3MBTL1 which affects DSB pathway choice (Acs et al., 2011). It also functions along with the E3 ligase RNF8 to remove substrates conjugated with the K48-ubiquitin chain linkage specifically at DSB sites, of which L3MBTL1 is one of them (Meerang et al., 2011; Singh et al., 2019). Antagonistic to this, the DUB, Ataxin-3, was found to form a complex with p97 and also acts to promote DSB repair (Singh et al., 2019). It does so by regulating the levels of K48 chains and the levels of RNF8 at DSB sites. Upstream of this, p97 also regulates the amount of MRE11 and Ku80 (Figure 8C) at DSB sites, thus having an influence on the amount of resection which occurs (Kilgas et al., 2021).

In addition to DSB repair, p97 also plays a role in NER, which is the primary repair pathway for UV-induced lesions. p97 acts on the lesion sensors DDB2 and XPC by removing them from DNA damage sites, it does so in concert with its cofactors NPL4-UFD1 and UBXD7 (Kusakabe et al., 2019).

Whereas the above describe p97 as a component of DNA repair signalling, it can also be a direct repair protein. It aides in the repair of DPCs (TOP1ccs) by unfolding the peptide component to allow its proteolytic degradation at the chromatin by SPRTN (Fielden et al., 2020). SPRTN which possesses its own SHP domain, can bind to p97 to form a complex

(Mosbech et al., 2012). Although SPRTN is a promiscuous protease, it is more efficient at cleaving disordered regions such as histone tails and also SPRTN *trans*-cleavage occurs at the disordered SPRTN c-terminus (Vaz et al., 2016, 2017). Therefore a possible mode of p97 cooperation with SPRTN for efficient DPC repair could be in the unfolding and presenting of substrates to SPRTN, as is suggested for TOP1ccs.

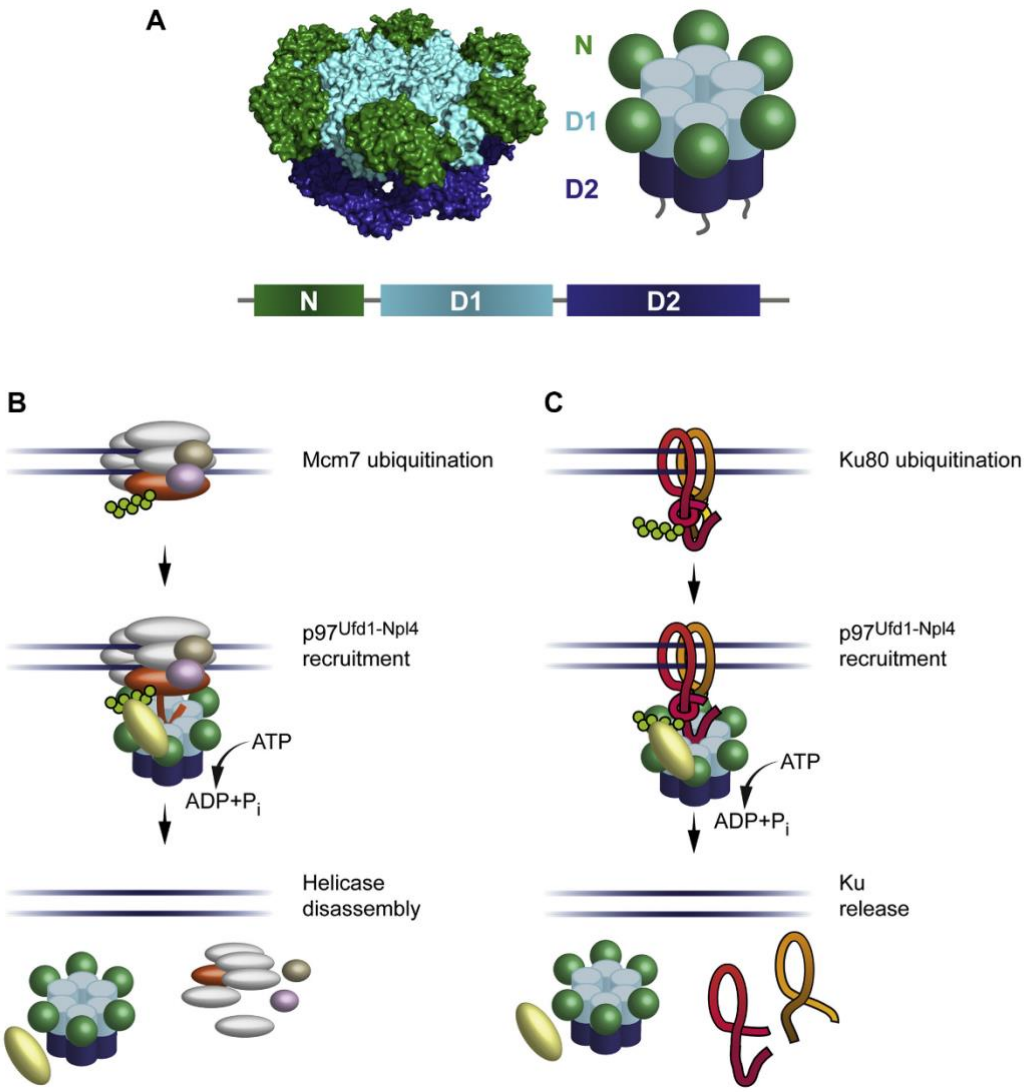


Figure 8. p97 unfolds proteins through its central pore

(**A**) Structure of p97 complex showing its hexameric structure containing its 3 functional domains. Its D1 and D2 domains each contain their own ATPase activity while the N-domain is responsible for the majority of p97 cofactor binding. These together make a central pore, through which it is thought p97 mechanically pulls substrates through. (**B**) p97 unfolds MCM7 and disassembles replicative helicases. MCM7 is ubiquitinated by $CRL2^{LRR1}$, this recruits p97 through ubiquitin binding by its heterodimeric cofactors UFD1-NPL4. p97 then uses ATP to unfold MCM7, causing the disassembly of CMG helicase at replication termination. (**C**) p97 removes Ku80 from DNA damage sites. Ku80 ubiquitination recruits p97-UFD1-NPL4 complex. Similarly to MCM7 removal, p97 uses its ATPase activity to unfold and release Ku80 from chromatin. Image taken from (van den Boom & Meyer, 2018).

1.6.1. p97 in cancer

Cancers thrive off a state of unregulated proliferation (Hanahan & Weinberg, 2011). It achieves such a state through oncogenic mutations which among other cellular stresses, causes loss of protein homeostasis (Vekaria et al., 2016). The unregulated transcription and production of proteins which are required for upregulated proliferation is mirrored by the upregulation of protein folders and chaperones (Nam & Jeon, 2019). p97 is also overexpressed to degrade misfolded proteins, its higher mRNA expression has been identified in 17 different cancers so far (Costantini et al., 2021). p97 expression positively correlated with greater invasion depth, higher tumour stage, higher recurrence rate, lower disease-free survival, shorter disease-free state, greater tumour size and more pro-oncogenic markers.

So far, no p97 interactions with DNA damage have been identified as a reason for its upregulation in malignancies. Instead, its functions in ERAD, mitochondria-associated degradation and ribosome-associated degradation have been proposed to be relevant in cancers (Costantini et al., 2021; Huryn et al., 2019). By aiding in the degradation of misfolded proteins which are the products of unregulated translation in transformed cells, it maintains a somewhat healthy protein machinery to allow cancer cell proliferation. This is achieved primarily through ERAD. One third of all proteins are translocated through and folded at the ER and represents the main source of misfolded proteins which are targets for p97 (Wang & Kaufman, 2016).

Indeed, drugs such as bortezomib, carfilzomib and ixazomib which target the proteasome have been approved for the treatment of multiple myeloma (X. Chen et al., 2021). Cytotoxicity to these drugs in cancer cells derives from stabilisation of tumour suppressors and induction of the unfolded protein response (UPR) (Obeng et al., 2006). This response occurs due to proteotoxic stress at the ER and can trigger apoptosis. This broadly targets cancer cells which are already under a high burden of proteotoxic stress and whose survival acutely depends on proteasomal degradation of misfolded proteins.

In 2015, a first-generation p97 inhibitor was created. CB-5083 triggered proteotoxic stress as poly-ubiquitinated substrates accumulated, causing the UPR followed by apoptosis (Anderson et al., 2015). Unfortunately, Phase I clinical trials were halted due to CB508's off-target inhibition on phosphodiesterase-6 (PDE6). This was hypothesised to be the cause of the adverse effects on patients which included photophobia and dyschromatopsia, as PDE6 is involved in signal transduction in photoreceptors (Leinonen et al., 2021). Promisingly in 2020, clinical trials for the second generation p97 inhibitor CB-5339 were started. This inhibitor showed 15 fold less activity against PDE6 and caused increased survival in patient-derived xenograft models of acute myeloid leukaemia (Roux et al., 2021).

The anti-alcohol abuse drug disulfiram also has p97-inhibitory properties. Originally found to have potent anti-cancer capabilities against BRCA1/2-deficient cells, an effect which was derived from the toxicity caused by acetaldehyde accumulation (Tacconi et al., 2017). A metabolite of disulfiram, CuET, a copper compound, was found to immobilise NPL4 and p97 into detergent-resistant clusters (Skrott et al., 2017, 2019). Copper was shown to be the key determinant for disulfiram cytotoxicity, as it is needed to generate CuET. Furthermore, it was found that CuET could recapitulate cytotoxicity but had no effect on aldehyde dehydrogenase (ALDH), the original proposed target of disulfiram (Skrott et al., 2019). These findings present an opportunity to repurpose disulfiram for cancer therapy use. Currently, clinical trials testing the use of disulfiram and copper are recruiting at the Phase II stage for breast cancer (clinicaltrial.gov: NCT04265274, NCT03323346) and Phase I stage for the treatment of multiple myelomas (clinicaltrial.gov: NCT04521335).

p97 has been newly identified as a protein extractor of RNF8 in DSB repair and a direct repair enzyme in TOP1ccs repair (Fielden et al., 2020; Kilgas et al., 2021; Singh et al., 2019). These findings give the real possibility of using p97 inhibitors in combination treatments with DNA-damaging chemotherapies and radiotherapies in addition to using p97 inhibitors as a singular treatment.

1.7. DNA damage in cancer

Cancers can gain an advantageous genotype to clonally expand either through direct genomic mutation or through epigenetic modifications (Hanahan & Weinberg, 2011). Although it is hypothetically possible to become malignant purely via epigenetic means, the prevalence of copy number variations, chromosomal instability and nucleotide polymorphisms throughout almost all cancers demonstrate that they have genomic instability (Lord & Ashworth, 2012). Mutations which are tumourigenic, occur as the result of either endogenous or exogenous agents. For example, it has been shown since the 18th century that environmental genotoxic agents such as soot, leads to high incidence of scrotal cancer in young men working as chimney sweeps (BROWN & THORNTON, 1957). Work since then on tobacco, radon and other exogenous agents which cause cancer show that DNA damage is the mechanism by which this is achieved.

Components of DDR pathways, as tumour suppressors, are themselves found mutated in cancers. For example, in high-grade serous ovarian adenocarcinomas, half are approximately defective in homologous recombination (Bell et al., 2011). This is caused by either epigenetic silencing of or gene mutations in *BRCA1* and *BRCA2*. Similarly in breast cancer, familial forms of cancer are often associated with mutations in HR genes such as *BRCA1, PALB2, ATM, RAD51C* and more (Shiovitz & Korde, 2015). Defects in mismatch repair (MMR) through *MSH2, MLH1* mutations predisposes to colorectal and endometrial cancers (Jiricny, 2006). Mutations in *XPA-XPG* causes Xeroderma pigmentosum, a form of skin cancer which occurs due to inability to repair UV-induced lesions (Jackson & Bartek, 2009). Although mutations in DDR proteins have been identified in familial forms of cancer as a driver of genomic instability, this phenomenon is less pronounced in sporadic cancer (Moon et al., 2019).

A different model, whereby DNA damage is caused by oncogene-induced replication stress, is used to explain the genomic instability observed in sporadic precancerous and

cancerous lesions (Berti & Vindigni, 2016; Macheret & Halazonetis, 2015, 2018). Replication stress broadly describes impediments in DNA replication characterised by replication fork stalling and collapse and caused by uncoupling of the helicase and polymerase machinery. This can be commonly observed by formation of phosphorylated RPA foci on ssDNA at these sites of uncoupling. Eventually, replication stress can lead to DSBs through fork collapse (Bartkova et al., 2006). Alternatively, replication fork stalling leads to reversed forks and the "chicken foot" structure which allows the lesion blocking the replication fork to be repaired (Neelsen & Lopes, 2015).

Overexpression of oncogenes which promote proliferation and inactivation of tumour suppressors which normally trigger cell-cycle checkpoints, can cause replication stress. For example overexpression of oncogenes such as, but not limited to, *Ras* and *c-MYC* can cause dysregulated firing of replication origins, depletion of nucleotides and increase in unregulated replication/transcription collisions (Macheret & Halazonetis, 2015). Eventual replication fork collapse and the resulting SSBs and possible DSBs can trigger chromosomal instability and chromosomal fusions observed in almost all cancers. The concepts of replication stress and DNA damage are not mutually exclusive, and there are several ways in which they interact and complement each other in cancers (Gaillard et al., 2015; Zeman & Cimprich, 2014).

In addition to oncogene-induced replication stress, various types of DNA damage are also causative agents. Unrepaired DNA lesions such as SSBs, UV lesions and DSBs all can cause replication fork stalling and associated replication stress (Gaillard et al., 2015; Zeman & Cimprich, 2014). This includes DPCs, as SPRTN deficiency and subsequent DPC accumulation causes widespread replication stress (Halder et al., 2019).

Overall, the altered DNA damage response and replication stress have an interdependent facilitating role in cancer. In somatic cells, a well regulated DDR response protects against the thousands of lesions formed every day through endogenous and exogenous agents (Jackson & Bartek, 2009). In cancers, mutations in DDR can be drivers for tumourigenesis due to their mutagenic capabilities (BRCA1, PALB2), this incidentally make

these cancer subtypes sensitive to certain DNA damaging agents (Lord & Ashworth, 2012). The ubiquitous phenomenon of replication stress in cancers can also be exploited by genotoxic agents which specifically cause obstacles to replication forks (Ubhi & Brown, 2019).

1.7.1. DNA damaging agents in cancer chemotherapy

The importance for studying DDR systems in cancers is not solely for learning about the tumourigenic role they may play, but in the possibility of exploiting the cancers' DDR defects for clinical treatment. Cancers addiction to proliferation and their mutated DDR components make them particularly sensitive to drugs which trigger and potentiate DNA damage (O'Connor, 2015; Ubhi & Brown, 2019). In comparison, somatic cells are mostly non-proliferative and have fully functioning DDR systems which can faithfully repair endogenous and exogenous sources of lesions.

As such, DNA damage, induced through chemotherapies, have long been used for the treatment of malignancies. Traditional chemotherapies used for their semi-selective ability towards proliferating cancer cells include: the nucleoside analogue 5-fluorouracil; the topoisomerase I inhibitor camptothecin and its derivatives such as irinotecan; and platinum salts such as cisplatin and carboplatin (Goldstein & Kastan, 2015; O'Connor, 2015; Ubhi & Brown, 2019). Their induced cytotoxicity is intrinsically linked to the unregulated DNA replication required for cell proliferation (Goldstein & Kastan, 2015). Irinotecan causes TOP1ccs, which blocks replication forks and eventually cause DSBs (Fujita et al., 2015). The same is true for platins which cause interstrand crosslinks and promiscuous DPCs which ultimately result in DSBs as a result of replication fork collpase (Dasari & Bernard Tchounwou, 2014). On the other hand, 5-fluouracil inhibits thymidylate synthase (TS), depleting the pool of dTMP and other nucleotide precursors leading to replication stress and DNA damage (Longley et al., 2003).

The initial use of these chemotherapeutics were not stratified based on cancer subtype. They were used for their ability to broadly inhibit proliferative malignancies. This was changed

by seminal work with PARPis (Bryant et al., 2005; Farmer et al., 2005). After the discovery that cancers specifically deficient in HR, are hypersensitive to PARPis, which cause DNA damage. A new era of targeted DNA damage therapy has emerged. This work highlights the importance of identifying underlying biomarkers which can indicate specific cancer treatment.

1.7.2. PARP1 inhibitors

In 2005, inhibitors of PARP1 were found to specifically kill cells which were absent of BRCA1/2 (Bryant et al., 2005; Farmer et al., 2005). They were proposed to work under the model of synthetic lethality, whereby cancers which were HR-deficient (HRD), due to BRCA1/2 mutations, could be specifically targeted (Figure 9A). At the time, PARPis were thought to cause SSBs which convert to DSB upon “replication fork-runoff”, a cytotoxic lesion in HRD cells, whereas in healthy somatic cells, DSBs are efficiently repaired by HR (Jackson & Bartek, 2009).

The main target of PARPis, PARP1, has 3 zinc-fingers which facilitate its binding to DNA. It also contains a BRCT domain which is the location of its catalytic auto-modification with PAR chains. PARP1’s catalytic activity derives from its catalytic (CAT) domain which is activated when conformational structural changes are transferred from zinc-finger-mediated binding through its WGR and helical domain (HD) (Figure 9B) (Alemasova & Lavrik, 2019; Kamaletdinova et al., 2019). PARP1’s CAT domain activity begins after binding to SSB and DSBs. It first binds to its substrate nicotinamide adenine dinucleotide (NAD), then it covalently link chains of ADP-ribose sugar on itself, nearby DNA and nearby proteins (Ray Chaudhuri & Nussenzweig, 2017).

It was initially thought that through its inhibition, there would be an accumulation of SSBs. More recent studies have uncovered a novel mechanism of cytotoxicity which better reflects observations of PARPi activity, namely, how PARPis do not induce higher levels of SSBs in cancer cells (Helleday, 2011; Ström et al., 2011). Furthermore, with the generation of new PARPis, it was discovered that their ability to inhibit PARP1 catalysis did not correlate

with their observed cellular cytotoxicity (Pommier et al., 2016). This was cleared up by the finding that PARPis cause trapping of PARP1 protein onto chromatin (Figure 9B) (Murai et al., 2012, 2014). It was confirmed that the cytotoxic ability of PARPis correlated with their ability to prevent PARP1 from leaving chromatin. A cytotoxicity ranking emerged where talazoparib, was the most potent PARPi followed by olaparib, a less potent trapper, and veliparib, which was the weakest PARP1 trapper (Pommier & Murai, 2015).

Since then, structural work has identified several different modes by which PARPis can cause cytotoxic PARP1 retention on chromatin. It was found that the clinically-approved PARPis causes trapping in a non-allosteric manner (Zandarashvili et al., 2020). While some PARPis can cause allosteric trapping of PARP1, including UKTT15, a newly synthesised derivative of the weak trapper veliparib. Talazoparib and olaparib both do not. Although the mechanisms of how talazoparib can cause 100-fold more PARP1 trapping and cytotoxicity than olaparib are yet not fully explained (Hopkins et al., 2015), the best model for the trapping mechanism of clinical PARPis is through inhibition of PARylation. This is because PARylation is thought to encourage PARP1 dissociation. ADP-ribose sugars are negatively charged, thus auto-modified PARP1 is repelled from the negatively-charged sugar-phosphate backbone. However, why PARPis' *in vitro* catalytic inhibition ability does not correlate well with their PARP1 trapping/cytotoxicity, remains an unanswered question (Hopkins et al., 2015). It is likely that within the cellular context, there are increased levels of regulation that may be affected by inhibitor binding. This includes the regulation of PARP1 activity by its co-factors such as HPF1. HPF1 was shown to contribute to PARP1's active site by providing critical amino acid residues for PARP1 catalysis and thus promoting PARP1's serine-ADP ribosylation activity in response to DNA damage (Bonfiglio et al., 2017; Suskiewicz et al., 2020).

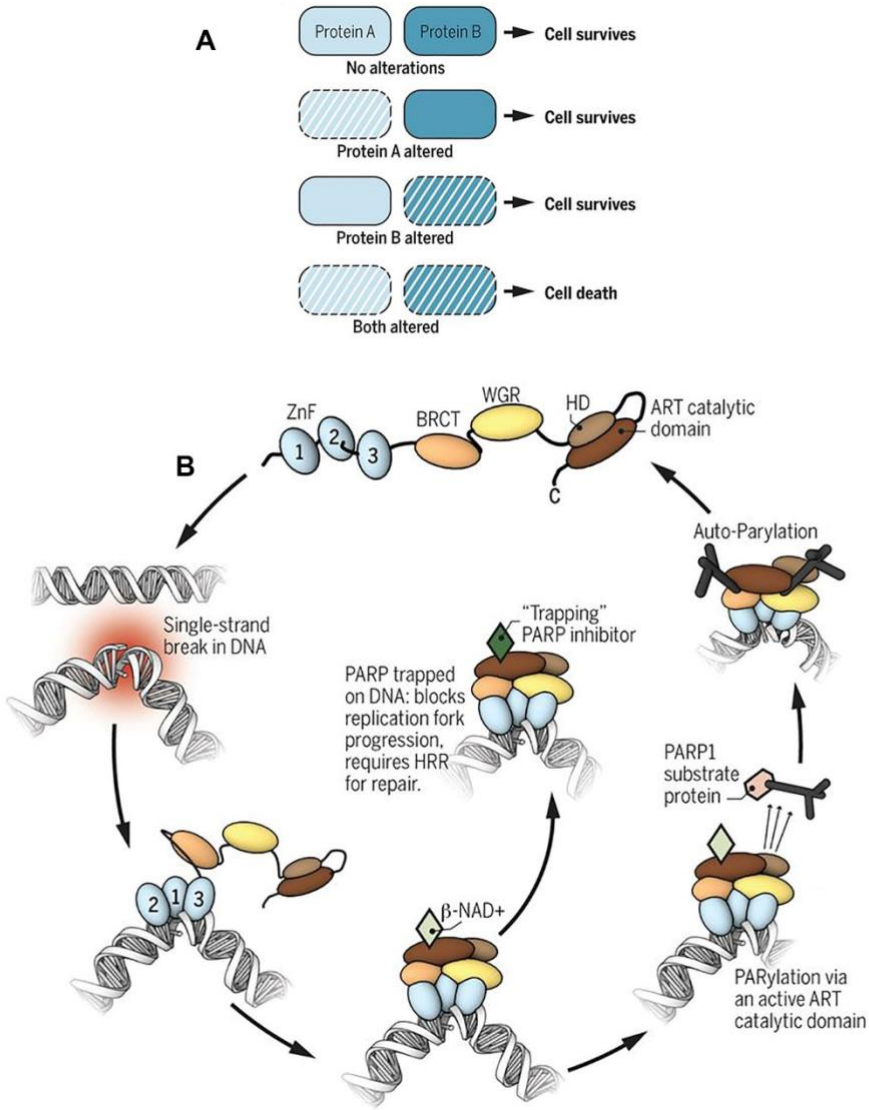


Figure 9. PARPi mechanism of action

(**A**) Model of synthetic lethal interactions between two proteins/genes. Alteration of either protein leads to cell survival however when both proteins/genes are altered, cell death occurs. (**B**) Diagram of PARP1 catalytic cycle. After a SSB occurs, PARP1 binds via its 3 ZNFs, this then allows binding to NAD which it uses to create PAR chains. In normal physiology, PARP1 actively PARylates itself and surrounding protein and DNA. This PARylation deposits negative charges which triggers its dissociation. In the presence of PARPis, of which the majority are NAD mimetics, PARP1 becomes trapped on DNA. This trapping is non-covalent and leads to the formation of an obstacle for replication and transcription. Image taken from (Lord & Ashworth, 2017).

Although we are only beginning to learn about trapped PARP1 biology, there is an extensive body of work on PARPi's differential sensitivity in HR-deficient cells (Dias et al., 2021). PARPis have been approved mainly for the use in BRCA1/2 deficient cancers, as trapped PARP1-induced replication stress and DSBs which cannot be repaired in BRCA1/2 deficient cells (Bayraktar et al., 2019; D. S. Kim et al., 2021; Pommier et al., 2016). However BRCA1/2 have been found to have roles outside of HR which affect PARPi cytotoxicity, namely, its role in protecting replication forks from degradation, which is independent of its HR promoting function (Chaudhuri et al., 2016). BRCA1/2 knockout cells showed increased nascent DNA degradation at replication forks when replication stress was induced. Degradation occurs due to PTIP-mediated recruitment of MRE11 which degrades reversed forks, these can eventually lead to DSBs and chromosomal abberations (Chaudhuri et al., 2016; Lemaçon et al., 2017).

The study by Chaudhuri et al. 2016 revealed not just a new mechanism of BRCA1/2 biology responsible for PARPi sensitisation, but also knowledge about the mechanisms of PARPi. They produced a mammary tumour in a BRCA2-deficient mouse model which was resistant to PARPis and found that they were also resistant to both cisplatin and topetecan. These resistant tumours also regained replication fork protection. The universality of resistance towards these different agents, derived from PARPi resistant tumours, point toward a shared mechanism of action. It suggests all three cause the formation of replication fork obstacles resulting in toxicity in backgrounds which lack fork protection.

There has also been a report that PARPi unexpectedly caused increased replication fork speed (Maya-Mendoza et al., 2018). In this study, BRCA2-deficient cells were observed after PARPi treatment to also cause loss of fork asymmetry, indicating the inability to stall replication forks. This finding is in contrast to more recent findings that PARPi-induced trapped PARP1 causes replication fork stalling (Saha et al., 2021).

Although the synthetic lethal model of PARPi does not seem as accurate as it originally did based on the unravelling of its molecular mechanisms, PARPis are still a success story for

their application in the clinic (D. S. Kim et al., 2021). They are an approved treatment and maintenance therapy for ovarian and breast cancers, prostate cancers with HR-deficiencies (Nizialek & Antonarakis, 2020) and pancreatic cancers as a maintenance therapy. For maintenance therapies, they are approved regardless of BRCA1/2 mutations but instead are reliant on the observation of platinum sensitivity, as this is a practical readout of HR-deficiencies which predispose to PARPi sensitivity (D. S. Kim et al., 2021; Pothuri et al., 2020; H. Zhu et al., 2020). PARPis are still being tested for their ability to be used as a first-line therapy in multiple malignancies (LaFargue et al., 2019).

Since their use in the clinic, several mechanisms of PARPi resistance have been discovered (Dias et al., 2021; Jiang et al., 2019). Although many have been proposed from preclinical experimentation, three resistance mechanism have been validated through analysis of patients. One is the restoration of HR through revertant mutation in BRCA1/2 which restores its function (Barber et al., 2013). Interestingly these mutations also causes resistance to platinum chemotherapy. The second mechanism of resistance is through the Shieldin complex, where PARPi-resistant patient-derived xenografts were revealed to correlate with lower levels/loss of SHLD1, SHLD2 and 53BP1 mRNA expression (Dev et al., 2018). The final mechanism of resistance was found in an ovarian cancer patient who possessed resistance to olaparib treatment, a mutation in PARP1's WGR domain was present (Pettitt et al., 2018). It was predicted that this mutation is critical for inter-domain communication in PARP1, particularly between its zinc-fingers and its catalytic domain. It was confirmed that this mutant PARP1 could not be trapped at DNA lesions by the PARPi talazoparib, even though it was successfully recruited to sites. This suggests that the molecular phenomenon of PARP1 trapping is not just a preclinical finding but plays a significant clinical role in determining patient outcome.

1.8. Aim of this study

The overall aim of this study was to reveal novel substrates and biological actions of p97 in DNA damage. This is because p97 inhibitors are currently being developed for cancer chemotherapy, and thus there exists a need to understand its mechanisms and interactors in greater detail for potential new therapeutic directions. Although previous work from our lab had revealed p97 is responsible for turnover of K48 linked ubiquitin chains in DSB repair, we looked to reveal the specific targets of p97 in the context of DSB and DPC repair. Specifically we looked at p97's physical and functional interactions with three chromatin-associated substrates: the ubiquitin E3 ligase RNF8, TOP1ccs and trapped PARP1.

My work especially focused on trapped PARP1. I chose to evaluate how PARPi-induced trapped PARP1 is repaired because PARPis represent the forefront of targeted chemotherapies for BRCA1/2-mutated tumours. And unlike TOP1ccs, which have been extensively studied, we believe there was a gap in the knowledge of PARPi cellular responses. Although there have been studies on PARPi and its differential cytotoxicity in different genetic backgrounds, there is still no study on how the cell responds directly to the trapped PARP1 lesion itself. We thus asked whether there was a physiological repair response to trapped PARP1 and whether it could be exploited for potentiating cytotoxicity. We had preliminary data showing that PARP1 could be proteolytically-cleaved by SPRTN. Thus, we believed that as SPRTN operates with p97, there could be a possibility that both are involved in trapped PARP1 repair. To this end, a mass spectrometry analysis was carried out to begin the elucidation for the physiological response to trapped PARP1.

2. Materials and methods

2.1. Buffers

2.1.1. 10x Phosphate buffer saline (PBS)

For 1 litre (L), the following were dissolved in 800 mL double-distilled (dd) H2O:

- 18.1 grams (g) Na2HPO4•2H2O
- 80 g NaCl
- 2 g KCl
- 2.4 g KH2PO4

The pH was adjusted to 7.4 with HCl and filled to a volume of 1 L with ddH2O. 1x PBS (working concentration: 137 mM NaCl, 10 mM Phosphate, 2.7 mM KCl, pH 7.4) was prepared by diluting the 10x PBS stock 1:10 in ddH2O

2.1.2. 10x Tris Buffered Saline (TBS)

For 1 L, the following were dissolved in 900 mL ddH2O:

- 88 g NaCl
- 24 g Trizma Base

The pH was adjusted to 7.6 with HCl and filled to a final volume filled of 1 L withddH2O.

1x TBS (20 mM Tris, 150 mM NaCl) was prepared by diluting the 10x TBS stock1:10 in ddH2O.

0.1% TBS-Tween (TBS-T) was prepared by adding 1 mL of Tween-20 to 1 L.

2.1.3. 10x Tris/Glycine buffer

For 1 L, the following were dissolved in ddH2O:

- 30g trizma base
- 144g glycine

The 10x stock of Tris/Glycine was diluted 1:10 for use as a running and transfer buffer for Immunoblotting. For running buffer, 1x Tris/Glycine was supplemented with SDS to a final concentration of 0.1%. For transfer buffer, 10x Tris/Glycine was diluted with ddH2O, 20% methanol, and supplemented with SDS to a final concentration of 0.025%.

2.1.4. 5x Laemmli Buffer

- Bromophenol Blue (SLS, 0.25%)
- Glycerol (Fisher Scientific, 50%)
- SDS (10%)
- Tris-HCl (0.25 M, pH 6.8)

1x LB (50 mM Tris-HCl pH 6.8, 2% SDS, 10% Glycerol, 0.05% bromophenol blue)was prepared in water supplemented with 15% β-mercaptoethanol (βMe).

2.1.5. Crystal violet staining (colony forming assays)

For 100 mL, 0.5 g crystal violet powder was dissolved in 80 ml water and 20 ml methanol.

2.2. Cell culture

2.2.1. Cell line buffers and maintenance

HEK293, U2OS, HeLa, RPE-1, DLD-1, CAL51 and MCF-7 cell lines were all cultured in DMEM (Sigma) containing 10% FBS (Sigma) and 5% Pencillin/Streptomycin (Life technologies). All cell lines, other than CAL51 which were obtained from DSMZ (DSMZ ACC 302) and DLD-1 BRCA2$^{-/-}$ which were obtained from Horizon (Horizon HD 105-007), were

obtained from ATCC. Cell lines were tested frequently with MycoAlert™ Mycoplasma Detection Kit.

2.2.2. Generation of cell lines

CAL51 PARP1$^{-/-}$ cells were previously described (Krastev et al., 2018). They were transfected with a corresponding PARP1-expressing piggyBac construct in combination with hyPBase-expressing plasmid (Yusa et al., 2011). 72 hours after transfection, single-cell clones were sorted by FACS and allowed to expand. These clones were characterized for the expression of the tagged protein by microscopy and western blotting. The HCT116 *PIAS4*$^{-/-}$ and MCF7 *RNF4*$^{-/-}$ cells were previously described (Sun, Jenkins, et al., 2020). HEK293 *PARP1*$^{-/-}$ cells were a kind gift from Ivan Ahel, University of Oxford. siRNAs

siRNAs were obtained from Dharmacon: RNF4 (L-006557-00-0005 and 3'UTR siRNA sequence 5'-GGGCAUGAAAGGUUGAGAAUU); UFD1L (L-017918-00-0005); NPL4 (L-020796-01-0005). PARP1 (Flexitube siRNA Hs_PARP1_5, catalog no. SI02662989). SPRTN (3'UTR sequence: GUCAGGAAGUUCUGGUUAA, D2 – Dharmacon onTarget J-015442-21-0050, Q1 sequence: AGCCAAUAUAACGGUAUACCA). TEX264 (3'UTR sequence: CUUCCAGGACCCAGAAUAA). ATXN3 (sequence: GCAGGGCUAUUCAGCUAAG).

2.2.3. Plasmids

To generate PB-PARP1-eGFP, PARP1 cDNA was cloned in a previously described piggyBac vector (Pettitt et al., 2017). To generate PARP1-Apex2-eGFP construct, the Apex2 gene was amplified from Addgene vector 49386 and inserted in between PARP1 and eGFP coding sequences via InFusion (Clonetek, 648910). PBZ-mRuby2 is described in (Krastev et al., 2018). UB-STREP-HA was a kind gift from Vincenzo D'angiolella, HA-SUMO2 (Gong & Yeh, 2006), FLAG-PARP1 was a kind gift from Ivan Ahel, p97-GFP was a kind gift from Hemmo Meyer.

The wild-type PIAS4 expressing construct was obtained from Addgene (#15208) and RNF4 from Origene (RC207273). The corresponding SAP and SIM mutants were generated as described (Sun, Jenkins, et al., 2020). The RNF4-M136S,R177A was a kind gift from Ronald Hay.

Plasmid DNA transfections were performed using polyethyleneimine (PEI) reagent, Lipofectamine 3000 (Thermo Fisher), or FuGENE HD Transfection Reagent (Promega), following the manufacturer's instructions.

2.2.4. Antibodies

Antibodies used were: GFP (Sigma-Aldrich, 11814460001, clones 7.1 and 13.1, dilution WB 1:5000 IF 1:500 PLA 1:1500); PARP (CST, 9532, 46D11, dilution 1:2000) for immunoblotting and PLA; p97 (Abcam, ab11433 [5], dilution WB 1:1000 PLA 1:2000) for immunoblotting and PLA; PAR (Trevigen, 4335-AMC-050, dilution WB 1:1000); HA (Roche, 11867423001, dilution WB 1:5000); FLAG (M2, Sigma-Aldrich, F1804, dilution WB 1:5000) for immunoprecipitation; FLAG (Sigma-Aldrich F7425, dilution WB 1:5000) for immunoblotting; Streptavidin-HRP (ThermoFisher, S911, WB dilution 1:1000); PARP1 (Sigma-Aldrich, WH0000142M1, dilution WB 1:1000 PLA 1:2000) for PLA; β-actin (Invitrogen, AM4302, dilution WB 1:5000); lamin-B1 (Thermo, PA5-19468, dilution WB 1:5000); vinculin (Abcam, ab18058. dilution WB 1:5000); phospho-H2AX (CST, 9718S, dilution 1:2000) for PLA; phospho-H2AX (Millipore, 05-636, dilution 1:1500) for foci immunostaining; RAD51 (Abcam, ab133534, dilution 1:1500) for foci immunostaining; Histone H3 (CST, 9715, dilution WB 1:5000); SUMO1 (CST, 4940, dilution WB 1:1000); SUMO2/3 (CST, 4971, dilution WB 1:1000); ubiquitin (Santa Cruz Biotechnology, sc-8017, dilution WB 1:1000); RNF4 (Novusbio, NBP2-13243, dilution WB 1:1000); UFD1L (Abcam, ab181080, dilution WB 1:1000); Anti-Rabbit IgG HRP (Rockland, 18-8816-31, dilution WB 1:5000); Anti-SPRTN (Atlas, HPA025073, Dilution 1:1000).

2.2.5. Cell treatment reagents

Talazoparib was supplied by Pfizer as part of the BCN Catalyst programme. Other small molecules were as follows: Olaparib (Selleckchem, S1060); Veliparib (Selleckchem, S1004); UKTT15 from in-house synthesis as described in[4], MMS (Sigma-Aldrich, 129925-5G); CB-5083 (Selleckchem, S8101); CuET from in-house synthesis as described in (Skrott et al., 2017a); MLN-7243 (Selleckchem, S8341); ML-792 (Medchemexpress, HY-108702).

2.2.6. Western blotting

Acrylamide gels were prepared in the laboratory. Separating and stacking buffers were prepared separately, as follows:

A 4x separating buffer composed of 1.5 M Tris, pH 8.8, 0.4% SDS was mixed with 30% acrylamide (to a final concentration of 5 – 18%) acrylamide/Bis solution and ddH2O and set with 0.5% ammonium persulfate and 0.06% Tetramethylethylenediamine. Stacking buffer was prepared as described for separating buffer, except the stacking buffer is composed of 0.5 M Tris, pH 6.8, 0.4% SDS and the final concentration of acrylamide was 4%.

SDS-PAGE was performed using the Mini-PROTEAN Tetra Electrophoresis System (Bio-Rad). Proteins were separated at 150 V in running buffer. SDS- PAGE gels were then either stained using the ProteoSilver Plus Silver Stain Kit (Sigma-Aldrich) or transferred in transfer buffer at 100 V for 75 mins onto a PVDF membrane (Bio-Rad), which had been activated with 100% methanol. Membranes were then washed once in 1 x TBS-T and blocked in 5% milk diluted in 1x TBS-T for 1 hr at room temperature. Primary antibodies against the protein of interest were diluted in 5% BSA (dissolved in in 1x TBS-T and supplemented with 0.02% sodium azide) and incubated with the membrane overnight 4˚C. The next day, membranes were washed three times in 1 x TBS-T (5 mins/wash) and incubated with the appropriate HRP-conjugated secondary antibody (diluted in 2.5% milk in TBS-T) for 1 hr at room temperature. Membranes were then washed three times in 1 x TBS-T (5 mins/wash),

dried, and incubated with enhanced chemiluminescent substrate detection reagent (Thermo Fisher) for 5 mins. Proteins were visualised using the ChemiDoc MP system (Bio-Rad).

2.2.7. Whole cell lysates

Cells were collected in 1x PBS and harvested by centrifugation at 600 x g. Cell pellets were lysed in Radioimmunoprecipitation assay buffer (RIPA buffer), composed of 25 mM Tris-HCl, pH 7.4, 150 mM NaCl, 0.1% SDS, 0.5% sodium deoxycholate, 1% Triton X-100). Pellets were lysed for 20 mins at 4°C with rotation. Samples were sonicated using a Bioruptor Plus sonicator (Diagenode) for 30 seconds ON, 30 seconds OFF for 5 cycles to fragment DNA. Samples were centrifuged at 21,800 x g for 15 minutes. The supernatant was collected, and protein concentrations were quantified using the RC DC Protein Assay (Bio-Rad).

2.2.8. Cellular fractionation immunoprecipitation

Cells were washed two times with PBS then resuspended in buffer A (10 mM HEPES, 10 mM KCl, 340 mM sucrose, 10% glycerol, 2 mM EDTA, protease and phosphatase inhibitors, N-ethylmaleimide (NEM)). Triton X-100 was added to achieve a final concentration of 0.1% and left on ice for 2-5 min depending on cell line. The supernatant was harvested as the cytosolic fraction and the pellet (nuclei) was then washed two times with buffer A. Buffer B (3 mM EDTA, 0.2 mM EGTA, 5 mM HEPES pH 7.9, protease and phosphatase inhibitors, NEM) was then added to burst nuclei, after which lysates were kept on ice for 10 min. Supernatant was then removed as the nuclear soluble fraction. Remaining chromatin pellet was then washed with buffer B in 0.5% Triton X-100 followed by benzonase buffer without $MgCl_2$ (50 mM Tris-HCl pH 7.9, 100 mM NaCl). Benzonase digestion buffer (50 mM Tris-HCl pH7.9, 10 mM $MgCl_2$, 100 mM NaCl, protease and phosphatase inhibitors, NEM) supplemented with 125 U of Benzonase enzyme (Merk Millipore) and rotated on wheel at 4°C for 1 hour. Samples were then centrifuged at 20,000 g for 15 min, chromatin input for the immunoprecipitation reaction was then taken from supernatant. The remaining supernatant was then incubated with respective beads on a rotating wheel for 3 hours at 4°C. For native IPs, 1:200 ethidium

bromide was added to remove unwanted DNA-protein interactions. Beads were then washed with IP wash buffer (50 mM Tris-HCl pH 7.4, 150 mM NaCl, 0.5 mM EDTA, 0.05% Triton X-100) three times before elution with lamelli buffer.

2.2.9. Whole cell Immunoprecipitation

Cells were lysed in IP lysis buffer (50 mM Tris HCl pH 7.4, 150 mM NaCl, 1 mM EDTA, 0.5% Triton X-100, protease and phosphatase inhibitors, NEM) and spun on wheel at 4°C for 10 min. The supernatant was removed and pellet was washed with benzonase buffer once and the supernatants were pooled together. Benzonase buffer (50 mM Tris-HCl pH 7.9, 10 mM $MgCl_2$, 100 mM NaCl, protease and phosphatase inhibitors, NEM) supplemented with 125 U of Benzonase enzyme (Merk Millipore) was added to the pellet and left on wheel at 4°C for 1 hour. Samples were then centrifuged at 20,000 g and all supernatants were pooled. Input for the IP was then removed and samples were incubated with respective beads on wheel for 3 hours at 4°C. Beads were then washed with IP wash buffer (50 mM Tris-HCl pH 7.4, 150 mM NaCl, 0.5 mM EDTA, 0.05% Triton X-100) three times before elution with Laemmlli buffer.

2.2.10. Denaturing IP

Cells were lysed either according to fractionation immunoprecipitation or whole cell immunoprecipitation protocol as stated above. Before incubation with beads, SDS was added to samples to a concentration of 1% and boiled at 95°C for 5 min. Samples were then diluted in 1% Triton X-100 to achieve a dilution of 1:10 (SDS at 0.1%) along with beads and rotated on wheel at 4°C for 3 hours. Beads were then washed with IP wash buffer (50 mM Tris-HCl pH 7.4, 150 mM NaCl, 0.5 mM EDTA, 0.05% Triton X-100) three times before elution with Laemmlli buffer.

2.2.11. Colony forming assay

HeLa/RPE-1 WT cells were seeded in triplicate on 6-well plates and allowed to attach for 16 hours. Cells were then treated with the indicated doses of CPT (Sigma-Aldrich) for 24 hours, after which they were washed with PBS, and released into normal media. 7- 10 days later, colonies were fixed with 100% methanol for 5 mins and stained with crystal violet. The number of colonies was counted using the automated colony counter, GelCount™ (DTI-Biotech). The number of colonies in treated samples is expressed as a percentage of the number of colonies in the untreated samples.

The viability of CAL51/DLD1 cells was measured after six days exposure to various concentrations of drugs using the Cell Titre-Glo assay (Promega). Long-term drug exposure effects were assessed by colony formation assay after 12–14 days exposure to a drug-containing medium (refreshed weekly) and cells stained at the end of the assay with sulforhodamine B. When plotting survival curves, the surviving fraction was calculated relative to DMSO (solvent)-exposed cells.

2.2.12. Apex2-mediated Proximity-Labelling

For each condition tested, 5-10 x 10^6 cells expressing PARP1-Apex2-eGFP were exposed to either 0.01% MMS or a combination of 0.01% MMS + 100 nM talazoparib for 1 hour. In the last 30 min of the incubation, 500 µM final concentration biotin-tyramide (Sigma-Aldrich, SML2135) was added to the media. To label proteins, 1 mM final concentration H_2O_2 (Sigma-Aldrich, H1009) was added for 60 s. The reaction was quenched by washing the cells tree times with freshly prepared quench solution (PBS containing 10 mM Sodium ascorbate, 10 mM Sodium Azide, 5 mM Trolox (Sigma-Aldrich, 238813)). Subsequently, the cells were scraped in quench solution and washed twice in 0.1% IGEPAL CA-630 quench solution. The remaining nuclei were lysed in nuclear RIPA buffer (50 mM Tris HCl pH 7.5, 1 M NaCl, 1% IGEPAL CA-630, 0.1% sodium deoxycholate, 1 mM EDTA) for 10 min on ice. The lysates were diluted with RIPA buffer not containing NaCl to final 200 mM NaCl, sonicated for 1 min

and incubated with 250 U benzonase for 20 min at room temperature. The lysates were clarified by centrifugation at 13000 g for 15 min at 4°C. Protein concentration was determined and 1 mg total protein was incubated with 30 µl streptavidin-magnetic beads (ThermoFisher, 88816) for 1 h at room temperature. The beads were washed stringently by sequential washes: twice with RIPA lysis buffer, once with 1 M KCl, once with 0.1 M Na_2CO_3, once with 2 M urea, twice with RIPA lysis buffer and processed further for MS analysis.

2.2.13. Rapid immunoprecipitation mass spectrometry of tagged protein (RIME-based approach)

For each condition tested, 5-10 x 10^6 cells were exposed to either 0.01% MMS or a combination of 0.01% MMS + 100 nM talazoparib for 1 hour. At the end of the incubation period, formaldehyde (ThermoFisher, 28908) was added to the media to 1% final concentration and incubated for 10 min at room temperature. The reaction was quenched by the addition of 125 mM glycine final concentration. The cells were collected and washed once in ice-cold PBS. The cells were resuspended in ice cold PBS containing 0.1% Triton X-100 and protease inhibitor cocktail (Merck, 4693116001). The nuclei were spun at 3000 g for 5 min at 4°C, and subsequently resuspended in PBS containing 1% IGEPAL CA-630 (Sigma-Aldrich) and protease inhibitors, and incubated on ice for 15 min. The remaining chromatin was spun at 13000 g for 5 min at 4°C and resuspended in PBS containing 0.1% IGEPAL CA-630 and protease inhibitors. The chromatin pellet was spun at 13000 g for 5 min at 4°C, resuspended in lysis buffer (20 mM HEPES pH 7.5, 150 mM NaCl, 0.5% sodium deoxycholate, 0.1% SDS, 10 mM $MgCl_2$) supplemented with 250 U benzonase (Sigma-Aldrich, E1014) and incubated for 30 min at room temperature with rotation to release the chromatin bound proteins. The supernatant was isolated after centrifugation (13000x g for 10 min at 4°C) and incubated with 25 µl GFP Trap (Chromotek, gtm-20) magnetic beads for 1 hour at 4°C with rotation. The beads were washed four times with the lysis buffer and processed further for MS analysis.

2.2.14. Mass spectrometry and data analysis

After initial washes according to the purification method, the beads were further washed twice with 50 mM ammonium bicarbonate. The proteins on the beads were digested with 0.1 µg/µl sequencing grade trypsin (Roche) overnight at 37°C. The peptide solution was neutralised with 5% formic acid, acetonitrile was added to 60% final concentration and the solution was filtered through a Millipore Mutiscreen HTS plate (pre washed with 60 % acetonitrile). The peptide solution was lyophilised on a SpeedVac and the peptides were dissolved in 20 mM TCEP-0.5% formic acid solution. The LC-MS/MS analysis was conducted on the Orbitrap Fusion Tribrid mass spectrometer coupled with U3000 RSLCnano UHPLC system (ThermoFisher). The peptides were first loaded on a PepMap C18 trap (100 µm i.d. x 20 mm, 100 Å, 5 µm) at 10 µl/min with 0.1% FA/H_2O, and then separated on a PepMap C18 column (75 µm i.d. x 500 mm, 100 Å, 2 µm) at 300 nl/min and a linear gradient of 4-32% ACN/0.1% FA in 90 min with the cycle at 120 min. Briefly, the Orbitrap full MS survey scan was m/z 375–1500 with the resolution 120,000 at m/z 200, with AGC (Automatic Gain Control) set at 40,000 and maximum injection time at 50 ms. Multiply charged ions (z = 2 – 5) with intensity above 8,000 counts (for Lumos) or 10,000 counts (for Fusion) were fragmented in HCD (higher collision dissociation) cell at 30% collision energy, and the isolation window at 1.6 Th. The fragment ions were detected in ion trap with AGC at 10,000 and 35 ms maximum injection time. The dynamic exclusion time was set at 40 s with ±10 ppm.

The mass spectrometry proteomics data have been deposited to the ProteomeXchange Consortium via the PRIDE partner repository with the dataset identifier PXD024337 (Perez-Riverol et al., 2019). Raw mass spectrometry data files were analysed with Proteome Discoverer 1.4 (Thermo). Database searches were carried out using Mascot (version 2.4) against the Uniprot human reference database (January 2018, 21123 sequences) with the following parameters: Trypsin was set as digestion mode with a maximum of two missed cleavages allowed. Precursor mass tolerance was set to 10 ppm, and fragment mass tolerance set to 0.5 Da. Acetylation at the N terminus, oxidation of methionine,

carbamidomethylation of cysteine, and deamidation of asparagine and glutamine were set as variable modifications. Peptide identifications were set at 1% FDR using Mascot Percolator. Protein identification required at least one peptide with a minimum score of 20. For the Apex2-based proximity-labelling MS the following steps were taken. Proteins identified with a single peptide were removed from further analysis. PARP1-eGFP MS profile under trapping conditions (MMS + talazoparib) was used as a negative control. Proteins identified with >2 unique peptides in this sample were removed from further analysis. Peptide Spectrum Matches (PSM) was used as a proxy of protein abundance in the samples. A ratio was built between PARP1-Apex2-eGFP MMS+talazoparib PSM and PARP1-Apex2-eGFP MMS PSM as an indicator for enrichment in the trapping conditions. Where PSM values were absent from the PARP1-Apex2-eGFP MMS PSM (i.e. no detection in the sample) a value of one was added in order to calculate a meaningful ratio (the data is provided in Supplementary Table 1). The list of genes was then searched on the STRING database to build a network of the hits. A high confidence threshold was set for mapping the network, using a minimum required interaction score of 0.7 for connecting nodes. Single, unconnected nodes were excluded from the network plots. The gene list was searched in the Enrichr database to assess which KEGG 2019 pathway annotations are enriched in the dataset. The list of annotations was filtered using -log(p) values of 1.3 ($p = 0.05$) or 2 ($p = 0.01$) (the data is provided in Supplementary Table 2). For RIME analysis the proteins identified with single peptides were removed from further analysis. Proteins identified in CAL51 *PARP1*$^{-/-}$ cells were considered as background and removed from further analysis when they were identified with more than two unique peptides. Subsequently the MS data obtained from PARP1^{WT}-eGFP or PARP1$^{del.p.119K120S}$-eGFP cells were considered separately. For each cell line a ratio was built between the MMS+talazoparib PSM and the MMS PSM as an indicator for enrichment in the trapping conditions. Where PSM values were absent from the MMS PSM (i.e. no detection in the sample) a value of one was added in order to calculate a meaningful ratio (the data is provided in Supplementary Table 3 and 4 for PARP1^{WT}-eGFP or PARP1$^{del.p.119K120S}$-eGFP, respectively). MS score is calculated by the MaxQuant software and is a measure of the probability of identification of an actual

proteomic peptides versus a match in a database of randomised scrambled peptides, effectively a measure of probability of a true match.

2.2.15. Proximity ligation assay (PLA)

Proximity ligation assays were carried out with Duolink® In Situ Red Starter Kit Mouse/Rabbit (Sigma-Aldrich) according to the manufacturer's protocol. The primary antibodies used were mouse anti-PARP1 (WH0000142M1-100UG), rabbit anti-PARP (Cell Signalling), mouse anti-p97 (ab11433) and rabbit anti-phospho-H2AX (Cell Signalling). The antibodies were used in 1:1500 dilution. Images were acquired on Marianas advanced spinning disk confocal microscope (3i) and analysed with a custom CellProfiler pipeline. Typically, several hundred nuclei were counted per condition from at least two independent biological repeats.

2.2.16. Immunofluorescence

Visualisation of TOP1ccs by immunofluorescence was performed as described by Patel et al, 2016. Briefly, cells were fixed in 4% formaldehyde for 15 mins at room temperature, then permeabilised in 0.5% Triton X-100 for 15 mins at 4°C. Cells were then treated with 0.5% SDS for 5 mins are room temperature and washed 5 times in a buffer containing 0.1% Triton X-100 and 0.1% BSA diluted in PBS. After blocking in 5% BSA/PBS for 1 hour at room temperature, cells were incubated with an anti-TOP1cc antibody (Merck) diluted 1:100 in 2.5% BSA/PBS. Following staining with secondary antibodies and DAPI, coverslips were mounted onto slides and imaged using a Nikon 90i microscope.

For visualisation of trapped PARP1. Cells attached on glass cloverslips for 2 days were washed 3 times with PBS before being pre-extracted with CSK buffer at 4°C for 3 mins (10mM PIPES/HEPES, 100mM NaCl, 0.3M sucrose, 3mM $MgCl_2$, 0.25% Triton-X100 made up in ddH_2O). Then cells were washed 2 times with CSK buffer with no Triton-X100. Cells were then fixed with 4% formaldehyde for 15 minutes at 4°C. After fixing, cells were stained with primary antibody in 5% BSA in PBS at 37°C for 1 hour, washed 3 times in PBS and then suitable

secondary fluorescent antibody (Alexa Fluor) used for staining in 5% BSA in PBS at 37°C for 1 hour. Repeat if second protein of interest needed for staining. After all staining achieved, Add DAPI to PBS and incubate cells are room temperature for 10 mins. Then fix coverslips with cells on microscope slide with Fluormount solution (Life technologies). Confocal microscopy was performed using Andor Dragonfly 200 on a Nikon Ti-E microscope. Z-stacks were taken at an interval of 0.1 µM across cells fixed identically to normal brightfield microscopy. ClearView-GPU™ deconvolution was carried out on samples where stated. Images were imported via Bio-Formats (ImageJ plugin) and analysis was carried out using ImageJ. Images displayed are single z-slices unless otherwise stated.

2.2.17. Rapid Approach to DNA Adduct Recovery (RADAR)

DPCs were isolated using a modified RADAR assay (Kiianitsa & Maizels, 2013). Cells were grown to ~70% confluency then lysed in M buffer (MB), containing 6 M guanidine thiocyanate, 10 mM Tris–HCl (pH 6.8), 20 mM EDTA, 4% Triton X-100, 1% N-lauroylsarcosine and 1% dithiothreitol. DNA was precipitated by adding 100% ethanol, then washed three times in wash buffer (20 mM Tris–HCl pH 7.4, 150 mM NaCl and 50% ethanol), and solubilised in 8 mM NaOH. DNA concentrations were quantified by NanoDropTM and confirmed by slot blot analysis on a Hybond N+ membrane followed by detection with an anti- dsDNA antibody. For TOP1ccs, samples were digested with Benzonase for 30 mins at 37°C and analysed by slot blot analysis on a Nitrocellulose membrane.

2.2.18. Statistics and reproducibility

No statistical method was used to predetermine sample size. No data were excluded from the analyses. The experiments were not randomized. The Investigators were not blinded to allocation during experiments and outcome assessment. Number of replicates for each experiment are stated in the figure legends. For statistical analysis, the type of test and indicated P-values are stated in the figure legends, these were calculated using GraphPad Prism.

3. Results

3.1. p97 functions in DNA damage repair and signalling

The first well-studied examples of p97 unfoldase/segregase function were in ER-associated degradation (Ye et al., 2001, 2004). Since 2007, seminal work from our lab and others showed that p97 also functions in the nucleus, often to remove proteins from chromatin. This established a novel compartment for p97 function, where similar to ERAD, proteins are embedded in an environment that makes them difficult to segregate. p97's chromatin targets include proteins vital for: DNA replication, CMG (Maric et al., 2014) and CDT1 (Raman et al., 2011); mitosis, Aurora B (Ramadan et al., 2007) and DNA damage, Ku80 (van den Boom et al., 2016). We focused our work on looking at p97's role in directly repairing DNA damage and its role in facilitating DDR through signalling, as DDR currently represents the forefront of targeted chemotherapy research.

3.1.1. p97 is a DNA damage repair protein

Camptothecin and its derivatives are used as treatment options for various cancers including bowel and lung malignancies (Fujita et al., 2015). Their mechanism of action is to induce TOP1 DPCs, TOP1ccs. As we know that cdc48, the p97 yeast homolog was implicated in TOP1cc repair, we reasoned that p97 may play a similar role in humans (Fielden et al., 2020) .

DPCs were measured by my colleague John Fielden using the RADAR assay, Rapid Approach to DNA Adducts Recovery (Kiianitsa & Maizels, 2013), where cells are lysed under stringent conditions to obtain only DPCs. When p97 was depleted by siRNA, an increase in TOP1ccs was observed (Figure 10A). The increase in TOP1ccs under p97 siRNA depletion was to a similar level as when cells were treated with camptothecin, demonstrating the importance of p97 in TOP1cc removal.

We know that p97 gains its specificity via its cofactors (Meyer et al., 2012; van den Boom & Meyer, 2018). From the analysis of p97's mass spectrometry interactome, we identified a previously uncharacterised protein, TEX264, which we believed to be a p97 cofactor due to presence of a p97 interacting SHP domain (Fielden et al., 2020). Since p97 is involved in TOP1cc repair and TEX264 also possesses a gyrase inhibitory-like domain (gyrase being the bacterial topoisomerase), we reasoned that TEX264 may play a role in TOP1ccs repair.

By performing native co-immunoprecipitation experiments, it was found that TEX264 indeed recruits p97 to TOP1ccs (Figure 10B, C). By using confocal immunofluorescence microscopy and an antibody specific for the covalent linkage between the TOP1 protein adduct and DNA, an increase in TOP1ccs was observed when TEX264 was depleted by siRNA (Figure 10D, E). This together shows that TEX264 acts as a p97 cofactor to specifically recruit p97 to TOP1ccs for its repair.

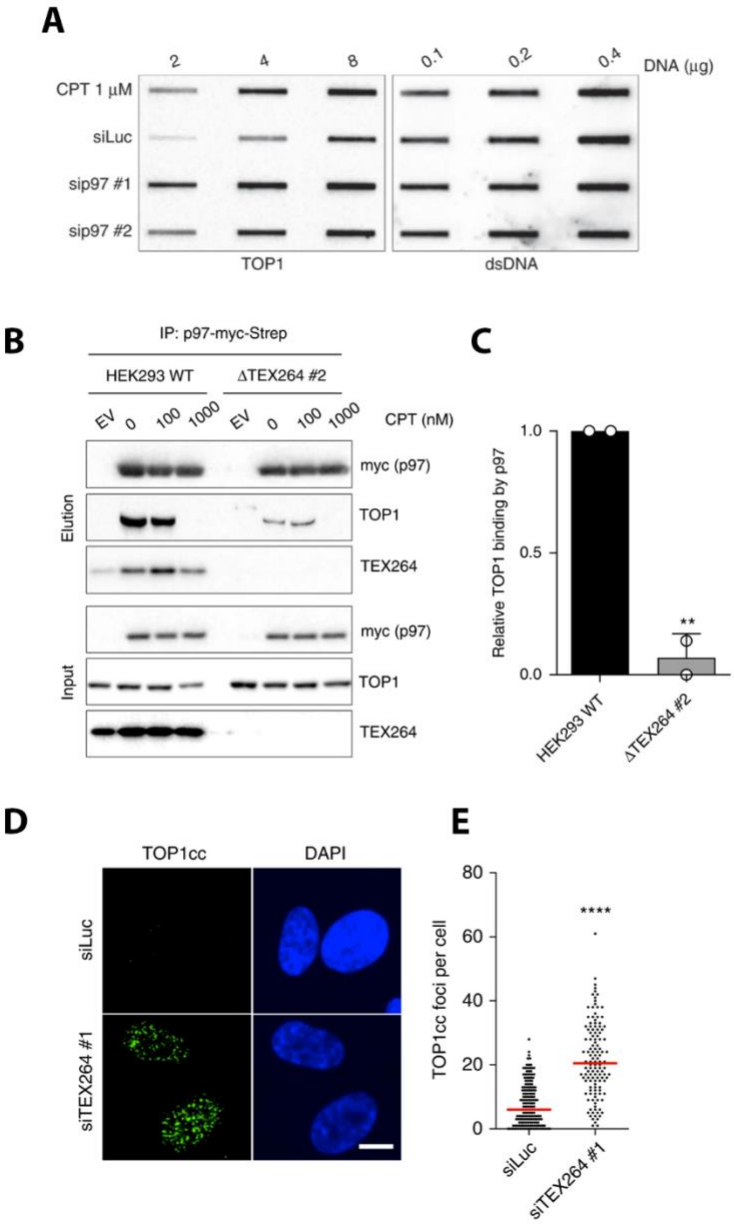


Figure 10. TEX264 acts to recruit p97 for TOP1cc repair

(**A**) Slot bots of HEK293 cells which were treated with CPT 1uM for 1 hour or depleted of p97 with two different siRNAs for 3 days. DPCs were isolated by RADAR assay and TOP1cc western blotted for using slot blot, dsDNA was used as a loading control, representative experiment shown of n=3. (**B**) Western blots of co-IP experiment where p97-MYC-STREP was immunoprecipitated via STREP-tag from HEK293 WT and TEX264$^{-/-}$ cells, n=2. (**C**) Quantification and statistical analysis of (**B**), (mean ± SEM; n = 3; **P < 0.01; Student's t-test). (**D**) U2OS cells where TEX264 was depleted for 3 days and stained for TOP1cc, images were then acquired using immunofluorescent microscopy, representative images shown for n=3. (**E**) Quantification of experiment shown in (**D**). Experiments (**A**-**C**) were performed by John Fielden.

Interestingly, while our manuscript was under revision, it was shown that TEX264 is also an ER associated protein (An et al., 2019). How it functions at the ER while also functioning as a nuclear cofactor for p97 and TOP1cc repair is unknown but would be important for improving our understanding of p97 nuclear biology.

Thus to learn more about TEX264 and p97 biology, we performed co-localisation experiments to validate that TEX264 is a nuclear cofactor of p97. We found TEX264^{WT} to be mostly localised to the nuclear periphery, likely the nuclear membrane (Figure 11A-C). The nuclear membrane consists of an inward-facing portion, the inner nuclear membrane (INM) which can interact with nuclear components. To see if TEX264 was capable of interacting with nuclear components, we checked the subcellular localisation of a TEX264$^{\Delta LRR}$ mutant which is unable to integrate into membranes due to deletion of its N-terminal transmembrane leucine-rich repeat (LRR). TEX264$^{\Delta LRR}$ was found both in the cytoplasm and the nucleus (Figure 11A-C). Importantly, we found that TEX264-ΔLRR colocalised with replication forks (Figure 11A), the protease SPRTN (Figure 11B) and TOP1ccs (Figure 11C), proving that TEX264 had the ability to interact with DPCs in a replication dependent manner (Fielden et al., 2020).

We propose that p97 performs its TOP1cc repair functions at the nuclear periphery, by forming a complex with TEX264 and its protease cofactor SPRTN. Altogether, p97-SPRTN-TEX264 form a novel TOP1cc repair complex that recognises (by TEX264), unfolds (by p97) and finally degrades (by SPRTN protease) the TOP1cc lesion (Figure 11D) (Fielden et al., 2020). This demonstrated one mode of p97 action in DDR where it is able to directly repair a DNA lesion (TOP1cc).

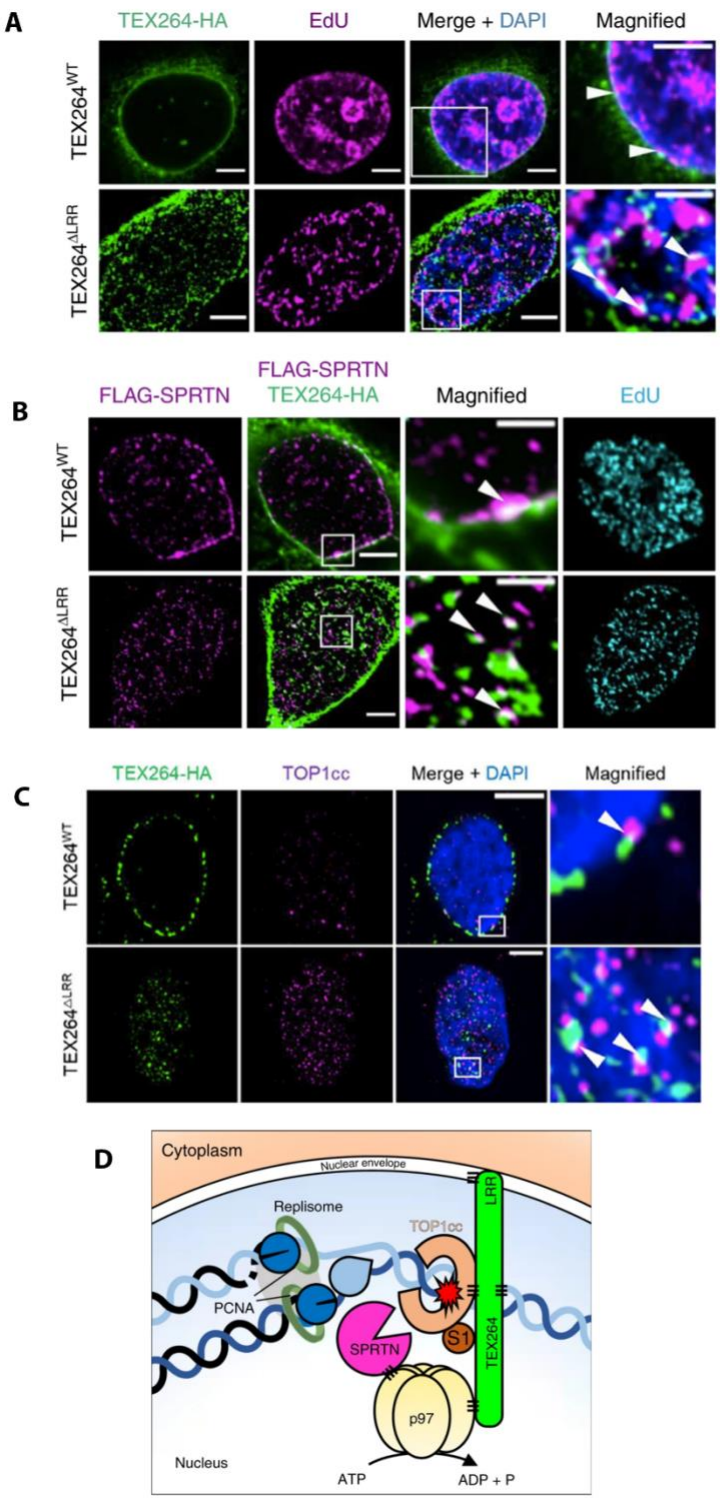


Figure 11. TEX264 functions at the nuclear periphery to recruit p97 to TOP1ccs

(**A**) Confocal immunofluorescent images of U2OS cells expressing TEX264^{WT}-HA and TEX264$^{\Delta LRR}$-HA, the latter being deconvolved images. Sites of replication activity were stained by EdU using a Click-iT reaction. Arrows point to presence of co-localisations, representative images shown, n=3. (**B**) Same as (**A**) but FLAG-SPRTN was expressed alongside TEX264-HA, n=3. (**C**) Same as (**A**) but TOP1cc was stained for and imaged alongside TEX264-HA expression, n=3. (**D**) Model of proposed complex of p97-TEX264-SPRTN which repairs TOP1ccs in replisome dependent manner, image taken from (Fielden et al., 2020).

3.1.2. p97 is a DNA damage signalling protein

In addition to direct lesion repair (TOP1ccs), p97 can also regulate DNA damage signalling by unfolding and releasing important signal transducers from chromatin (Meerang et al., 2011; Stach & Freemont, 2017; van den Boom & Meyer, 2018). DSBs are the most deleterious DNA lesion, formed as a result of wide range of chemotherapies from ionising radiation to irinotecan. The repair of DSBs is a process whereby efficient repair requires post-translation modifications (such as PARylation, ubiquitination and phosphorylation) and repair proteins to be coordinated (Khanna & Jackson, 2001). p97 regulates this process through its ability to unfold ubiquitinated substrates in a timely fashion to facilitate removal of signalling factors (Torrecilla et al., 2017).

Work by Singh and Oehler from our laboratory identified that p97 forms a novel complex with the DUB Ataxin-3 (ATXN3) and regulates DSB break repair (Singh et al., 2019). It does this by regulating the stability and association of the E3 ubiquitin ligase, RNF8, at DSBs (Acs et al., 2011; Meerang et al., 2011; Singh et al., 2019). RNF8 is one of the major signal transducers in DSB repair, where it ubiquitylates histones which ultimately recruits repair proteins such as BRCA1 and 53BP1. Using laser-stripe irradiation to generate DNA damage, we observed by immunofluorescence microscopy, increased RNF8 retention at lesion sites when either p97 and Ataxin-3 were depleted by siRNA or in ATX3-knock out cells (Figure 12A-C , KO data not shown). This occurred as RNF8 was retained for longer at damage sites due to misregulation of RNF8 ubiquitination levels (data not shown here) (Singh et al., 2019).

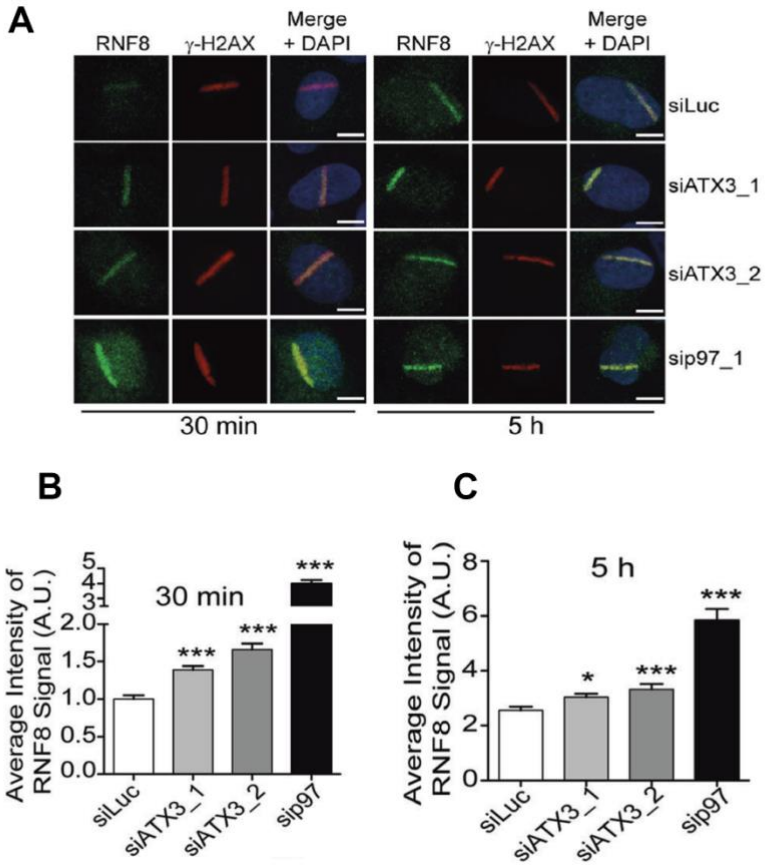


Figure 12. p97 regulates RNF8 E3 ubiquitin ligase at DSB sites (i)

(**A**) Representative microscopy images of UV-A laser stripes inducing DNA damage. RNF8 and γH2AX were stained for and observed in cells depleted of ATX3 and p97. (**B**) and (**C**) Quantification of (**A**), (*** $P < 0.001$; unpaired t-test, n = 3, mean ± SEM, on average, at least 70 nuclei per condition and experiment). Judith Oehler performed this experiment.

To gain a more accurate and *in vivo* understanding of the functional interaction between p97, Ataxin-3 and RNF8, I established a live imaging approach using a two photon laser to generate DNA damage. Recruitment of eGFP tagged proteins of interest to laser spots was then monitored. To first validate this method, we monitored the recruitment of one of the first DDR signalling proteins to be recruited to damage sites, PARP1 (Ray Chaudhuri & Nussenzweig, 2017). Stably expressed PARP1-WT-GFP was recruited to laser spots (Figure 13A, B), whereas deletion of 119K120S amino acid residues in the second zinc-finger (ZnF2) of PARP1, abolishing PARP1 DNA-binding ($PARP1^{KS}$ mutant), prevented PARP1 recruitment to laser spots (Pettitt et al., 2018).

Having validated this live-imaging method, we tested whether the p97-ATXN3 complex had an effect on RNF8 at DNA damage sites. Using CB5083, an ATPase inhibitor of p97, we found that in line with previous methods, RNF8-GFP was retained at DNA damage sites more strongly after p97 inhibition (Figure 13C).

p97 functions in complex with its cofactors, of which NPL4 and UFD1 are accepted to be its “core” cofactors (Meyer et al., 2012; van den Boom & Meyer, 2018). However, when NPL4, UFD1 and Ataxin3 was depleted, only Ataxin3 caused increased RNF8 retention (Figure 13D). This result suggests the existence of an independent p97-ATXN3 complex capable of regulating DSB repair (Singh et al., 2019). Through this work, we gained an additional understanding of how p97 can function via its enzymatic cofactors to modulate ubiquitinated substrates in DNA damage signalling.

In summary, in this chapter we showed previously unknown functions of p97, namely its role in directly repairing DNA lesions (TOP1ccs via its cofactor TEX264) (Fielden et al., 2020) and also signalling for the repair of lesions (DSBs via the DUB Ataxin-3) (Singh et al., 2019). Importantly, by revealing these mechanisms of p97 function in DNA damage response, we are able to make hypothesis-driven approaches to exploring chemotherapeutic options involving p97.

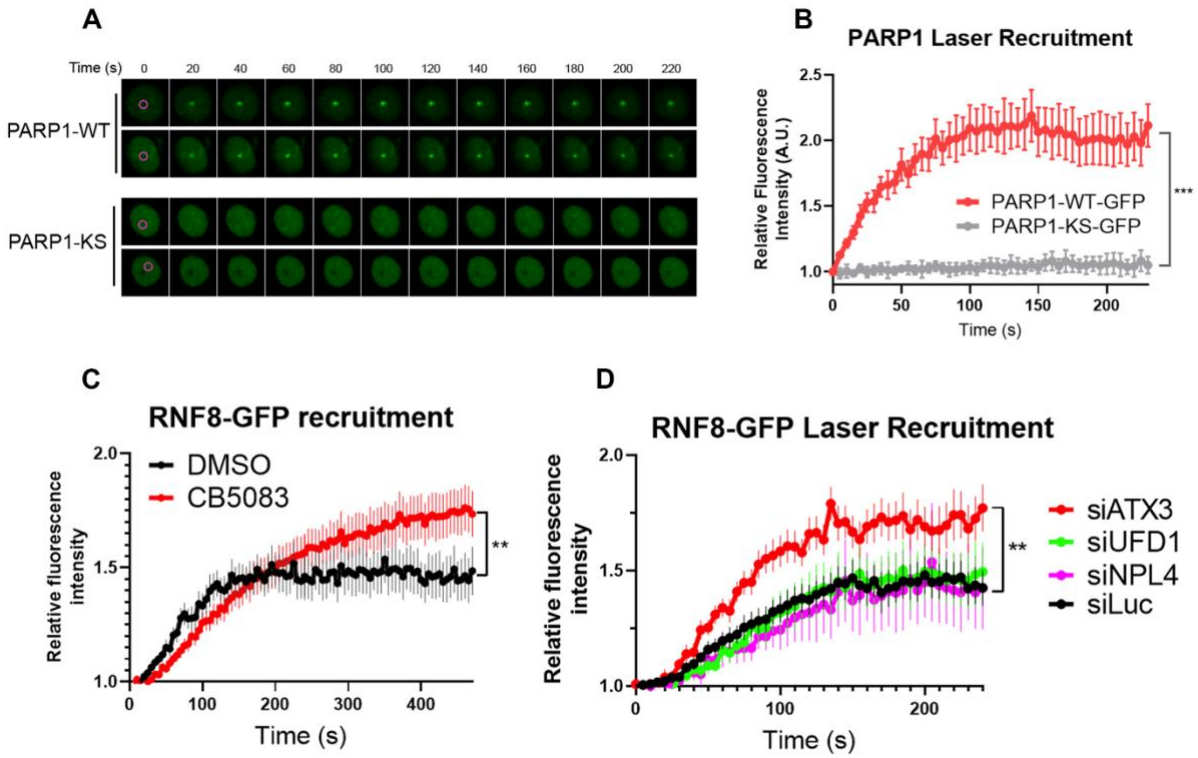


Figure 13. p97 regulates RNF8 E3 ubiquitin ligase at DSB sites (ii)

(**A**) Representative live-imaging confocal micrographs of two-photon (Mai Tai laser) micro-irradiation dots, inducing DNA damage in CAL51 cells and showing stably expressed PARP1-eGFP recruitment to lesion sites. (**B**) Quantification of (**A**) (*** P<0.001, unpaired t-test of area under curve, n=2, mean ± SEM, 8+ cells taken for each experiment). (**C**) Graph of RNF8-GFP recruitment to two-photon-induced DNA damage at micro-irradiation dots, quantified by live-imaging confocal microscopy. U2OS RNF8-GFP dox-inducible (24 hours dox induction) cells were treated with 10uM DMSO or CB5083 for 4 hours before acquisition of live-images. (** P<0.01, unpaired t-test of area under curve, n=3, mean ± SEM, 8+ cells taken for each experiment). (**D**) Similar to (**C**) but cells were depleted of ATX3, UFD1 and NPL4 by siRNA before RNF8-GFP recruitment to lesion sites was monitored, n=3.

3.2. Identifying the trapped PARP1 repair pathway

The DNA damage repair protein PARP1 is the target of PARP inhibitors which demonstrate exquisite sensitivity in HR-deficient cancers (Bryant et al., 2005; Farmer et al., 2005). We now know that PARPis trap PARP1 protein itself onto chromatin, forming a DPC-like DNA lesion (Murai et al., 2012; Stingele et al., 2017). This lead us to explore the possibility that like TOP1ccs, trapped PARP1 as a DPC-like protein, could be directly unfolded and repaired by p97. Preliminary data in the lab had previously shown that the p97-cofactor and DPC repair protease, SPRTN, could effectively cleave PARP1 *in vitro* (data not shown). To explore this interaction, we began a fruitful collaboration with the Chris Lord Lab and utilised mass spectrometric approaches to identify interaction partners of trapped PARP1.

3.2.1. Mass spectrometric analysis of trapped PARP1 protein interactions

To ascertain whether cells have a physiological repair pathway for PARPi-induced trapped PARP1, Dragomir Krastev from the Chris Lord Lab undertook two orthogonal mass spectrometry approaches to identify interaction partners of PARP1 upon PARPi treatment: (i) Rapid Immunoprecipitation Mass spectrometry of Endogenous proteins (RIME) (Mohammed et al., 2016) and (ii) *in vivo* Apex2 peroxidase-mediated labelling of proximal proteins (Hung et al., 2016) (Figure 14A). For both approaches, stable cell lines were firstly generated from a PARP1$^{-/-}$ CAL51 breast cancer cell line.

For RIME, constitutively expressing constructs containing PARP1^{WT} and PARP1^{KS} (PARP1 trapping defective mutant with deletion of 119K120S in ZnF2 of PARP1) tagged with eGFP were inserted into PARP1$^{-/-}$ CAL51 cells. PARP1$^{-/-}$ CAL51 cells are resistant to PARPi due to the lack of PARP1 trapping (Pettitt et al., 2018). Single-cell cloning produced cell lines which demonstrated regained sensitivity to PARPi in PARP1^{WT}-eGFP expressing cells and resistance to PARPi in PARP1^{KS}-eGFP expressing cells (Figure 14B, C).

For the proximity-labelling approach, an insertion of a construct expressing $PARP1^{WT}$ with Apex2 peroxidase and eGFP attached to PARP1's C terminus was similarly selected for from single cell clones and obtained. The $PARP1^{WT}$-APEX2-eGFP cell line also rescued PARPi sensitivity that was previously absent in the $PARP1^{-/-}$ CAL51 cell line (Figure 14B, C). To validate efforts in creating a functional PARP1 protein fusion protein with Apex2, live-imaging microirradiation was used to observe PARP1-APEX2-eGFP recruitment and PAR generation at DNA lesion sites (Figure 14D). Strong PARP1-APEX2-eGFP recruitment upon UV microirradiation and importantly, trapping of the fusion protein upon talazoparib treatment was observed (red line, indicating increased retention at lesion sites). Using the PAR-binding PBZ-mRuby2 probe (Krastev et al., 2018), PARP1-APEX2-eGFP also faithfully generated PAR chains at lesion sites, an event abolished by talazoparib (Figure 14D).

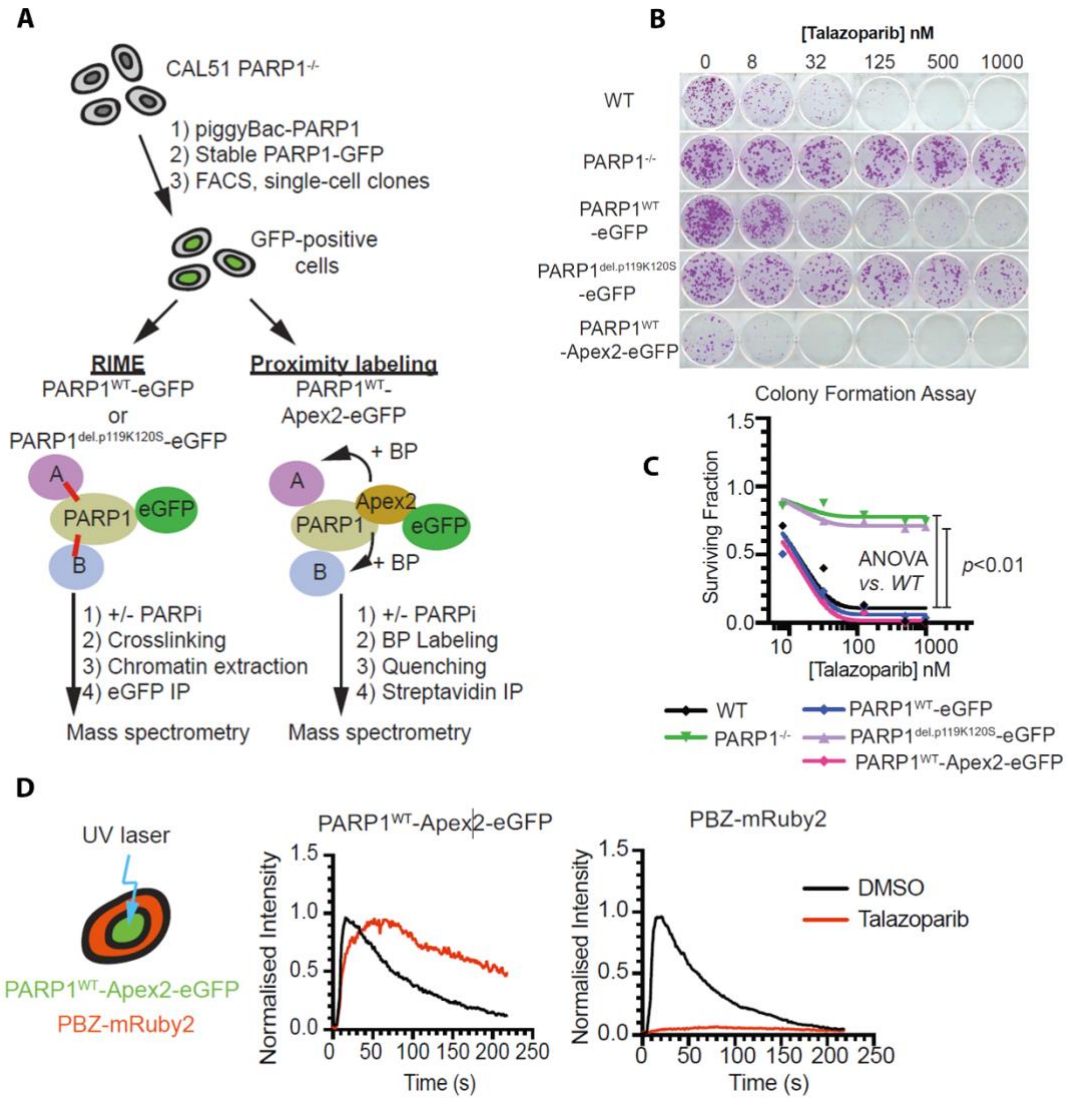


Figure 14. Generating and validating model cell lines for trapped PARP1 mass spectrometry

(A) Schematic showing the full protocol for cell line generation and the following orthogonal mass spectrometry approaches taken, more details in Methods section. (**B**) Images of fixed colonies from a clonogenic assay of various stated CAL51 cell lines. Cells were exposed to talazoparib for 14 days and then colonies quantified. (**C**) Quantified data from (**B**) ($p<0.01$, one-way ANOVA, n=2). (**D**) Left: Schematic of live imaging experiment performed to monitor PARP1^{WT}-Apex2-eGFP recruitment to UV laser sites. Middle: Graph of PARP1^{WT}-Apex2-eGFP recruitment to laser sites, quantified by confocal live-imaging microscopy, cells treated with 100nM talazoparib 1 hour prior and during image acquisition. Right: Same as middle except PBZ-mRuby2 was expressed and recruitment monitored to assess PARylation at DNA lesion sites in CAL51 PARP1^{WT}-Apex2-eGFP expressing cell lines, n=2. Experiments (**A**-**D**) were performed by Dragomir Krastev.

With the validated cell lines, Dragomir moved on to identifying protein interactions with trapped PARP1. He first used the RIME approach on untreated cells and cells treated with the DNA damaging agent methyl methanesulfonate (MMS) to generate PARP1 binding sites and the PARPi, talazoparib, to trap PARP1 at the generated DNA lesions. This treatment condition is commonly used to create the trapping conditions for PARP1 (Michelena et al., 2018; Murai et al., 2012). Formaldehyde was then used to stabilise and crosslink protein-protein interactions and the chromatin fraction was separated and subject to immunoprecipitation using GFP-trap beads (which contain high-affinity nanobodies for GFP). The pulldown-products were then analysed by mass spectrometry. As a control for non-specific binding to GFP-TRAP beads, PARP1$^{-/-}$ CAL51 cells were subjected to the same protocol, and identified proteins from this condition were removed from the final analyses of PARP1^{WT}-eGFP and PARP1^{KS}-eGFP expressing cell lines.

The analysis identified 50 interaction partners for wild-type PARP1, and 144 interaction partners for PARP1^{KS}. MS score was used (a combination score representing peptide abundance and quality of identification) and the enrichment ratio of peptide spectrum matches (PSM) in MMS + talazoparib-treated vs untreated cells to identify proteins for biochemical validation (Figure 15A, B). As a proof of the experimental protocol, upon MMS + talazoparib treatment, there was a PSM enrichment ratio of PARP1 in PARP1^{WT}-eGFP expressing cells of 2.5 (Figure 15A). In cells expressing the trapping mutant PARP1^{KS}, the enrichment ratio was only 1.1 (Figure 15B). Interestingly, even though PARP1^{KS} is not able to be trapped at DNA lesion sites by talazoparib, it still interacted with chromatin-associated proteins such as the cohesion complex subunit PDS5A and the chromatin remodeler CHD4 (Figure 15A, B). This suggests PARP1^{KS} still is able to retain some of its chromatin binding functions. Importantly, it was evident that only PARP1^{WT} demonstrated increased interaction with the family of small ubiquitin-like modifiers, SUMO1 and SUMO2 upon MMS + talazoparib treatment (Figure 15A). As this was not observed in PARP1^{KS} cells, it represents a possible post-translational modification that only occurs upon PARP1 trapping on chromatin.

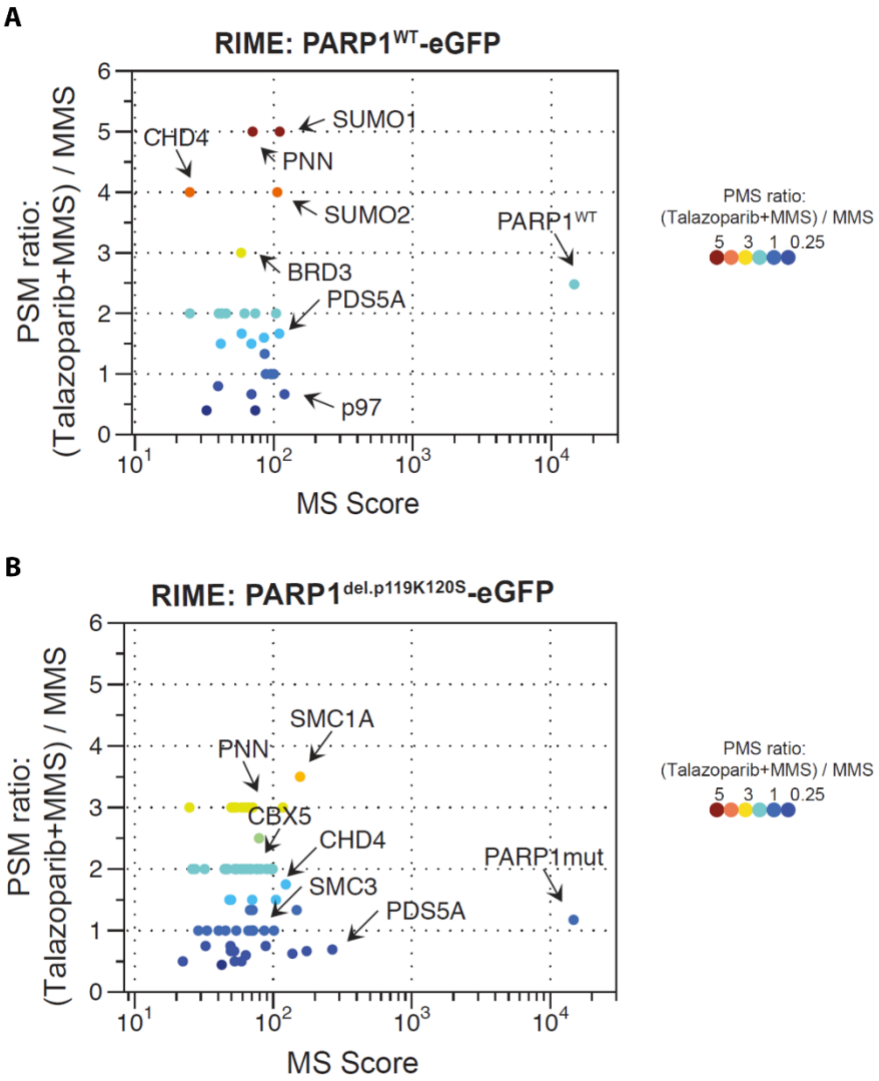


Figure 15. RIME mass spectrometry approaches identifies trapped PARP1 interaction partners

(**A**) and (**B**), Scatter plots of PARP1 interactions for PARP1^{WT}-eGFP and PARP1$^{del.p119K120S}$-eGFP (PARP1^{KS}) respectively. Interactions were assessed by plotting PSM ratio (treatment/untreated) against MS Score – see Methods. Experiments (**A**-**B**) were performed by Dragomir Krastev.

In the orthogonal proteomics approach, PARP1^{WT}-APEX2-eGFP fusion protein was used to proximity-label interaction partners of PARP1. Apex2 is a peroxidase which in the presence of biotin-phenol and hydrogen peroxide (H_2O_2) generates highly reactive biotin-phenol radicals (Figure 16A). These radicals then label proteins within ~20nm with biotin, and labelled proteins can then be purified via streptavidin-binding. Similar to RIME, samples of cells expressing PARP1^{WT}-APEX2-eGFP were either untreated or treated with MMS + talazoparib and then analysed by mass spectrometry. To identify non-specific background interactions with the streptavidin beads, a negative control of cells lacking the Apex2 fusion protein and only expressing PARP1^{WT}-eGFP was also analysed in parallel. These identified hits were then removed from further analysis.

The identified proteins from the proximity-labelling approach were plotted based on PSM enrichment ratio versus MS score (Figure 16A). The most abundant proteins identified included PARP1, UBA1, p97, while proteins which were heavily enriched upon MMS + talazoparib treatment such as USP7 and FUS were detected at low abundance (MS score). This is made evident when PSM (from treated cells) of the identified proteins were plotted against their MS score (Figure 16B). Unfortunately, PARP1^{KS}-Apex2-eGFP expressing cells were unable to be obtained to perform identical analysis to the RIME mass spectrometry approach. Thus MS score was prioritised over PSM ratio for *bona fide* PARP1 interactors, as the low abundance of peptides seen for USP7 and FUS likely lead to the high enrichment ratios observed from their PSM scores and thus do not represent relevant interactions.

The identification of ubiquitin-like modifier-activating enzyme 1 (UBA1) and the ubiquitin dependent segregase/unfoldase p97 as trapped PARP1 associated proteins (Figure 16A), suggested that ubiquitin-mediated degradation of trapped PARP1 is a possible conclusion to trapped PARP1 induction by PARPi. Indeed, in addition to p97's role in DDR shown above, UBA1, has also been shown to be involved in DDR pathways (Moudry et al., 2012). To test this hypothesis, we first asked whether PARP1 is post-translationally modified by ubiquitin.

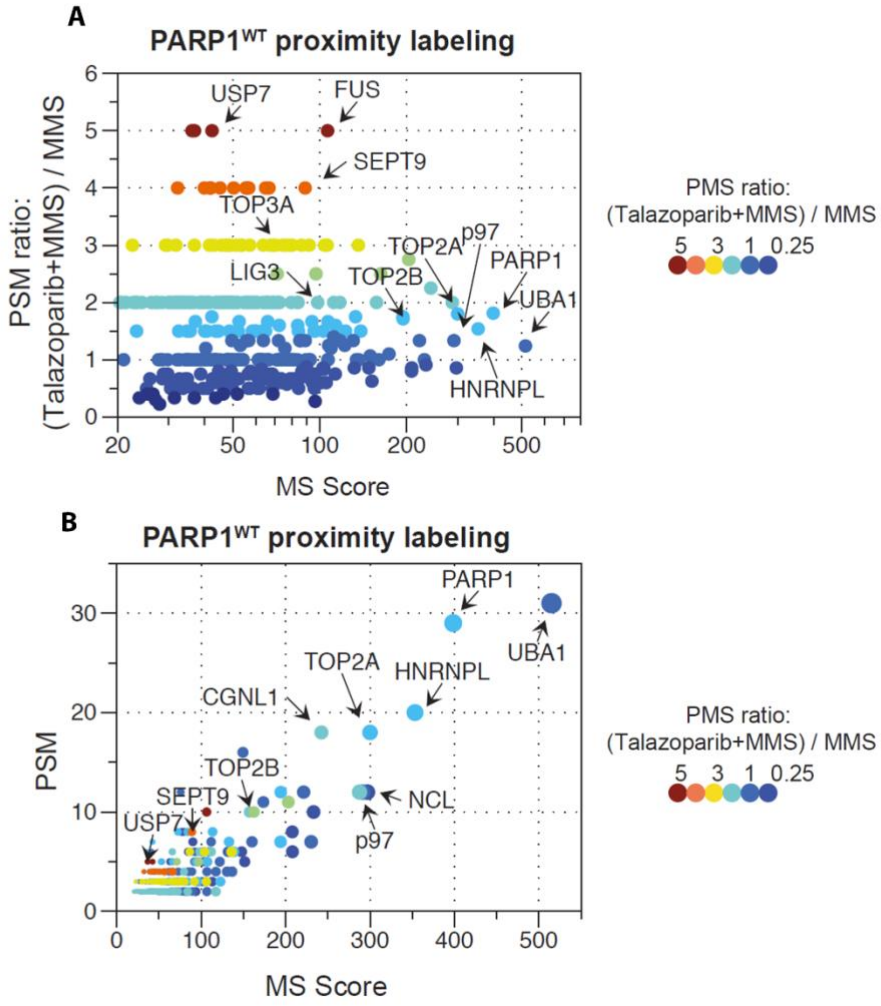


Figure 16. Apex2-mediated proximity-labelling mass spectrometry approach identifies trapped PARP1 interaction partners

(**A**) Graph of PARP1 interactions identified for PARP1^{WT}-Apex2-eGFP cells after proximity-labelling and immunoprecipitation of biotinylated proteins, hits are plotted by PSM ratio vs MS score. (**B**) A graph of PARP1 interactions from PARP1^{WT}-Apex2-eGFP cells where PSM from MMS + talazoparib treated samples is plotted against MS score. Experiments (**A**-**B**) was performed by Dragomir Krastev.

3.2.2. Ubiquitination and SUMOylation of trapped PARP1

To validate whether trapped PARP1 is modified upon trapping by PARPis, HEK293 cells were treated with MMS + talazoparib to induce PARP1 trapping and then cellular fractionation was carried out. This allowed us to separate proteins into chromatin bound and nuclear soluble fractions, from which PARP1 was immunoprecipitated using PARP1-TRAP beads (containing high affinity nanobody for PARP1). Upon western blotting of both cellular fractions, we only observed modified high MW forms of PARP1 in the chromatin fraction upon MMS + talazoparib treatment (Figure 17A). This suggests PARP1 is modified when it is trapped at MMS-induced DNA lesions by PARPi.

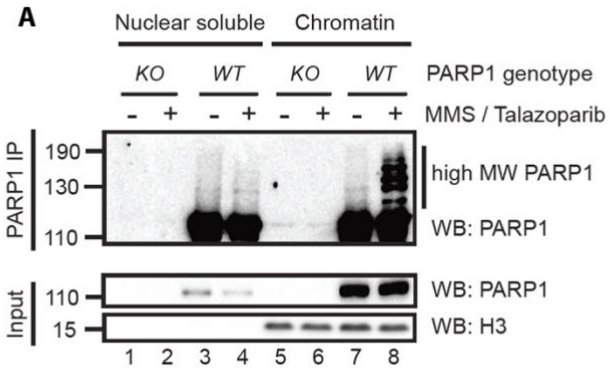


Figure 17. PARP1 forms high MW isoforms upon trapping on chromatin by PARPi.

(**A**) Western blots of an immunoprecipitation experiment where HEK293 WT and PARP$^{-/-}$ cells were treated with 0.01% MMS + 100nM talazoparib for 2 hours and cells were fractionated into nuclear-soluble and chromatin-bound fractions. Endogenous PARP1 was then pulled down by PARP1-TRAP (Chromotek) beads, representative western blots shown for n=2.

We tested whether these high MW forms of PARP1 represent ubiquitination by performing a immunoprecipitation (IP) under denaturing conditions, where 1% SDS detergent was used in samples post-cell lysis to prevent protein-protein interactions. This enables one to obtain only proteins of interest and probe for post-translational modifications from the IP reaction. To this end, ubiquitin tagged with HA and STREP, UB-STREP-HA, was expressed in HEK293 cells and we carried out a denaturing IP over streptactin beads. From the immunoprecipitated pool of ubiquitinated proteins, PARP1 was then blotted for (Figure 18A). We observed strong bands of ubiquitinated PARP1 only when cells were treated with both MMS and talazoparib (lane 5, Figure 18A). Furthermore, when we used an inhibitor of ubiquitin activating enzymes E1 ligases, MLN-7243 (M. et al., 2014), we were able to almost completely abrogate the formation of these high MW forms of PARP1 (Figure 18A).

To verify that PARP1 ubiquitination is truly PARPi-induced trapping-dependent, we utilised veliparib; veliparib has similar PARP1 catalytic inhibition effectiveness to talazoparib but considerably lower PARP1 trapping potency (Pommier & Murai, 2015). We also used an analogue of veliparib, UKT115, which was engineered to have strong PARP1 trapping ability (Zandarashvili et al., 2020). Using these PARPis, we observed that only the PARPis capable of strong PARP1 trapping, talazoparib and UKT115, were capable of causing PARP1 ubiquitination in the chromatin fraction (lane 3 and 7, Figure 18B). These results show that upon DNA damage and PARPi treatment, PARP1 is ubiquitinated on the chromatin.

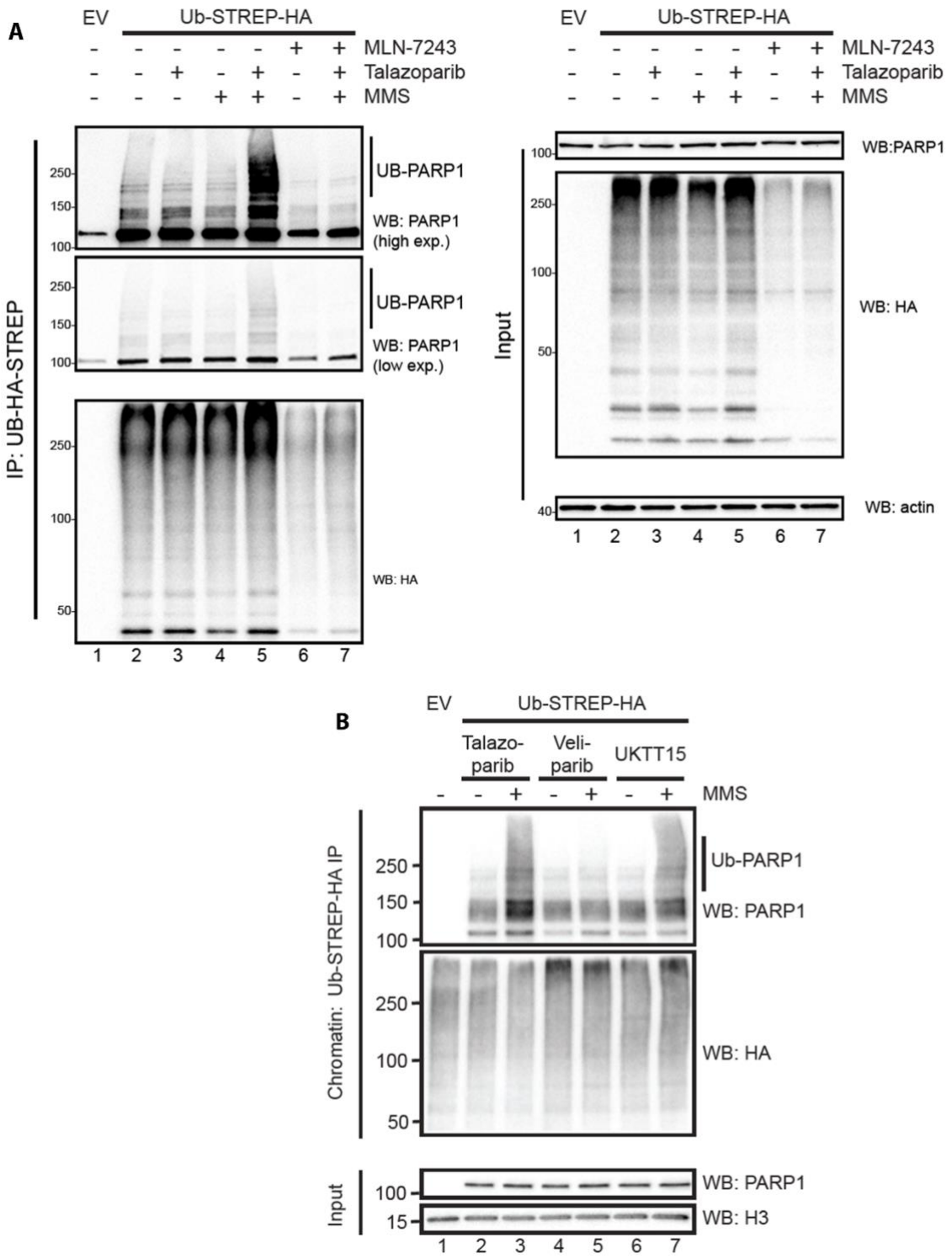


Figure 18. Trapped PARP1 is modified by ubiquitin on chromatin.

(**A**) Western blots of HEK293 immunoprecipitates under denaturing conditions (1% SDS). Cells were transfected with either UB-STREP-HA or empty vector (EV) control for 24 hours and treated with 0.01% MMS + 100nM talazoparib and 5uM MLN-7243 as stated for 2 hrs. Streptactin beads were used to pull down ubiquitinated pool of proteins, representative experiment shown, n=3. (**B**) Western blots of immunoprecipitates from HEK293 cells transfected with UB-STREP-HA and treated with 0.01% MMS and either 100nM talazoparib, 10uM veliparib or 10uM UKTT15. Streptactin beads were used to isolate ubiquitinated pool of proteins from the chromatin-bound fraction, representative experiment shown, n=2.

In addition to the ubiquitination machinery identified by the proximity-labelling approach using PARP1^{WT}-APEX2-eGFP, we also identified SUMO1 and SUMO2 as PARP1 associated proteins via the RIME experiment. This lead us to explore whether PARP1 is also SUMOylated upon trapping by PARPis.

We employed a similar approach to assessing PARP1 ubiquitination, this time, HA-SUMO2 was expressed in HEK293 cells and the total SUMOylated pool of proteins was immunoprecipitated under denaturing conditions. We chose SUMO2 as it appeared in our RIME mass spectrometry analysis of interacting proteins and also of previously identified interactions with PARP1 (Martin et al., 2009). Blotting for PARP1 revealed that, identically to ubiquitination, PARP1 is only SUMOylated when treated with MMS and talazoparib (Figure 19A). We also noticed that MMS treatment alone triggered SUMO2 depletion from the cell extract (lane 4, Figure 19A) and caused observable PARP1 SUMOylation when the western blot was subject to high exposure (red arrows, Figure 19A). The depletion of cellular SUMO pools upon MMS has been previously observed (Hendriks et al., 2015) and is discussed later.

In collaboration with the Yves Pommier lab, Yilun Sun tested for whether PIAS4 is the E3 SUMO-ligase responsible for trapped PARP1 SUMOylation, as it was previously shown that upon heat-shock PARP1 is modified by PIAS4 (Martin et al., 2009). Using HCT116 cells which had a *PIAS4*$^{-/-}$ background, he found that upon PARP1 trapping, there was only a minimal increase in PARP1 SUMOylation compared to WT cells which showed robust PARP1 SUMOylation upon trapping (Figure 19B).

From these experiments, we show that trapped PARP1 is both SUMOylated by PIAS4 and ubiquitinated.

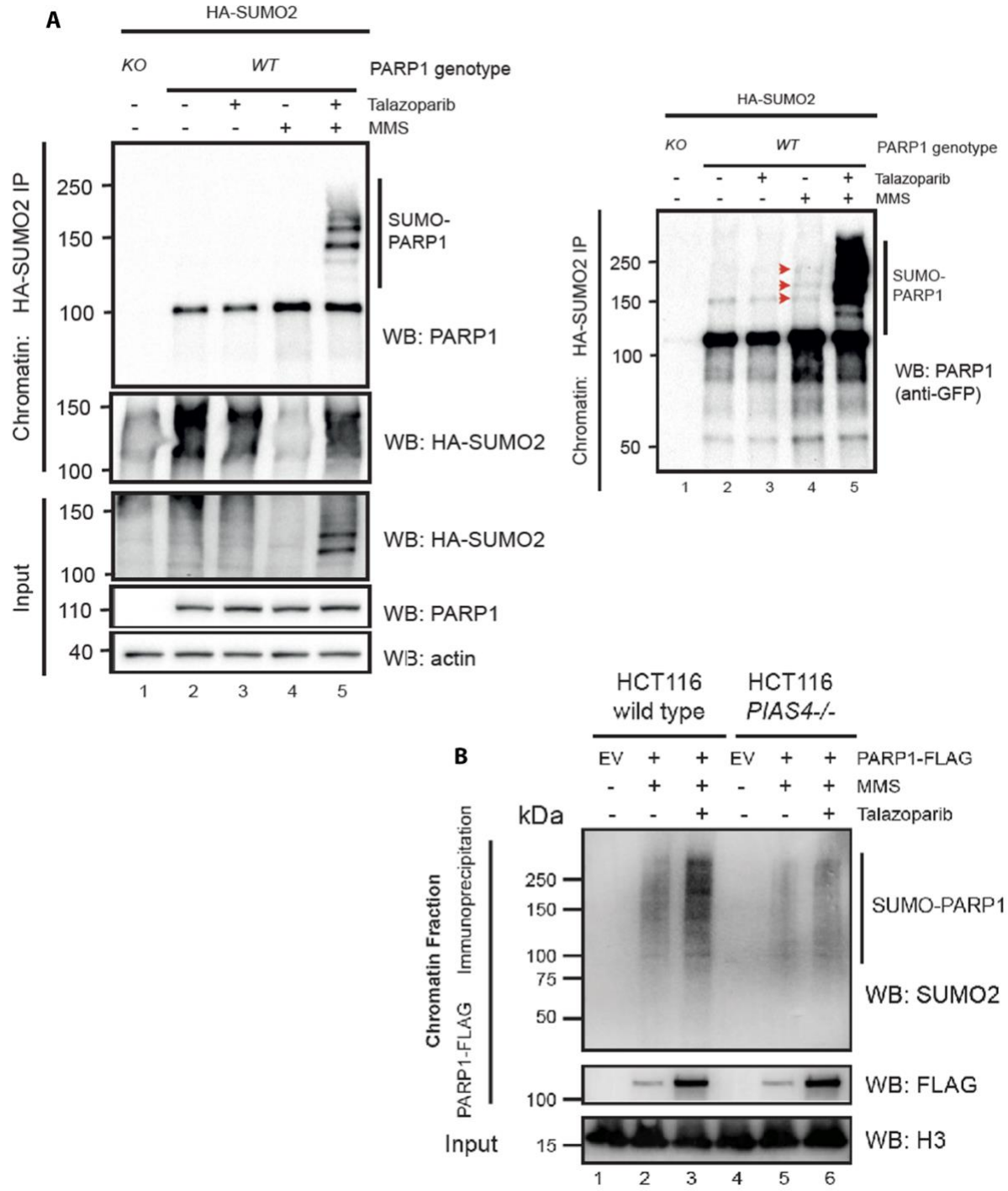


Figure 19. Trapped PARP1 is modified by SUMOylation

(A) Western blots of immunoprecipitates from HEK293 cells expressing HA-SUMO2. HA-affinity beads (Pierce) were used to isolated SUMOylated proteins from the chromatin bound fraction. Cells were treated with 0.01% MMS and 100nM talazoparib as stated then harvested. Right: high exposure blot of PARP1-SUMOylation, red arrows indicate high MW SUMOylated PARP1 species present in MMS treatment alone, representative experiment shown, n=3. (**B**) WT and PIAS4$^{-/-}$ HCT116 cells were transfected with PARP1-FLAG and pulled down under denaturing conditions with FLAG beads from the chromatin fraction. 0.01% MMS and 100nM talazoparib were used in combinations stated for treatment before harvesting and blotting, (**B**) was performed by Yilun Sun.

We then tested to see if there was any cross-talk between trapped PARP1 SUMOylation and ubiquitination, to do this we used the ubiquitin E1 activating enzyme inhibitor MLN7243 and the SUMO activating enzyme inhibitor ML-792 (He et al., 2017).

Using HEK293 cells, we isolated the ubiquitinated pool of proteins after treatment with MMS + talazoparib alongside concurrent treatment with ML-7243 and ML-792. We discovered that inhibition of SUMOylation also lead to a decrease in high MW forms of ubiquitinated PARP1 (Lane 4, Figure 20A).

In the case of PARP1 SUMOylation, we found inhibiting ubiquitination of PARP1 had no effect on SUMOylated trapped PARP1 (lane 5, Figure 20B). This demonstrates that PARP1 ubiquitination is dependent on its SUMOylation however its SUMOylation is independent of its ubiquitination state.

The nature of this cross-talk pointed towards the function of an E3 SUMO-targeted ubiquitin ligase (STUbL) (Prudden et al., 2007), of which two have so far been identified, RNF4 and RNF111 (Poulsen et al., 2013). As RNF4 has previously been identified to be a component of DDR and has also been shown to target PARP1 in relation to PARP1's transcriptional roles (Martin et al., 2009), we tested for RNF4 interaction with PARP1. When we immunoprecipitated PARP1 under native conditions, we observed increased interaction with RNF4 upon treatment with MMS + talazoparib (Figure 20B). This interaction was abrogated when SUMOylation was inhibited by ML-792 and stabilised when ubiquitination was inhibited by ML-7243, indicative of a STUbL-substrate interaction.

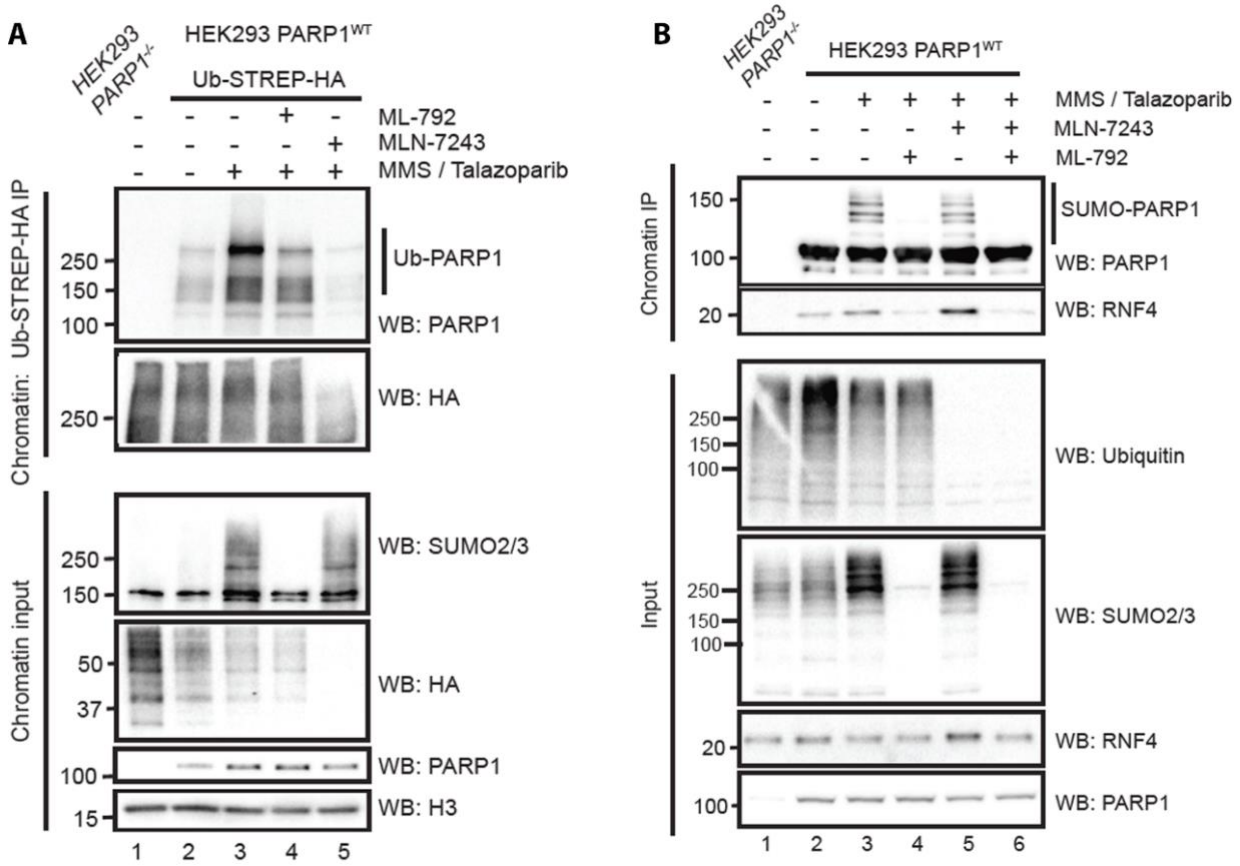


Figure 20. SUMOylation triggers ubiquitination of trapped PARP1 and recruits RNF4

(**A**) Western blots of immunoprecipitates from HEK293 WT and PARP1$^{-/-}$ cells expressing UB-STREP-HA, streptactin beads were used isolate ubiquitinated pool of proteins from denatured samples as before. Cells were treated for 2 hours with 0.01% MMS + 100nM talazoparib, 5uM MLN-7243 and 1uM ML-792 as stated and harvested via cellular fractionation into chromatin-bound fractions, from which the immunoprecipitation step was performed, representative experiment shown, n=3. (**B**) Western blots of co-immunoprecipitation experiment performed at native conditions to reveal PARP1^{WT} interactions. HEK293 cells were treated as in (**A**) and fractionated into chromatin-bound fractions, from which PARP1-TRAP beads were employed to pulldown endogenous PARP1. PARP1 interactions with RNF4 were probed and blotting for PARP1 revealed high MW modifications which were abrogated by SUMO E1 inhibition, suggesting these observed bands (labelled as SUMO-PARP1) are SUMOylated species of trapped PARP1, representative experiment shown, n=2.

3.2.3. RNF4 ubiquitinates trapped PARP1

To test that RNF4 is the E3 ubiquitin ligase which modifies trapped PARP1, we depleted RNF4 using two different siRNA approaches. One of these targeted its 5'UTR and another was a SMARTpool of 4 different siRNAs against RNF4. Then, similarly to above experiments, the ubiquitinated pool of proteins was immunoprecipitated under denaturing conditions. Using this method we observed a strong reduction of ubiquitinated PARP1 when RNF4 was depleted (Figure 21A).

We also tested whether the only alternative STUbL, RNF111, could contribute to PARP1 ubiquitination. Using the same experimental setup, we depleted RNF4 and RNF111 and assayed for PARP1 ubiquitination under PARP1 trapping conditions. We again observed RNF4 contribution to trapped PARP1 ubiquitination. We also observed that when depleted alone, RNF111 did not decrease PARP1 ubiquitination (lane 6, Figure 21B). However, there was a slight additive effect on trapped PARP1 ubiquitination when both STUbLs were depleted when compared to RNF4 alone (lane 8 versus lane 4, Figure 21B). This suggests that RNF111 is not the primary E3 ligase for this reaction when RNF4 is available, but may offer minimal E3 ligase activity on trapped PARP1 when RNF4 is absent. However, we do note that better techniques to cause RNF111 deficiency are needed to confirm this finding.

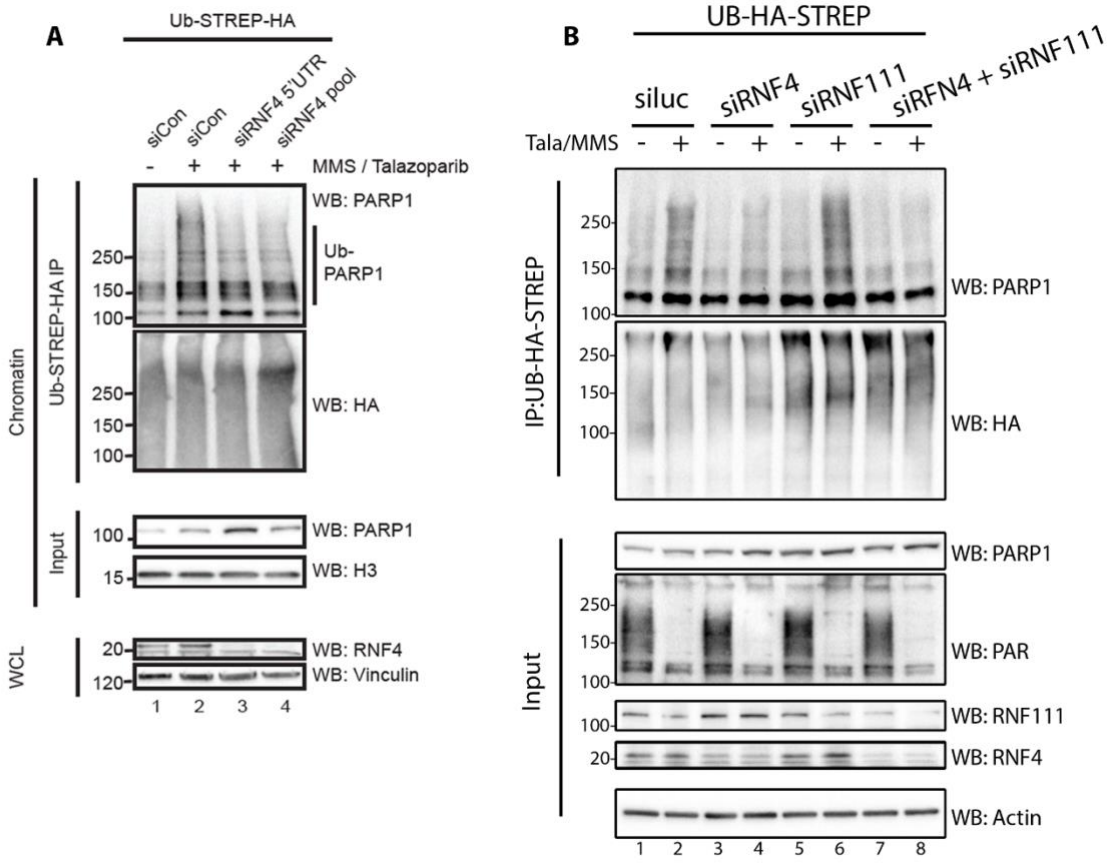


Figure 21. RNF4 siRNA depletion prevents trapped PARP1 ubiquitination

(**A**) Western blots of immunoprecipitates of HEK293 cells expressing UB-STREP-HA and depleted of RNF4 by two different siRNA approaches. Cells were fractionated into chromatin bound proteins and ubiquitinated pool of proteins pulled down under denaturing conditions using Streptactin bead. RNF4 depletion was confirmed in whole cell lysate, representative experiment shown, n=3. (**B**) Same as (**A**), except siRNAs targeting RNF4 and RNF111, were used as labelled, n=3.

To confirm that RNF4 is the primary E3 ligase for trapped PARP1, MCF7 RNF4$^{-/-}$ cell lines were used, a reciprocal IP was performed. PARP1-FLAG was expressed and immunoprecipitated using FLAG beads under denaturing conditions (Figure 22A). Western blots for ubiquitination on PARP1-FLAG immunoprecipitates revealed that PARP1 is more strongly modified under trapping conditions in MCF7 wild type cells when compared to cells in the RNF4$^{-/-}$ background.

We were then able to confirm that RNF4 is a ligase capable of ubiquitinating PARP1 by overexpression of RNF4^{WT} and a dominant negative E2-binding mutant (as RNF4 functions as an obligate dimer), RNF4$^{M136S/R177A}$ (Rojas-Fernandez et al., 2014). We observed a large increase in trapped PARP1 ubiquitination upon overexpression of RNF4^{WT}, whereas overexpression of RNF4$^{M136S/R177A}$ abrogated PARP1 ubiquitination entirely (Figure 22B).

Altogether these results show that upon trapping by talazoparib, trapped PARP1 is SUMOylated and then primarily ubiquitinated by the STUbL RNF4.

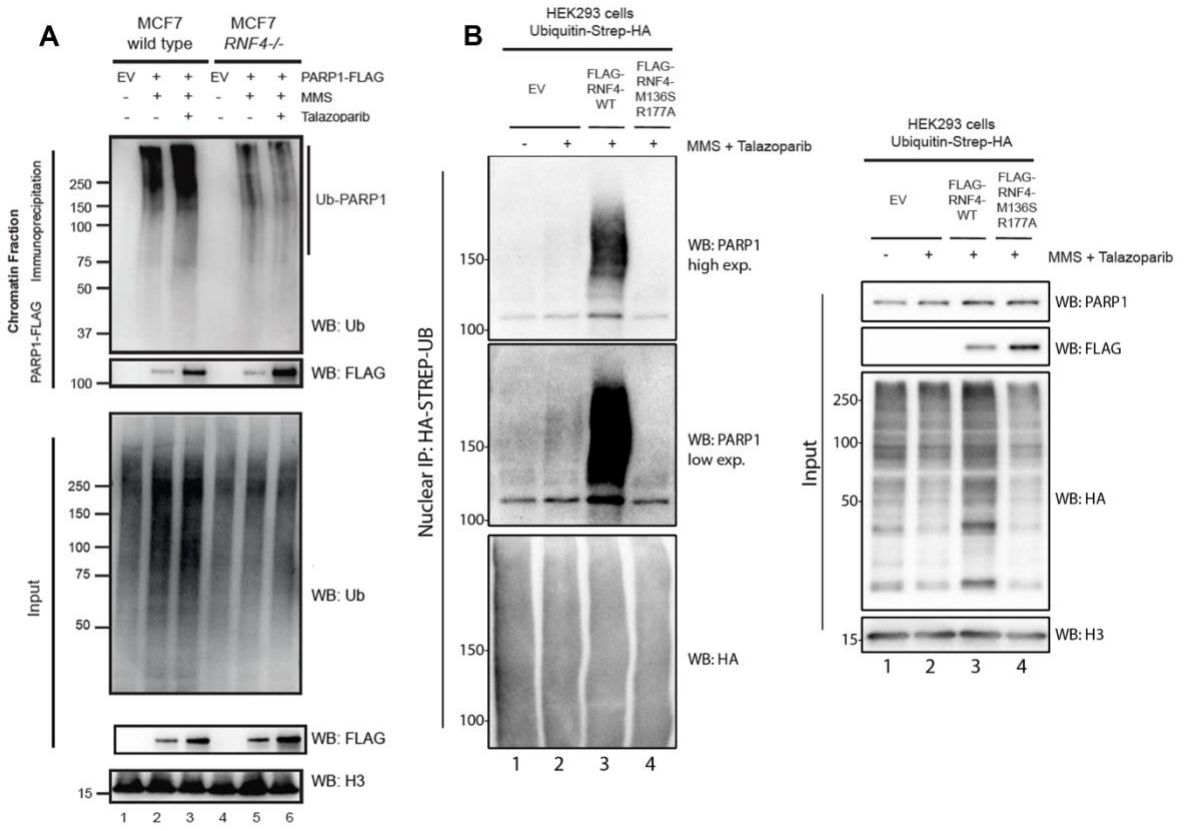


Figure 22. RNF4$^{-/-}$ cells and RNF4 dominant negative mutant confirms E3 ubiquitin ligase activity on trapped PARP1

(**A**) Western blots of immunoprecipitated PARP1-FLAG under denaturing conditions from the chromatin-bound fraction, performed in MCF7 WT and RNF4$^{-/-}$ cells. Cells were treated with 0.01% MMS and 100nM talazoparib for 2 hours in stated combinations prior to harvest, representative experiment shown, n=2. (**B**) Same as (**A**), except no siRNAs was used, instead RNF4-WT and RNF4$^{M136S/R177A}$ (dominant negative E2-binding mutant) were expressed alongside UB-STREP-HA and trapped PARP1 ubiquitination blotted for, n=2. (**A**) was performed by Yilun Sun.

3.2.4. Trapped PARP1 triggers ubiquitin-dependent p97 activity

From our mass spectrometry analysis, the ubiquitin-dependent unfoldase/segregase p97 was identified via both RIME and proximity-labelling approaches as an abundant interaction partner of trapped PARP1. To validate whether p97 interacts with trapped PARP1, we performed a co-IP experiment using CAL51 cell lines stably expressing PARP1^{WT}-eGFP and PARP1^{KS}-eGFP. Under MMS + talazoparib treatment and after cell lysis under native conditions, GFP-trap beads were used to pulldown PARP1 along with its interaction partners. Western blotting firstly revealed that under untreated conditions, cells in the PARP1^{WT}-eGFP background displayed a PARylation signal that was abrogated by talazoparib treatment (lane 2 versus lane 3, Figure 23A). Interestingly in the PARP1^{KS}-eGFP background, there was a lack of PARylation in all conditions. This suggests that the PARP1^{WT}-eGFP PARylation signal seen in lane 2 is likely due to physiological DNA damage signalling dependent on PARP1 binding to lesion sites via its 2nd zinc-finger domain.

Importantly, the interaction between endogenous p97 and PARP1^{WT}-eGFP strongly increased under trapping conditions (Figure 23A). This was not observed with the PARP1^{KS}-eGFP mutant, where the minimal interaction with p97 under untreated conditions remained the same after treatment.

To further confirm the interaction between p97 and PARP1 was dependent on the amount of trapped PARP1, we used the weak PARP1 trapping PARPi, veliparib, and its engineered potent PARP1 trapping analogue UKTT15. We performed a co-IP experiment from the chromatin fraction to probe trapped PARP1-p97 interaction. To observe the interaction in the chromatin fraction, we maintained the samples under 100nM concentration of NaCl and cleaved the DNA via a benzonase reaction rather than sonication (see Methods). We observed that UKTT15 caused the strongest interaction between p97 and PARP1 followed by talazoparib, then veliparib (Figure 23B). This mirrors the known trapping potencies of the three PARPis, suggesting the more trapped PARP1 present, the stronger the interaction between p97 and PARP1.

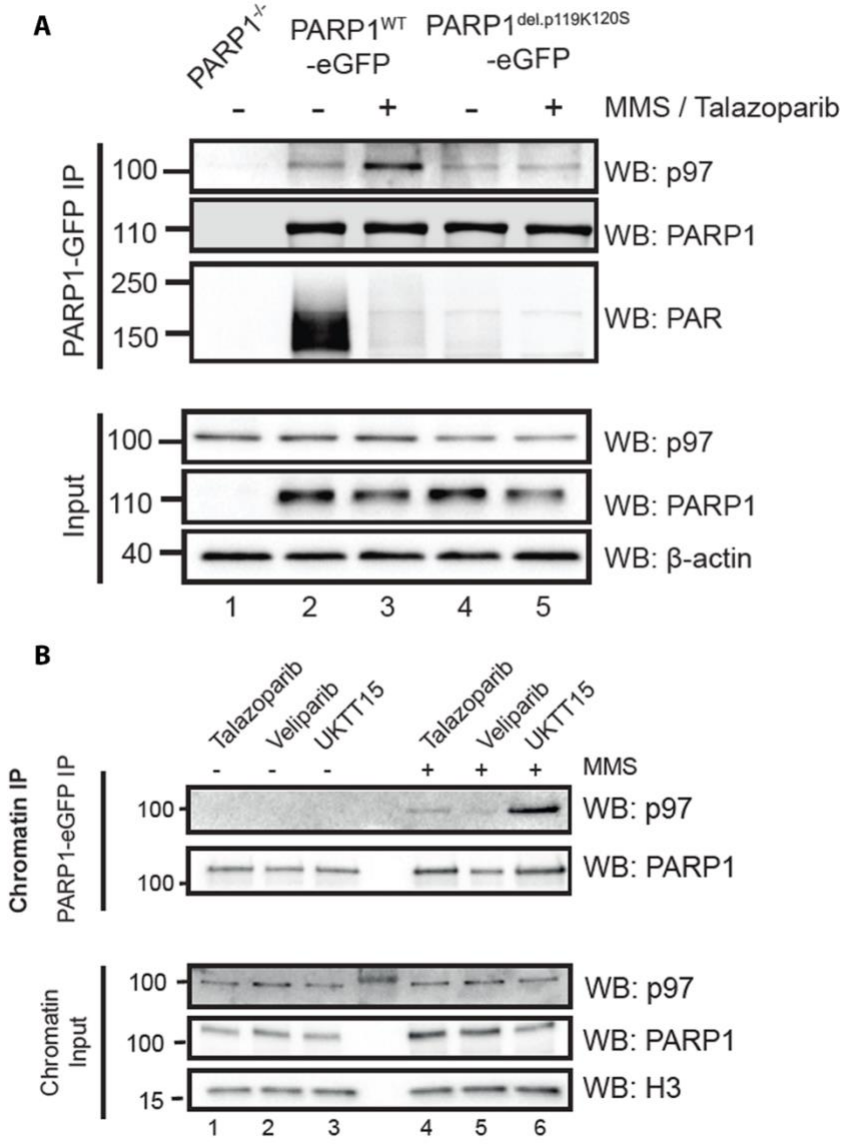


Figure 23. p97 interacts with PARP1 in a trapped PARP1 dependent manner

(**A**) Western blots of immunoprecipitates from CAL51 PARP1$^{-/-}$ cells stably expressing PARP1^{WT}-eGFP and PARP1^{KS}-eGFP. Cells were treated with 0.01% MMS + 100nM talazoparib for 2 hours and harvested. Then PARP1 and its interaction partners were isolated under native conditions using GFP-TRAP beads, representative experiment shown, n=3. (**B**) same as (**A**) except cells were treated with three different PARPis with different abilities to trap PARP1. In order of strongest PARP1 trapper, 10uM UKTT15, 100nM talazoparib and 10uM veliparib were used with 0.01% MMS, representative experiment shown n=2.

We showed above that PARP1 is ubiquitinated upon its trapping on chromatin (Figure 18). We thus asked whether this ubiquitination is the signal which recruits p97 to trapped PARP1. To do this, we used MLN-7243 to prevent ubiquitination processes under trapping conditions and we were able to decrease the interaction between p97 and trapped PARP1 (Figure 24A). Our collaborators were able to confirm this by using proximity ligation assays as an alternative technique. Using antibodies against p97 and PARP1, proximity ligation assays generate a signal when the two antibody targets are in proximity to each other. They first confirmed that PARP1-p97 interaction does indeed increase upon trapping conditions (MMS + talazoparib). Furthermore, by inhibiting both ubiquitination (MLN-7243) and SUMOylation (ML-792), they prevented the interaction between p97 and trapped PARP1 (Figure 24B).

These results demonstrate that trapped PARP1 SUMOylation/ubiquitination acts as the signal which recruits p97 to trapped PARP1. As p97 itself lacks ubiquitin binding domains, to bind to ubiquitinated substrates, p97 requires a binding cofactor to bridge this interaction. We tested the two “core” p97 cofactors which are thought to function as an obligate dimer, NPL4 and UFD1 (Stach & Freemont, 2017). Both of these proteins possess ubiquitin binding domains, however when we depleted them separately using siRNA and performed a co-IP experiment under PARP1 trapping conditions, we found that only UFD1 was required for trapped PARP1-p97 interaction (Figure 24C). This peculiar observation showing delineated functions of the apparent obligate dimer for p97 activity is explored in the discussion section.

In conclusion from our results so far, we show that upon induction of PARP1 trapping, PARP1 is SUMOylated, leading to recruitment of RNF4 which then ubiquitinates trapped PARP1. Trapped PARP1 ubiquitination then sustains its interaction with p97 via its cofactor UFD1.

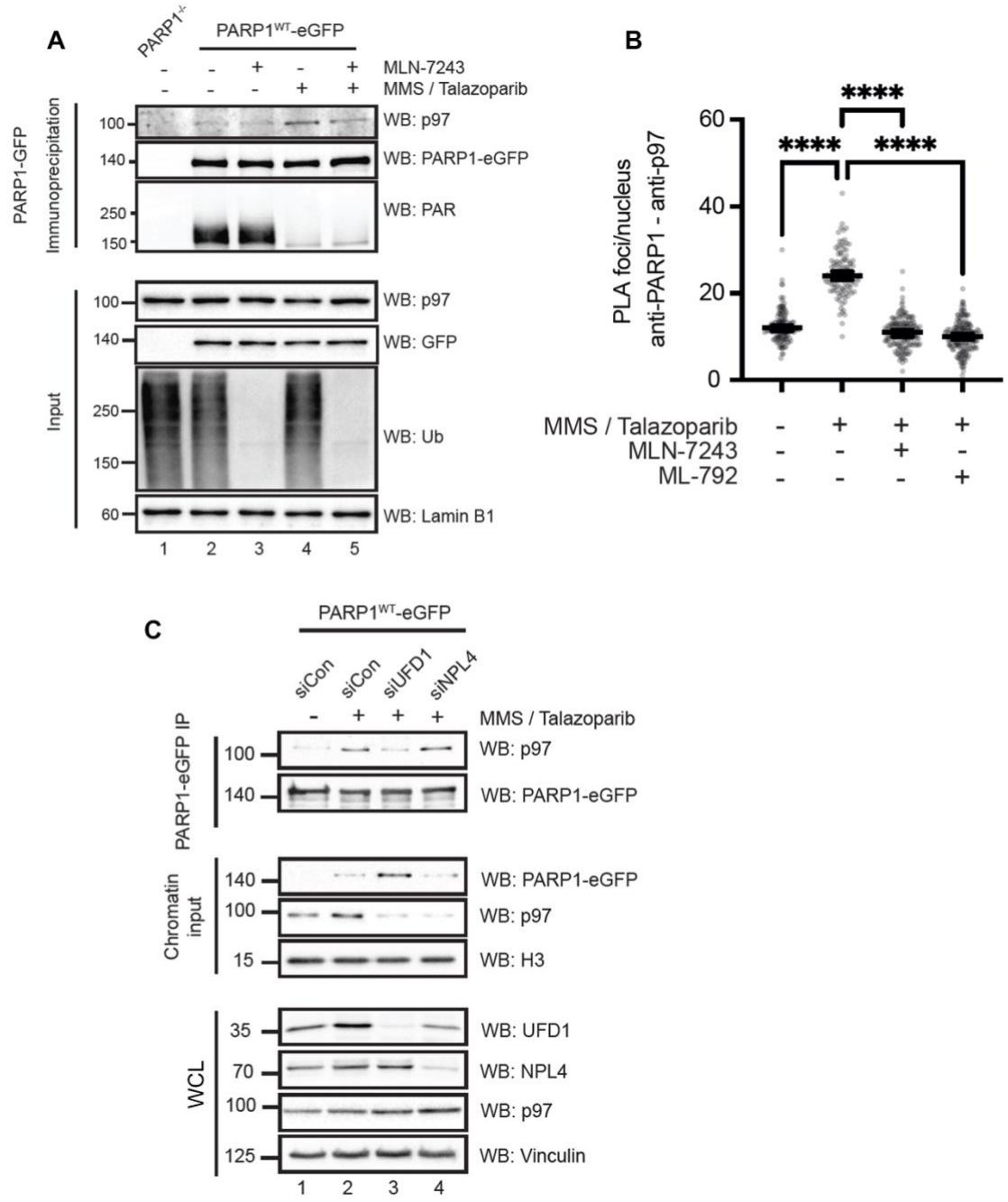


Figure 24. p97 interacts with trapped PARP1 in a ubiquitin/UFD1 dependent manner.

(**A**) Western blots of immunoprecipitates from CAL51 PARP1$^{-/-}$ cells and PARP1^{WT}-eGFP expressing cells. Cells were treated with 0.01% MMS + 100nM talazoparib and 5uM MLN-7243 for 2 hours as labelled. Then PARP1 and its interaction partners were isolated under native conditions using GFP-TRAP beads, representative experiment shown, n=3. (**B**) Graph of results from proximity ligation assay using antibodies against PARP1 and p97 to quantify interaction under combinations of 0.01% MMS + 100nM talazoparib, 5uM MLN-7243 and 1uM ML-792 as labelled, n=2. (**C**) Same as (**A**) except CAL51 cells expressing PARP1^{WT}-eGFP were depleted of UFD1 and NPL4 by siRNA for 3 days then harvested under physiological conditions, n=3. (**B**) was performed by Dragomir Krastev.

In addition to depleting p97 cofactors to modulate p97's activity, small molecule inhibitors such as CB-5083, which directly inhibit p97 ATP binding have been synthesised (Tang et al., 2019). As p97 uses its catalytic ATPase activity to unfold substrates through its central pore, inhibiting this activity causes p97 to increase in its interaction with its substrates, which remains ubiquitinated and folded (van Nguyen et al., 2017). Our collaborators, using PLA with anti-PARP1 and anti-p97 antibodies to detect PARP1-p97 interaction, concurrently treated cells with MMS + talazoparib and the p97 inhibitor CB-5083. They discovered that CB-5083 caused a substrate trapping effect on PARP1-p97 interaction, where interaction increased when compared to MMS + talazoparib treatment alone (Figure 25A, B).

In further support of this, we performed a denaturing IP in HEK293 cells and pulled down the ubiquitinated pool of proteins. We found that CB-5083 treatment with MMS + talazoparib also caused an accumulation of ubiquitinated trapped PARP1 when compared with MMS + talazoparib treatment alone (Figure 25C). This suggests that p97 is involved with the processing/unfolding of ubiquitinated trapped PARP1.

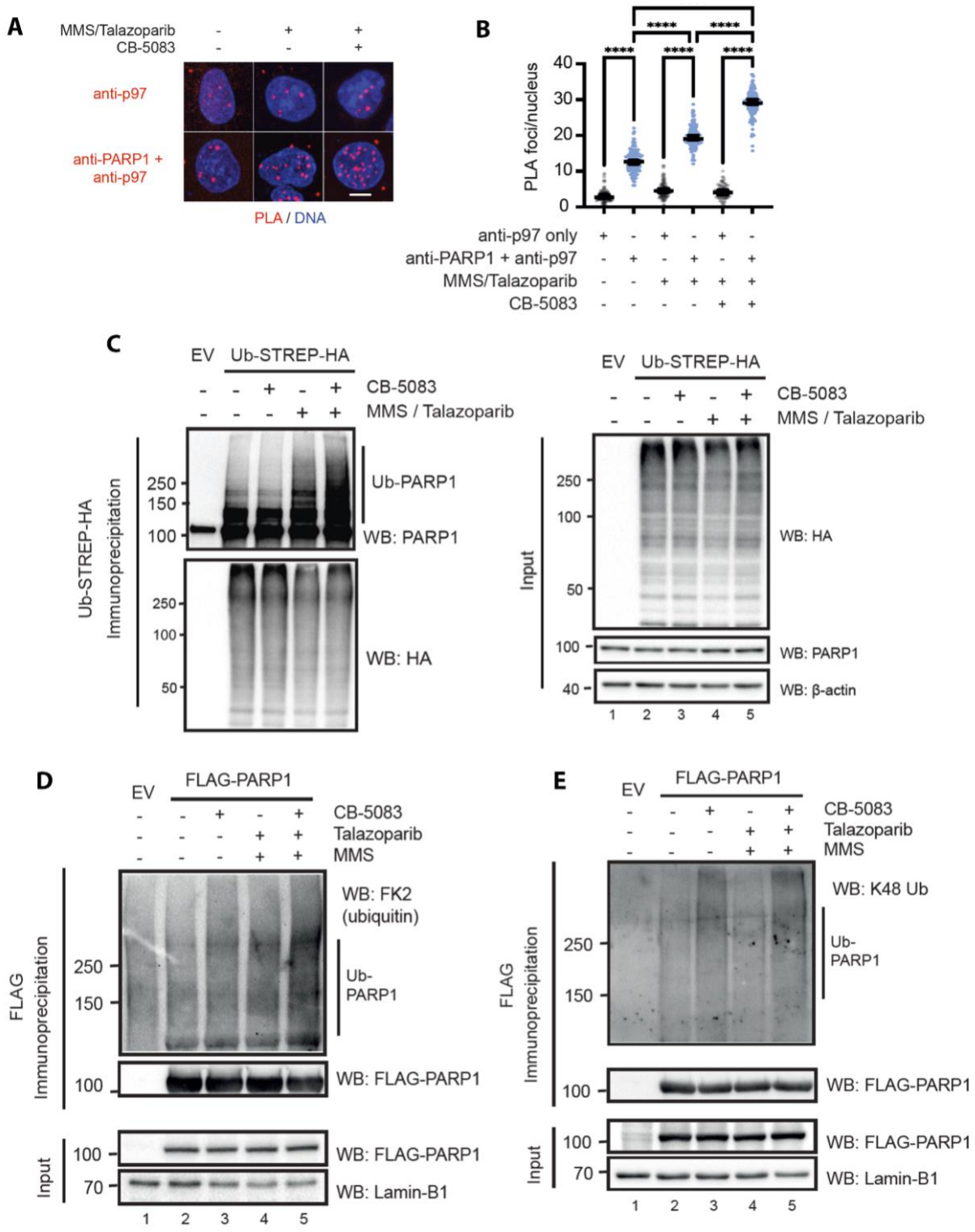

A
MMS/Talazoparib
CB-5083
anti-p97
anti-PARP1 + anti-p97
PLA / DNA
B
PLA foci/nucleus
anti-p97 only
anti-PARP1 + anti-p97
MMS/Talazoparib
CB-5083
C
EV
Ub-STREP-HA
CB-5083
MMS / Talazoparib
Ub-STREP-HA Immunoprecipitation
Ub-PARP1
WB: PARP1
WB: HA
Input
WB: HA
WB: PARP1
WB: β-actin
D
FLAG-PARP1
Talazoparib
MMS
FLAG Immunoprecipitation
WB: FK2 (ubiquitin)
WB: FLAG-PARP1
WB: Lamin-B1
E
WB: K48 Ub

Figure 25. p97 ATPase inhibition by CB-5083 treatment causes increased trapped PARP1 ubiquitination (K48 linked) and p97 interaction

(**A**) Representative images of PLA assay using anti-p97 and anti-PARP1 antibodies after 0.01% MMS + 100nM talazoparib and 10uM CB-5083 treatment for 2 hours. (**B**) Quantification of PLA assay in (**A**), **** P<0.0001, one-way ANOVA, n=2. (**C**) Western blots of immunoprecipitates from HEK293 cells transfected with UB-STREP-HA, under denaturing conditions. Cells were treated with 0.01% MMS + talazoparib and 10uM CB-5083, then streptactin beads were used for pull-down, representative experiment shown, n=2. (**D**) Western blots of reciprocal IP to (**C**), where FLAG-PARP1 was expressed then immunoprecipitated and ubiquitin blotted for, representative experiment shown n=3. (**E**) Same as (**D**) but antibody against K48 linked ubiquitin chains was used to probe immunoprecipitated PARP1 after treatment, n=2. (**B**) was performed by Dragomir Krastev.

To validate this finding, we performed a reciprocal denaturing IP where we expressed and pulled down PARP1-FLAG and western blotted for ubiquitin. We again found that CB-5083 caused an accumulation of ubiquitinated trapped PARP1 (Figure 25D). We were able to probe the ubiquitin modifications further by using an antibody specific for K48 ubiquitin chains and indeed, we found that trapped PARP1 is modified with K48-linked ubiquitin chains upon MMS + talazoparib (Figure 25E). This specific type of ubiquitin chains has been shown to direct p97 towards the degradation/recycling activity (Stach & Freemont, 2017; van den Boom & Meyer, 2018).

In conclusion, we show that inhibition of p97's ATPase activity by CB5083 caused increased interaction between p97-PARP1, indicative of a p97 enzyme-substrate interaction. We also showed that this lead to an accumulation of unprocessed ubiquitinated trapped PARP1. These results suggest that trapped PARP1 is a p97 substrate and that this pathway can be targeted by CB-5083.

We can also employ genetic approaches to probe p97-substrate interaction, by using the well characterised p97 point mutation E578Q in its D2 domain (Dalal et al., 2004). This mutation, similarly to CB-5083, causes p97 to lose its ATPase activity and subsequently causes it to become trapped in binding to its substrates. Furthermore, this mutant is dominant negative because active p97 functions in a hexameric quartenary structure, where disruption of individual subunits inhibit its catalytic cycle (DeLaBarre et al., 2006).

Thus we expressed the $p97^{E578Q}$ substrate mutant in a variety of experimental settings and monitored its interactions with trapped PARP1. Using HEK293 cells which have a dox-inducible expression system for $p97^{WT}$-MYC-STREP and $p97^{E578Q}$-MYC-STREP, we performed a co-IP by pulling down PARP1 after MMS + talazoparib treatment and western blotting for p97 (Figure 26A). We observed a stronger interaction between $p97^{E578Q}$ and trapped PARP1 versus $p97^{WT}$ and trapped PARP1, indicative of a substrate trapping effect.

To determine whether this interaction was trapping dependent, we performed co-IP experiments by immunoprecipitating PARP1^{WT} and PARP1^{KS} under trapping conditions in cells which were expressing p97^{E578Q}-MYC-STREP (Figure 26B). Although p97^{E578Q}-MYC-STREP transfection efficiency in CAL51 cells was low (p97^{E578Q}-MYC-STREP is the upper band compared to endogenous p97 band in input, Figure 26B), we only saw an increase in interaction between trapped PARP1^{WT} and p97^{E578Q}-MYC-STREP in trapping conditions (lane 3 versus lane 1, Figure 26B), whereas there was no increase in interaction between PARP1^{KS} and p97^{E578Q}-MYC-STREP (lane 2 versus lane 4, Figure 26B).

Taken together, we show that p97 is recruited to trapped PARP1 in a ubiquitin and UFD1-dependent manner. We also show that p97 utilises its ATPase activity in PARP1 trapping conditions, inhibition of which, causes an increase in interaction with trapped PARP1 and the accumulation of unprocessed ubiquitinated trapped PARP1. These findings strongly suggest that trapped PARP1 is a p97 substrate.

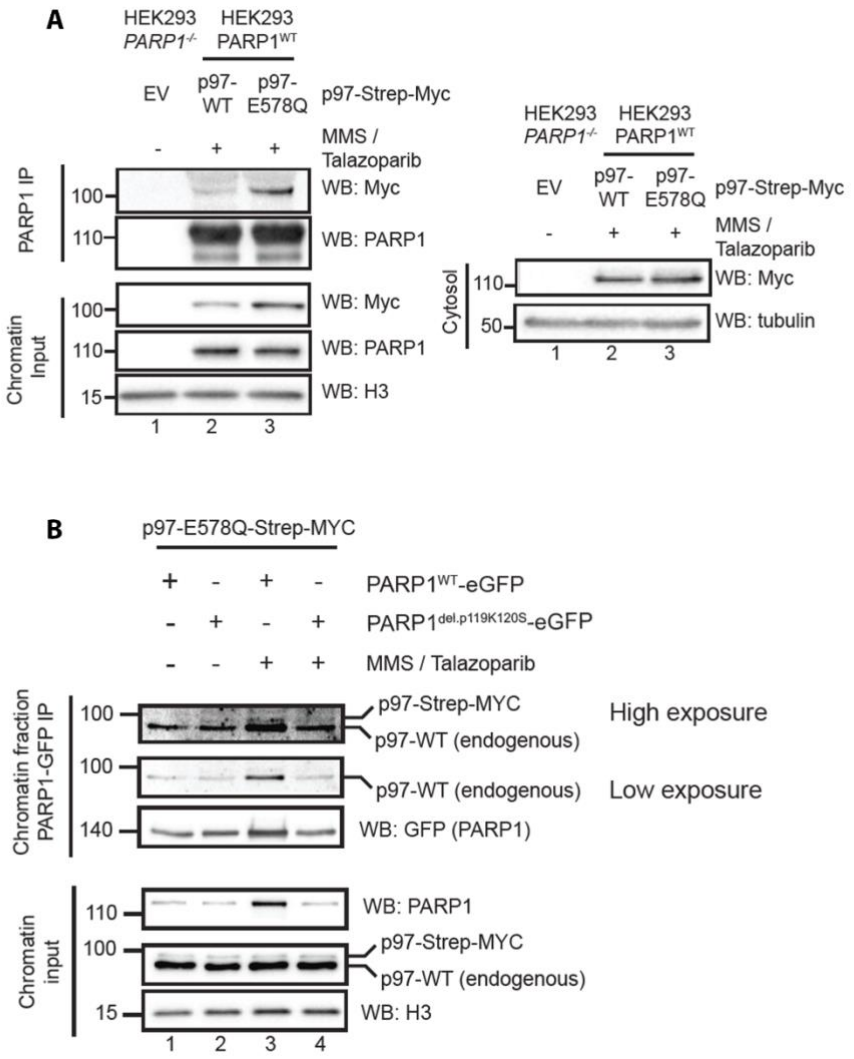


Figure 26. ATPase deficient p97^{E578Q} mutant interacts with trapped PARP1 upon PARPi treatment

(**A**) Western blots showing immunoprecipitates from HEK293 cells under native conditions which have doxycycline-inducible expression system for p97^{WT}-MYC-STREP and p97^{E578Q}-MYC-STREP. Cells were treated with doxycycline for 18 hours and then treated with 0.01% MMS + talazoparib, endogenous PARP1 was then immunoprecipitated from the chromatin-bound fraction using PARP1-trap beads, representative experiment shown, n=2. (**B**) Western blots of immunoprecipitates from CAL51 PARP1^{WT}-eGFP and PARP1^{KS}-eGFP expressing cells transfected with p97^{E578Q}-MYC-STREP. Cells were treated with 0.01 % MMS + 100nM talazoparib and harvested, GFP-TRAP beads were incubated with the chromatin-bound fraction to immunoprecipitate PARP1-eGFP and its interaction partners. Upper band in p97 blot represents the expression of the slightly larger MW p97-MYC-STREP construct, representative experiment shown, n=2.

3.2.5. The RNF4-UFD1-p97 axis repairs trapped PARP1

If the RNF4-UFD1-p97 axis does indeed remove trapped PARP1 on chromatin then one would expect inhibition of individual components to cause an accumulation of trapped PARP1 itself.

To inhibit RNF4, we utilised the dominant negative RNF4 E2-binding mutant M136S/R177A and expressed it in PARP1^{WT}-eGFP expressing CAL51 cells. We treated cells with MMS + talazoparib and carried out a cellular fractionation to observe chromatin bound proteins. The expression of the dominant negative RNF4 mutant lead to an increased accumulation of trapped PARP1 on the chromatin when compared to cells expressing RNF4-WT (Figure 27A).

To inhibit UFD1, we depleted the protein by siRNA and similarly treated cells with MMS + talazoparib. Interestingly, after cellular fractionation we observed an increased accumulation of chromatin bound trapped PARP1 both in untreated and MMS + talazoparib treated sample (Figure 27B). This suggests that UFD1 may also have a role in regulating the amount of trapped PARP1 on chromatin in both a physiological and PARPi treated context. This observation is discussed with recent literature below.

To inhibit p97, we expressed the dominant negative ATPase mutant p97^{E578Q}-MYC-STREP and p97^{WT}-MYC-STREP in HeLa cells and isolated the chromatin bound protein fraction as above. We found that p97^{E578Q}-MYC-STREP expression caused a slight increase in accumulation of trapped PARP1 when treated with MMS + talazoparib in comparison to p97^{WT}-MYC STREP expression (lane 2 versus lane 4, Figure 27C).

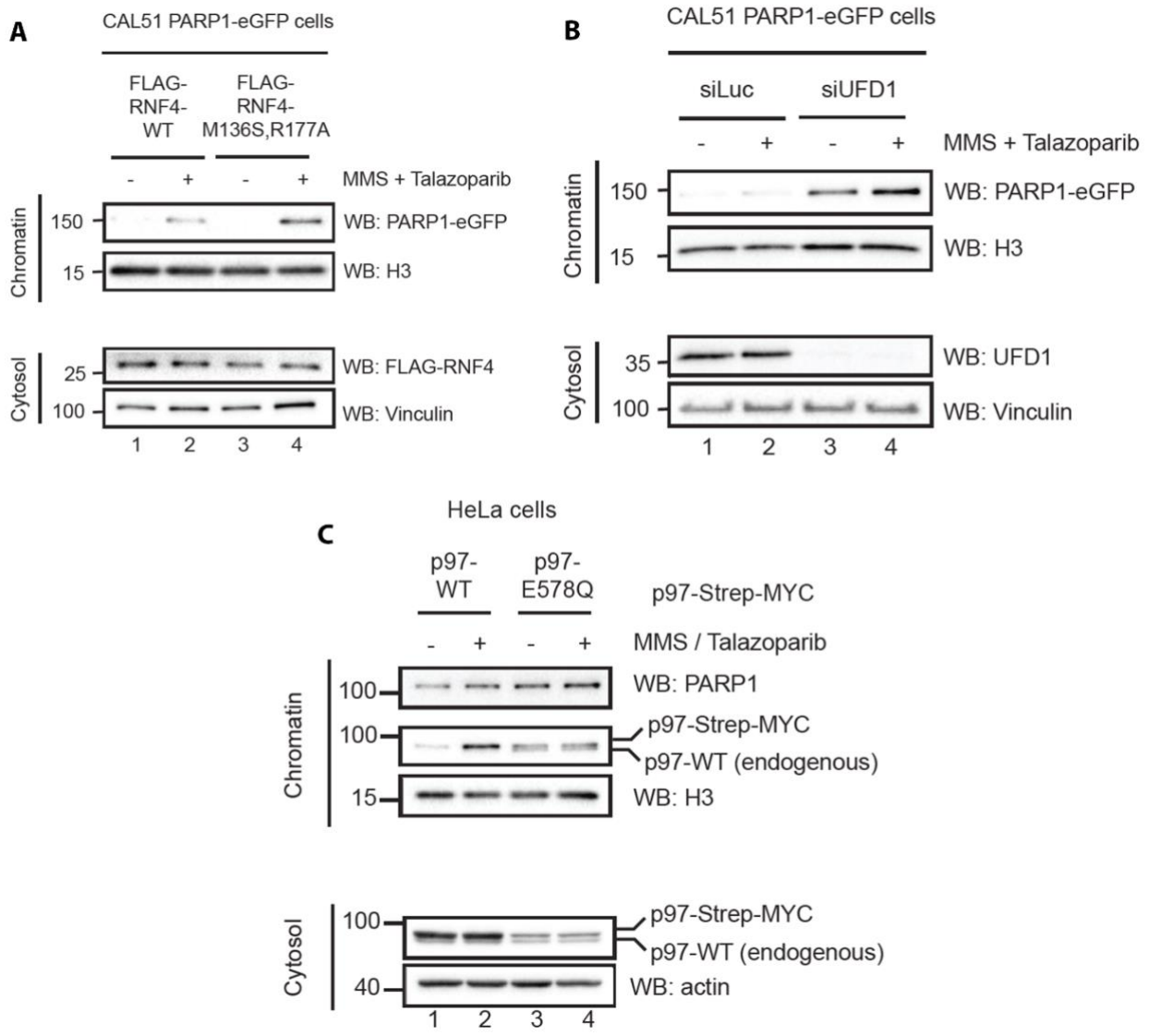


Figure 27. Inhibiting the RNF4-UFD1-p97 axis causes increased trapped PARP1 on chromatin

(**A**) Western blots of CAL51 PARP1^{WT}-EGFP expressing cells transfected with constructs expressing FLAG-RNF4^{WT} and dominant-negative FLAG-RNF4$^{M136S/R177A}$. Cells were treated with 0.01% MMS + talazoparib for 2 hours then fractionated into chromatin-bound fractions where trapped PARP1 was then probed for, representative experiment shown, n=2. (**B**) Same as (**A**) except cells were depleted of UFD1 by siRNA, n=3. (**C**) Same as (**A**) except HeLa wildtype cells were transfected with constructs expressing p97^{WT}-MYC-STREP or p97^{E578Q}-MYC-STREP for 18 hours before treatment with MMS + talazoparib.

In addition to using cellular fractionation, we attempted to develop a immunofluorescence based approach to directly quantify the amount of trapped PARP1 on chromatin. We first attempted a normal fluorescence microscopy protocol where cells were treated with MMS and talazoparib, then fixed before permeabilisation and stained for PAR and PARP1. We observed robust induction of PARylation by MMS, a sign of PARP1 activity, which was inhibited when talazoparib was used in combination (Figure 28A, B). However under normal cell fixation protocol, the amount of PARP1 signal in the nuclei remained unchanged upon PARP1 trapping conditions (MMS + talazoparib treatment) (Figure 28C).

To rectify this, we reasoned that a pre-extraction step could be used to wash the chromatin before fixation. This should remove loosely bound and nuclear soluble PARP1, to only leave PARPi-induced trapped PARP1. Thus we used a mild detergent (0.25% Triton-X100) on cells in a wash step before fixation to only leave proteins that were tightly bound to chromatin. This has previously been used to visualise DNA damage repair proteins such as Ku70/80, which are recruited to the ends of double strand breaks (Britton et al., 2013).

When we employed pre-extraction and quantified the PARP1 signal, we observed a strong retention of PARP1 on chromatin under PARP1 trapping conditions of MMS + talazoparib treatment (Figure 28D, E).

These experiments show that using pre-extraction and immunofluorescence, trapped PARP1 can be directly observed. Since these experiments were performed, this method has been confirmed and replicated in subsequent published literature (Michelena et al., 2018).

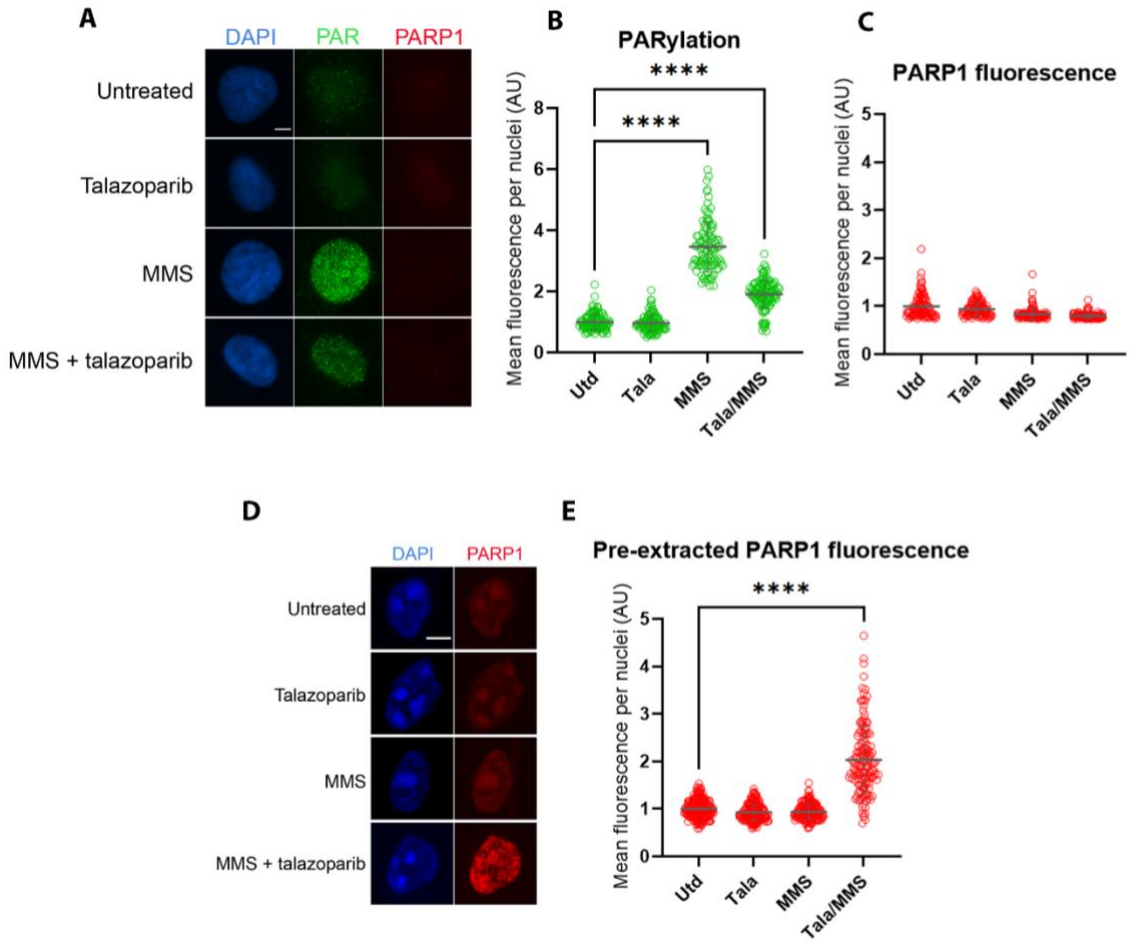


Figure 28. Pre-extraction based immunofluorescence microscopy enables visualisation of trapped PARP1

(**A**) Representative images of HeLa nuclei after 0.01% MMS and 100nM talazoparib treatment. HeLa cells were fixed using 4% formaldehyde before permeabilisation staining using stated antibodies. (**B**) and (**C**) Scatter plots showing quantification of (**A**), over 100 nuclei were quantified for each condition and the mean ± SD is displayed (**** P<0.0001, one-way ANOVA, n=3). (**D**) Representative images of pre-extracted HeLa nuclei after 0.01% MMS and 100nM talazoparib treatment as labelled. After treatment, HeLa cells were first washed with buffer containing 0.25% Triton-X100 then washed twice with buffer alone before fixing. (**E**) Scatter blot of (**D**), where the mean ± SD is displayed (**** P<0.0001, one-way ANOVA, n=3).

We then used this pre-extraction immunofluorescent microscopy method to see if p97 inhibition affects the amount of trapped PARP1 after MMS + talazoparib. To inhibit p97 we expressed the dominant negative ATPase mutant p97^{E578Q}-MYC-STREP in CAL51 cells. Upon MMS + talazoparib treatment and pre-extraction of cells, trapped PARP1 signal was analysed by confocal microscopy. We observed a significant increase of trapped PARP1^{WT}-eGFP in cells expressing the dominant negative p97^{E578Q}-MYC-STREP mutant compared to p97^{WT}-MYC-STREP expression (Figure 29A and B). As an additional control, we also expressed the p97^{E578Q}-MYC-STREP mutant in CAL51 cells expressing PARP1^{KS}-eGFP. As expected we failed to see retention of trapped PARP1^{KS} in these cells after p97^{E578Q}-MYC-STREP expression and MMS + talazoparib treatment.

Using this approach we were also able to perform co-localisation experiments and we observed clear nuclear colocalization between p97^{E578Q} and trapped PARP1^{WT} signal, in support of our hypothesis (yellow arrows, Figure 29C).

From these results, we validated a new microscopy based approach to directly observe trapped PARP1. Using this approach, we were able to visualise trapped PARP1-p97 nuclear interaction and found that inhibiting p97 caused an increase in retention of trapped PARP1 on the chromatin.

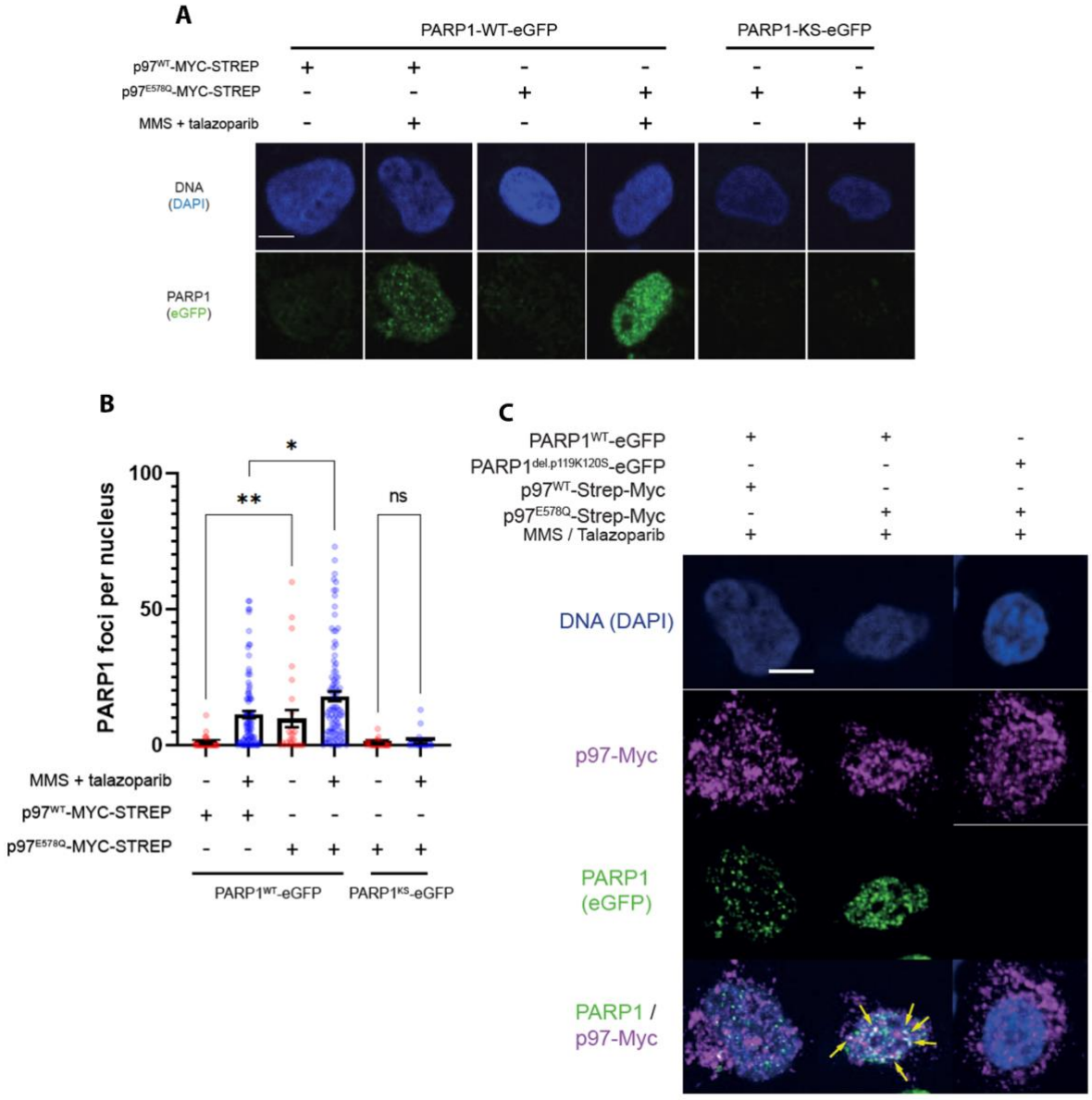


Figure 29. Immunofluorescence microscopy shows p97^{E578Q} expression causes trapped PARP1 accumulation

Representative images of experiment where CAL51 PARP1^{WT}-eGFP and PARP1^{KS}-eGFP expressing cells were transfected with p97^{WT}-MYC-STREP and p97^{E578Q}-MYC-STREP as labelled. Cells were then treated with 0.01% MMS + 100nM talazoparib before being pre-extracted as in (Figure 28D, E) and stained for PARP1-eGFP, (**B**) Quantification of (**A**) (** P<0.01, **** P<0.0001, one-way ANOVA, n=2). (**C**) Confocal microscopy images of immunofluorescence in CAL51 PARP1^{WT}-eGFP expressing cells transfected with p97^{WT}-MYC-STREP and p97^{E578Q}-MYC-STREP. Yellow arrows indicate colocalisation (white) between p97^{E578Q}-eGFP and PARP1-eGFP, n=2. Experiments (**A**-**B**) were performed by Gwendoline Hoslett.

So far, we have shown that inhibiting RNF4-UFD1-p97 leads to an increased accumulation of PARPi-induced trapped PARP1 on chromatin via cellular fractionation and pre-extraction based immunofluorescence microscopy. To further show that this pathway repairs trapped PARP1, we tested whether inhibiting RNF4-UFD1-p97 also leads to slower kinetics of trapped PARP1 repair using chromatin fractionation and PLA (Figure 30A).

Using MCF7 RNF4$^{-/-}$ cells, which were previously shown to have decreased trapped PARP1 ubiquitination (Figure 22A), a treatment of MMS + talazoparib was used before releasing into a mixture containing talazoparib only. PARPi was maintained in the chase treatment as it is a reversible inhibitor. During this chase step, the amount of trapped PARP1 on the chromatin was monitored by cellular fractionation. Over a period of 12 hours, the repair of trapped PARP1 occurred with significantly slower kinetics in RNF4$^{-/-}$ cells when compared to wild-type MCF7 (Figure 30B, C).

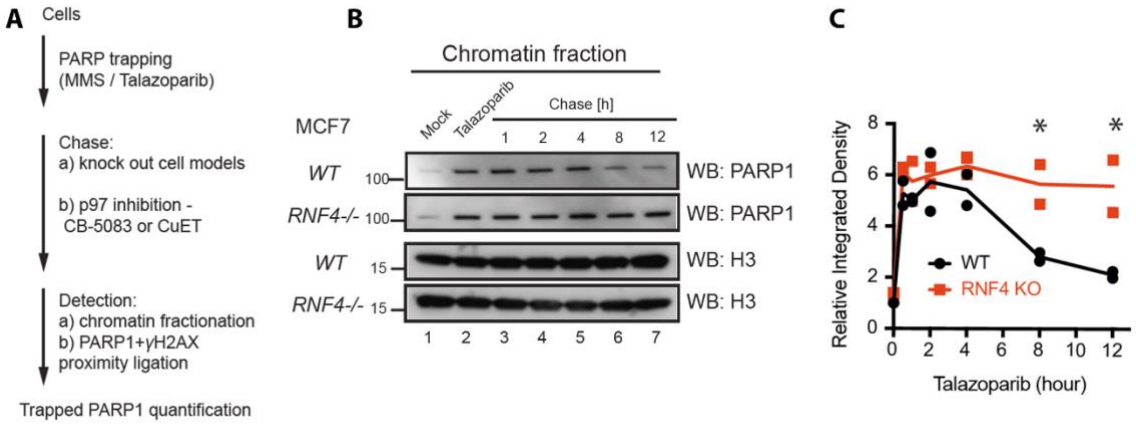


Figure 30. Inhibiting RNF4 and p97 slows the kinetics of trapped PARP1 repair (i)

(**A**) Schematic of experiments carried out to quantify trapped PARP1 repair kinetics, including those shown in Figure 31. (**B**) Western blots of chromatin fractions of MCF7 WT and RNF4$^{-/-}$ cells after 0.01% MMS + 100nM talazoparib treatment and released in 100nM talazoparib only media for the stated lengths of time. (**C**) Quantification of (**B**), (* P<0.05 on a two sided t-test, n=2). Experiments (**B**-**C**) were performed by Yilun Sun.

To test whether inhibiting p97 function causes slower kinetics of trapped PARP1 repair, we utilised two small molecular inhibitors of p97, CB-5083 and CuET. The former which, caused an accumulation of ubiquitinated trapped PARP1 and increased p97-PARP1 interaction as a sign of enzyme-substrate trapping through it inhibiting p97 ATPase activity (Figure 25). The latter, CuET, is a metabolite of the anti-alcohol abuse drug disulfiram and was shown to exhibit inhibitory properties on p97 by sequestering it away from its substrates (Skrott et al., 2017). We confirmed this effect by performing a co-IP experiment in PARP1^{WT}-EGFP expressing CAL51 cells, we found that CuET treatment prevented interaction between trapped PARP1 and p97 (Figure 31A). We thus have shown two different mechanisms of how p97 inhibitors, CB-5083 and CuET, prevent processing of trapped PARP1.

Our collaborator Dragomir Krastev then used an established PLA protocol whereby antibodies against γH2AX and PARP1 was used to measure their proximity, the quantification of which provides a readout for the amount of trapped PARP1 within a cell (Figure 31B) (Hopkins et al., 2019). Cells were treated with MMS + talazoparib then released in media containing talazoparib and different combinations of CB-5083 and CuET (Figure 31B, C). Both p97 inhibitors when used in combination with talazoparib in the chase step, prevented the repair of trapped PARP1, whereas any chase step which contained PARPi, CB-5803 or CuET alone had no effect. Using this same method, trapped PARP1 repair kinetics in cells depleted of the trapped PARP1 ubiquitin E3 ligase RNF4 were also significantly impaired (Figure 31D).

In conclusion from our results so far, we show that the RNF4-UFD1-p97 axis acts to remove PARPi-induced trapped PARP1 from chromatin.

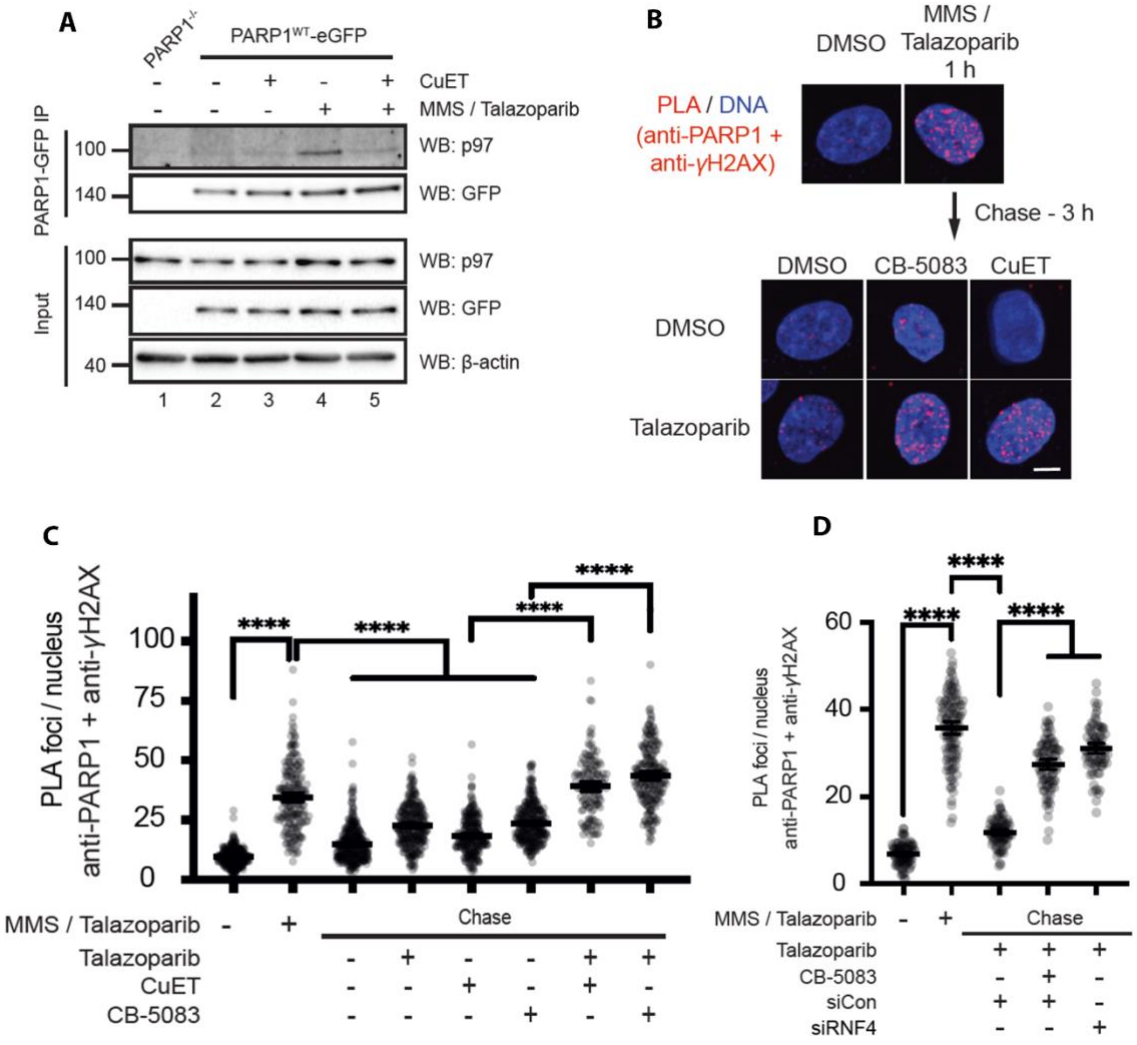


Figure 31. Inhibiting RNF4 and p97 slows the kinetics of trapped PARP1 repair (ii)

(**A**) Western blots showing immunoprecipitates from CAL51 PARP1^{WT}-eGFP expressing cells after treatment with 0.01% MMS + 100nM talazoparib and 1uM CuET as labelled, GFP-Trap beads were used for pull-down under native conditions, representative experiment is shown, n=3. (**B**) Representative microscopy images of PLA experiment where anti-PARP1 and anti-γH2AX were used in CAL51 PARP1^{WT}-eGFP expressing cells. Cells were treated with 0.01% MMS and 100nM talazoparib then released into media containing combinations of 100nM talazoparib, 1uM CuET and 10uM CB-5083 for 3 hours as labelled. (**C**) Quantification of (**B**), >200 nuclei quantified for each condition from three independent experiments. (****P<0.0001, one-way ANOVA, n=3). (**D**) Same as (**C**) except CAL51 cells were depleted of RNF4 by siRNA (****P<0.0001, one-way ANOVA, n=3). (**B-D**) were performed by Dragomir Krastev.

3.2.6. Targeting RNF4-UFD1-p97 sensitises to PARPi

Since we showed that inhibiting the RNF4-UFD1-p97 axis leads to the accumulation of trapped PARP1 on chromatin, we reasoned that this should lead to increased cytotoxicity. This is important for demonstrating clinical relevance of our identified pathway. Furthermore, currently there are drugs in development that target p97 to cause anti-cancer effects. This includes drugs we have used so far; CB-5083 and its recent analogues (Aftab et al., 2014; Roux et al., 2021) and CuET along with its clinically approved precursor disulfiram (Skrott et al., 2017). Therefore, if targeting our proposed trapped PARP1 repair pathway causes increased cytotoxicity to PARPi, there would be further impetus to study the use of these p97 inhibitory drugs for combination therapy with PARPi.

To this end, clonogenic assays using CAL51 revealed that both CB-5083 and CuET caused sensitivity to the PARPis, olaparib and talazoparib (Figure 32A-C). This effect was only present in CAL51 WT cells, whereas in CAL51 PARP1$^{-/-}$ cells, no sensitivity was observed. The lack of sensitivity in CAL51 PARP1$^{-/-}$ cells demonstrate that PARP1 protein itself, as a DNA adduct, is essential to mediate the effects of CB-5083/CuET and PARPi.

We know that PARPi traps PARP1 at DNA lesion sites which occur physiologically or via induction by the alkylating agent, MMS, the latter being what we and others have used for biochemical analysis of trapped PARP1. This opens the possibility that our use of p97 inhibitors may be preventing the efficient repair of MMS-induced lesions, and thus leading to the increased trapped PARP1 phenotypes we have observed. To test this, sensitivity were checked to increasing concentrations of CB-5083 and MMS. We made sure to include concentrations used in previous biochemical experiments (Figure 32D). In both CAL51 PARP1^{WT} and CAL51 PARP$^{-/-}$ cells, no sensitivity to increasing concentrations of combination CB-5083 and MMS treatment was present.

Having validated p97's role in modulating PARPi sensitivity, we wanted to see if synergistic sensitisation existed in the cellular background in which PARPis are prescribed for, cancers with HR deficiency. CB-5083 was found to have a mild synthetic lethal effect by itself on DLD1 BRCA2$^{-/-}$ cells when compared to wild-type DLD1 cells (Figure 32E). When CB-5083 was used in combination with talazoparib, the same synergistic sensitisation effect in DLD1 BRCA2$^{-/-}$ cells was observed (Figure 32F-H). This increased cytotoxicity of combination treatment occurs in both DLD1 WT and BRCA2$^{-/-}$ cells.

In summary, our results demonstrated that p97 acts in a physiological ubiquitin-dependent pathway which removes PARPi-induced trapped PARP1 from chromatin. This is achieved by RNF4-dependent ubiquitination of SUMOylated trapped PARP1 which recruits p97 via its cofactor UFDf1 (Figure 33). Furthermore, we show that by inhibiting p97, we are able to potentiate the effects of PARPis by increasing the retention of trapped PARP1 on the chromatin. This leads to increased cytotoxicity in cancer cells, including ones with HR-deficiency.

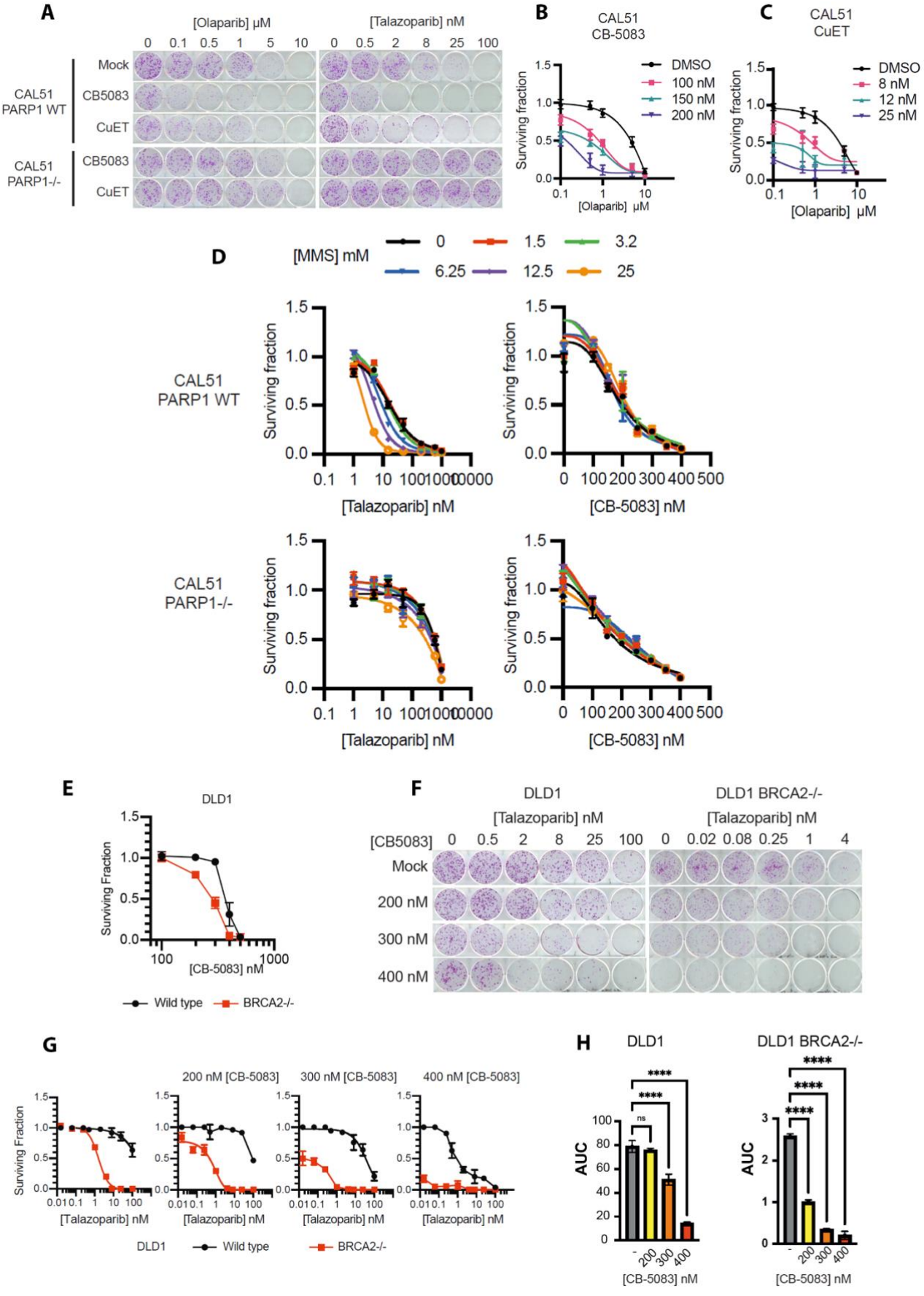

A
[Olaparib] µM
0 0.1 0.5 1 5 10
[Talazoparib] nM
0 0.5 2 8 25 100
CAL51 PARP1 WT
Mock
CB5083
CuET
CAL51 PARP1-/-
CB5083
CuET
B
CAL51 CB-5083
DMSO
100 nM
150 nM
200 nM
Surviving fraction
[Olaparib] µM
C
CAL51 CuET
DMSO
8 nM
12 nM
25 nM
Surviving fraction
[Olaparib] µM
D
[MMS] mM
0
1.5
3.2
6.25
12.5
25
CAL51 PARP1 WT
Surviving fraction
[Talazoparib] nM
[CB-5083] nM
CAL51 PARP1-/-
Surviving fraction
[Talazoparib] nM
[CB-5083] nM
E
DLD1
Surviving Fraction
[CB-5083] nM
Wild type
BRCA2-/-
F
DLD1
[Talazoparib] nM
DLD1 BRCA2-/-
[Talazoparib] nM
[CB5083] 0 0.5 2 8 25 100 0 0.02 0.08 0.25 1 4
Mock
200 nM
300 nM
400 nM
G
200 nM [CB-5083]
300 nM [CB-5083]
400 nM [CB-5083]
Surviving Fraction
[Talazoparib] nM
DLD1
Wild type
BRCA2-/-
H
DLD1
DLD1 BRCA2-/-
AUC
ns
****
[CB-5083] nM

Figure 32. CB5083 and CuET sensitises to PARPi in a trapped PARP1 dependent manner

(**A**) Representative images of clonogenic assay of CAL51 wildtype and CAL51 PARP1$^{-/-}$ cells treated with increasing concentrations of PARPis, olaparib and talazoparib in the presence of CB-5083 and CuET as labelled. (**B**) and (**C**), Drug-response curves for (**A**), Talazoparib was used at a concentrations around 100-fold less than olaparib due to its stronger trapping potency, n=3. (**D**) Drug-response curves of CAL51 PARP1^{WT}-eGFP expressing and PARP1$^{-/-}$ cells treated with increasing concentrations of talazoparib or CB-5083 in combination with MMS as stated, n=3. (**E**) Drug response curve of DLD1 wild type and isogenic BRCA2$^{-/-}$ cells to CB-5083 alone. (**F**) Representative images of clonogenic assay of DLD1 wild type and BRCA2$^{-/-}$ cells to CB-5083 and talazoparib treatment. (**G**) Drug response curves of (**F**), n=3. (**H**) Area under curve (AUC) quantification of (**G**) (**** P<0.0001, one-way ANOVA, n=3). Experiments (**A**-**H**) were performed by Dragomir Krastev.

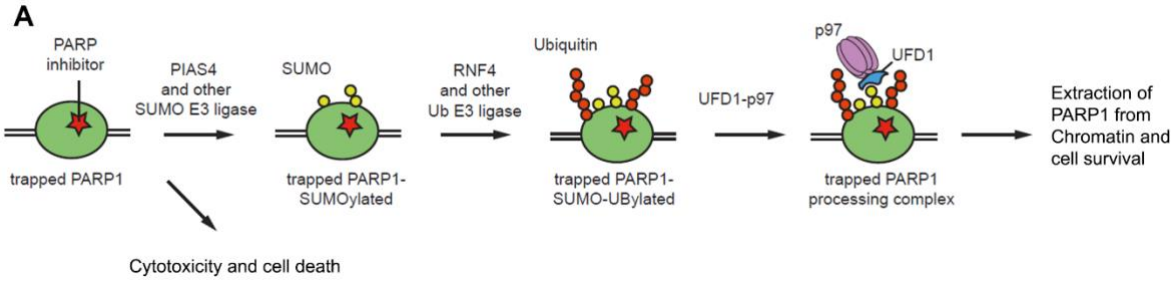


Figure 33. Proposed model for trapped PARP1 repair by p97

PARP inhibitors trap PARP1, which causes it to be sequentially SUMOylated by PIAS4 and then ubiquitylated by RNF4. This ubiquitination recruits p97 which uses its ATPase activity to remove trapped PARP1 from the chromatin.

3.3. The p97 cofactor SPRTN and trapped PARP1

3.3.1. Deficiency in the p97 cofactor SPRTN causes PARPi sensitivity

In the previous chapter, we identified the RNF4-UFD1-p97 axis for trapped PARP1 repair. In this axis, p97 acts to extract trapped PARP1 from chromatin for recycling/degradation. From our previous work, it has been shown that the protease and p97 cofactor, SPRTN, can function in concert with p97, to proteolytically degrade DPCs (Fielden et al., 2020). As PARPi-induced trapped PARP1 is a DPC-like protein adduct (Stingele et al., 2017), we wanted to evaluate whether SPRTN may also have a role in the repair of trapped PARP1. Furthermore, preliminary data in the lab showed SPRTN efficiently cleaves PARP1 *in vitro* and lead to sensitivity to the PARPi olaparib.

To validate these results, we performed colony forming assays where SPRTN was depleted using siRNAs in HeLa and RPE cells and treated with 3 different PARPis (Figure 34A-G). We found that SPRTN deficiency caused increased sensitivity to PARPis, olaparib, talazoparib and veliparib in both Hela and RPE cell lines. Furthermore, in both cell lines, the strongest PARP1 trapper, talazoparib caused the strongest cytotoxic effects in SPRTN deficient cells (Figure 34A, D). We verified that protein depletion occurred by western blotting for SPRTN (Figure 34G).

To further reinforce our findings, we performed the same experiment using 3 different siRNAs targeting SPRTN. We found that in all instances, SPRTN deficiency caused sensitivity to talazoparib in Hela cells (Figure 34H-I). However, there were variability in the resulting sensitivities, suggesting the need for a more robust cellular system for inducing SPRTN deficiency.

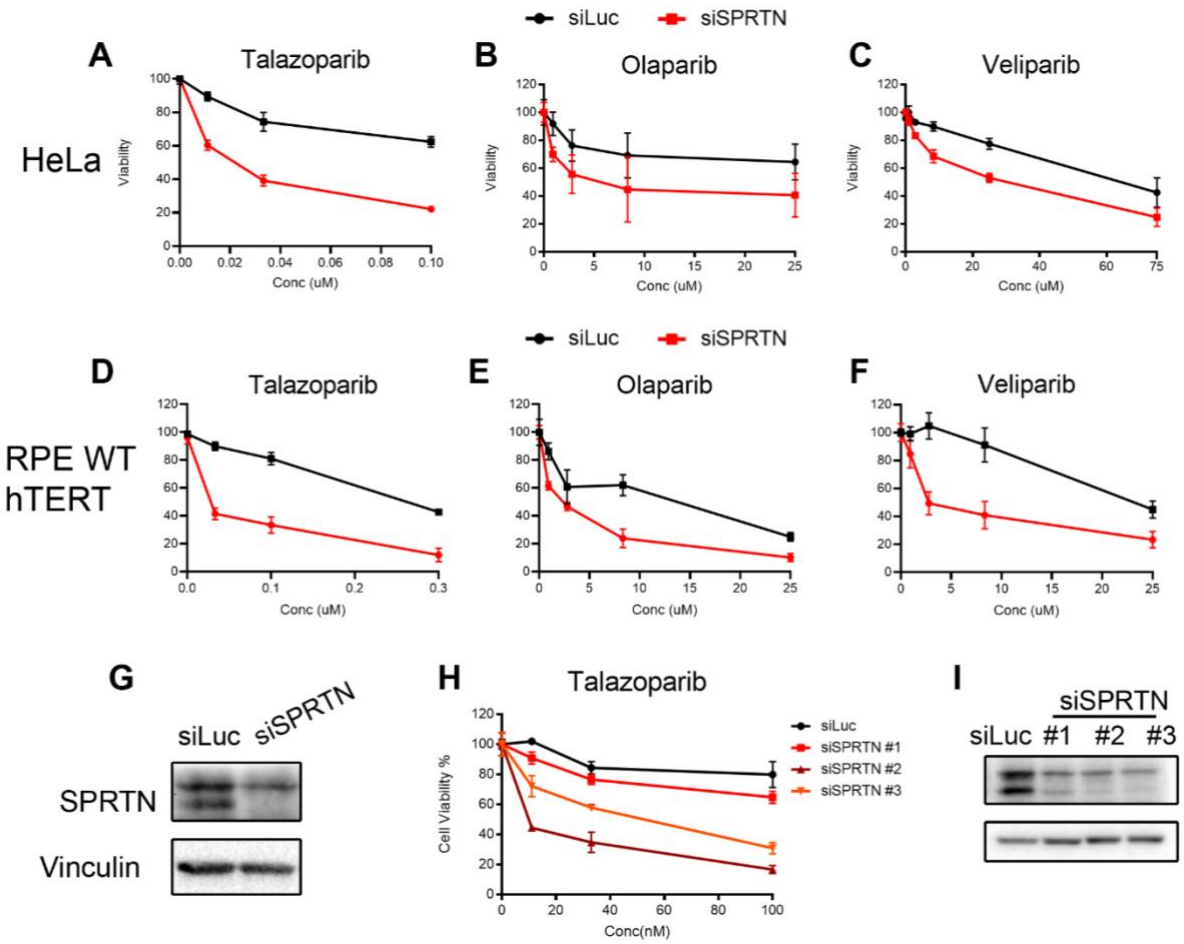


Figure 34. SPRTN deficiency causes increased cytotoxicity to PARPis in HeLa and RPE WT hTERT

(**A**-**C**) Graphs of colony forming assays from a single experiment where talazoparib, olaparib and veliparib, respectively, were used at increasing concentrations in HeLa cells for 24 hours and then allowed to grow for 10-14 days. Cells were depleted of SPRTN using siRNA targeting the 3'UTR, cells were depleted for 2 days before the beginning of PARPi treatment (mean ± SEM is displayed, n=3). (**D**-**F**) Same as (**A**-**C**) except the experiment was performed in RPE WT hTERT cells. (**G**) Western blot showing SPRTN depletion check for (**A**-**C**). (**H**) Graph of colony forming assay, same as (**A**) except 3 different siRNAs were used against SPRTN, (mean ± SD is displayed, n=1). (**I**) Western blot of depletion check for (**H**).

We and others have shown, the PARP1 protein itself is required for PARPi-induced sensitivity (Figure 32) (Murai et al., 2014; Pettitt et al., 2018).

Thus, we asked whether this same phenomenon is observed in the sensitivity of SPRTN deficient cells to PARPi. In Hela cells, SPRTN was depleted along with PARP1 and treated with talazoparib in the colony forming assay. The depletion of PARP1 completely rescued the cytotoxic effects of PARPi in SPRTN deficient cells (Figure 35A, B). This reinforced the hypothesis that it was indeed trapped PARP1 that was causing the cytotoxic effects in PARPi treated SPRTN deficient cells.

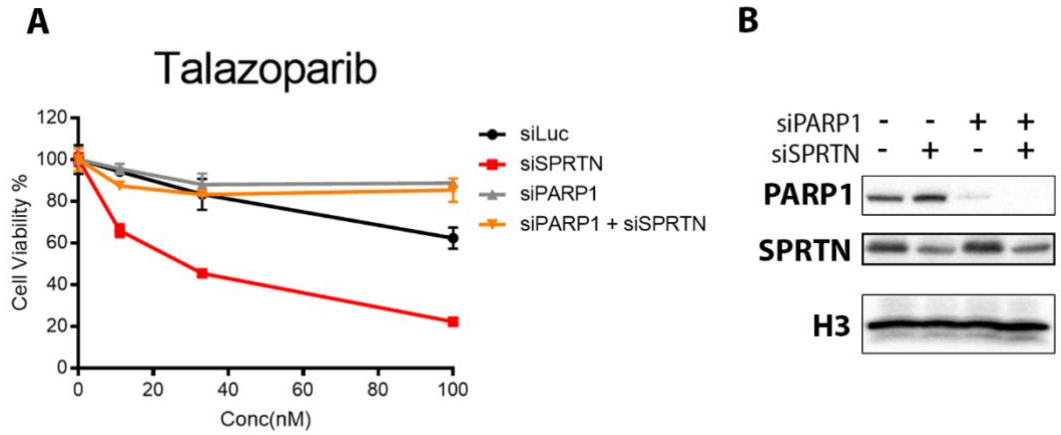


Figure 35. PARPi-induced cytotoxicity in SPRTN deficient cells is PARP1 trapping dependent

(**A**) Graphs of colony forming assay in HeLa cells where SPRTN and PARP1 were depleted via siRNA for 3 days as stated and treated with increasing concentrations of talazoparib for 24 hours after 2 days. Cells were then allowed to grow for 10 to 14 days (mean ± SEM is displayed, n=3). (**B**) Western blots showing depletion checks for (**A**).

3.3.2. SPRTN deficiency causes ineffective trapped PARP1 repair

Using the pre-extraction based immunofluorescence microscopy approach established in the previous chapter (Figure 28), we looked to see if SPRTN deficiency leads to trapped PARP1 accumulation.

SPRTN was depleted in Hela cells and treated with MMS + talazoparib. We discovered that SPRTN deficiency caused significant increased accumulation of trapped PARP1 when compared to non-depleted cells, there was also an according increase in γH2AX signal (Figure 36A-C). This indicates that upon MMS + talazoparib-induced PARP1 trapping there is increased trapped PARP1 and DNA damage present in SPRTN deficient cells (Figure 36C).

We further treated cells with formaldehyde (induces crosslinking of chromatin binding proteins), CPT and H2O2 (induces SSBs). We failed to see an increase in PARP1 signal by any of these exogenous agents alone, even though they induced a γ-H2AX response (Figure 36A-C). This shows that the induction of TOP1cc lesions, SSBs and global DPCs do not, by themselves, cause trapped PARP1.

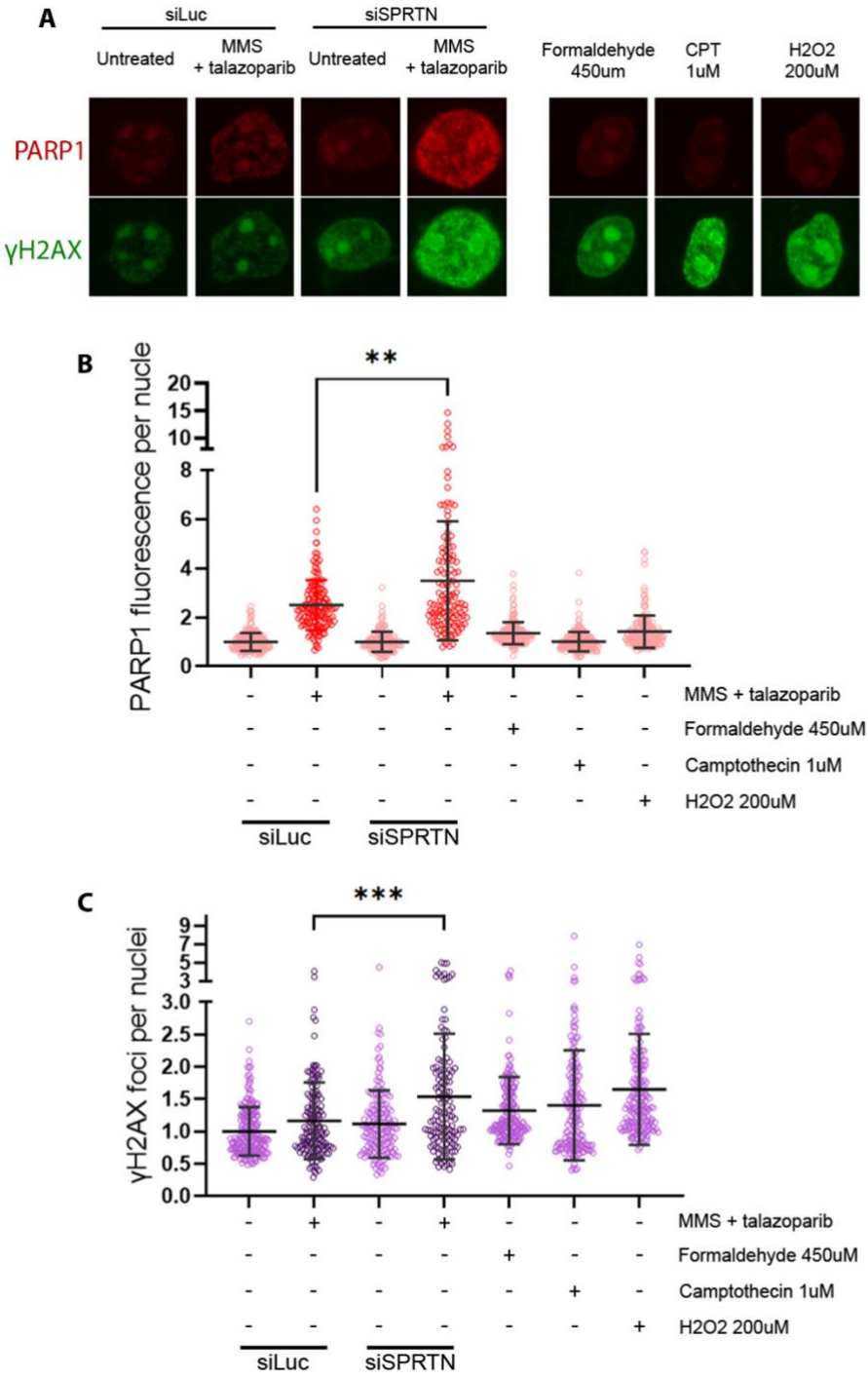


Figure 36. PARPi induces more trapped PARP1 in SPRTN deficient cells

(**A**) Representative images showing HeLa cells depleted of SPRTN and treated with 0.01% MMS + 100nM talazoparib for 2 hours. Cells were also treated with 450uM formaldehyde, 1uM CPT and 200uM H2O2 for 1 hour. Cells were pre-extracted and fixed before staining with PARP1 and γH2AX antibodies. (**B**) Trapped PARP1 and (**C**) γH2AX scatter plots showing quantification of (**A**). (** P<0.01, *** P<0.001, one-way ANOVA, n=2).

We then assessed the effect of continuous MMS + talazoparib treatment in SPRTN deficient cells and observed significantly increased accumulation of trapped PARP1 over 4 hours treatment (Figure 37A). This again was reflected in a more significant robust γ-H2AX DNA damage response in SPRTN deficient cells, indicative of increased DNA damage present from trapped PARP1 in SPRTN deficient cells (Figure 37B).

Using cellular fractionation to measure trapped PARP1 repair kinetics, we released cells into fresh media after 4 hours of MMS + talazoparib treatment. From this, we observed a loss of trapped PARP1 repair kinetics in SPRTN deficient cells, as trapped PARP1 remained on the chromatin rather than being released (Figure 37C). These results show that SPRTN, a protease and p97 cofactor, plays a critical role in the release of trapped PARP1 from chromatin after PARPi treatment.

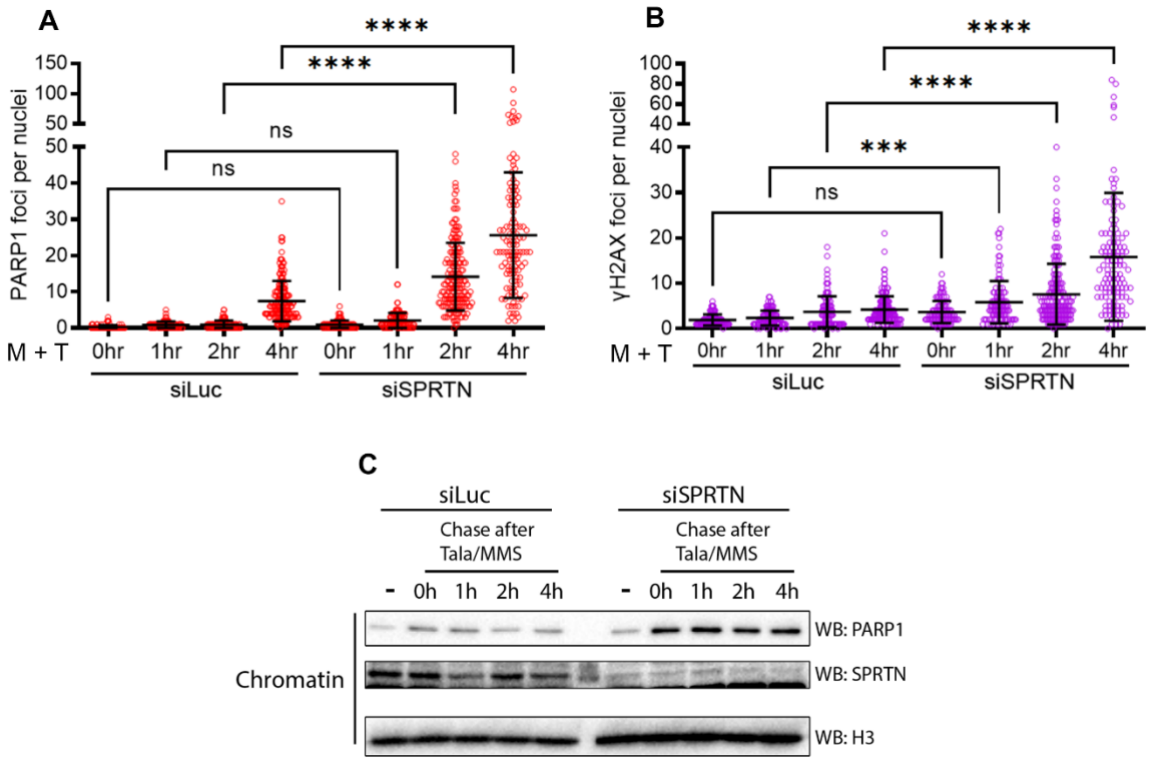


Figure 37. SPRTN deficiency causes trapped PARP1 accumulation and inhibits repair

(**A**) and (**B**) Scatter blots quantifying trapped PARP1 and γH2AX foci in HeLa cells after pre-extraction. Cells were treated with 0.01% MMS + 100nM talazoparib for durations stated (M + T), n=2. (**C**) Western blots of chromatin fractions from SPRTN deficient HeLa cells treated for 4 hours with 0.01% MMS + 100nM talazoparib and released to allow trapped PARP1 repair. SPRTN was depleted by siRNA for 3 days, representative experiment is shown, n=3.

4. Discussion

We show here that p97 unfolds and segregates specific substrates in multiple DNA repair pathways (Torrecilla et al., 2017). It achieves this through ubiquitin and SUMO directed targeting, regulating protein turnover at DNA lesion sites and participating in direct DNA damage repair (Dantuma et al., 2014; Ramadan, 2012).

We show in the repair of DSBs, p97 regulates turnover of the crucial DSB signalling E3 ubiquitin ligase RNF8 (Singh et al., 2019). This is in addition to several other DSB related roles that have been discovered for p97, all of which require p97 ATPase activity to correctly remove ubiquitinated substrates from the chromatin during DSB repair (Torrecilla et al., 2017). The wide variety of p97's roles, not limited to HR or NHEJ in DSB repair, demonstrates the ubiquitous regulatory role p97 plays in DDR.

In addition to DSB repair signalling, we show here that p97 now joins the list of *bona fide* DNA damage repair proteins through its actions in DPC repair. We find that p97 is able to facilitate the removal of DPCs by either (i) directly unfolding the peptide component of DPCs leading to its proteolytic cleavage (TOP1ccs) (Fielden et al., 2020), (ii) directly unfolding DPC-like lesions, facilitating its dissociation from chromatin (Trapped PARP1). For both TOP1ccs and trapped PARP1, the pathway of detection (PIAS4, RNF4) and repair, via p97-SPRTN, seem almost identical (Fielden et al., 2020; Sun, Jenkins, et al., 2020). Work on these two different substrates suggest an indiscriminate pathway for DPC and DPC-like signalling that is dependent on PIAS4-RNF4. A pathway that acts through SUMO-ubiquitin signalling to remove deleterious protein blocks to DNA transcription and replication.

Furthermore, our work identifying the novel interactions between p97 and trapped PARP1 is particularly pertinent at the current time. There are over 200 ongoing clinical trials using PARP inhibitors registered on clinicaltrials.gov, most of which are against BRCA1/2-mutated lung, ovarian, breast, pancreatic and prostate cancers. PARPis are the first targeted DNA damaging chemotherapy, however the mechanistic biology of how PARPis trigger

sensitivity has been revised (Lord & Ashworth, 2017). Originally thought to be through their ability to inhibit SSB repair, this hypothesis has been re-evaluated since the finding that PARPi and its analogues trap PARP1 on chromatin (Murai et al., 2012). Multiple studies have pointed towards a more complex mode of action that we are yet to fully realise. We add to this debate by demonstrating that cells have a physiological apparatus of PIAS4-RNF4-p97 which removes trapped PARP1. Our data suggests that this machinery is active even in the absence of PARPis, as trapped PARP1 seems to form physiologically after p97 inhibition, an observation supported by recent studies (Demin et al., 2021). Under PARPis, this physiological machinery proceeds to remove trapped PARP1, producing innate cytotoxic resistance. Importantly, we showed that we can potentiate cytotoxicity by combining FDA approved PARPis with p97 inhibitors which are themselves in clinical trials (CuET and CB5083 analogues).

p97 has a unique role functioning in a wide range of DNA repair pathways through its ability to unfold and segregate substrates. From repairing DPCs to DSB signalling, the more we gain an understanding of p97 biology in DNA repair, the more opportunities arise for possible chemotherapy treatments with p97 inhibitors.

4.1. p97 and DNA damage

p97 is found overexpressed in multiple cancers, its expression has strong prognostic value and also is a predictor of treatment outcome (Costantini et al., 2021). In cases such as liver cancer, pancreatic cancer, gastric cancer, breast cancer, its high expression is associated with shorter overall survival. Cancers have unregulated proliferation, gene amplification and mutations which lead to a higher burden on the protein folding machinery (Guang et al., 2019). This phenomenon is called proteotoxic stress, and it is characterised by increased protein misfolding and aggregation. To account for this, p97 is upregulated (Vekaria et al., 2016). Thus p97 represents a target for therapeutic inhibition as a monotherapy for the treatment of cancers with especially high proteotoxic stress.

Interestingly, p97's newfound functions in DNA damage repair means that many cancers which have upregulation for p97 are likely innately more resistant to certain DNA damaging chemotherapies. Thus the more we reveal regarding p97 and its role in DNA damage repair, the more opportunities arise for potentiating DNA damaging chemotherapeutics.

4.1.1. p97 and DSBs

DSBs are the most cytotoxic lesions and are directly induced by ionising radiation during radiotherapy treatment for cancers (Khanna & Jackson, 2001). Since the discovery that p97 depletion leads to the accumulation of K48-linked ubiquitin chains and the reduced loading of RAD51 at DSB sites (Meerang et al., 2011), there have been several studies (Acs et al., 2011; Kilgas et al., 2021; van den Boom et al., 2016), including work presented here, that attempts to reveal the p97 mechanisms behind facilitating DSB repair. As p97 is not a DSB specific protein but instead a multitool which regulates protein presence at DNA lesion sites, a wide range of substrates and mechanisms have been revealed (Stach & Freemont, 2017). These have begun to establish p97 as an orchestrator of DSB repair, acting on multiple substrates during different steps of DDR.

Recently it was shown that MRE11 is a p97 substrate (Kilgas et al., 2021). MRE11 is part of the MRN complex which promotes HR by initiating DNA resection at DSBs. When p97 was inhibited by the ATPase inhibitor CB-5083 (the same used in this study), MRE11 accumulated at DSB sites. This led to increased resection and RPA accumulation, ultimately causing a switch from error-free HR repair to the error-prone single-strand annealing repair pathway. By treating the cells with ionising radiation in combination with CB-5083, an increased cytotoxic effect was observed both *in vitro* and *in vivo*.

In addition to the regulation of DSB resection, we show here that p97 also plays a crucial role in regulating ubiquitin signalling at sites of DSB. It does this in concert with ATXN3 to control the amount of RNF8 at DSB sites (Figure 12, 13). RNF8 is the initial E3 ubiquitin ligase which decorates damage sites with K48 and K63-linked ubiquitin chains. We showed by live-imaging micro-irradiation microscopy that p97 inhibition by CB-5083 causes the retention of RNF8 at DNA lesion sites (Figure 13).

In these studies, two different mechanisms by which p97 regulates DSB repair are proposed. Both showed an increasing cytotoxicity when CB-5083 was used with ionising radiation. In the case of MRE11, this was shown in a xenograft model of bladder cancer (Kilgas et al., 2021). Interestingly, p97 was also found to be highly expressed in more aggressive forms of bladder cancer. This neatly demonstrates the dual context in which p97 is important in cancers, (i) as a highly expressed protein, which cancers rely on for maintaining protein homeostasis, (ii) as an important regulator of DNA damage chemotherapeutic responses. Thus the “addiction” cancers have to p97 for proteostasis also makes them resistant to DNA damage induced by chemotherapies. It would also follow that in addition to using p97 inhibitors as a monotherapy to treat the “addiction”, combination p97 inhibitor therapies with DNA damaging chemotherapies would potentiate cytotoxicity.

4.1.2. p97 and TOP1ccs – nuclear periphery-based repair

In addition to a regulatory role in DDR, we show here that p97 plays a direct repair role in removing DPCs. DPCs are triggered by approved chemotherapeutic agents such as platinum salts, topotecan, irinotecan and 5-aza-dC to cause cell death to highly proliferative cancer cells (Stingele et al., 2017). We found that p97 and its cofactor, the metalloprotease SPRTN, play a crucial role in unfolding and catalytically cleaving the peptide component of TOP1ccs (Fielden et al., 2020). TOP1ccs are formed physiologically as the result of failed TOP1 enzymatic activity and are also induced by CPT and its derivatives. p97-SPRTN as a complex, is recruited to TOP1ccs by the novel p97 cofactor TEX264. Recently it was also shown that TEX264 is an ER-phagy (reticulophagy) receptor, facilitating ER degradation by bridging it with autophagosomes during nutrient stress (An et al., 2019). Our work supported this notion as we also found TEX264 to be localised to the nuclear periphery where the ER is located (Figure 10, 11). Interestingly when we created a truncated version of TEX264 which is unable to associate with membranes, we found it strongly localised inside the nucleus (Figure 11). Furthermore, we found it colocalised to SPRTN, the replication machinery and TOP1ccs inside the nucleus. This is supported by two published TEX264 interaction mass spectrometry analyses which found multiple nuclear components including TOP1, PARP1 and MCM components (Raman et al., 2011).

The mass spectrometry data and our work show that in cancer cells, TEX264 is actively engaged under untreated conditions in the replication dependent repair of TOP1ccs (Figure 10). We can postulate that under the highly proliferative conditions in cancer cells, normal physiological mechanisms which safeguard processes such as DNA replication are overwhelmed. This includes TOP1 which is required for unwinding of DNA during replication. Therefore oncogene-induced DNA replication could cause more abortive TOP1 complexes which form physiological DPCs. These processes force cells to respond by utilising autophagy dependent mechanisms to remove and recycle TOP1ccs and the associated DNA replication machinery. Indeed, p97 has been implicated in autophagic pathways (Dargemont & Ossareh-

Nazari, 2012). There have also been studies which show that autophagy pathways are involved in DNA damage repair, specifically DSB repair. Although these have conflicting models, the general trend is that inhibiting autophagy can inhibit HR-mediated repair (G & VI, 2017).

The localisation of SPRTN-p97 by the ER-phagy receptor TEX264 to the nuclear periphery for TOP1cc repair is an evocative finding. It pinpoints the nuclear periphery as an important locale of DNA repair that remains mechanistically unexplored and also links DPC repair with autophagy. It also establishes p97 as a DNA damage repair enzyme which uses its ATPase activity to directly repair DPC lesions. Our later findings on the mechanism of trapped PARP1 repair expands on this to show that the p97 machinery is not restricted to TOP1ccs, but is likely a universal component for the repair of different DPC and DPC-like lesions.

4.2. Trapped PARP1 - mechanistic insights into DPC repair

Unlike TOP1ccs, trapped PARP1 is not covalently bound to DNA, instead it is reversibly trapped by its inhibitor (Stingele et al., 2017). Indeed, similarly to TOP1ccs, it has been shown that PARP inhibitors, depending on its ability to trap PARP1, causes slowing down of replication fork speed (Saha et al., 2021). This indicates it is a deleterious protein block which requires removal. We know from our previous work on TOP1ccs (Fielden et al., 2020), that DPCs which slow down replication forks elicit a cellular response to remove those lesions. So to look for components of such a response, we carried out dual orthogonal mass spectrometric approaches to identify interactors with trapped PARP1.

4.2.1. Insights from mass spectrometric analysis

We used two separate mass spectrometry-based approaches. One approach using formaldehyde crosslinking to fix protein complexes, in essence, taking a snapshot of protein interactions (RIME) (Mohammed et al., 2016). The other required a fusion protein of PARP1-APEX2, with the engineered APEX2 enzyme, capable of proximity biotinylation (Lam et al., 2015). For these techniques, accuracy of results heavily depends on negative controls to filter out non-specific hits from the mass spectrometer. For RIME, we were able to create both PARP1^{WT}-eGFP and PARP1^{KS}-eGFP (mutant incapable of chromatin trapping) expressing cell lines (Figure 14, 15), unfortunately we were unable to obtain clones for PARP1^{KS}-APEX2-eGFP (Figure 16). However, we used PARP1-/- cells and PARP1^{WT}-GFP expressing cells respectively, as a negative control for bead-binding and any hits obtained in this condition were filtered out for subsequent analysis.

It was evident that more PARP1 interaction hits were identified for the APEX2 based proximity-labelling approach, 360 hits for PARP1^{WT}-APEX2-eGFP PARP1 versus 50 for RIME PARP1^{WT} and 144 for RIME PARP1^{KS} (Figure 16). This is likely due to the nature of the

different techniques, whereas APEX2 proximity-labelling occurred over a span of 30 mins, RIME formaldehyde crosslinking occurs over 10 mins. Furthermore, the formaldehyde used for crosslinking causes irreversible crosslinking of protein interactions and within proteins themselves. So once fixed, complexes can become non-functional due to loss of ability to change in conformation, whereas the PARP1^{WT}-APEX2 fusion protein maintains its normal physiological function throughout its labelling period.

When we analysed interaction hits, we began to gain a picture of the cellular response to trapped PARP1 lesions (Figure 15, 16). Notably, p97 was one of three proteins found through both mass spectrometry approaches. We know that p97 shows activity towards SUMOylated (TOP1ccs) (Fielden et al., 2020) and ubiquitinated substrates (Ku80, DDB2) (Puumalainen et al., 2014; van den Boom et al., 2016) in DNA damage. In our combined approaches we found hints of SUMO and ubiquitin machinery being engaged at trapped PARP1, notably, interaction hits for UBA1, SUMO1 and SUMO2. These findings guided us to eventually finding trapped PARP1 to be sequentially SUMOylated by PIAS4 followed by StUBL-mediated ubiquitination (Figure 17-22).

Interestingly, we observed that PARP1^{KS}-eGFP still maintained interactions with chromatin associated proteins such as PDS5A and the chromatin remodeller CHD4 (Figure 15). This is in counter to the fact that PARP1^{KS} cannot bind to DNA lesions due to a mutation in its ZnF2 (Pettitt et al., 2018). This is possibly due to PARP1 possessing non-DNA-damage binding modes for chromatin. For example, reports show that PARP1's CAT domain is capable of binding histone H4, this is further backed up by the finding that the C-terminal end of PARP1 (WGR and CAT domains) have strong interaction with nucleosomes (Clark et al., 2012). Interestingly we also found that PARP1^{KS} maintained low background binding to p97 to a similar extent to PARP1^{WT} when both were under untreated conditions (Figure 23A). Importantly, only PARP1^{WT} increased in interaction with p97 after treatment with PARPis, whereas interaction between PARP1^{KS} and p97 remained the same (Figure 23A). The fact that the mass spectrometry analysis shows PARP1^{KS} still binds chromatin, suggests that the

interaction between PARP1^{KS} and p97 could be occurring on DNA. Further study could elucidate whether p97 also removes PARP1^{KS} from chromatin. This would be interesting in affirming whether p97 acts as a ubiquitous method of PARP1 removal. The biology of p97 and its other substrates such as TOP1ccs, suggests that it likely acts in the physiological removal of chromatin binding proteins, and also as a response to unnaturally trapped chromatin proteins. This could be the same for PARP1. Our data only focuses on how p97 removes trapped PARP1, with details of the physiological role of p97 and PARP1 remaining unprobed.

4.2.2. Novel mechanism of PARP1 dissociation

PARP1 binds to SSBs and DSBs on DNA and catalytically modifies itself, surrounding proteins and DNA with ADP-ribose sugars. Auto-modification accounts for the majority of PARP1's activity (Langelier et al., 2012; Ray Chaudhuri & Nussenzweig, 2017). As these sugar moieties are negatively charged, auto-modification leads to dissociation of modified-PARP1 from chromatin. This is due to repulsion towards the negatively charged phosphate-backbone of DNA (Krüger et al., 2020). Our study and others show an alternative route for PARP1 dissociation, through SUMO/ubiquitin.

Ours is not the first study to show engagement of the SUMO/ubiquitin machinery leading to PARP1 removal from chromatin. It is known that PIAS4 SUMOylates and RNF4 ubiquitinates PARP1 upon cellular heat shock (Martin et al., 2009). PARP1 is removed from binding to HSP70 promoters upon heat shock, while under physiological conditions, it negatively regulates HSP70 gene expression. Its dissociation facilitates HSP70 expression and the response to heat shock. In this setting, there is no DNA damage to activate PARP1's catalytic activity. Upon heat shock, PARP1 dissociates from the promoter regions of HSP70 by the recruitment of PIAS4 and subsequent SUMO modification then RNF4 ubiquitination. Interestingly in response to heat shock, PARP1 has been shown to be active, it is partially responsible for PARylation occurring at the HSP70 promoter region along with PARP13 (Martin et al., 2009). PARP1's activity is required for dissociation from its binding partner PARP13 and for effective binding to the gene body during a redistribution step. However,

importantly, its activity was not needed for the initial dissociation from the HSP70 promoter as this is likely the identified SUMO/ubiquitin dependent step (Martin et al., 2009). These data point towards a dual mode of PARP1 dissociation from chromatin, one dependent on auto-PARylation and another dependent on SUMO/ubiquitin.

In our case we identify p97 as the downstream effector for PARP1 dissociation. In the case of heat shock, the authors suggest that the proteasome is partially responsible for PARP1 removal (Martin et al., 2009). Although we cannot fully rule out proteasome involvement in trapped PARP1 degradation, we show that p97, often an upstream component of proteasome-mediated degradation, is involved (Stach & Freemont, 2017). In our study, the endpoint of interest was the removal of PARP1 from chromatin, as this represents the cytotoxic lesion with clinical relevance. We did not explore further whether, once removed, PARP1 was recycled, or degraded by the proteasome.

We did find that trapped PARP1 is likely proteolytically degraded by the protease SPRTN. We observed that SPRTN causes a loss of trapped PARP1 removal kinetics and the accumulation of trapped PARP1 under SPRTN deficient conditions (Figure 36, 37). Interestingly it was recently found that SPRTN is also regulated by SUMOylation and ubiquitination of its substrates (Ruggiano et al., 2021). SPRTN deficiency leads to an accumulation of SUMOylated DPCs. It is possible that p97 coordinates this function of SPRTN by recruiting it to trapped PARP1. Since our studies were carried out, it was published that SPRTN colocalised to trapped PARP1 lesions and extracted trapped PARP1 from chromatin to prevent replication fork stalling (Saha et al., 2021). How exactly SUMOylation and ubiquitination of substrates regulates SPRTN-mediated degradation and whether this is the same as p97 dependent pathways is unclear. However, trapped PARP1 now represents one of the best model substrates to use for the elucidation of the mechanistic details of DPC repair.

Our data presents a model of PARP1 dissociation that has only been lightly explored so far. It is evident that PARP1 has many transcriptional roles (Schiewer & Knudsen, 2014). In these conditions, the removal of PARP1 maybe reliant on pathways such as the p97-

mediated pathway. Indeed, p97 has a well established role in regulating transcription by the non-proteolytic release of transcription factors from chromatin (Franz et al., 2016). PARP1 could be a new member of transcription factors modulated by p97.

4.2.3. SUMOylation and STUbLs

The SUMOylation of PARP1 and its STUbL-mediated removal from chromatin has important implications for DPC repair and p97 biology. Several p97 substrates are now known to be both SUMOylated and ubiquitinated. These include XPC removal for efficient NER repair (Poulsen et al., 2013; Puumalainen et al., 2014), CMG disassembly via MCM7 unfolding (Maric et al., 2014) and TOP1ccs (Fielden et al., 2020). We are beginning to generate a complex picture of modifications where DPCs such as TOP1ccs are modified by SUMO-1 which recruits p97 via TEX264 (Fielden et al., 2020) while also being modified by SUMO-2/3 by PIAS4 (Sun, Jenkins, et al., 2020). This suggests there are multiple pathways for the repair of TOP1ccs which are difficult to experimentally differentiate and thus make identifying DPC repair pathways particularly difficult.

Our results showing that trapped PARP1 is a substrate for PIAS4-RNF4 dependent removal suggest that the SUMO-STUbL pathway is likely a promiscuous mechanism for chromatin protein removal. In fact, PARP1 is a known target of SUMOylation upon MMS treatment and ensuing BER (Hendriks et al., 2015). We also observed this and show that this is potently potentiated by the introduction of PARPi and associated trapping (Figure 19). A possible explanation of this is that PARP1 is actively SUMOylated and removed during its physiological cycle, however trapping by PARPi prevents its removal and leads to the accumulation of SUMOylation and ubiquitination.

Since our study was completed, work has been published which confirmed some of the presented findings here. It was shown that DPCs, including trapped PARP1 are sequentially SUMOylated and ubiquitinated by PIAS4 and RNF4 respectively. This work performed in *Xenopus laevis* egg extracts showed that DPCs are modified independently of

DNA replication (Liu et al., 2021). Using nucleoplasmic extracts from interphase, the authors utilised a model DPC crosslinked to plasmid DNA to show modifications in the absence of replication. From this, they propose that PIAS4-RNF4 directly shuttles DPCs to proteasome-mediated degradation, which is inferred from the loss of the soluble form of DPCs. It does suggest that similar to DSB repair pathway choice, cell cycle also plays a critical role in DPC repair pathway choice. Perhaps, in the absence of DNA replication, PIAS4-RNF4-mediated signalling on DPCs occurs. This could then recruit proteasome and p97 for DPC repair pre and post-replicatively, whereas DPCs which are encountered by replication machinery are repaired in a SPRTN-dependent manner. Complicating the mechanistic understanding of this is the overlap of SUMO-ubiquitin signalling which are needed for both p97- and SPRTN-dependent DPC repair (Ruggiano et al., 2021).

In the frog extract system, SUMO-ubiquitin modification leads to the proteasomal degradation of its targets. When we looked at PARP1, we failed to see a drop in soluble levels of PARP1 suggesting that degradation by the proteasome is not the end-point of trapped PARP1 (Figure 24, 26, 27, 29). This is likely due to trapped PARP1 not being covalently linked to DNA, therefore once unfolded, it can naturally detach from the DNA. This is in contrast to TOP1ccs, where it is covalently bonded to DNA, requiring them to be unfolded and degraded first before its dedicated nuclease TDP1 can excise the protein-DNA remnant (Pouliot et al., 1999). Only then are TOP1ccs repaired and no longer present as an obstacle to replication forks. Furthermore, the high abundancy of PARP1 may also be a factor which buffers any observation of increase or degradation at the soluble level as a result of chromatin-related processes.

In yeast, the STUbL pathway is conserved, and direct binding between the p97 cofactor UFD1 to SUMOylated substrates and the yeast homolog of RNF4 has been observed (Nie et al., 2012). This interaction is lost upon mutation of SIMs on UFD1. However, the SUMO binding function of UFD1 has not been observed in mammalian cells yet. Our data strongly suggest that UFD1 is an essential cofactor for binding of p97 to trapped PARP1 (Figure 24C,

27B). We observed loss of interaction between p97 and trapped PARP1 upon UFD1 depletion (Figure 24C). Under the same conditions we also observed a strong retention of trapped PARP1 on chromatin (Figure 27B). Both these phenotypes were not observed under robust NPL4 depletion (Figure 24C). Our data and these observations point towards a blind spot in the current p97 field. It is commonly assumed that NPL4-UFD1 functions as an obligate dimer for p97 processing, we show this is not likely the case for trapped PARP1.

Indeed, structural data identifies NPL4 as the essential cofactor for p97 binding to ubiquitinated substrates. However, our data show that NPL4 has minimal contribution towards PARP1 removal. This same observation was seen for p97 substrates such as CDT1 (Raman et al., 2011) and MCM7 (Maric et al., 2017), where UFD1 has the larger contribution. A complication is that in certain cell lines and biological settings, NPL4 depletion leads to UFD1 loss and vice versa. However, in our systems, we observed individual depletion of UFD1 or NPL4, as was seen for the case of CDT1 and MCM7 (Figure 24C, 27B). These point towards a yet unexplored phenomenon where UFD1 is essential for certain substrates. In yeast this has been shown by large scale elucidation of UFD1 substrates, by comparing quantities of SUMOylated proteins between wild type and UFD1 mutant clones (Køhler et al., 2015). There were around 40 proteins which showed increase in SUMOylation upon UFD1 deficiency. From these results, a hypothesis by which UFD1 is essential for mammalian p97 binding to certain SUMOylated substrates emerges and warrants further exploration.

One unique difference between SUMO and ubiquitin is the critical role SUMO plays in facilitating phase condensates and non-membranous organisation. By modifying substrates and allowing novel protein-protein interactions, SUMO has been shown to build membraneless organelle structures such as PML bodies and maintain nucleolar structures (X. Zhao, 2018). In the context of DNA damage, SUMO has been shown to regulate the relocation of DNA damage sites such as damaged telomeres and DSBs to the nuclear periphery (Caridi et al., 2018; Churikov et al., 2016; Horigome et al., 2016; Ryu et al., 2015). There is the possibility that DPCs such as trapped PARP1 are SUMOylated and localised towards the

nuclear periphery for their repair. Indeed, this is location for TEX264-mediated TOP1cc repair (Fielden et al., 2020). The fact that the identical signalling pathway (PIAS4, RNF4) and repair pathway effectors (p97, SPRTN) are seen for trapped PARP1 and TOP1ccs repair, suggest that trapped PARP1 could also be repaired at the nuclear periphery. It would be interesting to see if TEX264 also plays a role in trapped PARP1 repair, this would strongly indicate that the nuclear periphery is a centre for trapped PARP1 repair.

Another candidate protein which may regulate trapped PARP1 is the DUB ATXN3. We showed that ATXN3 binds to p97 and regulates the amount of RNF8 ubiquitination at DSB sites, by inhibiting ATXN3, RNF8 becomes retained and causes hyper-K48-ubiquitination at DSB sites (Singh et al., 2019). ATXN3 is recruited by SUMO to DSBs and also has been suggested to antagonise ubiquitination of MDC1 by RNF4 (Pfeiffer et al., 2017). Thus it could be playing the same role on trapped PARP1, as for MDC1. We would expect that ATXN3 deficiency would cause an increase in trapped PARP1 K48 ubiquitination and dysfunctional processing by p97 as seen for RNF8. The exact mechanism of how increased ubiquitination of RNF8 due to ATXN3 deficiency, leads to increased p97 binding but lower processing, is yet unrevealed. However this phenomenon has also been observed in a recent study which demonstrated that inhibition of the DUB, USP7, increases p97 binding via its cofactor FAF1 to its SUMOylated substrates (Franz et al., 2021). However, USP7 DUB inhibition also increases a deleterious DNA replication phenotype associated with loss of substrate processing. Thus it seems a balance of ubiquitination is required for efficient processing. One possible explanation is that p97 activity may be similar to the proteasome, where proteasomal subunits which possess DUB activity are needed to trim ubiquitin before substrates can enter the proteolytic core (Lee et al., 2011). This could explain why ATXN3 is required for p97 processing as ubiquitin chains on RNF8 need to be trimmed before they can begin p97-mediated unfolding as was shown *in vitro* (Bodnar & Rapoport, 2017).

By identifying the SUMO-ubiquitin signalling pathway for trapped PARP1 repair, we are able to gain key insights into DPC repair. We show that the PIAS4-RNF4 pathway is likely

ubiquitous for many DPC and DPC-like lesions. Recent studies suggest that this particular signalling mode occurs independently of DNA replication (Liu et al., 2021). However, our identification that the replication dependent protease SPRTN performs trapped PARP1 repair shows that there are likely multiple mechanisms for DPC repair. These include replication-independent PIAS4-RNF4-mediated signalling resulting in p97/proteasome-mediated repair and replication-dependent SPRTN proteolytic repair. This points toward cell cycle being a possible determinant of DPC repair pathway choice similar to DSB repair. The identification of SUMOylation for trapped PARP1 being a key step in signalling for repair also brings in the possibility of relocalisation of trapped PARP1 lesion to the nuclear periphery, as is found for TOP1ccs.

4.2.4. Physiological trapped PARP1

By looking at the cellular response to the trapped PARP1 lesion itself rather than its cytotoxic downstream effects, we discovered that trapped PARP1 does not only occur after PARPi treatment, but are also found after genetic perturbations. This is exemplified by our finding that depletion of the p97 cofactor UFD1 or expression of the dominant negative $p97^{E578Q}$ mutant increased trapped PARP1 in the absence of PARPi (Figure 27B, C and 29A, B). Recent studies have begun to unravel the different possibilities of where and how physiologically trapped PARP1 can occur in absence of PARPi-induced trapping.

Seminal work from the Caldecott laboratory published in 2021, revealed the occurrence of physiologically trapped PARP1 during BER (Demin et al., 2021). Up until now, the concept of trapped PARP1 centred around the use of exogenous PARPis to cause PARP1 trapping. *Demin et al. 2021* showed that in cells that are XRCC1 deficient, treatment with MMS alone to activate BER causes extensive PARP1 trapping on chromatin. This was not observed in wild-type cells. This trapping was proposed to be due to the role XRCC1 plays in antagonising PARP1 retention. Importantly, they demonstrated exquisite sensitivity towards MMS in $XRCC1^{-/-}$ cells that was completely rescued in $XRCC1^{-/-}$ $PARP1^{-/-}$ cells. This validated that no matter its origins, endogenous or exogenous, trapped PARP1 is severely cytotoxic.

It would be interesting to see if under these conditions of physiological trapped PARP1 (MMS treatment in XRCC1$^{-/-}$ cells), PARP1 SUMOylation/ubiquitination and p97 dependent removal occurs. Interestingly, when we co-treated cells with p97 inhibitor and MMS, we failed to observe a cytotoxic effect. This suggests that p97 is likely not removing PARP1 from BER lesions under physiological conditions, however perhaps in cells that are XRCC1-/- background, p97 may play a role.

Previous work from the Caldecott laboratory also revealed a novel role of PARP1 during normal cell physiology. PARP1 was shown to be highly active during DNA replication, where it signalled for Okazaki fragment maturation on the lagging strand of DNA replication forks (Hanzlikova et al., 2018). This activity was revealed by PARGi treatment which unveiled the new centre of PARylation. It thus seems possible that throughout the use of PARPi, proliferative cancer cells which spend majority of its time in S-phase, experience a high burden of trapped PARP1 specifically at replication forks. This could also be the location of physiological trapped PARP1 which we observed upon p97 inhibition.

During our work with p97, we found that TOP1cc repair is heavily reliant on DNA replication and its replication dependent cofactor SPRTN (Fielden et al., 2020). We present data here that shows p97 and SPRTN is also important for trapped PARP1 repair (Figure 34-37). Thus if trapped PARP1 is occurring at the replication fork, whether physiologically or via PARPis, p97 and SPRTN should be primary candidates for mediating its removal. One way to test this would be to perform an iPOND (Isolation of Proteins On Nascent DNA) experiment to determine whether the amount of PARP1 accumulates at the replication fork upon PARP1 and p97 inhibition.

Another regulatory layer of PARP1's physiological activity was revealed by a series of work from the Ahel laboratory. PARP1 was shown to have a catalytic preference towards serine ribosylation on histones in response to DNA damage (Palazzo et al., 2018), and this was shown to be dependent on its cofactor, HPF1 (Bonfiglio et al., 2017). It was shown structurally that PARP1 and HPF1 bind and complete a single active site, through which it is

able to modify histones (Suskiewicz et al., 2020). HPF1-PARP1 reconfigures PARP1 away from auto-modification of itself, which is thought to be the mechanism which release PARP1 from chromatin.

It is thus possible that mis-regulation of PARP1-HPF1 interaction could lead to increased trapped PARP1 on the chromatin. A situation where HPF1-PARP1 binding could not be released, could lead to increased PARP1 trapping and associated cytotoxicity. Indeed, the clinical relevance of HPF1 was shown when it was found that HPF1 binding to PARP1 increased the binding of the PARPi, olaparib, to PARP1 (Rudolph et al., 2021). Furthermore, the presence of HPF1 caused stronger retention of PARP1 to DNA. HPF1 is the only known cofactor of PARP1 which completes an active site. This additional cofactor which affects PARPi binding could explain the differential cytotoxicity exhibited by talazoparib versus olaparib. It represents an unexplored reason as to why *in vitro* data, which suggests talazoparib and olaparib should have the same potency of trapping (Hopkins et al., 2015; Zandarashvili et al., 2020), actually show hundred fold difference in cellular PARP1 trapping and cytotoxicity (Murai et al., 2014). These small molecular inhibitors of PARP1 may be exhibiting additional interactions with cofactors of PARP1. This begs the question whether there are other unidentified cofactors which function to determine PARPi sensitivity.

Our findings that show p97 inhibition increases trapped PARP1 in the absence of PARPi, along with recent findings that trapped PARP1 increases upon DNA damage induction in XRCC1-/- cells, point towards a previously unknown phenomenon in PARP1 biology. They show the likelihood that trapped PARP1 is a physiological phenomenon which is extremely deleterious for cell survival.

4.3. PARPis and cancer

PARP inhibitors are the first targeted cancer chemotherapy against DNA damage, specifically targeting HR deficient cancers (Bayraktar et al., 2019). Currently, it can be used

for the treatment of prostate, pancreatic, breast and ovarian HR-deficient cancers as a first line treatment and maintenance therapy (Dias et al., 2021a).

4.3.1. PARPi synthetic lethality revised

It was originally found that PARP1 inhibition in BRCA1/2 deficient cells demonstrate marked cytotoxicity when compared to BRCA1/2 wild-type (Bryant et al., 2005; Farmer et al., 2005). From this, four PARPis, rucaparib, niraparib, olaparib and talazoparib were developed and approved by the FDA (Dias et al., 2021; Lord & Ashworth, 2017). Back In 2005, when the initial interaction was discovered, PARP1 was primarily known as a SSB repair protein. In consideration with its effects on HR-deficient cancers, a model for the mechanism of action of PARPis was proposed. This model was based on synthetic lethality, which posits PARPi treatment causes an increase in SSBs, where fork run-off then coverts these SSBs to DSBs (Lord & Ashworth, 2017). These DSBs overwhelm HR-deficient cancers and cell death occurs through mitotic catastrophe. In somatic cells, it was suggested that the induced DSBs are promptly repaired in an error-free process by HR.

However since this proposal, several findings have led to a redrawing of the model for PARPi-induced specific killing in HR deficient cancers. The main findings were: (i) PARPi cytotoxicity correlates with PARP1 trapping ability rather than catalytic inhibition (Murai et al., 2012), (ii) PARPis do not increase SSBs (Helleday, 2011; Ström et al., 2011). The new revised model is one where PARPis trap PARP1 protein to form a DPC-like lesion that causes cytotoxicity in HR-deficient cells through replication stress and DSBs (Murai & Pommier, 2019). This mechanism is similar to TOP1cc-induced cytotoxicity, where PARP1 remains bound at the ends of SSBs and becomes an obstacle for replication forks and transcription.

Our data supports the notion that trapped PARP1 is the main cytotoxic lesion of PARPis. We showed that there exists an innate response to trapped PARP1 within cancer cells. A pathway consisting of PIAS4-RNF4-UFD1-p97 which we can target to increase the amount of trapped PARP1 and to slow down the kinetics of trapped PARP1 repair (Figure 30,

31). By using p97 inhibitors we were able to potentiate cytotoxicity of PARPi (Figure 32). This effect was entirely trapping dependent as PARP1$^{-/-}$ cells did not respond to combination treatment of p97 inhibitor and PARPi (Figure 32 A-C). By revealing the cellular response to the trapping of PARP1, we validated the new trapped PARP1 model of PARPi-induced specific killing in HR-deficient cancers. We showed that the weak PARP1 trapper veliparib, when compared to its derivative UKTT15, which has potent PARP1 trapping abilities, produced weaker responses within the cell. Veliparib caused weak PARP1 ubiquitination, whereas UKTT15 was able to trigger a strong ubiquitin response followed by strong PARP1-p97 interaction (Figure 18B, 23B). These results along with previously observed increased cytotoxicity of cancers to UKTT15 when compared to veliparib, validate the presence and deleterious result of PARP1 trapping (Zandarashvili et al., 2020).

Our results support the redrawing of the original synthetic lethal model for PARPi specific cytotoxicity in HR-deficient cells. Whereas the synthetic lethal model proposes that PARP1 loss is the mechanism for cell killing, it is the presence of PARP1 and its protein bulk as a DPC-like lesion that causes cell death in HR-deficient cancers (Hopkins et al., 2019; Murai et al., 2012, 2014; Murai & Pommier, 2019; Pommier et al., 2016; Pommier & Murai, 2015; Saha et al., 2021). In contradiction of the synthetic lethality model, higher levels of PARP1 actually leads to greater toxicity to PARPis (Pettitt et al., 2013). This is explained by the fact that there is more PARP1 protein to be trapped.

PARPi's mechanism of action is actually more akin to CPT, its derivatives, and platinum salts such as cisplatin, which cause covalently linked TOP1ccs and promiscuous DPCs/ICLs respectively (Stingele et al., 2017). These agents also cause, to a similar extent to PARPis, exquisite sensitivity to BRCA-deficient cancers (Nakamura et al., 2010; Tassone et al., 2003). This demonstrates that rather than a mechanism of genetic interaction and synthetic lethality, PARPis achieve its cytotoxicity by directly causing genotoxic lesions in cells which lack the DDR capabilities to survive the insult. The exact mechanisms of why BRCA1/2

deficient cells are so sensitive to trapped PARP1 is still being actively researched and expanded.

On this topic, it was shown that HR repair factors including BRCA1/2 play an important role in protecting replication forks against degradation (Chaudhuri et al., 2016). Importantly, this process was revealed to play a role in regulating sensitivity to PARPis and other DNA damaging agents. Unprotected forks recruit MRE11 via PTIP and MRE11 uncontrollably resects DNA at stalled replication forks. This was suggested to cause increased cell death via *in vivo* models, where tumours resistant to PARPis were found to have less fork degradation. Interestingly, these tumours were resistant not just to PARPi, but also to platinum salts and topotecan due to increased fork protection in the BRCA2 deficient background. This suggests that all three cause cell death by a similar mechanism, namely replication stress as the result of replication fork obstacles. The discovery of fork degradation provides an alternative explanation as to why BRCA1/2-deficient cells are more sensitive to PARPis and other DNA damaging agents. This hypothesis suggests that HR-deficiency alone cannot explain the targeted sensitivity, and that one needs to take into account the role DDR proteins play in fork protection.

These studies looking to reveal the functions of HR and BRCA1/2 are downstream of the majority of the work presented here. Whereas they look to explain the reasoning for differential sensitivity of BRCA1/2-deficient cancers to PARPis, we looked to explore the lesion which causes the differential sensitivity.

Our results show that increasing the amount of PARPi-induced trapped PARP1 by inhibiting p97, leads to increased synergistic cytotoxicity in both HR-proficient and deficient cell lines (Figure 32E-H). This result is also illustrated in the study by Zandarashvili et al., where UKTT15 caused greater cell death when compared to veliparib. However, UKTT15 maintained the same therapeutic window, as veliparib, between BRCA1 dysfunctional mutant and revertant mutant cell lines (Zandarashvili et al., 2020). In essence, the more PARP1 trapping one causes, the greater the cellular cytotoxicity one observes. In our study, if one is

to rule out the mild cytotoxic effect we observed for CB-5083 on DLD1 BRCA2$^{-/-}$ cells (Figure 32E). The cytotoxic profiles of PARPi + CB-5083 would be a near equidistant shift towards increased cytotoxicity, irrespective of BRCA2 status. Increasing the amount of trapped PARP1 by combination treatment, effectively maintains the same therapeutic window as PARPi alone, as both cell backgrounds are equally permeable to trapped PARP1 generation and repair (Figure 32G). The difference in cytotoxicity which creates the therapeutic window is in the cells' tolerance towards trapped PARP1, of which cells with BRCA1/2 deficiencies is much less. Thus, our results confirm that HR plays a role downstream of trapped PARP1 lesion repair.

Although this situation may be different *in vivo*, as the cells you hope to create the therapeutic window between are somatic cells versus cancerous cells, whereas we determined the therapeutic window after increasing trapped PARP1 in WT versus BRCA2$^{-/-}$ cancer cell lines. There exists the possibility that the higher p97 activity abnormally found in cancer cells may make them more sensitive to combinations of PARPi and p97 inhibition. As cancer cells have a cellular background that makes them more resistant to PARPi when compared with somatic cells, irrespective of their BRCA1/2 status.

We find that under the use of PARPis, trapped PARP1 is the cause of cytotoxicity in both HR-proficient and HR-deficient cancer cell lines. When we increase the amount of trapped PARP1 by p97 inhibition, we caused more cell death in both backgrounds (Figure 32). By removing BRCA1/2 and causing HR-deficiency and loss of fork protection, cells are able to tolerate much lower amounts of trapped PARP1. Thus rather than a model of redundant repair mechanisms as proposed by synthetic lethality, the differential sensitivity observed is built on the bedrock of cytotoxic trapped PARP1. It seems to be the case that cancers which are deficient in DSB repair are unable to repair DPC/DPC-like causing chemotherapeutics, whether that is PARPi, CPT derivatives or platinum salts.

4.3.2. Clinical implications

The concept of synthetic lethality proposes that somatic cells would be resistant to PARPi's cytotoxicity due to their functional HR pathway, thereby enabling targeting of HR-deficient cancers (Lord & Ashworth, 2017). However, the biggest drawback of PARPis is currently the emergence of therapeutic resistance in tumours (Dias et al., 2021). In addition, the clinical trials for PARPis have unfortunately identified a range of adverse events and side effects it was thought to be free of (LaFargue et al., 2019). These events often include haematological toxicities such as anaemia and thrombocytemia; and gastrointestinal toxicities such as nausea and vomiting. These side effects are common to anti-proliferative traditional chemotherapies such as irinotecan and platinum salts (Shi et al., 2015). This suggests that PARPi and its cytotoxic lesion trapped PARP1, still has effects on physiological cellular proliferation within the body, found during haematopoiesis and in the gastrointestinal lining. This is likely due to the similar cytotoxic mechanisms both PARPis and CPTs possess.

Importantly, the outstanding recent interest in PARPis, have led to possible methods of tweaking the treatment for increased sensitivity. For example, it was shown that there are ways of manipulating PARPi dosing regimes to reduce toxicity in normal cells, in particular with combinatorial PARPi therapies. This was done in a preclinical study exploring the effects of PARPi in combination with Wee1 inhibitor (Fang et al., 2019). Rather than concurrent treatment, authors found that sequential therapy leads to low replication stress in normal cells. However in cancer cells, sequential treatment still lead to a maintenance of high replication stress and associated cell death. This shows that with combination treatments of PARPi, there may be more flexibility to obtain the best therapeutic window. Our study which shows the synergistic cytotoxicity between the use of p97 inhibitors CB-5083/CuET and PARPi could also benefit from optimised dosing regimes.

CB-5083 was tested in two phase I trials in solid tumours and multiple myelomas, the trials were halted due to off-target effects on phosphodiesterase 6 (PDE6) (Roux et al., 2021). Since then, a second generation inhibitor CB-5339 has been developed and is currently in

phase I clinical trial. CB-5339 showed 15 times less activity *in vitro* to PDE6 when compared to CB-5083 (Roux et al., 2021). Its cytotoxic effects on cell lines and cancers, specifically acute myeloid leukamia, were validated to be almost identical to CB-5083.

CuET on the other hand was discovered as a metabolite of an already approved clinical treatment for alcohol abuse, disulfiram, (Skrott et al., 2017). The metabolite, CuET, which forms upon incubating disulfiram with copper, is another promising step towards using a p97 inhibitor in the clinic. In fact, disulfiram's anti-cancer capabilities have already led to several ongoing clinical trials as a single treatment (NCT03323346, NCT04521335). Our results showed synergistic cytotoxicity of CuET with PARPis and suggested a mechanism for this cytotoxicity, providing impetus to study this combination further (Figure 31, 32A, C). Unlike other PARPi combination treatments, our proposed combination treatment targets two distinct vulnerabilities of cancer, DNA damage from trapped PARP1 and proteotoxic stress from p97 inhibition.

In summary, the recent focus on PARPis and combination treatments have shed light on many ways to potentiate PARPi effects. These include modifying dosing regimes to remove some of the side-effects and adverse events common to anti-proliferative drugs (Fang et al., 2019). Encouragingly, our identified combination target of p97 and PARP1 is a treatment that is possible without the need for *de novo* drug development. The second generation p97 inhibitor, CB-5339, has been developed for cancer monotherapy, and the approved drug disulfiram, whose metabolite CuET has also been found to inhibit p97 (Benajiba et al., 2020; Skrott et al., 2017, 2019). These results combined with the solid mechanistic understanding we show, make it an attractive combination for further preclinical testing.

4.3.3. Further Work

To delineate the different pathways of DPC repair, I would use trapped PARP1 as a model substrate. Work shown here and from other labs have used trapped PARP1 to reveal its repair by PIAS4/RNF4, p97 and SPRTN (Liu et al., 2021; Saha et al., 2021). The increasing complexity of the cellular response to DPCs involving SUMOylation and ubiquitination requires a model system to delineate the overlapping pathways. Although promising work have begun to discern some of these mechanisms through the use of model substrates in frog extracts, their differential expression of many important DDR factors and lack of translatability to a mammalian cancer setting leaves much to be desired. Using trapped PARP1, we can begin by exploring the role of the cell cycle has on the various signalling and repair pathways. By arresting cells in G1 phase of the cell cycle, we can remove the contribution of replication-dependent SPRTN repair and isolate the effects of PIAS4/RNF4 repair and begin to reveal their different mechanisms. Trapped PARP1 is both an attractive substrate to use due to its clinical implications but also due to the wealth of research resources available. It may provide the gateway to realising the full details of DPC repair signalling.

Expanding on this, trapped PARP1 is also an appropriate substrate to use for the testing of nuclear autophagy. There are indications as mentioned above which suggest trapped PARP1 could be repaired at the nuclear periphery. This presents an opportunity to study whether autophagy may play a role in repairing DPCs. Using the various different inhibitors with differential trapping capabilities, it would be possible to discern the role that autophagy plays upon DPC induction. This would increase our understanding of both DPC repair and reveal possible novel biomarkers for PARPi treatment.

5. References

Acs, K., Luijsterburg, M. S., Ackermann, L., Salomons, F. A., Hoppe, T., & Dantuma, N. P. (2011a). The AAA-ATPase VCP/p97 promotes 53BP1 recruitment by removing L3MBTL1 from DNA double-strand breaks. *Nature Structural and Molecular Biology*, *18*(12). https://doi.org/10.1038/nsmb.2188

Acs, K., Luijsterburg, M. S., Ackermann, L., Salomons, F. A., Hoppe, T., & Dantuma, N. P. (2011b). The AAA-ATPase VCP/p97 promotes 53BP1 recruitment by removing L3MBTL1 from DNA double-strand breaks. *Nature Structural and Molecular Biology*, *18*(12). https://doi.org/10.1038/nsmb.2188

Aftab, B. T., Anderson, D. J., le Moigne, R., Djakovic, S., Dhimolea, E., Murnane, M., King, E., Rice, J., Wong, S., Kumar, B., Valle, E., Menon, M.-K., Kiss von Soly, S., Wang, J., Yao, B., Soriano, F., Kampmann, M., Alcost-Alvear, D., Chesi, M., … Rolfe, M. (2014). Pre-Clinical Activity of the Novel, First-in-Class p97 Inhibitor, CB-5083, in Multiple Myeloma. *Blood*, *124*(21). https://doi.org/10.1182/blood.v124.21.4701.4701

Aleksandrov, R., Dotchev, A., Poser, I., Krastev, D., Georgiev, G., Panova, G., Babukov, Y., Danovski, G., Dyankova, T., Hubatsch, L., Ivanova, A., Atemin, A., Nedelcheva-Veleva, M. N., Hasse, S., Sarov, M., Buchholz, F., Hyman, A. A., Grill, S. W., & Stoynov, S. S. (2018). Protein Dynamics in Complex DNA Lesions. *Molecular Cell*, *69*(6). https://doi.org/10.1016/j.molcel.2018.02.016

Alemasova, E. E., & Lavrik, O. I. (2019). Poly(ADP-ribosyl)ation by PARP1: reaction mechanism and regulatory proteins. *Nucleic Acids Research*, *47*(8), 3811. https://doi.org/10.1093/NAR/GKZ120

An, H., Ordureau, A., Paulo, J. A., Shoemaker, C. J., Denic, V., & Harper, J. W. (2019). TEX264 Is an Endoplasmic Reticulum-Resident ATG8-Interacting Protein Critical for ER Remodeling during Nutrient Stress. *Molecular Cell*, *74*(5). https://doi.org/10.1016/j.molcel.2019.03.034

Anand, R., Ranjha, L., Cannavo, E., & Cejka, P. (2016). Phosphorylated CtIP Functions as a Co-factor of the MRE11-RAD50-NBS1 Endonuclease in DNA End Resection. *Molecular Cell*, *64*(5). https://doi.org/10.1016/j.molcel.2016.10.017

Anderson, D. J., le Moigne, R., Djakovic, S., Kumar, B., Rice, J., Wong, S., Wang, J., Yao, B., Valle, E., Kiss von Soly, S., Madriaga, A., Soriano, F., Menon, M. K., Wu, Z. Y., Kampmann, M., Chen, Y., Weissman, J. S., Aftab, B. T., Yakes, F. M., … Rolfe, M. (2015). Targeting the AAA ATPase p97 as an Approach to Treat Cancer through Disruption of Protein Homeostasis. *Cancer Cell*, *28*(5), 653–665. https://doi.org/10.1016/J.CCELL.2015.10.002

Audebert, M., Salles, B., & Calsou, P. (2004). Involvement of poly(ADP-ribose) polymerase-1 and XRCC1/DNA ligase III in an alternative route for DNA double-strand breaks rejoining. *Journal of Biological Chemistry*, *279*(53). https://doi.org/10.1074/jbc.M404524200

Balakirev, M. Y., Mullally, J. E., Favier, A., Assard, N., Sulpice, E., Lindsey, D. F., Rulina, A. v., Gidrol, X., & Wilkinson, K. D. (2015). Wss1 metalloprotease partners

with Cdc48/Doa1 in processing genotoxic SUMO conjugates. *ELife*, *4*(September2015). https://doi.org/10.7554/eLife.06763

Barber, L. J., Sandhu, S., Chen, L., Campbell, J., Kozarewa, I., Fenwick, K., Assiotis, I., Rodrigues, D. N., Filho, J. S. R., Moreno, V., Mateo, J., Molife, L. R., de Bono, J., Kaye, S., Lord, C. J., & Ashworth, A. (2013). Secondary mutations in BRCA2 associated with clinical resistance to a PARP inhibitor. *The Journal of Pathology*, *229*(3), 422–429. https://doi.org/10.1002/PATH.4140

Barnes, D. E., & Lindahl, T. (2004). Repair and genetic consequences of endogenous DNA base damage in mammalian cells. In *Annual Review of Genetics* (Vol. 38). https://doi.org/10.1146/annurev.genet.38.072902.092448

Bartkova, J., Rezaei, N., Liontos, M., Karakaidos, P., Kletsas, D., Issaeva, N., Vassiliou, L. V. F., Kolettas, E., Niforou, K., Zoumpourlis, V. C., Takaoka, M., Nakagawa, H., Tort, F., Fugger, K., Johansson, F., Sehested, M., Andersen, C. L., Dyrskjot, L., Ørntoft, T., … Gorgoulis, V. G. (2006). Oncogene-induced senescence is part of the tumorigenesis barrier imposed by DNA damage checkpoints. *Nature 2006 444:7119*, *444*(7119), 633–637. https://doi.org/10.1038/nature05268

Basu, A. K. (2018). DNA Damage, Mutagenesis and Cancer. *International Journal of Molecular Sciences*, *19*(4). https://doi.org/10.3390/IJMS19040970

Bauer, N. C., Corbett, A. H., & Doetsch, P. W. (2015). The current state of eukaryotic DNA base damage and repair. In *Nucleic Acids Research* (Vol. 43, Issue 21). https://doi.org/10.1093/nar/gkv1136

Baumann, P., Benson, F. E., & West, S. C. (1996). Human Rad51 protein promotes ATP-dependent homologous pairing and strand transfer reactions in vitro. *Cell*, *87*(4). https://doi.org/10.1016/S0092-8674(00)81394-X

Bayraktar, S., Glück, S., & Darling, H. (2019). Update on PARP inhibitor therapy for solid tumors. *Journal of Cancer Prevention & Current Research*, *Volume 10*(Issue 4). https://doi.org/10.15406/JCPCR.2019.10.00400

Bell, D., Berchuck, A., Birrer, M., Chien, J., Cramer, D. W., Dao, F., Dhir, R., Disaia, P., Gabra, H., Glenn, P., Godwin, A. K., Gross, J., Hartmann, L., Huang, M., Huntsman, D. G., Iacocca, M., Imielinski, M., Kalloger, S., Karlan, B. Y., … Thomson, E. (2011). Integrated genomic analyses of ovarian carcinoma. *Nature 2011 474:7353*, *474*(7353), 609–615. https://doi.org/10.1038/nature10166

Benajiba, L., Carraway, H. E., Hamad, N., Stein, E. M., Yannakou, C. K., Burroughs, A., Harris, S., Lane, H., Nguyen, D. D., Stuart, M., Vargas, J., Puissant, A., Stegmaier, K., & DiNardo, C. D. (2020). Trials in Progress: A Phase I Study to Evaluate the Safety and Pharmacokinetic Profiles of CB-5339 in Participants with Relapsed/Refractory Acute Myeloid Leukemia or Relapsed/Refractory Intermediate or High-Risk Myelodysplastic Syndrome. *Blood*, *136*(Supplement 1). https://doi.org/10.1182/blood-2020-140636

Benson, F. E., Baumann, P., & West, S. C. (1998). Synergistic actions of Rad51 and Rad52 in recombination and DNA repair. *Nature*, *391*(6665). https://doi.org/10.1038/34937

Berti, M., & Vindigni, A. (2016). Replication stress: getting back on track. *Nature Structural & Molecular Biology*, *23*(2), 103. https://doi.org/10.1038/NSMB.3163

Bhargava, R., Onyango, D. O., & Stark, J. M. (2016). Regulation of Single-Strand Annealing and its Role in Genome Maintenance. In *Trends in Genetics* (Vol. 32, Issue 9). https://doi.org/10.1016/j.tig.2016.06.007

Bishop, A. J. R., & Schiestl, R. H. (2000). Homologous recombination as a mechanism for genome rearrangements: environmental and genetic effects. *Human Molecular Genetics*, *9*(16), 2427–2334. https://doi.org/10.1093/HMG/9.16.2427

Blackford, A. N., & Jackson, S. P. (2017). ATM, ATR, and DNA-PK: The Trinity at the Heart of the DNA Damage Response. In *Molecular Cell* (Vol. 66, Issue 6). https://doi.org/10.1016/j.molcel.2017.05.015

Blythe, E. E., Olson, K. C., Chau, V., & Deshaies, R. J. (2017). Ubiquitin- A nd ATP-dependent unfoldase activity of P97/VCP•NPLOC4•UFD1L is enhanced by a mutation that causes multisystem proteinopathy. *Proceedings of the National Academy of Sciences of the United States of America*, *114*(22). https://doi.org/10.1073/pnas.1706205114

Bodnar, N. O., & Rapoport, T. A. (2017a). Molecular Mechanism of Substrate Processing by the Cdc48 ATPase Complex. *Cell*, *169*(4). https://doi.org/10.1016/j.cell.2017.04.020

Bodnar, N. O., & Rapoport, T. A. (2017b). Molecular Mechanism of Substrate Processing by the Cdc48 ATPase Complex. *Cell*, *169*(4), 722-735.e9. https://doi.org/10.1016/J.CELL.2017.04.020

Bonfiglio, J. J., Fontana, P., Zhang, Q., Colby, T., Gibbs-Seymour, I., Atanassov, I., Bartlett, E., Zaja, R., Ahel, I., & Matic, I. (2017a). Serine ADP-Ribosylation Depends on HPF1. *Molecular Cell*, *65*(5). https://doi.org/10.1016/j.molcel.2017.01.003

Bonfiglio, J. J., Fontana, P., Zhang, Q., Colby, T., Gibbs-Seymour, I., Atanassov, I., Bartlett, E., Zaja, R., Ahel, I., & Matic, I. (2017b). Serine ADP-Ribosylation Depends on HPF1. *Molecular Cell*, *65*(5), 932-940.e6. https://doi.org/10.1016/J.MOLCEL.2017.01.003

Borgermann, N., Ackermann, L., Schwertman, P., Hendriks, I. A., Thijssen, K., Liu, J. C., Lans, H., Nielsen, M. L., & Mailand, N. (2019). SUMO ylation promotes protective responses to DNA -protein crosslinks . *The EMBO Journal*, *38*(8). https://doi.org/10.15252/embj.2019101496

Bothmer, A., Robbiani, D. F., Feldhahn, N., Gazumyan, A., Nussenzweig, A., & Nussenzweig, M. C. (2010). 53BP1 regulates DNA resection and the choice between classical and alternative end joining during class switch recombination. *The Journal of Experimental Medicine*, *207*(4), 855. https://doi.org/10.1084/JEM.20100244

Botuyan, M. V., Lee, J., Ward, I. M., Kim, J. E., Thompson, J. R., Chen, J., & Mer, G. (2006). Structural Basis for the Methylation State-Specific Recognition of Histone H4-K20 by 53BP1 and Crb2 in DNA Repair. *Cell*, *127*(7), 1361–1373. https://doi.org/10.1016/J.CELL.2006.10.043/ATTACHMENT/1E24C5EA-5D93-4E9E-96A9-E39731599FA9/MMC1.PDF

Britton, S., Coates, J., & Jackson, S. P. (2013). A new method for high-resolution imaging of Ku foci to decipher mechanisms of DNA double-strand break repair. *Journal of Cell Biology*, *202*(3). https://doi.org/10.1083/jcb.201303073

BROWN, J. R., & THORNTON, J. L. (1957). Percivall Pott (1714-1788) and chimney sweepers' cancer of the scrotum. *British Journal of Industrial Medicine*, *14*(1), 68–70. https://doi.org/10.1136/OEM.14.1.68

Bruce Alberts. (2015). *Molecular biology of the cell* (Sixth edition.).

Bryant, H. E., Schultz, N., Thomas, H. D., Parker, K. M., Flower, D., Lopez, E., Kyle, S., Meuth, M., Curtin, N. J., & Helleday, T. (2005). Specific killing of BRCA2-deficient tumours with inhibitors of poly(ADP-ribose) polymerase. *Nature*, *434*(7035). https://doi.org/10.1038/nature03443

Caldecott, K. W. (2008). Single-strand break repair and genetic disease. In *Nature Reviews Genetics* (Vol. 9, Issue 8). https://doi.org/10.1038/nrg2380

Caldecott, K. W. (2019). XRCC1 protein; Form and function. In *DNA Repair* (Vol. 81). https://doi.org/10.1016/j.dnarep.2019.102664

Cao, L., Xu, X., Bunting, S. F., Liu, J., Wang, R. H., Cao, L. L., Wu, J. J., Peng, T. N., Chen, J., Nussenzweig, A., Deng, C. X., & Finkel, T. (2009). A Selective Requirement for 53BP1 in the Biological Response to Genomic Instability Induced by Brca1 Deficiency. *Molecular Cell*, *35*(4). https://doi.org/10.1016/j.molcel.2009.06.037

Caridi, C. P., D'agostino, C., Ryu, T., Zapotoczny, G., Delabaere, L., Li, X., Khodaverdian, V. Y., Amaral, N., Lin, E., Rau, A. R., & Chiolo, I. (2018). Nuclear F-actin and myosins drive relocalization of heterochromatic breaks. *Nature*, *559*(7712). https://doi.org/10.1038/s41586-018-0242-8

Ceccaldi, R., Liu, J. C., Amunugama, R., Hajdu, I., Primack, B., Petalcorin, M. I. R., O'Connor, K. W., Konstantinopoulos, P. A., Elledge, S. J., Boulton, S. J., Yusufzai, T., & D'Andrea, A. D. (2015). Homologous-recombination-deficient tumours are dependent on Polθ -mediated repair. *Nature*, *518*(7538). https://doi.org/10.1038/nature14184

Chang, H. H. Y., Pannunzio, N. R., Adachi, N., & Lieber, M. R. (2017). Non-homologous DNA end joining and alternative pathways to double-strand break repair. *Nature Reviews Molecular Cell Biology 2017 18:8*, *18*(8), 495–506. https://doi.org/10.1038/nrm.2017.48

Chatterjee, N., & Walker, G. C. (2017). Mechanisms of DNA damage, repair, and mutagenesis. In *Environmental and Molecular Mutagenesis* (Vol. 58, Issue 5). https://doi.org/10.1002/em.22087

Chaudhuri, A. R., Callen, E., Ding, X., Gogola, E., Duarte, A. A., Lee, J. E., Wong, N., Lafarga, V., Calvo, J. A., Panzarino, N. J., John, S., Day, A., Crespo, A. V., Shen, B., Starnes, L. M., de Ruiter, J. R., Daniel, J. A., Konstantinopoulos, P. A., Cortez, D., … Nussenzweig, A. (2016a). Replication fork stability confers chemoresistance in BRCA-deficient cells. *Nature*, *535*(7612). https://doi.org/10.1038/nature18325

Chaudhuri, A. R., Callen, E., Ding, X., Gogola, E., Duarte, A. A., Lee, J. E., Wong, N., Lafarga, V., Calvo, J. A., Panzarino, N. J., John, S., Day, A., Crespo, A. V., Shen, B., Starnes, L. M., de Ruiter, J. R., Daniel, J. A., Konstantinopoulos, P. A., Cortez,

D., … Nussenzweig, A. (2016b). Replication fork stability confers chemoresistance in BRCA-deficient cells. *Nature 2016 535:7612*, *535*(7612), 382–387. https://doi.org/10.1038/nature18325

Chen, B. R., Wang, Y., Shen, Z. J., Bennett, A., Hindi, I., Tyler, J. K., & Sleckman, B. P. (2021). The RNF8 and RNF168 Ubiquitin Ligases Regulate Pro- and Anti-Resection Activities at Broken DNA Ends During Non-Homologous End Joining. *DNA Repair*, *108*. https://doi.org/10.1016/J.DNAREP.2021.103217

Chen, X., Dou, Q. P., Liu, J., & Tang, D. (2021). Targeting Ubiquitin–Proteasome System With Copper Complexes for Cancer Therapy. *Frontiers in Molecular Biosciences*, *8*, 116. https://doi.org/10.3389/FMOLB.2021.649151/BIBTEX

Churikov, D., Charifi, F., Eckert-Boulet, N., Silva, S., Simon, M. N., Lisby, M., & Géli, V. (2016). SUMO-Dependent Relocalization of Eroded Telomeres to Nuclear Pore Complexes Controls Telomere Recombination. *Cell Reports*, *15*(6). https://doi.org/10.1016/j.celrep.2016.04.008

Ciccia, A., & Elledge, S. J. (2010). The DNA Damage Response: Making It Safe to Play with Knives. In *Molecular Cell* (Vol. 40, Issue 2). https://doi.org/10.1016/j.molcel.2010.09.019

Clark, N. J., Kramer, M., Muthurajan, U. M., & Luger, K. (2012). Alternative modes of binding of poly(ADP-ribose) polymerase 1 to free DNA and nucleosomes. *Journal of Biological Chemistry*, *287*(39). https://doi.org/10.1074/jbc.M112.397067

Costantini, S., Capone, F., Polo, A., Bagnara, P., & Budillon, A. (2021). Valosin-Containing Protein (VCP)/p97: A Prognostic Biomarker and Therapeutic Target in Cancer. *International Journal of Molecular Sciences*, *22*(18), 10177. https://doi.org/10.3390/IJMS221810177

Dalal, S., Rosser, M. F. N., Cyr, D. M., & Hanson, P. I. (2004). Distinct Roles for the AAA ATPases NSF and p97 in the Secretory Pathway. *Molecular Biology of the Cell*, *15*(2). https://doi.org/10.1091/mbc.E03-02-0097

Damgaard, R. B. (2021). The ubiquitin system: from cell signalling to disease biology and new therapeutic opportunities. In *Cell Death and Differentiation* (Vol. 28, Issue 2). https://doi.org/10.1038/s41418-020-00703-w

Dantuma, N. P., Acs, K., & Luijsterburg, M. S. (2014). Should I stay or should I go: VCP/p97-mediated chromatin extraction in the DNA damage response. In *Experimental Cell Research* (Vol. 329, Issue 1). https://doi.org/10.1016/j.yexcr.2014.08.025

Dargemont, C., & Ossareh-Nazari, B. (2012). Cdc48/p97, a key actor in the interplay between autophagy and ubiquitin/proteasome catabolic pathways. *Biochimica et Biophysica Acta (BBA) - Molecular Cell Research*, *1823*(1), 138–144. https://doi.org/10.1016/J.BBAMCR.2011.07.011

Das, B. B., Huang, S. N., Murai, J., Rehman, I., Amé, J. C., Sengupta, S., Das, S. K., Majumdar, P., Zhang, H., Biard, D., Majumder, H. K., Schreiber, V., & Pommier, Y. (2014). PARP1–TDP1 coupling for the repair of topoisomerase I–induced DNA damage. *Nucleic Acids Research*, *42*(7), 4435–4449. https://doi.org/10.1093/NAR/GKU088

Dasari, S., & Bernard Tchounwou, P. (2014). Cisplatin in cancer therapy: molecular mechanisms of action. *European Journal of Pharmacology*, *740*, 364. https://doi.org/10.1016/J.EJPHAR.2014.07.025

Davis, A. J., & Chen, D. J. (2013). DNA double strand break repair via non-homologous end-joining. *Translational Cancer Research*, *2*(3), 130. https://doi.org/10.3978/J.ISSN.2218-676X.2013.04.02

DeLaBarre, B., Christianson, J. C., Kopito, R. R., & Brunger, A. T. (2006). Central Pore Residues Mediate the p97/VCP Activity Required for ERAD. *Molecular Cell*, *22*(4). https://doi.org/10.1016/j.molcel.2006.03.036

Demin, A. A., Hirota, K., Tsuda, M., Adamowicz, M., Hailstone, R., Brazina, J., Gittens, W., Kalasova, I., Shao, Z., Zha, S., Sasanuma, H., Hanzlikova, H., Takeda, S., & Caldecott, K. W. (2021). XRCC1 prevents toxic PARP1 trapping during DNA base excision repair. *Molecular Cell*, *81*(14), 3018-3030.e5. https://doi.org/10.1016/J.MOLCEL.2021.05.009

Deshaies, R. J. (2014). Proteotoxic crisis, the ubiquitin-proteasome system, and cancer therapy. In *BMC Medicine* (Vol. 12, Issue 1). https://doi.org/10.1186/s12915-014-0094-0

Dev, H., Chiang, T. W. W., Lescale, C., de Krijger, I., Martin, A. G., Pilger, D., Coates, J., Sczaniecka-Clift, M., Wei, W., Ostermaier, M., Herzog, M., Lam, J., Shea, A., Demir, M., Wu, Q., Yang, F., Fu, B., Lai, Z., Balmus, G., … Jackson, S. P. (2018a). Shieldin complex promotes DNA end-joining and counters homologous recombination in BRCA1-null cells. *Nature Cell Biology*, *20*(8), 954. https://doi.org/10.1038/S41556-018-0140-1

Dev, H., Chiang, T. W. W., Lescale, C., de Krijger, I., Martin, A. G., Pilger, D., Coates, J., Sczaniecka-Clift, M., Wei, W., Ostermaier, M., Herzog, M., Lam, J., Shea, A., Demir, M., Wu, Q., Yang, F., Fu, B., Lai, Z., Balmus, G., … Jackson, S. P. (2018b). Shieldin complex promotes DNA end-joining and counters homologous recombination in BRCA1-null cells. *Nature Cell Biology*, *20*(8), 954. https://doi.org/10.1038/S41556-018-0140-1

Dewar, J. M., Low, E., Mann, M., Räschle, M., & Walter, J. C. (2017). CRL2Lrr1 promotes unloading of the vertebrate replisome from chromatin during replication termination. *Genes and Development*, *31*(3). https://doi.org/10.1101/gad.291799.116

Dias, M. P., Moser, S. C., Ganesan, S., & Jonkers, J. (2021a). Understanding and overcoming resistance to PARP inhibitors in cancer therapy. *Nature Reviews Clinical Oncology 2021*, 1–19. https://doi.org/10.1038/s41571-021-00532-x

Dias, M. P., Moser, S. C., Ganesan, S., & Jonkers, J. (2021b). Understanding and overcoming resistance to PARP inhibitors in cancer therapy. *Nature Reviews Clinical Oncology 2021*, 1–19. https://doi.org/10.1038/s41571-021-00532-x

Fang, Y., McGrail, D. J., Sun, C., Labrie, M., Chen, X., Zhang, D., Ju, Z., Vellano, C. P., Lu, Y., Li, Y., Jeong, K. J., Ding, Z., Liang, J., Wang, S. W., Dai, H., Lee, S., Sahni, N., Mercado-Uribe, I., Kim, T. beom, … Mills, G. B. (2019). Sequential Therapy with PARP and WEE1 Inhibitors Minimizes Toxicity while Maintaining Efficacy. *Cancer Cell*, *35*(6). https://doi.org/10.1016/j.ccell.2019.05.001

Farmer, H., McCabe, H., Lord, C. J., Tutt, A. H. J., Johnson, D. A., Richardson, T. B., Santarosa, M., Dillon, K. J., Hickson, I., Knights, C., Martin, N. M. B., Jackson, S. P., Smith, G. C. M., & Ashworth, A. (2005). Targeting the DNA repair defect in BRCA mutant cells as a therapeutic strategy. *Nature*, *434*(7035). https://doi.org/10.1038/nature03445

Fell, V. L., & Schild-Poulter, C. (2012). Ku Regulates Signaling to DNA Damage Response Pathways through the Ku70 von Willebrand A Domain. *Molecular and Cellular Biology*, *32*(1), 76. https://doi.org/10.1128/MCB.05661-11

Fielden, J., Ruggiano, A., Popović, M., & Ramadan, K. (2018). DNA protein crosslink proteolysis repair: From yeast to premature ageing and cancer in humans. *DNA Repair*, *71*, 198–204. https://doi.org/10.1016/J.DNAREP.2018.08.025

Fielden, J., Wiseman, K., Torrecilla, I., Li, S., Hume, S., Chiang, S. C., Ruggiano, A., Narayan Singh, A., Freire, R., Hassanieh, S., Domingo, E., Vendrell, I., Fischer, R., Kessler, B. M., Maughan, T. S., El-Khamisy, S. F., & Ramadan, K. (2020). TEX264 coordinates p97- and SPRTN-mediated resolution of topoisomerase 1-DNA adducts. *Nature Communications*, *11*(1). https://doi.org/10.1038/s41467-020-15000-w

Fortini, P., & Dogliotti, E. (2007). Base damage and single-strand break repair: Mechanisms and functional significance of short- and long-patch repair subpathways. *DNA Repair*, *6*(4). https://doi.org/10.1016/j.dnarep.2006.10.008

Fradet-Turcotte, A., Canny, M. D., Escribano-Díaz, C., Orthwein, A., Leung, C. C. Y., Huang, H., Landry, M. C., Kitevski-Leblanc, J., Noordermeer, S. M., Sicheri, F., & Durocher, D. (2013). 53BP1 is a reader of the DNA-damage-induced H2A Lys 15 ubiquitin mark. *Nature 2013 499:7456*, *499*(7456), 50–54. https://doi.org/10.1038/nature12318

Franz, A., Ackermann, L., & Hoppe, T. (2016). Ring of change: CDC48/p97 drives protein dynamics at chromatin. In *Frontiers in Genetics* (Vol. 7, Issue MAY). https://doi.org/10.3389/fgene.2016.00073

Franz, A., Valledor, P., Ubieto-Capella, P., Pilger, D., Galarreta, A., Lafarga, V., Fernández-Llorente, A., de la Vega-Barranco, G., den Brave, F., Hoppe, T., Fernandez-Capetillo, O., & Lecona, E. (2021). USP7 and VCPFAF1 define the SUMO/Ubiquitin landscape at the DNA replication fork. *Cell Reports*, *37*(2). https://doi.org/10.1016/j.celrep.2021.109819

Fujita, K. I., Kubota, Y., Ishida, H., & Sasaki, Y. (2015). Irinotecan, a key chemotherapeutic drug for metastatic colorectal cancer. *World Journal of Gastroenterology*, *21*(43), 12234. https://doi.org/10.3748/WJG.V21.I43.12234

G, H., & VI, K. (2017). Repair, Reuse, Recycle: The Expanding Role of Autophagy in Genome Maintenance. *Trends in Cell Biology*, *27*(5), 340–351. https://doi.org/10.1016/J.TCB.2016.11.011

Gaillard, H., García-Muse, T., & Aguilera, A. (2015). Replication stress and cancer. *Nature Reviews Cancer 2015 15:5*, *15*(5), 276–289. https://doi.org/10.1038/nrc3916

Gianfaldoni, S., Gianfaldoni, R., Wollina, U., Lotti, J., Tchernev, G., & Lotti, T. (2017). An Overview on Radiotherapy: From Its History to Its Current Applications in

Dermatology. *Open Access Macedonian Journal of Medical Sciences*, *5*(4), 521. https://doi.org/10.3889/OAMJMS.2017.122

Goldberg, M., Stucki, M., Falck, J., D'Amours, D., Rahman, D., Pappin, D., Bartek, J., & Jackson, S. P. (2003). MDC1 is required for the intra-S-phase DNA damage checkpoint. *Nature 2003 421:6926*, *421*(6926), 952–956. https://doi.org/10.1038/nature01445

Goldstein, M., & Kastan, M. B. (2015). The DNA Damage Response: Implications for Tumor Responses to Radiation and Chemotherapy. *Https://Ezproxy-Prd.Bodleian.Ox.Ac.Uk:2102/10.1146/Annurev-Med-081313-121208*, *66*, 129–143. https://doi.org/10.1146/ANNUREV-MED-081313-121208

Gong, L., & Yeh, E. T. H. (2006). Characterization of a family of nucleolar SUMO-specific proteases with preference for SUMO-2 or SUMO-3. *The Journal of Biological Chemistry*, *281*(23), 15869–15877. https://doi.org/10.1074/JBC.M511658200

Gottifredi, V., & Wiesmüller, L. (2020). Current understanding of RAD52 functions: Fundamental and therapeutic insights. In *Cancers* (Vol. 12, Issue 3). https://doi.org/10.3390/cancers12030705

Graham, T. G. W., Walter, J. C., & Loparo, J. J. (2016). Two-Stage Synapsis of DNA Ends during Non-homologous End Joining. *Molecular Cell*, *61*(6). https://doi.org/10.1016/j.molcel.2016.02.010

Gravel, S., Chapman, J. R., Magill, C., & Jackson, S. P. (2008). DNA helicases Sgs1 and BLM promote DNA double-strand break resection. *Genes and Development*, *22*(20). https://doi.org/10.1101/gad.503108

Guang, M. H. Z., Kavanagh, E. L., Dunne, L. P., Dowling, P., Zhang, L., Lindsay, S., Bazou, D., Goh, C. Y., Hanley, C., Bianchi, G., Anderson, K. C., O'Gorman, P., & McCann, A. (2019). Targeting Proteotoxic Stress in Cancer: A Review of the Role that Protein Quality Control Pathways Play in Oncogenesis. *Cancers*, *11*(1), 66. https://doi.org/10.3390/CANCERS11010066

Gupta, R., Somyajit, K., Narita, T., Maskey, E., Stanlie, A., Kremer, M., Typas, D., Lammers, M., Mailand, N., Nussenzweig, A., Lukas, J., & Choudhary, C. (2018). DNA Repair Network Analysis Reveals Shieldin as a Key Regulator of NHEJ and PARP Inhibitor Sensitivity. *Cell*, *173*(4), 972. https://doi.org/10.1016/J.CELL.2018.03.050

Haince, J. F., McDonald, D., Rodrigue, A., Déry, U., Masson, J. Y., Hendzel, M. J., & Poirier, G. G. (2008). PARP1-dependent kinetics of recruitment of MRE11 and NBS1 proteins to multiple DNA damage sites. *Journal of Biological Chemistry*, *283*(2). https://doi.org/10.1074/jbc.M706734200

Halabelian, L., Ravichandran, M., Li, Y., Zeng, H., Rao, A., Aravind, L., & Arrowsmith, C. H. (2019). Structural basis of HMCES interactions with abasic DNA and multivalent substrate recognition. *Nature Structural and Molecular Biology*, *26*(7). https://doi.org/10.1038/s41594-019-0246-6

Halder, S., Torrecilla, I., Burkhalter, M. D., Popović, M., Fielden, J., Vaz, B., Oehler, J., Pilger, D., Lessel, D., Wiseman, K., Singh, A. N., Vendrell, I., Fischer, R., Philipp, M., & Ramadan, K. (2019). SPRTN protease and checkpoint kinase 1 cross-

activation loop safeguards DNA replication. *Nature Communications 2019 10:1*, *10*(1), 1–18. https://doi.org/10.1038/s41467-019-11095-y

Hanahan, D., & Weinberg, R. A. (2011). Hallmarks of cancer: The next generation. In *Cell* (Vol. 144, Issue 5). https://doi.org/10.1016/j.cell.2011.02.013

Hanzlikova, H., Kalasova, I., Demin, A. A., Pennicott, L. E., Cihlarova, Z., & Caldecott, K. W. (2018). The Importance of Poly(ADP-Ribose) Polymerase as a Sensor of Unligated Okazaki Fragments during DNA Replication. *Molecular Cell*, *71*(2). https://doi.org/10.1016/j.molcel.2018.06.004

He, X., Riceberg, J., Soucy, T., Koenig, E., Minissale, J., Gallery, M., Bernard, H., Yang, X., Liao, H., Rabino, C., Shah, P., Xega, K., Yan, Z. H., Sintchak, M., Bradley, J., Xu, H., Duffey, M., England, D., Mizutani, H., … Pulukuri, S. M. (2017). Probing the roles of SUMOylation in cancer cell biology by using a selective SAE inhibitor. *Nature Chemical Biology*, *13*(11). https://doi.org/10.1038/nchembio.2463

Helleday, T. (2011). The underlying mechanism for the PARP and BRCA synthetic lethality: clearing up the misunderstandings. *Molecular Oncology*, *5*(4), 387–393. https://doi.org/10.1016/J.MOLONC.2011.07.001

Hendriks, I. A., Treffers, L. W., Verlaan-deVries, M., Olsen, J. v., & Vertegaal, A. C. O. (2015). SUMO-2 Orchestrates Chromatin Modifiers in Response to DNA Damage. *Cell Reports*, *10*(10). https://doi.org/10.1016/j.celrep.2015.02.033

Hicks, W. M., Kim, M., & Haber, J. E. (2010). Increased mutagenesis and unique mutation signature associated with mitotic gene conversion. *Science*, *329*(5987). https://doi.org/10.1126/science.1191125

Hopkins, T. A., Ainsworth, W. B., Ellis, P. A., Donawho, C. K., DiGiammarino, E. L., Panchal, S. C., Abraham, V. C., Algire, M. A., Shi, Y., Olson, A. M., Johnson, E. F., Wilsbacher, J. L., & Maag, D. (2019). PARP1 trapping by PARP inhibitors drives cytotoxicity in both cancer cells and healthy bone marrow. *Molecular Cancer Research*, *17*(2). https://doi.org/10.1158/1541-7786.MCR-18-0138

Hopkins, T. A., Shi, Y., Rodriguez, L. E., Solomon, L. R., Donawho, C. K., di Giammarino, E. L., Panchal, S. C., Wilsbacher, J. L., Gao, W., Olson, A. M., Stolarik, D. F., Osterling, D. J., Johnson, E. F., & Maag, D. (2015). Mechanistic Dissection of PARP1 Trapping and the Impact on In Vivo Tolerability and Efficacy of PARP Inhibitors. *Molecular Cancer Research : MCR*, *13*(11), 1465–1477. https://doi.org/10.1158/1541-7786.MCR-15-0191-T

Horigome, C., Bustard, D. E., Marcomini, I., Delgoshaie, N., Tsai-Pflugfelder, M., Cobb, J. A., & Gasser, S. M. (2016). PolySUMOylation by Siz2 and Mms21 triggers relocation of DNA breaks to nuclear pores through the Slx5/Slx8 STUbL. *Genes and Development*, *30*(8). https://doi.org/10.1101/gad.277665.116

Huen, M. S. Y., Grant, R., Manke, I., Minn, K., Yu, X., Yaffe, M. B., & Chen, J. (2007). RNF8 Transduces the DNA-Damage Signal via Histone Ubiquitylation and Checkpoint Protein Assembly. *Cell*, *131*(5). https://doi.org/10.1016/j.cell.2007.09.041

Hung, V., Udeshi, N. D., Lam, S. S., Loh, K. H., Cox, K. J., Pedram, K., Carr, S. A., & Ting, A. Y. (2016). Spatially resolved proteomic mapping in living cells with the

engineered peroxidase APEX2. *Nature Protocols*, *11*(3). https://doi.org/10.1038/nprot.2016.018

Huryn, D. M., Kornfilt, D. J. P., & Wipf, P. (2019). p97: An Emerging Target for Cancer, Neurodegenerative Diseases, and Viral Infections. *Journal of Medicinal Chemistry*, *63*(5), 1892–1907. https://doi.org/10.1021/ACS.JMEDCHEM.9B01318

Jackson, S. P., & Bartek, J. (2009). The DNA-damage response in human biology and disease. *Nature*, *461*(7267), 1071–1078. https://doi.org/10.1038/NATURE08467

Jensen, R. B., Carreira, A., & Kowalczykowski, S. C. (2010). Purified human BRCA2 stimulates RAD51-mediated recombination. *Nature*, *467*(7316). https://doi.org/10.1038/nature09399

Jiang, X., Li, X., Li, W., Bai, H., & Zhang, Z. (2019). PARP inhibitors in ovarian cancer: Sensitivity prediction and resistance mechanisms. *Journal of Cellular and Molecular Medicine*, *23*(4), 2303. https://doi.org/10.1111/JCMM.14133

Jiricny, J. (2006). The multifaceted mismatch-repair system. *Nature Reviews. Molecular Cell Biology*, *7*(5), 335–346. https://doi.org/10.1038/NRM1907

Kamaletdinova, T., Fanaei-Kahrani, Z., & Wang, Z. Q. (2019). The Enigmatic Function of PARP1: From PARylation Activity to PAR Readers. *Cells*, *8*(12). https://doi.org/10.3390/CELLS8121625

Kciuk, M., Marciniak, B., & Kontek, R. (2020). Irinotecan—still an important player in cancer chemotherapy: A comprehensive overview. In *International Journal of Molecular Sciences* (Vol. 21, Issue 14). https://doi.org/10.3390/ijms21144919

Khanna, K. K., & Jackson, S. P. (2001). DNA double-strand breaks: Signaling, repair and the cancer connection. *Nature Genetics*, *27*(3). https://doi.org/10.1038/85798

Kiianitsa, K., & Maizels, N. (2013). A rapid and sensitive assay for DNA-protein covalent complexes in living cells. *Nucleic Acids Research*, *41*(9). https://doi.org/10.1093/nar/gkt171

Kilgas, S., Singh, A. N., Paillas, S., Then, C.-K., Torrecilla, I., Nicholson, J., Browning, L., Vendrell, I., Konietzny, R., Kessler, B. M., Kiltie, A. E., & Ramadan, K. (2021). p97/VCP inhibition causes excessive MRE11-dependent DNA end resection promoting cell killing after ionizing radiation. *Cell Reports*, *35*(8). https://doi.org/10.1016/J.CELREP.2021.109153

Kim, D. S., Camacho, C. v., & Kraus, W. L. (2021). Alternate therapeutic pathways for PARP inhibitors and potential mechanisms of resistance. *Experimental & Molecular Medicine 2021 53:1*, *53*(1), 42–51. https://doi.org/10.1038/s12276-021-00557-3

Kim, H., Chen, J., & Yu, X. (2007). Ubiquitin-binding protein RAP80 mediates BRCA1-dependent DNA damage response. *Science*, *316*(5828), 1202–1205. https://doi.org/10.1126/SCIENCE.1139621/SUPPL_FILE/KIM.SOM.PDF

Kliza, K., & Husnjak, K. (2020). Resolving the Complexity of Ubiquitin Networks. In *Frontiers in Molecular Biosciences* (Vol. 7). https://doi.org/10.3389/fmolb.2020.00021

Køhler, J. B., Tammsalu, T., Jørgensen, M. M., Steen, N., Hay, R. T., & Thon, G. (2015). Targeting of SUMO substrates to a Cdc48-Ufd1-Npl4 segregase and STUbL pathway in fission yeast. *Nature Communications*, *6*. https://doi.org/10.1038/ncomms9827

Kolas, N. K., Chapman, J. R., Nakada, S., Ylanko, J., Chahwan, R., Sweeney, F. D., Panier, S., Mendez, M., Wildenhain, J., Thomson, T. M., Pelletier, L., Jackson, S. P., & Durocher, D. (2007). Orchestration of the DNA-damage response by the RNF8 ubiquitin ligase. *Science*, *318*(5856). https://doi.org/10.1126/science.1150034

Kozlov, S. v., Graham, M. E., Jakob, B., Tobias, F., Kijas, A. W., Tanuji, M., Chen, P., Robinson, P. J., Taucher-Scholz, G., Suzuki, K., So, S., Chen, D., & Lavin, M. F. (2011). Autophosphorylation and ATM Activation. *Journal of Biological Chemistry*, *286*(11). https://doi.org/10.1074/jbc.m110.204065

Krastev, D. B., Pettitt, S. J., Campbell, J., Song, F., Tanos, B. E., Stoynov, S. S., Ashworth, A., & Lord, C. J. (2018). Coupling bimolecular PARylation biosensors with genetic screens to identify PARylation targets. *Nature Communications*, *9*(1). https://doi.org/10.1038/s41467-018-04466-4

Krokan, H. E., & Bjørås, M. (2013). Base excision repair. *Cold Spring Harbor Perspectives in Biology*, *5*(4). https://doi.org/10.1101/cshperspect.a012583

Krüger, A., Bürkle, A., Hauser, K., & Mangerich, A. (2020). Real-time monitoring of PARP1-dependent PARylation by ATR-FTIR spectroscopy. *Nature Communications*, *11*(1). https://doi.org/10.1038/s41467-020-15858-w

Kusakabe, M., Onishi, Y., Tada, H., Kurihara, F., Kusao, K., Furukawa, M., Iwai, S., Yokoi, M., Sakai, W., & Sugasawa, K. (2019). Mechanism and regulation of DNA damage recognition in nucleotide excision repair. *Genes and Environment*, *41*(1). https://doi.org/10.1186/s41021-019-0119-6

Kuzminov, A. (1999). Recombinational Repair of DNA Damage in Escherichia coli and Bacteriophage λ . *Microbiology and Molecular Biology Reviews*, *63*(4). https://doi.org/10.1128/mmbr.63.4.751-813.1999

LaFargue, C. J., Molin, G. Z. D., Sood, A. K., & Coleman, R. L. (2019). Exploring and comparing adverse events between PARP inhibitors. *The Lancet. Oncology*, *20*(1), e15. https://doi.org/10.1016/S1470-2045(18)30786-1

Lam, S. S., Martell, J. D., Kamer, K. J., Deerinck, T. J., Ellisman, M. H., Mootha, V. K., & Ting, A. Y. (2015). Directed evolution of APEX2 for electron microscopy and proteomics. *Nature Methods*, *12*(1), 51. https://doi.org/10.1038/NMETH.3179

Langelier, M. F., Planck, J. L., Roy, S., & Pascal, J. M. (2012). Structural basis for DNA damage-dependent poly(ADP-ribosyl)ation by human PARP-1. *Science*, *336*(6082). https://doi.org/10.1126/science.1216338

Larsen, N. B., Gao, A. O., Sparks, J. L., Gallina, I., Wu, R. A., Mann, M., Räschle, M., Walter, J. C., & Duxin, J. P. (2019). Replication-Coupled DNA-Protein Crosslink Repair by SPRTN and the Proteasome in Xenopus Egg Extracts. *Molecular Cell*, *73*(3). https://doi.org/10.1016/j.molcel.2018.11.024

Lee, M. J., Lee, B. H., Hanna, J., King, R. W., & Finley, D. (2011). Trimming of ubiquitin chains by proteasome-associated deubiquitinating enzymes. In *Molecular and Cellular Proteomics* (Vol. 10, Issue 5). https://doi.org/10.1074/mcp.R110.003871

Leinonen, H., Cheng, C., Pitkänen, M., Sander, C. L., Zhang, J., Saeid, S., Turunen, T., Shmara, A., Weiss, L., Ta, L., Ton, T., Koskelainen, A., Vargas, J. D., Kimonis, V., & Palczewski, K. (2021). A p97/valosin-containing protein inhibitor drug CB-5083 has a potent but reversible off-target effect on phosphodiesterase-6. *Journal of Pharmacology and Experimental Therapeutics*, *378*(1). https://doi.org/10.1124/jpet.120.000486

Lemaçon, D., Jackson, J., Quinet, A., Brickner, J. R., Li, S., Yazinski, S., You, Z., Ira, G., Zou, L., Mosammaparast, N., & Vindigni, A. (2017). MRE11 and EXO1 nucleases degrade reversed forks and elicit MUS81-dependent fork rescue in BRCA2-deficient cells. *Nature Communications 2017 8:1*, *8*(1), 1–12. https://doi.org/10.1038/s41467-017-01180-5

Lessel, D., Vaz, B., Halder, S., Lockhart, P. J., Marinovic-Terzic, I., Lopez-Mosqueda, J., Philipp, M., Sim, J. C. H., Smith, K. R., Oehler, J., Cabrera, E., Freire, R., Pope, K., Nahid, A., Norris, F., Leventer, R. J., Delatycki, M. B., Barbi, G., von Ameln, S., … Kubisch, C. (2014). Mutations in SPRTN cause early onset hepatocellular carcinoma, genomic instability and progeroid features. *Nature Genetics*, *46*(11). https://doi.org/10.1038/ng.3103

Li, X., Stith, C. M., Burgers, P. M., & Heyer, W. D. (2009). PCNA Is Required for Initiation of Recombination-Associated DNA Synthesis by DNA Polymerase δ. *Molecular Cell*, *36*(4). https://doi.org/10.1016/j.molcel.2009.09.036

Liu, J. C. Y., Kühbacher, U., Larsen, N. B., Borgermann, N., Garvanska, D. H., Hendriks, I. A., Ackermann, L., Haahr, P., Gallina, I., Guérillon, C., Branigan, E., Hay, R. T., Azuma, Y., Nielsen, M. L., Duxin, J. P., & Mailand, N. (2021). Mechanism and function of DNA replication-independent DNA-protein crosslink repair via the SUMO-RNF4 pathway. *The EMBO Journal*, *40*(18). https://doi.org/10.15252/embj.2020107413

Longley, D. B., Harkin, D. P., & Johnston, P. G. (2003). 5-Fluorouracil: mechanisms of action and clinical strategies. *Nature Reviews Cancer 2003 3:5*, *3*(5), 330–338. https://doi.org/10.1038/nrc1074

Lord, C. J., & Ashworth, A. (2012). The DNA damage response and cancer therapy. *Nature 2012 481:7381*, *481*(7381), 287–294. https://doi.org/10.1038/nature10760

Lord, C. J., & Ashworth, A. (2017). PARP inhibitors: Synthetic lethality in the clinic. In *Science* (Vol. 355, Issue 6330). https://doi.org/10.1126/science.aam7344

Luo, K., Zhang, H., Wang, L., Yuan, J., & Lou, Z. (2012). Sumoylation of MDC1 is important for proper DNA damage response. *EMBO Journal*, *31*(13). https://doi.org/10.1038/emboj.2012.158

M., M., D., S., J., D., K., H., J., H., P., S., E., K., M., H., & J., C. (2014). Characterization of the cellular mechanism of action of the first in class investigational inhibitor of the Ubiquitin Activating Enzyme, MLN7243. In *European Journal of Cancer* (Vol. 50).

Macheret, M., & Halazonetis, T. D. (2015). DNA Replication Stress as a Hallmark of Cancer. *Http://Ezproxy-Prd.Bodleian.Ox.Ac.Uk:2197/10.1146/Annurev-Pathol-012414-040424*, *10*, 425–448. https://doi.org/10.1146/ANNUREV-PATHOL-012414-040424

Macheret, M., & Halazonetis, T. D. (2018). Intragenic origins due to short G1 phases underlie oncogene-induced DNA replication stress. *Nature*, *555*(7694), 112. https://doi.org/10.1038/NATURE25507

Mailand, N., Bekker-Jensen, S., Faustrup, H., Melander, F., Bartek, J., Lukas, C., & Lukas, J. (2007). RNF8 Ubiquitylates Histones at DNA Double-Strand Breaks and Promotes Assembly of Repair Proteins. *Cell*, *131*(5). https://doi.org/10.1016/j.cell.2007.09.040

Malu, S., de Ioannes, P., Kozlov, M., Greene, M., Francis, D., Hanna, M., Pena, J., Escalante, C. R., Kurosawa, A., Erdjument-Bromage, H., Tempst, P., Adachi, N., Vezzoni, P., Villa, A., Aggarwal, A. K., & Cortes, P. (2012). Artemis C-terminal region facilitates V(D)J recombination through its interactions with DNA Ligase IV and DNA-pkcs. *Journal of Experimental Medicine*, *209*(5). https://doi.org/10.1084/jem.20111437

Mari, P. O., Florea, B. I., Persengiev, S. P., Verkaik, N. S., Brüggenwirth, H. T., Modesti, M., Giglia-Mari, G., Bezstarosti, K., Demmers, J. A. A., Luider, T. M., Houtsmuller, A. B., & van Gent, D. C. (2006). Dynamic assembly of end-joining complexes requires interaction between Ku70/80 and XRCC4. *Proceedings of the National Academy of Sciences of the United States of America*, *103*(49). https://doi.org/10.1073/pnas.0609061103

Maric, M., Maculins, T., de Piccoli, G., & Labib, K. (2014). Cdc48 and a ubiquitin ligase drive disassembly of the CMG helicase at the end of DNA replication. *Science*, *346*(6208). https://doi.org/10.1126/science.1253596

Maric, M., Mukherjee, P., Tatham, M. H., Hay, R., & Labib, K. (2017). Ufd1-Npl4 Recruit Cdc48 for Disassembly of Ubiquitylated CMG Helicase at the End of Chromosome Replication. *Cell Reports*, *18*(13). https://doi.org/10.1016/j.celrep.2017.03.020

Martin, N., Schwamborn, K., Schreiber, V., Werner, A., Guillier, C., Zhang, X. D., Bischof, O., Seeler, J. S., & Dejean, A. (2009). PARP-1 transcriptional activity is regulated by sumoylation upon heat shock. *EMBO Journal*, *28*(22). https://doi.org/10.1038/emboj.2009.279

Martino, E., della Volpe, S., Terribile, E., Benetti, E., Sakaj, M., Centamore, A., Sala, A., & Collina, S. (2017). The long story of camptothecin: From traditional medicine to drugs. *Bioorganic & Medicinal Chemistry Letters*, *27*(4), 701–707. https://doi.org/10.1016/J.BMCL.2016.12.085

Maskey, R. S., Kim, M. S., Baker, D. J., Childs, B., Malureanu, L. A., Jeganathan, K. B., Machida, Y., van Deursen, J. M., & Machida, Y. J. (2014). Spartan deficiency causes genomic instability and progeroid phenotypes. *Nature Communications*, *5*. https://doi.org/10.1038/ncomms6744

Maslov, A. Y., Lee, M., Gundry, M., Gravina, S., Strogonova, N., Tazearslan, C., Bendebury, A., Suh, Y., & Vijg, J. (2012). 5-Aza-2′-deoxycytidine-induced genome rearrangements are mediated by DNMT1. *Oncogene*, *31*(50). https://doi.org/10.1038/onc.2012.9

Masuda, T., Shinohara, H., & Kondo, M. (1980). Reactivity of Nucleotides and Polynucleotides Toward Hydroxyl Radical in Aqueous Solution. *Journal of Radiation Research*, *21*(2). https://doi.org/10.1269/jrr.21.173

Mateos-Gomez, P. A., Gong, F., Nair, N., Miller, K. M., Lazzerini-Denchi, E., & Sfeir, A. (2015). Mammalian polymerase θ promotes alternative NHEJ and suppresses recombination. *Nature*, *518*(7538). https://doi.org/10.1038/nature14157

Matsuoka, S., Huang, M., & Elledge, S. J. (1998). Linkage of ATM to cell cycle regulation by the Chk2 protein kinase. *Science*, *282*(5395). https://doi.org/10.1126/science.282.5395.1893

Maya-Mendoza, A., Moudry, P., Merchut-Maya, J. M., Lee, M., Strauss, R., & Bartek, J. (2018). High speed of fork progression induces DNA replication stress and genomic instability. *Nature 2018 559:7713*, *559*(7713), 279–284. https://doi.org/10.1038/s41586-018-0261-5

Meerang, M., Ritz, D., Paliwal, S., Garajova, Z., Bosshard, M., Mailand, N., Janscak, P., Hübscher, U., Meyer, H., & Ramadan, K. (2011). The ubiquitin-selective segregase VCP/p97 orchestrates the response to DNA double-strand breaks. *Nature Cell Biology*, *13*(11). https://doi.org/10.1038/ncb2367

Mehta, K. P. M., Lovejoy, C. A., Zhao, R., Heintzman, D. R., & Cortez, D. (2020). HMCES Maintains Replication Fork Progression and Prevents Double-Strand Breaks in Response to APOBEC Deamination and Abasic Site Formation. *Cell Reports*, *31*(9). https://doi.org/10.1016/j.celrep.2020.107705

Meyer, H., Bug, M., & Bremer, S. (2012). Emerging functions of the VCP/p97 AAA-ATPase in the ubiquitin system. In *Nature Cell Biology* (Vol. 14, Issue 2). https://doi.org/10.1038/ncb2407

Michelena, J., Lezaja, A., Teloni, F., Schmid, T., Imhof, R., & Altmeyer, M. (2018). Analysis of PARP inhibitor toxicity by multidimensional fluorescence microscopy reveals mechanisms of sensitivity and resistance. *Nature Communications*, *9*(1). https://doi.org/10.1038/s41467-018-05031-9

Mimitou, E. P., & Symington, L. S. (2008). Sae2, Exo1 and Sgs1 collaborate in DNA double-strand break processing. *Nature*, *455*(7214). https://doi.org/10.1038/nature07312

Mimitou, E. P., & Symington, L. S. (2010). Ku prevents Exo1 and Sgs1-dependent resection of DNA ends in the absence of a functional MRX complex or Sae2. *EMBO Journal*, *29*(19), 3358–3369. https://doi.org/10.1038/EMBOJ.2010.193

Ming, X., Groehler, A., Michaelson-Richie, E. D., Villalta, P. W., Campbell, C., & Tretyakova, N. Y. (2017). Mass Spectrometry Based Proteomics Study of Cisplatin-Induced DNA-Protein Cross-Linking in Human Fibrosarcoma (HT1080) Cells. *Chemical Research in Toxicology*, *30*(4). https://doi.org/10.1021/acs.chemrestox.6b00389

Mirman, Z., Lottersberger, F., Takai, H., Kibe, T., Gong, Y., Takai, K., Bianchi, A., Zimmermann, M., Durocher, D., & de Lange, T. (2018). 53BP1/Rif1/Shieldin counteract DSB resection through CST/Polα-dependent fill-in. *Nature*, *560*(7716), 112. https://doi.org/10.1038/S41586-018-0324-7

Mohammed, H., Taylor, C., Brown, G. D., Papachristou, E. K., Carroll, J. S., & D'Santos, C. S. (2016a). Rapid immunoprecipitation mass spectrometry of endogenous proteins (RIME) for analysis of chromatin complexes. In *Nature Protocols* (Vol. 11, Issue 2). https://doi.org/10.1038/nprot.2016.020

Mohammed, H., Taylor, C., Brown, G. D., Papachristou, E. K., Carroll, J. S., & D'Santos, C. S. (2016b). Rapid immunoprecipitation mass spectrometry of endogenous proteins (RIME) for analysis of chromatin complexes. *Nature Protocols 2015 11:2*, *11*(2), 316–326. https://doi.org/10.1038/nprot.2016.020

Mohni, K. N., Wessel, S. R., Zhao, R., Wojciechowski, A. C., Luzwick, J. W., Layden, H., Eichman, B. F., Thompson, P. S., Mehta, K. P. M., & Cortez, D. (2019). HMCES Maintains Genome Integrity by Shielding Abasic Sites in Single-Strand DNA. *Cell*, *176*(1–2). https://doi.org/10.1016/j.cell.2018.10.055

Moon, J. J., Lu, A., & Moon, C. (2019). Role of genomic instability in human carcinogenesis. *Experimental Biology and Medicine*, *244*(3), 227. https://doi.org/10.1177/1535370219826031

Morris, J. R., Boutell, C., Keppler, M., Densham, R., Weekes, D., Alamshah, A., Butler, L., Galanty, Y., Pangon, L., Kiuchi, T., Ng, T., & Solomon, E. (2009). The SUMO modification pathway is involved in the BRCA1 response to genotoxic stress. *Nature 2009 462:7275*, *462*(7275), 886–890. https://doi.org/10.1038/nature08593

Mosbech, A., Gibbs-Seymour, I., Kagias, K., Thorslund, T., Beli, P., Povlsen, L., Nielsen, S. V., Smedegaard, S., Sedgwick, G., Lukas, C., Hartmann-Petersen, R., Lukas, J., Choudhary, C., Pocock, R., Bekker-Jensen, S., & Mailand, N. (2012). DVC1 (C1orf124) is a DNA damage-targeting p97 adaptor that promotes ubiquitin-dependent responses to replication blocks. *Nature Structural and Molecular Biology*, *19*(11). https://doi.org/10.1038/nsmb.2395

Moudry, P., Lukas, C., Macurek, L., Hanzlikova, H., Hodny, Z., Lukas, J., & Bartek, J. (2012). Ubiquitin-activating enzyme UBA1 is required for cellular response to DNA damage. *Cell Cycle*, *11*(8). https://doi.org/10.4161/cc.19978

Muñoz, M. C., Laulier, C., Gunn, A., Cheng, A., Robbiani, D. F., Nussenzweig, A., & Stark, J. M. (2012). Ring finger nuclear factor RNF168 is important for defects in homologous recombination caused by loss of the breast cancer susceptibility factor BRCA1. *Journal of Biological Chemistry*, *287*(48). https://doi.org/10.1074/jbc.M112.410951

Murai, J., Huang, S. Y. N., Das, B. B., Renaud, A., Zhang, Y., Doroshow, J. H., Ji, J., Takeda, S., & Pommier, Y. (2012). Trapping of PARP1 and PARP2 by clinical PARP inhibitors. *Cancer Research*, *72*(21). https://doi.org/10.1158/0008-5472.CAN-12-2753

Murai, J., Huang, S. Y. N., Renaud, A., Zhang, Y., Ji, J., Takeda, S., Morris, J., Teicher, B., Doroshow, J. H., & Pommier, Y. (2014). Stereospecific PARP trapping by BMN 673 and comparison with olaparib and rucaparib. *Molecular Cancer Therapeutics*, *13*(2). https://doi.org/10.1158/1535-7163.MCT-13-0803

Murai, J., & Pommier, Y. (2019). PARP trapping beyond homologous recombination and platinum sensitivity in cancers. In *Annual Review of Cancer Biology* (Vol. 3, Issue 1). https://doi.org/10.1146/annurev-cancerbio-030518-055914

Nakamura, K., Kogame, T., Oshiumi, H., Shinohara, A., Sumitomo, Y., Agama, K., Pommier, Y., Tsutsui, K. M., Tsutsui, K., Hartsuiker, E., Ogi, T., Takeda, S., & Taniguchi, Y. (2010). Collaborative action of Brca1 and CtIP in elimination of covalent modifications from double-strand breaks to facilitate subsequent break repair. *PLoS Genetics*, *6*(1). https://doi.org/10.1371/journal.pgen.1000828

Nam, S. M., & Jeon, Y. J. (2019). Proteostasis in the endoplasmic reticulum: Road to cure. In *Cancers* (Vol. 11, Issue 11). https://doi.org/10.3390/cancers11111793

Neelsen, K. J., & Lopes, M. (2015). Replication fork reversal in eukaryotes: from dead end to dynamic response. *Nature Reviews Molecular Cell Biology 2015 16:4*, *16*(4), 207–220. https://doi.org/10.1038/nrm3935

Nie, M., Aslanian, A., Prudden, J., Heideker, J., Vashisht, A. A., Wohlschlegel, J. A., Yates, J. R., & Boddy, M. N. (2012). Dual recruitment of Cdc48 (p97)-Ufd1-Npl4 ubiquitin-selective segregase by small ubiquitin-like modifier protein (SUMO) and ubiquitin in SUMO-targeted ubiquitin ligase-mediated genome stability functions. *Journal of Biological Chemistry*, *287*(35). https://doi.org/10.1074/jbc.M112.379768

Nimonkar, A. v., Sica, R. A., & Kowalczykowski, S. C. (2009). Rad52 promotes second-end DNA capture in double-stranded break repair to form complement-stabilized joint molecules. *Proceedings of the National Academy of Sciences of the United States of America*, *106*(9). https://doi.org/10.1073/pnas.0813247106

Nizialek, E., & Antonarakis, E. S. (2020). PARP Inhibitors in Metastatic Prostate Cancer: Evidence to Date. *Cancer Management and Research*, *12*, 8105. https://doi.org/10.2147/CMAR.S227033

Noordermeer, S. M., Adam, S., Setiaputra, D., Barazas, M., Pettitt, S. J., Ling, A. K., Olivieri, M., Álvarez-Quilón, A., Moatti, N., Zimmermann, M., Annunziato, S., Krastev, D. B., Song, F., Brandsma, I., Frankum, J., Brough, R., Sherker, A., Landry, S., Szilard, R. K., … Durocher, D. (2018). The Shieldin complex mediates 53BP1-dependent DNA repair. *Nature*, *560*(7716), 117. https://doi.org/10.1038/S41586-018-0340-7

Obeng, E. A., Carlson, L. M., Gutman, D. M., Harrington, W. J., Lee, K. P., & Boise, L. H. (2006). Proteasome inhibitors induce a terminal unfolded protein response in multiple myeloma cells. *Blood*, *107*(12), 4907–4916. https://doi.org/10.1182/BLOOD-2005-08-3531

O'Connor, M. J. (2015). Targeting the DNA Damage Response in Cancer. *Molecular Cell*, *60*(4), 547–560. https://doi.org/10.1016/J.MOLCEL.2015.10.040

Oh, E., Akopian, D., & Rape, M. (2018). Principles of Ubiquitin- Dependent Signaling. In *Annual Review of Cell and Developmental Biology* (Vol. 34). https://doi.org/10.1146/annurev-cellbio-100617-062802

Palazzo, L., Leidecker, O., Prokhorova, E., Dauben, H., Matic, I., & Ahel, I. (2018). Serine is the major residue for ADP-ribosylation upon DNA damage. *ELife*, *7*. https://doi.org/10.7554/eLife.34334

Panier, S., Ichijima, Y., Fradet-Turcotte, A., Leung, C. C. Y., Kaustov, L., Arrowsmith, C. H., & Durocher, D. (2012). Tandem Protein Interaction Modules Organize the Ubiquitin-Dependent Response to DNA Double-Strand Breaks. *Molecular Cell*, *47*(3). https://doi.org/10.1016/j.molcel.2012.05.045

Perez-Riverol, Y., Csordas, A., Bai, J., Bernal-Llinares, M., Hewapathirana, S., Kundu, D. J., Inuganti, A., Griss, J., Mayer, G., Eisenacher, M., Pérez, E., Uszkoreit, J., Pfeuffer, J., Sachsenberg, T., Yilmaz, Ş., Tiwary, S., Cox, J., Audain, E., Walzer, M., … Vizcaíno, J. A. (2019). The PRIDE database and related tools and resources in 2019: improving support for quantification data. *Nucleic Acids Research*, *47*(D1), D442–D450. https://doi.org/10.1093/NAR/GKY1106

Pettitt, S. J., Krastev, D. B., Brandsma, I., Dréan, A., Song, F., Aleksandrov, R., Harrell, M. I., Menon, M., Brough, R., Campbell, J., Frankum, J., Ranes, M., Pemberton, H. N., Rafiq, R., Fenwick, K., Swain, A., Guettler, S., Lee, J. M., Swisher, E. M., … Lord, C. J. (2018). Genome-wide and high-density CRISPR-Cas9 screens identify point mutations in PARP1 causing PARP inhibitor resistance. *Nature Communications*, *9*(1). https://doi.org/10.1038/s41467-018-03917-2

Pettitt, S. J., Krastev, D. B., Pemberton, H. N., Fontebasso, Y., Frankum, J., Rehman, F. L., Brough, R., Song, F., Bajrami, I., Rafiq, R., Wallberg, F., Kozarewa, I., Fenwick, K., Armisen-Garrido, J., Swain, A., Gulati, A., Campbell, J., Ashworth, A., & Lord, C. J. (2017). Genome-wide barcoded transposon screen for cancer drug sensitivity in haploid mouse embryonic stem cells. *Scientific Data*, *4*. https://doi.org/10.1038/SDATA.2017.20

Pettitt, S. J., Rehman, F. L., Bajrami, I., Brough, R., Wallberg, F., Kozarewa, I., Fenwick, K., Assiotis, I., Chen, L., Campbell, J., Lord, C. J., & Ashworth, A. (2013). A Genetic Screen Using the PiggyBac Transposon in Haploid Cells Identifies Parp1 as a Mediator of Olaparib Toxicity. *PLoS ONE*, *8*(4). https://doi.org/10.1371/journal.pone.0061520

Petukhova, G., Stratton, S., & Sung, P. (1998). Catalysis of homologous DNA pairing by yeast Rad51 and Rad54 proteins. *Nature*, *393*(6680). https://doi.org/10.1038/30037

Pfeiffer, A., Luijsterburg, M. S., Acs, K., Wiegant, W. W., Helfricht, A., Herzog, L. K., Minoia, M., Böttcher, C., Salomons, F. A., Attikum, H. van, & Dantuma, N. P. (2017). Ataxin-3 consolidates the MDC1-dependent DNA double-strand break response by counteracting the SUMO-targeted ubiquitin ligase RNF4. *The EMBO Journal*, *36*(8), 1066–1083. https://doi.org/10.15252/EMBJ.201695151

Pommier, Y., Huang, S. yin N., Gao, R., Das, B. B., Murai, J., & Marchand, C. (2014). Tyrosyl-DNA-phosphodiesterases (TDP1 and TDP2). *DNA Repair*, *19*. https://doi.org/10.1016/j.dnarep.2014.03.020

Pommier, Y., & Murai, J. (2015). Classification of PARP inhibitors based on PARP trapping and catalytic inhibition, and rationale for combinations. *Annals of Oncology*, *26*. https://doi.org/10.1093/annonc/mdv084.1

Pommier, Y., O'Connor, M. J., & de Bono, J. (2016). Laying a trap to kill cancer cells: PARP inhibitors and their mechanisms of action. *Science Translational Medicine*, *8*(362). https://doi.org/10.1126/SCITRANSLMED.AAF9246/ASSET/1F45A43D-50DA-4BF6-AE64-5BFD85AA9C83/ASSETS/GRAPHIC/8-362PS17-F3.JPEG

Pothuri, B., O'Cearbhaill, R., Eskander, R., & Armstrong, D. (2020). Frontline PARP inhibitor maintenance therapy in ovarian cancer: A Society of Gynecologic Oncology practice statement. *Gynecologic Oncology*, *159*(1), 8–12. https://doi.org/10.1016/J.YGYNO.2020.07.097

Pouliot, J. J., Yao, K. C., Robertson, C. A., & Nash, H. A. (1999). Yeast gene for a Tyr-DNA phosphodiesterase that repairs topoisomerase I complexes. *Science*, *286*(5439). https://doi.org/10.1126/science.286.5439.552

Poulsen, S. L., Hansen, R. K., Wagner, S. A., van Cuijk, L., van Belle, G. J., Streicher, W., Wikström, M., Choudhary, C., Houtsmuller, A. B., Marteijn, J. A., Bekker-Jensen, S., & Mailand, N. (2013). RNF111/Arkadia is a SUMO-targeted ubiquitin ligase that facilitates the DNA damage response. *Journal of Cell Biology*, *201*(6). https://doi.org/10.1083/jcb.201212075

Prudden, J., Pebernard, S., Raffa, G., Slavin, D. A., Perry, J. J. P., Tainer, J. A., McGowan, C. H., & Boddy, M. N. (2007). SUMO-targeted ubiquitin ligases in genome stability. *EMBO Journal*, *26*(18). https://doi.org/10.1038/sj.emboj.7601838

Puumalainen, M.-R., Lessel, D., Rüthemann, P., Kaczmarek, N., Bachmann, K., Ramadan, K., & Naegeli, H. (2014). Chromatin retention of DNA damage sensors DDB2 and XPC through loss of p97 segregase causes genotoxicity. *Nature Communications 2014 5:1*, *5*(1), 1–10. https://doi.org/10.1038/ncomms4695

Ramadan, K. (2012). p97/VCP- and Lys48-linked polyubiquitination form a new signaling pathway in DNA damage response. In *Cell Cycle* (Vol. 11, Issue 6). https://doi.org/10.4161/cc.11.6.19446

Ramadan, K., Bruderer, R., Spiga, F. M., Popp, O., Baur, T., Gotta, M., & Meyer, H. H. (2007). Cdc48/p97 promotes reformation of the nucleus by extracting the kinase Aurora B from chromatin. *Nature*, *450*(7173). https://doi.org/10.1038/nature06388

Raman, M., Havens, C. G., Walter, J. C., & Harper, J. W. (2011). A Genome-wide Screen Identifies p97 as an Essential Regulator of DNA Damage-Dependent CDT1 Destruction. *Molecular Cell*, *44*(1). https://doi.org/10.1016/j.molcel.2011.06.036

Ray Chaudhuri, A., & Nussenzweig, A. (2017). The multifaceted roles of PARP1 in DNA repair and chromatin remodelling. In *Nature Reviews Molecular Cell Biology* (Vol. 18, Issue 10). https://doi.org/10.1038/nrm.2017.53

Reinking, H. K., Kang, H. S., Götz, M. J., Li, H. Y., Kieser, A., Zhao, S., Acampora, A. C., Weickert, P., Fessler, E., Jae, L. T., Sattler, M., & Stingele, J. (2020). DNA Structure-Specific Cleavage of DNA-Protein Crosslinks by the SPRTN Protease. *Molecular Cell*, *80*(1). https://doi.org/10.1016/j.molcel.2020.08.003

Reyes-Turcu, F. E., Ventii, K. H., & Wilkinson, K. D. (2009). Regulation and cellular roles of ubiquitin-specific deubiquitinating enzymes. In *Annual Review of Biochemistry* (Vol. 78). https://doi.org/10.1146/annurev.biochem.78.082307.091526

Rich, T., Allen, R. L., & Wyllie, A. H. (2000). Defying death after DNA damage. In *Nature* (Vol. 407, Issue 6805). https://doi.org/10.1038/35037717

Rogakou, E. P., Pilch, D. R., Orr, A. H., Ivanova, V. S., & Bonner, W. M. (1998). DNA double-stranded breaks induce histone H2AX phosphorylation on serine 139. *Journal of Biological Chemistry*, *273*(10). https://doi.org/10.1074/jbc.273.10.5858

Rojas-Fernandez, A., Plechanovová, A., Hattersley, N., Jaffray, E., Tatham, M. H., & Hay, R. T. (2014). SUMO chain-induced dimerization activates RNF4. *Molecular Cell*, *53*(6). https://doi.org/10.1016/j.molcel.2014.02.031

Rothenberg, E., Grimme, J. M., Spies, M., & Ha, T. (2008). Human Rad52-mediated homology search and annealing occurs by continuous interactions between overlapping nucleoprotein complexes. *Proceedings of the National Academy of Sciences of the United States of America*, *105*(51). https://doi.org/10.1073/pnas.0810317106

Roux, B., Vaganay, C., Vargas, J. D., Alexe, G., Benaksas, C., Pardieu, B., Fenouille, N., Ellegast, J. M., Malolepsza, E., Ling, F., Sodaro, G., Ross, L., Pikman, Y., Conway, A. S., Tang, Y., Wu, T., Anderson, D. J., le Moigne, R., Zhou, H. J., … Benajiba, L. (2021a). Targeting acute myeloid leukemia dependency on VCP-mediated DNA repair through a selective second-generation small-molecule inhibitor. *Science Translational Medicine*, *13*(587). https://doi.org/10.1126/scitranslmed.abg1168

Roux, B., Vaganay, C., Vargas, J. D., Alexe, G., Benaksas, C., Pardieu, B., Fenouille, N., Ellegast, J. M., Malolepsza, E., Ling, F., Sodaro, G., Ross, L., Pikman, Y., Conway, A. S., Tang, Y., Wu, T., Anderson, D. J., le Moigne, R., Zhou, H. J., … Benajiba, L. (2021b). Targeting acute myeloid leukemia dependency on VCP-mediated DNA repair through a selective second-generation small-molecule inhibitor. *Science Translational Medicine*, *13*(587), 31. https://doi.org/10.1126/SCITRANSLMED.ABG1168/SUPPL_FILE/ABG1168_TABLES_S1_TO_S9.XLSX

Rudolph, J., Roberts, G., & Luger, K. (2021). Histone Parylation factor 1 contributes to the inhibition of PARP1 by cancer drugs. *Nature Communications*, *12*(1). https://doi.org/10.1038/s41467-021-20998-8

Ruggiano, A., & Ramadan, K. (2021). DNA–protein crosslink proteases in genome stability. In *Communications Biology* (Vol. 4, Issue 1). https://doi.org/10.1038/s42003-020-01539-3

Ruggiano, A., Vaz, B., Kilgas, S., Popović, M., Rodriguez-Berriguete, G., Singh, A. N., Higgins, G. S., Kiltie, A. E., & Ramadan, K. (2021). The protease SPRTN and SUMOylation coordinate DNA-protein crosslink repair to prevent genome instability. *Cell Reports*, *37*(10), 110080. https://doi.org/10.1016/J.CELREP.2021.110080

Ryu, T., Spatola, B., Delabaere, L., Bowlin, K., Hopp, H., Kunitake, R., Karpen, G. H., & Chiolo, I. (2015). Heterochromatic breaks move to the nuclear periphery to continue recombinational repair. *Nature Cell Biology*, *17*(11). https://doi.org/10.1038/ncb3258

Saha, L. K., Murai, Y., Saha, S., Jo, U., Tsuda, M., Takeda, S., & Pommier, Y. (2021). Replication-dependent cytotoxicity and Spartan-mediated repair of trapped PARP1–DNA complexes. *Nucleic Acids Research*, *49*(18). https://doi.org/10.1093/nar/gkab777

Savage, K. I., & Harkin, D. P. (2015). BRCA1, a 'complex' protein involved in the maintenance of genomic stability. *The FEBS Journal*, *282*(4), 630–646. https://doi.org/10.1111/FEBS.13150

Schiewer, M. J., & Knudsen, K. E. (2014). Transcriptional roles of PARP1 in cancer. In *Molecular Cancer Research* (Vol. 12, Issue 8). https://doi.org/10.1158/1541-7786.MCR-13-0672

Schwertman, P., Bekker-Jensen, S., & Mailand, N. (2016). Regulation of DNA double-strand break repair by ubiquitin and ubiquitin-like modifiers. In *Nature Reviews Molecular Cell Biology* (Vol. 17, Issue 6). https://doi.org/10.1038/nrm.2016.58

Scully, R., Panday, A., Elango, R., & Willis, N. A. (2019). DNA double-strand break repair-pathway choice in somatic mammalian cells. *Nature Reviews Molecular Cell Biology 2019 20:11*, *20*(11), 698–714. https://doi.org/10.1038/s41580-019-0152-0

Sczepanski, J. T., Wong, R. S., McKnight, J. N., Bowman, G. D., & Greenberg, M. M. (2010). Rapid DNA-protein cross-linking and strand scission by an abasic site in a nucleosome core particle. *Proceedings of the National Academy of Sciences of the United States of America*, *107*(52). https://doi.org/10.1073/pnas.1012860108

Setiaputra, D., & Durocher, D. (2019). Shieldin – the protector of DNA ends. *EMBO Reports*, *20*(5). https://doi.org/10.15252/EMBR.201847560

Shi, Y., Hu, Y., Hu, X., Li, X., Lin, L., & Han, X. (2015). Cisplatin combined with irinotecan or etoposide for untreated extensive-stage small cell lung cancer: A multicenter randomized controlled clinical trial. *Thoracic Cancer*, *6*(6), 785–791. https://doi.org/10.1111/1759-7714.12303

Shi, Y., Lan, F., Matson, C., Mulligan, P., Whetstine, J. R., Cole, P. A., Casero, R. A., & Shi, Y. (2004). Histone demethylation mediated by the nuclear amine oxidase homolog LSD1. *Cell*, *119*(7). https://doi.org/10.1016/j.cell.2004.12.012

Shiovitz, S., & Korde, L. A. (2015). Genetics of breast cancer: a topic in evolution. *Annals of Oncology*, *26*(7), 1291. https://doi.org/10.1093/ANNONC/MDV022

Simsek, D., Brunet, E., Wong, S. Y. W., Katyal, S., Gao, Y., McKinnon, P. J., Lou, J., Zhang, L., Li, J., Rebar, E. J., Gregory, P. D., Holmes, M. C., & Jasin, M. (2011). DNA ligase III promotes alternative nonhomologous end-joining during chromosomal translocation formation. *PLoS Genetics*, *7*(6). https://doi.org/10.1371/journal.pgen.1002080

Singh, A. N., Oehler, J., Torrecilla, I., Kilgas, S., Li, S., Vaz, B., Guérillon, C., Fielden, J., Hernandez-Carralero, E., Cabrera, E., Tullis, I. D., Meerang, M., Barber, P. R., Freire, R., Parsons, J., Vojnovic, B., Kiltie, A. E., Mailand, N., & Ramadan, K. (2019). The p97–Ataxin 3 complex regulates homeostasis of the DNA damage response E3 ubiquitin ligase RNF 8 . *The EMBO Journal*, *38*(21). https://doi.org/10.15252/embj.2019102361

Skrott, Z., Majera, D., Gursky, J., Buchtova, T., Hajduch, M., Mistrik, M., & Bartek, J. (2019). Disulfiram's anti-cancer activity reflects targeting NPL4, not inhibition of aldehyde dehydrogenase. *Oncogene 2019 38:40*, *38*(40), 6711–6722. https://doi.org/10.1038/s41388-019-0915-2

Skrott, Z., Mistrik, M., Andersen, K. K., Friis, S., Majera, D., Gursky, J., Ozdian, T., Bartkova, J., Turi, Z., Moudry, P., Kraus, M., Michalova, M., Vaclavkova, J., Dzubak, P., Vrobel, I., Pouckova, P., Sedlacek, J., Miklovicova, A., Kutt, A., … Bartek, J. (2017a). Alcohol-abuse drug disulfiram targets cancer via p97 segregase adaptor NPL4. *Nature*, *552*(7684). https://doi.org/10.1038/nature25016

Skrott, Z., Mistrik, M., Andersen, K. K., Friis, S., Majera, D., Gursky, J., Ozdian, T., Bartkova, J., Turi, Z., Moudry, P., Kraus, M., Michalova, M., Vaclavkova, J., Dzubak, P., Vrobel, I., Pouckova, P., Sedlacek, J., Miklovicova, A., Kutt, A., …

Bartek, J. (2017b). Alcohol-abuse drug disulfiram targets cancer via p97 segregase adaptor NPL4. *Nature 2017 552:7684*, *552*(7684), 194–199. https://doi.org/10.1038/nature25016

Solinger, J. A., Kiianitsa, K., & Heyer, W. D. (2002). Rad54, a Swi2/Snf2-like recombinational repair protein, disassembles Rad51:dsDNA filaments. *Molecular Cell*, *10*(5). https://doi.org/10.1016/S1097-2765(02)00743-8

Stach, L., & Freemont, P. S. (2017). The AAA+ ATPase p97, a cellular multitool. In *Biochemical Journal* (Vol. 474, Issue 17). https://doi.org/10.1042/BCJ20160783

Stingele, J., Bellelli, R., Alte, F., Hewitt, G., Sarek, G., Maslen, S. L., Tsutakawa, S. E., Borg, A., Kjær, S., Tainer, J. A., Skehel, J. M., Groll, M., & Boulton, S. J. (2016). Mechanism and Regulation of DNA-Protein Crosslink Repair by the DNA-Dependent Metalloprotease SPRTN. *Molecular Cell*, *64*(4). https://doi.org/10.1016/j.molcel.2016.09.031

Stingele, J., Bellelli, R., & Boulton, S. J. (2017). Mechanisms of DNA-protein crosslink repair. In *Nature Reviews Molecular Cell Biology* (Vol. 18, Issue 9). https://doi.org/10.1038/nrm.2017.56

Ström, C. E., Johansson, F., Uhlén, M., Szigyarto, C. A. K., Erixon, K., & Helleday, T. (2011). Poly (ADP-ribose) polymerase (PARP) is not involved in base excision repair but PARP inhibition traps a single-strand intermediate. *Nucleic Acids Research*, *39*(8), 3166–3175. https://doi.org/10.1093/NAR/GKQ1241

Sun, Y., Jenkins, L. M. M., Su, Y. P., Nitiss, K. C., Nitiss, J. L., & Pommier, Y. (2020). A conserved SUMO pathway repairs topoisomerase DNA-protein cross-links by engaging ubiquitin-mediated proteasomal degradation. *Science Advances*, *6*(46). https://doi.org/10.1126/sciadv.aba6290

Sun, Y., Miller Jenkins, L. M., Su, Y. P., Nitiss, K. C., Nitiss, J. L., & Pommier, Y. (2019). A conserved SUMO-Ubiquitin pathway directed by RNF4/SLX5-SLX8 and PIAS4/SIZ1 drives proteasomal degradation of topoisomerase DNA-protein crosslinks. *BioRxiv*. https://doi.org/10.1101/707661

Sun, Y., Saha, S., Wang, W., Saha, L. K., Huang, S. Y. N., & Pommier, Y. (2020). Excision repair of topoisomerase DNA-protein crosslinks (TOP-DPC). In *DNA Repair* (Vol. 89). https://doi.org/10.1016/j.dnarep.2020.102837

Surova, O., & Zhivotovsky, B. (2012). Various modes of cell death induced by DNA damage. *Oncogene 2013 32:33*, *32*(33), 3789–3797. https://doi.org/10.1038/onc.2012.556

Suskiewicz, M. J., Zobel, F., Ogden, T. E. H., Fontana, P., Ariza, A., Yang, J. C., Zhu, K., Bracken, L., Hawthorne, W. J., Ahel, D., Neuhaus, D., & Ahel, I. (2020). HPF1 completes the PARP active site for DNA damage-induced ADP-ribosylation. *Nature*, *579*(7800). https://doi.org/10.1038/s41586-020-2013-6

Tacconi, E. M., Lai, X., Folio, C., Porru, M., Zonderland, G., Badie, S., Michl, J., Sechi, I., Rogier, M., García, V. M., Batra, A. S., Rueda, O. M., Bouwman, P., Jonkers, J., Ryan, A., Reina-San-Martin, B., Hui, J., Tang, N., Bruna, A., … Tarsounas, M. (2017). BRCA1 and BRCA2 tumor suppressors protect against endogenous acetaldehyde toxicity. *EMBO Molecular Medicine*, *9*(10), 1398–1414. https://doi.org/10.15252/EMMM.201607446

Tang, W. K., Odzorig, T., Jin, W., & Xia, D. (2019). Structural basis of p97 inhibition by the site-selective anticancer compound CB-5083. *Molecular Pharmacology*, *95*(3). https://doi.org/10.1124/mol.118.114256

Tassone, P., Tagliaferri, P., Perricelli, A., Blotta, S., Quaresima, B., Martelli, M. L., Goel, A., Barbieri, V., Costanzo, F., Boland, C. R., & Venuta, S. (2003). BRCA1 expression modulates chemosensitivity of BRCA1-defective HCC1937 human breast cancer cells. *British Journal of Cancer*, *88*(8), 1285. https://doi.org/10.1038/SJ.BJC.6600859

Thorslund, T., Ripplinger, A., Hoffmann, S., Wild, T., Uckelmann, M., Villumsen, B., Narita, T., Sixma, T. K., Choudhary, C., Bekker-Jensen, S., & Mailand, N. (2015). Histone H1 couples initiation and amplification of ubiquitin signalling after DNA damage. *Nature*, *527*(7578). https://doi.org/10.1038/nature15401

Torrecilla, I., Oehler, J., & Ramadan, K. (2017). The role of ubiquitin-dependent segregase p97 (VCP or Cdc48) in chromatin dynamics after DNA double strand breaks. In *Philosophical Transactions of the Royal Society B: Biological Sciences* (Vol. 372, Issue 1731). https://doi.org/10.1098/rstb.2016.0282

Ubhi, T., & Brown, G. W. (2019). Exploiting DNA Replication Stress for Cancer Treatment. *Cancer Research*, *79*(8), 1730–1739. https://doi.org/10.1158/0008-5472.CAN-18-3631

Uematsu, N., Weterings, E., Yano, K. I., Morotomi-Yano, K., Jakob, B., Taucher-Scholz, G., Mari, P. O., van Gent, D. C., Chen, B. P. C., & Chen, D. J. (2007). Autophosphorylation of DNA-PKCS regulates its dynamics at DNA double-strand breaks. *Journal of Cell Biology*, *177*(2). https://doi.org/10.1083/jcb.200608077

van den Boom, J., & Meyer, H. (2018). VCP/p97-Mediated Unfolding as a Principle in Protein Homeostasis and Signaling. In *Molecular Cell* (Vol. 69, Issue 2). https://doi.org/10.1016/j.molcel.2017.10.028

van den Boom, J., Wolf, M., Weimann, L., Schulze, N., Li, F., Kaschani, F., Riemer, A., Zierhut, C., Kaiser, M., Iliakis, G., Funabiki, H., & Meyer, H. (2016a). VCP/p97 Extracts Sterically Trapped Ku70/80 Rings from DNA in Double-Strand Break Repair. *Molecular Cell*, *64*(1). https://doi.org/10.1016/j.molcel.2016.08.037

van den Boom, J., Wolf, M., Weimann, L., Schulze, N., Li, F., Kaschani, F., Riemer, A., Zierhut, C., Kaiser, M., Iliakis, G., Funabiki, H., & Meyer, H. (2016b). VCP/p97 extracts sterically trapped Ku70/80 rings from DNA in double strand break repair. *Molecular Cell*, *64*(1), 189. https://doi.org/10.1016/J.MOLCEL.2016.08.037

van Nguyen, T., Li, J., Lu, C. C. J., Mamrosh, J. L., Lu, G., Cathers, B. E., & Deshaies, R. J. (2017). P97/VCP promotes degradation of CRBN substrate glutamine synthetase and neosubstrates. *Proceedings of the National Academy of Sciences of the United States of America*, *114*(14). https://doi.org/10.1073/pnas.1700949114

Vaz, B., Popovic, M., Newman, J. A., Fielden, J., Aitkenhead, H., Halder, S., Singh, A. N., Vendrell, I., Fischer, R., Torrecilla, I., Drobnitzky, N., Freire, R., Amor, D. J., Lockhart, P. J., Kessler, B. M., McKenna, G. W., Gileadi, O., & Ramadan, K. (2016). Metalloprotease SPRTN/DVC1 Orchestrates Replication-Coupled DNA-Protein Crosslink Repair. *Molecular Cell*, *64*(4). https://doi.org/10.1016/j.molcel.2016.09.032

Vaz, B., Popovic, M., & Ramadan, K. (2017). DNA–Protein Crosslink Proteolysis Repair. In *Trends in Biochemical Sciences* (Vol. 42, Issue 6). https://doi.org/10.1016/j.tibs.2017.03.005

Vekaria, P. H., Home, T., Weir, S., Schoenen, F. J., & Rao, R. (2016). Targeting p97 to disrupt protein homeostasis in cancer. In *Frontiers in Oncology* (Vol. 6, Issue AUG). https://doi.org/10.3389/fonc.2016.00181

Villa, F., Fujisawa, R., Ainsworth, J., Nishimura, K., Lie-A-Ling, M., Lacaud, G., & Labib, K. P. (2021). CUL2 LRR1 , TRAIP and p97 control CMG helicase disassembly in the mammalian cell cycle . *EMBO Reports*, *22*(3). https://doi.org/10.15252/embr.202052164

Wang, M., & Kaufman, R. J. (2016). Protein misfolding in the endoplasmic reticulum as a conduit to human disease. *Nature 2016 529:7586*, *529*(7586), 326–335. https://doi.org/10.1038/nature17041

Weith, M., Seiler, J., van den Boom, J., Kracht, M., Hülsmann, J., Primorac, I., del Pino Garcia, J., Kaschani, F., Kaiser, M., Musacchio, A., Bollen, M., & Meyer, H. (2018). Ubiquitin-Independent Disassembly by a p97 AAA-ATPase Complex Drives PP1 Holoenzyme Formation. *Molecular Cell*, *72*(4), 766-777.e6. https://doi.org/10.1016/J.MOLCEL.2018.09.020/ATTACHMENT/4B8B0D4E-DF84-4CE9-8505-CFF4D5CCD70A/MMC2.XLSX

Wold, M. S. (1997). Replication protein A: A heterotrimeric, single-stranded DNA-binding protein required for eukaryotic DNA metabolism. In *Annual Review of Biochemistry* (Vol. 66). https://doi.org/10.1146/annurev.biochem.66.1.61

Xie, A., Kwok, A., & Scully, R. (2009). Role of mammalian Mre11 in classical and alternative nonhomologous end joining. *Nature Structural & Molecular Biology*, *16*(8), 814–818. https://doi.org/10.1038/NSMB.1640

Yang, G., Liu, C., Chen, S. H., Kassab, M. A., Hoff, J. D., Walter, N. G., & Yu, X. (2018). Super-resolution imaging identifies PARP1 and the Ku complex acting as DNA double-strand break sensors. *Nucleic Acids Research*, *46*(7). https://doi.org/10.1093/nar/gky088

Yang, S. W., Burgin, A. B., Huizenga, B. N., Robertson, C. A., Yao, K. C., & Nash, H. A. (1996). A eukaryotic enzyme that can disjoin dead-end covalent complexes between DNA and type I topoisomerases. *Proceedings of the National Academy of Sciences of the United States of America*, *93*(21), 11534–11539. https://doi.org/10.1073/PNAS.93.21.11534

Yano, K. I., Morotomi-Yano, K., Wang, S. Y., Uematsu, N., Lee, K. J., Asaithamby, A., Weterings, E., & Chen, D. J. (2008). Ku recruits XLF to DNA double-strand breaks. *EMBO Reports*, *9*(1). https://doi.org/10.1038/sj.embor.7401137

Ye, Y., Meyer, H. H., & Rapoport, T. A. (2001a). The AAA ATPase Cdc48/p97 and its partners transport proteins from the ER into the cytosol. *Nature*, *414*(6864). https://doi.org/10.1038/414652a

Ye, Y., Meyer, H. H., & Rapoport, T. A. (2001b). The AAA ATPase Cdc48/p97 and its partners transport proteins from the ER into the cytosol. *Nature 2001 414:6864*, *414*(6864), 652–656. https://doi.org/10.1038/414652a

Ye, Y., Meyer, H. H., & Rapoport, T. A. (2003). Function of the p97–Ufd1–Npl4 complex in retrotranslocation from the ER to the cytosol. *Journal of Cell Biology*, *162*(1). https://doi.org/10.1083/jcb.200302169

Ye, Y., Shibata, Y., Yun, C., Ron, D., & Rapoport, T. A. (2004). A membrane protein complex mediates retro-translocation from the ER lumen into the cytosol. *Nature*, *429*(6994). https://doi.org/10.1038/nature02656

Ye, Y., Tang, W. K., Zhang, T., & Xia, D. (2017). A mighty "protein extractor" of the cell: Structure and function of the p97/CDC48 ATPase. In *Frontiers in Molecular Biosciences* (Vol. 4, Issue JUN). https://doi.org/10.3389/fmolb.2017.00039

Yin, Y., Seifert, A., Chua, J. S., Maure, J. F., Golebiowski, F., & Hay, R. T. (2012). SUMO-targeted ubiquitin E3 ligase RNF4 is required for the response of human cells to DNA damage. *Genes and Development*, *26*(11). https://doi.org/10.1101/gad.189274.112

Yusa, K., Zhou, L., Li, M. A., Bradley, A., & Craig, N. L. (2011). A hyperactive piggyBac transposase for mammalian applications. *Proceedings of the National Academy of Sciences of the United States of America*, *108*(4), 1531–1536. https://doi.org/10.1073/PNAS.1008322108/-/DCSUPPLEMENTAL

Zandarashvili, L., Langelier, M. F., Velagapudi, U. K., Hancock, M. A., Steffen, J. D., Billur, R., Hannan, Z. M., Wicks, A. J., Krastev, D. B., Pettitt, S. J., Lord, C. J., Talele, T. T., Pascal, J. M., & Black, B. E. (2020). Structural basis for allosteric PARP-1 retention on DNA breaks. In *Science* (Vol. 368, Issue 6486). https://doi.org/10.1126/science.aax6367

Zeman, M. K., & Cimprich, K. A. (2014). Causes and Consequences of Replication Stress. *Nature Cell Biology*, *16*(1), 2. https://doi.org/10.1038/NCB2897

Zhao, B., Rothenberg, E., Ramsden, D. A., & Lieber, M. R. (2020). The molecular basis and disease relevance of non-homologous DNA end joining. In *Nature Reviews Molecular Cell Biology* (Vol. 21, Issue 12). https://doi.org/10.1038/s41580-020-00297-8

Zhao, S., Kieser, A., Li, H. Y., Reinking, H. K., Weickert, P., Euteneuer, S., Yaneva, D., Acampora, A. C., Götz, M. J., Feederle, R., & Stingele, J. (2021). A ubiquitin switch controls autocatalytic inactivation of the DNA-protein crosslink repair protease SPRTN. *Nucleic Acids Research*, *49*(2). https://doi.org/10.1093/nar/gkaa1224

Zhao, W., Steinfeld, J. B., Liang, F., Chen, X., Maranon, D. G., Jian Ma, C., Kwon, Y., Rao, T., Wang, W., Sheng, C., Song, X., Deng, Y., Jimenez-Sainz, J., Lu, L., Jensen, R. B., Xiong, Y., Kupfer, G. M., Wiese, C., Greene, E. C., & Sung, P. (2017). BRCA1–BARD1 promotes RAD51-mediated homologous DNA pairing. *Nature 2017 550:7676*, *550*(7676), 360–365. https://doi.org/10.1038/nature24060

Zhao, X. (2018). SUMO-Mediated Regulation of Nuclear Functions and Signaling Processes. In *Molecular Cell* (Vol. 71, Issue 3). https://doi.org/10.1016/j.molcel.2018.07.027

Zhu, H., Wei, M., Xu, J., Hua, J., Liang, C., Meng, Q., Zhang, Y., Liu, J., Zhang, B., Yu, X., & Shi, S. (2020). PARP inhibitors in pancreatic cancer: Molecular mechanisms

and clinical applications. *Molecular Cancer*, *19*(1), 1–15. https://doi.org/10.1186/S12943-020-01167-9/FIGURES/2

Zhu, Z., Chung, W. H., Shim, E. Y., Lee, S. E., & Ira, G. (2008). Sgs1 Helicase and Two Nucleases Dna2 and Exo1 Resect DNA Double-Strand Break Ends. *Cell*, *134*(6). https://doi.org/10.1016/j.cell.2008.08.037